BIOBASED POLYURETHANES AND NANOCOMPOSITES

From structure/properties relationship to shape-memory behavior

Tamara Calvo Correas

eman ta zabal zazu

Universidad del País Vasco   Euskal Herriko Unibertsitatea

Donostia-San Sebastian, 2017

BIOBASED POLYURETHANES AND NANOCOMPOSITES

From structure/properties relationship to shape-memory behavior

PhD Dissertation presented by

TAMARA CALVO CORREAS

Under the supervision of

Dr. Mª Aranzazu Eceiza Mendiguren

Dr. Mª Ángeles Corcuera Maeso

Donostia-San Sebastian, May 2017

ACKNOWLEDGMENTS

SUMMARY

This work deals with the synthesis of polyurethane rigid foams, as well as, thermoplastic and crosslinked polyurethanes and bionanocomposites with high biobased carbon content. To this end, different reactants and nanoentities derived from renewable sources, such as vegetable oils, aminoacids, fatty acids and polysaccharides, have been employed. Regarding rigid polyurethanes foams, the use of different hydroxyl-containing modifiers in their formulation leads to the obtaining of foams with different properties, since their final properties are directly influenced by the nature and content of hydroxyl-containing modifiers. As far as crosslinked and thermoplastic polyurethanes is concerned two different biobased diisocyanates were used and in the case of the thermoplastic polyurethanes in addition to the diisocyanates, two different chain extenders derived from renewable sources were also employed in order to analyze their effect over the final properties of the material. The microphase separation between domains, thermal properties, the overall crystallinity and mechanical properties are closely affected by the nature of the reactants and the content of diisocyanate/chain extender or crosslinker content. Therefore, the control of these parameters leads to the obtaining of crosslinked and thermoplastic polyurethanes with tailored properties. In addition, the synthesized thermoplastic and crosslinked polyurethanes show a high biocompatibility, denoting that these materials can be good candidate for biomedical applications. Different bionanocomposites have been prepared by incorporating chitin and cellulose nanocrystals and magnetite nanoparticles. The final properties of the bionanocomposites are influenced by the nature of the nanoentity, as well as, by their content, since the rod-like nanocrystals (chitin and cellulose) would preferably interact with diisocyanate/chain extender rich domain, while magnetite nanoparticles interact with macrodiol rich domain.

Furthermore, the crosslinked and thermoplastic polyurethanes and bionanocomposites show thermally activated shape-memory properties. All the synthesized polyurethanes and bionanocomposites have presented high shape fixity and shape recovery ratios. Moreover, it has been observed that shape-memory properties are strongly dependent to the chosen programming conditions, dynamic mechanical behavior and the overall crystallinity of the material. In the case of the bionanocomposites, the addition of nanoentities would promote shape fixity or shape recovery ratios depending on the nature of the domain that interacts with them. In this way, the shape-memory properties of bionanocomposites, in addition to the factors previously mentioned, are tightly influenced by the nature of the nanoentities, as well as, by the preparation process.

INDEX

CHAPTER 1

INTRODUCTION

1. INTRODUCTION

1.1 Motivation

The demand for the development of polymers derived from renewable sources has increased in the last decades due to the depletion of the world crude oil stock and economical, environmental and social concerns.[1,2] Among polymers, polyurethanes are one of the most employed due to their versatility regarding properties, which make possible their use in multiple applications.[3–5] Hence the use of renewably sourced precursors has also extended to their synthesis. Polyurethanes are formed by addition polymerization of hydroxyl containing components, mainly polyols, and isocyanates. Biobased polyols are usually derived from vegetables oils such as castor, rapeseed and linseed oil, among others. Over the past few years, different vegetable oils derived polyols have been proved competitive for the synthesis of a wide range of polyurethanes.[6–13] Nowadays, the most employed isocyanates for the synthesis of polyurethanes are derived from petroleum. However, it is noteworthy the increased use of biobased isocyanates such as L-lysine diisocyanate (LDI), which is derived from L-lysine amino acid[14–17] and dimeryldiisocyanate (DDI), based on fatty acids.[18–20]

Furthermore, the development of smart materials has drawn increasing attention, especially shape-memory polymers (SMPs), since they can find broad range of applications in different sectors.[21–27] SMPs are a type of polymeric smart materials which are able to remember their original shape after being deformed, and recover it as a response to an external stimulus, being heat the most common one.[7,28,29]

In order to improve the shape-memory properties or modify the external stimulus, which triggers the shape recovery, different nanoentities can be used. These properties would be influenced depending on the nature of the segment that interacts with the nanoentities.[30,31] Besides, the use of nanoentities from

renewable sources is gaining attention since they are employed to enhance the final properties of the synthesized nanocomposites, to increase the amount of biobased carbon content in the final nanocomposites formulation and also the biocompatibility of the polymers.[30,32,33] Among biobased nanoentities polysaccharides nanocrystals, such as chitin and cellulose nanocrystals, are noteworthy. Furthermore, the incorporation of magnetic nanoparticles, such as magnetite, in addition to improve thermally-activated shape-memory properties,[34,35] they also allow triggering shape recovery by applying an alternative magnetic field.

Furthermore, due to the nature of biobased diisocyanates, polyurethanes with high biocompatibility can be obtained which makes them a very interesting candidates for being used in biomedical applications.[17,36–40]

Therefore, biobased polyurethanes (foams, crosslinked and thermoplastic) as well as bionanocomposites, based on biobased thermoplastic polyurethanes and renewable nanoentities and magnetic nanoparticles, were synthesized and characterized by means of physico-chemical, thermal, mechanical and surface properties and by analyzing their morphology. In the case of the crosslinked and thermoplastic polyurethanes their biocompatibility was also analyzed. In addition, shape-memory behavior of the synthesized crosslinked and thermoplastic polyurethanes and bionanocomposites was also studied.

1.2   Polyurethanes

As mentioned before, due to the wide range of properties of polyurethanes they can found multiple applications in different fields, such as automotive, textile, construction, biomedical and aerospace industry.[3–5,41,21,42–46]

The urethane functional group results from the addition reaction of alcohol and isocyanate groups, as observed in Scheme 1.1.

$$R_1{-}OH \ + \ R_2{-}NCO \longrightarrow R_2{-}\overset{\overset{\displaystyle H}{|}}{N}{-}\overset{\overset{\displaystyle O}{\|}}{C}{-}O{-}R_1$$

Alcohol   Isocyanate   Urethane
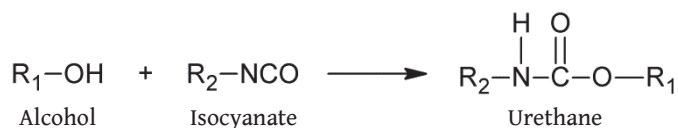
Scheme 1.1. Addition reaction between alcohol and isocyanate.

Furthermore, depending on the functionality of the starting reactants different kind of polyurethanes can be obtained. For instance, when reactants with functionality equal to two are used thermoplastic polyurethanes are obtained, whereas when functionality is higher than two the resultant polyurethanes are crosslinked. Among crosslinked polyurethanes they can be either solids or porous (foams). One of the most sustainable routes for the obtaining of porous polyurethanes is the use of water as blowing agent. The reaction of isocyanate groups with water results in the formation of urea functional groups and carbon dioxide (Scheme 1.2). The generated carbon dioxide allows the growth of the foam and the formation of a porous material takes place.

$$2\ R{-}NCO + H_2O \longrightarrow R{-}\overset{\overset{\displaystyle H}{|}}{N}{-}\overset{\overset{\displaystyle O}{\|}}{C}{-}\overset{\overset{\displaystyle H}{|}}{N}{-}R \ + \ CO_2{\uparrow}$$

Isocyanate   Water   Urea   Carbon dioxide
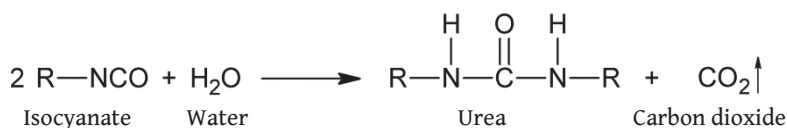
Scheme 1.2. Urea formation reaction.

1.2.1 Polyurethane foams

The main components of polyurethane foams are polyols, isocyanates, blowing agents, reactive modifiers, surfactants and catalysts. These porous materials are obtained by means of two different reactions. On the one hand, gelling reaction, in which a polyol is reacted with an isocyanate forming polyurethane and on the other hand, the reaction between the isocyanate and water takes place, blowing reaction, which as mentioned before generates carbon dioxide allowing the growth of the foam and forming the porous structure. A scheme of both reactions is shown in Scheme 1.3.

$$R_1-NCO \ + \ R_2-OH \longrightarrow R_1-\overset{\overset{\displaystyle H}{|}}{N}-\overset{\overset{}{\underset{\displaystyle O}{\|}}}-O-R_2$$

Isocyante   Alcohol   Urethane

Gelling reaction

$$2 \ R_1-NCO + H_2O \longrightarrow R_1-\overset{\overset{\displaystyle H}{|}}{N}-\overset{\overset{}{\underset{\displaystyle O}{\|}}}-\overset{\overset{\displaystyle H}{|}}{N}-R_1 + CO_2\uparrow$$

Isocyanate   Water   Urea   Carbon dioxide
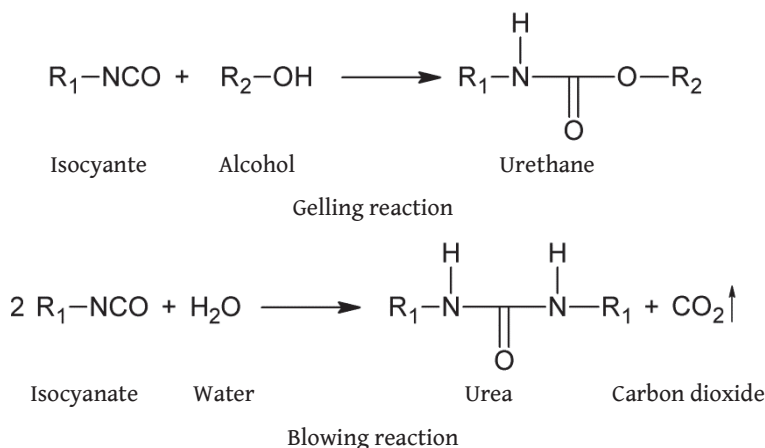
Blowing reaction

Scheme 1.3. Polyurethane foams forming reactions.

The use of precursors with different functionality leads to the modification of crosslink density of the polymer network obtaining flexible (low crosslink density) or rigid (high crosslink density) foams. An schematic representation of foams with low and high crosslink density is shown in Figure 1.1.
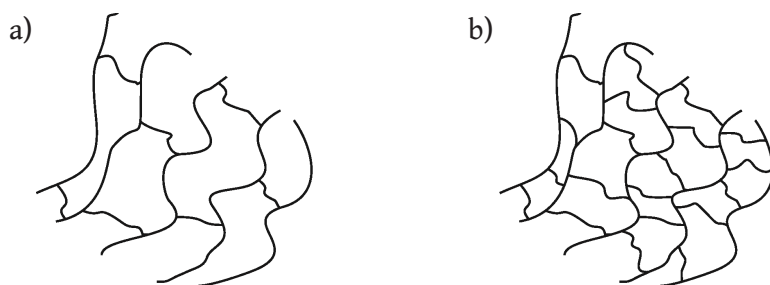
Figure 1.1. Schematic representation of a) low crosslinked polymer network and b) high crosslinked network.

The classification of polyurethane foams depending on the hydroxyl index value (I_{OH}) and functionality of the polyol is shown in Table 1.1.

Table 1.1. Classification of polyurethane foams.[46,47]

Polyol	Flexible foam	Semirigid foam	Rigid foam
I_{OH}	5.6-70	100-200	250-560
Functionality	2.0-3.1	3.0-3.5	3.0-8.0

Flexible foams show a density range from 10 to 80 Kg m^{-3}. This kind of foams show a high tensile strength and elongation at break, as well as high resilience or fast recovery from deformation. In the case of rigid foams, these foams have a density range from 10 to 1100 Kg m^{-3}. Moreover they are characterized for showing a high strength to weight ratio, high heat distortion temperature, high resistance to impact damage and insulation properties.

Regarding the preparation of the foams, there are different foaming reaction processes, being one-step process the most employed in industry and in lab scale. First the components of the B-side (polyol, blowing agent, reactive modifiers, surfactant and catalysts) are premixed at high speed to introduce air bubbles to the mixture. Subsequently, the component of A-side (isocyanate) is added to the homogeneous mixture and simultaneously both gelling and blowing reactions take place. Foam growth can be carried out in open or closed molds. A diagram of the one-step process is shown in Figure 1.2.
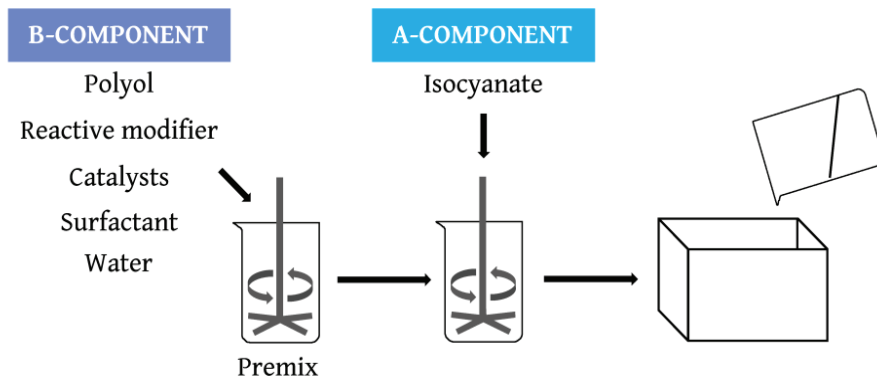
Figure 1.2. Scheme of the one-step foaming process.

1.2.2 Solid (segmented) polyurethanes

Segmented polyurethanes can be obtained through the reaction of a polyol with a medium molecular weight, usually diol type (macrodiol), a isocyanate (typically diisocyanate) and a chain extender or crosslinker with low molecular weight, and keeping the stoichiometric ratio between hydroxyl and isocyanate

functional groups close to one. Furthermore, these polymers are block copolymers with two main structural segments: the constituted by the macrodiol and the obtained by the reaction of a diisocyanate and a low-molecular weight chain extender or crosslinker.

Segmented polyurethanes can be obtained in bulk or in solution. In order to synthesize segmented polyurethanes in bulk two different preparation methods can be followed: one step and two step polymerization methods. In this work two step or prepolymer polymerization method was used, since a more accurate control over the chemistry is possible, which has influence on the structure, physical properties and reactivity of the obtained polyurethane.[48–51] Scheme 1.4 the general scheme of the two step polymerization method is shown.

First step
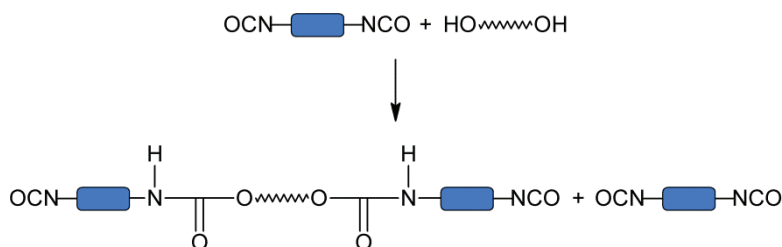
Second step
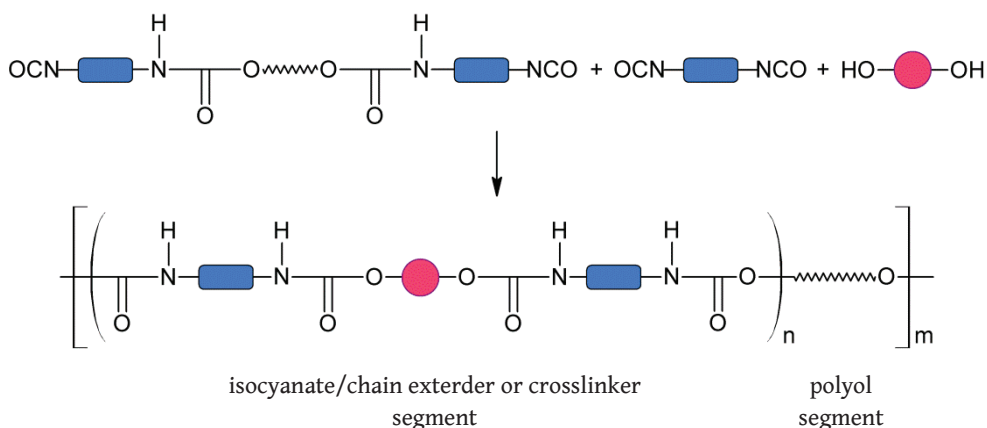
Scheme 1.4. General scheme of the two step polymerization method.

During the first step of the synthesis the macrodiol reacts with an excess of diisocyanate, obtaining prepolymer chains with isocyanate end groups and unreacted diisocyanate. After that, on the second step, the chain extender or crosslinker (depending if the desired segmented polyurethane is thermoplastic or crosslinked, respectively) is added stoichiometrically, in order to react with the unreacted isocyanate groups from the first step, joining prepolymer chains though urethane linkages to obtain a polymer with a high molecular weight. In

The use of different ratios of isocyanate, macrodiol and chain extender or crosslinker leads to the preparation of polyurethanes with segments of different lengths. Furthermore, the thermodynamic incompatibility between both segments promotes a microphase separation, which is strongly dependent on chemical structure and block lengths, and it is influenced by factors such as hydrogen bonding, the extent of crystallization and crosslinking degree.[13,52–56] In general, the isocyanate/chain extender or crosslinker segment provides both physical crosslinking points (in thermoplastics) and chemical crosslinking net points (in crosslinked) and filler-like reinforcement. In addition, this segment commonly rules the properties at high temperatures.[57] The physical crosslinking points among segments are formed by hydrogen bonding interactions between the N-H group of a segment and the C=O group of other segment.[58] The polyol segment is the responsible of the flexibility of the polymer as usually controls the properties of the material at low temperatures.[56,57,59] Nevertheless, if polyol segments form crystalline domains, they can also behave as reinforcing units.[13] Furthermore, depending on the structure of the isocyanate the segments which constitute polyurethanes could behave in a different way. When conventional petroleum derived isocyanates, such as 4,4'-diphenylmethane diisocyanate (MDI) or 1,6-hexamethylene diisocyanate (HDI), are used, the segment formed by the isocyanate and chain extender is mainly crystalline and shows a high glass transition.[10,12,13,60] However, the use of aliphatic and nonsymmetrical diisocyanates with long

chains or dangling chains results in the formation of amorphous urethane-based domains with low glass transition temperatures.[18,61,62] In addition, as mentioned before, semicrystalline macrodiols could also behave as reinforcing units.[13] Thus when semicrystalline polyols with a melting temperature much higher than room temperature are used, together with aliphatic and nonsymmetrical diisocyanates with long or dangling chains, the role of the segments could be inverted, acting the macrodiol as the hard phase, while the domain formed by the diisocyanate and the chain extender or crosslinker would act as the soft phase.

In Figure 1.1 a representation of the microstructure of microphase separated segmented thermoplastic and crosslinked polyurethane are shown.
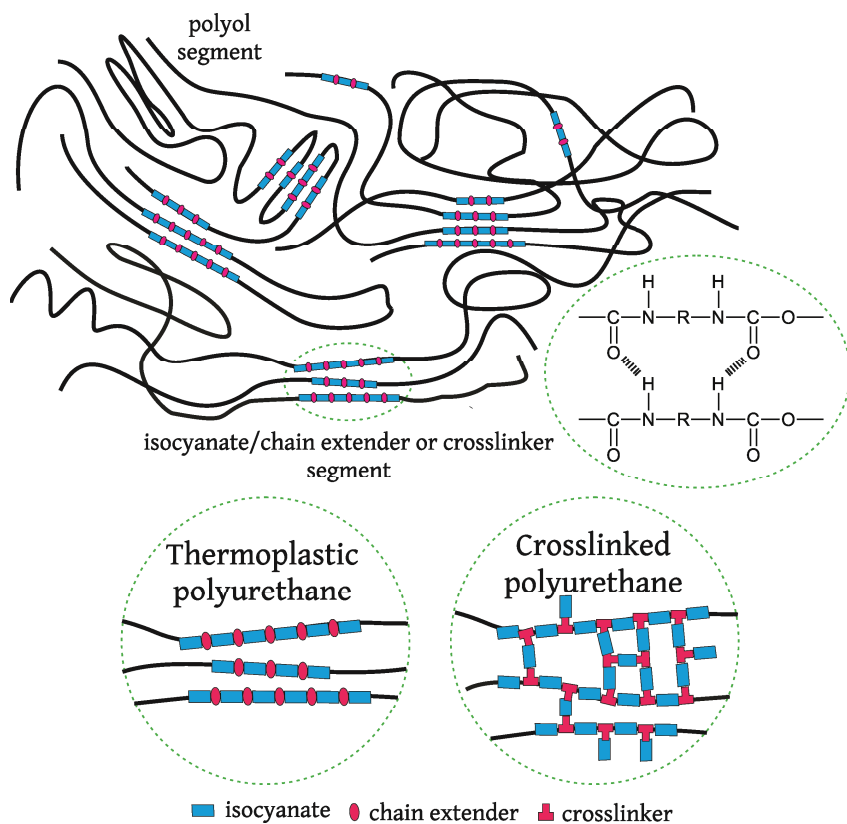
Figure 1.3. Schematic representation of the microphase separated segmented thermoplastic and crosslinked polyurethane microstructures.

1.2.3   Reactants for the formulation of polyurethanes

The final properties of polyurethanes are mainly governed by the choice of the reactants used for their synthesis. In this way polyurethanes with tailored properties can be obtained just by changing the nature of one of the reactant or by varying their composition. In general, polyurethanes are constituted by three reactants: a macrodiol or polyol, an isocyanate that has more than one reactive isocyanate group per molecule (diisocyanate or polyisocyanate) and a chain extender or crosslinker.

1.2.3.1   Macrodiols and polyols

Macrodiol and polyols are characterized for having a molecular weight range from 250 to 8000 g mol^{-1} and hydroxyl functional groups at the end of the chain. Macrodiols have two reactive hydroxyl functional groups per molecule, while polyols have a functionality between 2 and 8. Generally macrodiols are use in the synthesis of solid polyurethanes. Their use provides flexibility to the polyurethane, due to their glass transition temperature is usually far below from room temperature. Furthermore, macrodiols could also behave as reinforcement when they are semicrystalline.[13] In contrast, the use of polyols are more often used in the obtaining of polyurethanes foams, due to their high functionality which allows the synthesis of polyurethanes with a high crosslink density.

Different kind of macrodiols and polyols can be used in the synthesis of polyurethanes; however the most employed are polyether and polyester type.

In addition, in the last decades the interest in the use of macrodiols and polyols based on vegetable oils, such as soybean, linseed, palm, rapeseed and castor oil, is gaining attention as a result of economic, environmental and social concerns.[6,8,11,63–70] The use of macrodiols and polyols based on vegetable oils is one of the cheapest and most abundant natural alternative, which is available in

large quantities. These macrodiols and polyols provide numerous benefits to the material, such as high resistance, high stiffness, low toxicity and usually inherent biodegradability.[66,68,71]

Vegetal oils are formed by triglycerides, which are the result of the condensation of glycerol and three fatty acids (R_1, R_2 and R_3). In each vegetable oil the fatty acids from which it is formed varies. The general structure of triglycerides is shown in Scheme 1.5.
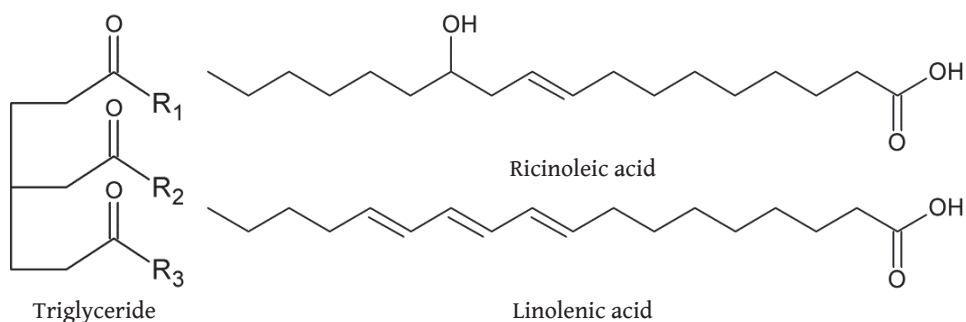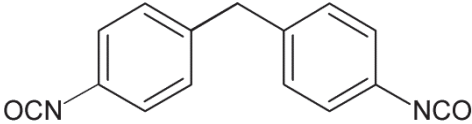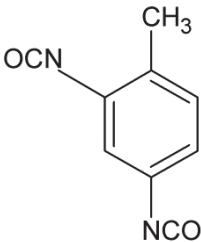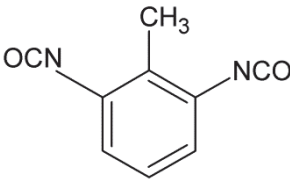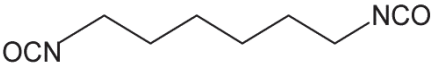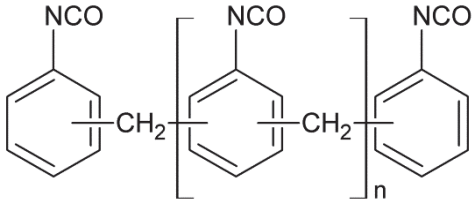
Scheme 1.5. Chemical structure of a triglyceride and ricinoleic and linolenic fatty acids.

One of the most employed vegetable oils in the synthesis of polyurethanes is castor oil due to it is mainly composed by ricinoleic acid (around 90%) and it is the only fatty acid with an inherent hydroxyl group in its structure, as can be observed in Scheme 1.5. Furthermore, linseed oil could be easily hydroxylated to obtain a polyol and employed in the synthesis of rigid polyurethane foams.[72,73] This oil is principally constituted by linolenic acid (around 57%), which chemical structure is shown in Scheme 1.5.

1.2.3.2 Isocyanates

Isocyanates are usually obtained from the phosgenation of amines and they are often derived from petrochemical sources. In Table 1.2 the chemical structure of the most employed isocyanates for the synthesis of solid and porous polyurethanes is shown.

Table 1.2. Chemical structure of the most common isocyanates used in the polyurethane synthesis.

Isocyanate (abbreviation)	Chemical structure
4,4'-Diphenylmethane diisocyanate (MDI)	
Toluene diisocyanate (TDI)	 2,4-TDI isomer 2,6-TDI isomer
1,6-Hexamethylene diisocyanate (HDI)	
Polymeric MDI (pMDI)	

The final properties of the polyurethanes are closely related with the structure of the isocyanate. In general, polyurethanes with aromatic diisocyanates such as MDI and toluene diisocyanate (TDI) show a high reactivity, and results in materials with elastic modulus, tensile strength and glass transition temperatures.[60,74–76] However, this kind of isocyanates tend to yellow gradually on exposure to daylight.[46] Whereas, aliphatic diisocyanates, such as HDI, in despite of their lower reactivity if comparing with aromatic diisocyanates, they

show a higher biocompatibility, lower hydrolytic degradation and higher resistance to yellowing.[46,77,78] The most employed diisocyanates for the synthesis of solid polyurethanes, either thermoplastic or crosslinked, are MDI and TDI.

Regarding the synthesis of porous polyurethanes, for flexible foams TDI is one of the most employed diisocyanate. TDI usually is composed by a mixture of 2,4-TDI and 2,6-TDI isomers (80:20). While for rigid foams polymeric MDI (pMDI) is the most used due to leads the obtaining of polymers with a high crosslink density.

In the last decades, the use of diisocyanates derived from renewable sources is gaining attention due to the reasons previously mentioned. Diisocyanates based on renewable sources could be obtained from fatty acids,[18–20,65,79] aminoacids,[14,16,17,61] biomass wastes[65,80–83] and polysaccharides,[84] among others. In Table 1.3 the most remarkable diisocyanates derived from renewable sources are gathered.

These diisocyanates are mainly used for the synthesis of thermoplastic and crosslinked polyurethanes. The use of biobased diisocyanates increases the amount of renewable carbon in the polymer.[65] However, the principal advantage of employing these diisocyanates for the synthesis of polyurethanes is their low toxicity which allows the obtaining of polymers with high biocompatibility, making them ideal candidates for their use in biomedical applications.[17,36–40]

Furthermore, diisocyanates such as LDI and DDI leads to the obtaining of polyurethanes with innovative properties since due to their nonsymmetrical and aliphatic chemical structure the resultant polyurethanes present urethane-based domains with low glass transition temperature. In this way, the diisocyanate rich segment could behave as a soft phase and rule the properties at low temperatures, as well as the flexibility of the material.[18,19]

Table 1.3. Some of the most remarkable biobased isocyanates.

Isocyanate (abbreviation)	Chemical structure
Ethyl ester L-lysine diisocyanate (LDI) **Renewable source:** aminoacids	
2-heptyl-3,4-bis(9-isocyanatononyl)-1-pentylcyclohexane (DDI) **Renewable source:** fatty acids	
5,5'-Isopropylidenebis(2-furfuryl isocyanate) (EDFI) **Renewable source:** biomass wastes	

Isocyanates could also leads to crosslinking side reactions during the synthesis of the polyurethanes, Scheme 1.6. For instance, isocyanate groups in excess can react with urethane or urea groups at high temperatures or in presence of organometallic catalysts forming allophanate and biuret groups, respectively. Usually for the synthesis of thermoplastic polyurethanes, these reactions are not desirable therefore in order to avoid them mild temperature conditions should be used. However, in the synthesis of crosslinked polyurethanes these reactions can be promoted in order to obtain polymers with a higher crosslink density.
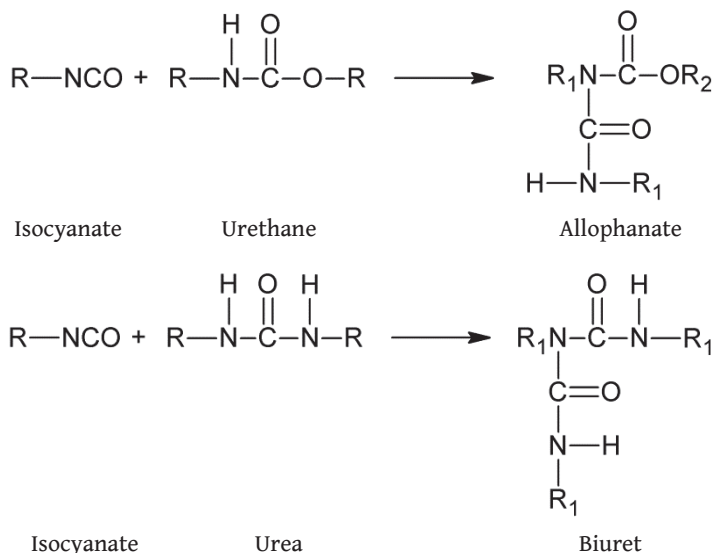
Scheme 1.6. Main isocyanate crosslinking side reactions.

1.2.3.3   Chain extenders and crosslinkers

Chain extenders and crosslinkers are polyols and diamines with low molecular weight. Chain extenders are difunctional compounds, while crosslinkers have functionality greater than two. The reaction of chain extenders or crosslinkers with isocyanate produces a urethane bond (a urea bond when diamines are used), and as mentioned before isocyanate/chain extender or crosslinker segments are formed along the polymer chain. Although the amount of this reactant in the final formulation is usually the lowest, their nature, chemical structure and proportion have a noteworthy effect on the final properties of the polymer.[85,86]

The addition of chain extenders leads to isocyanate/chain extender segment segregation by means of hydrogen bond formation between segments resulting in an increase in the elastic modulus and the glass transition of the polyurethanes.[46,86–88] Whereas the addition of crosslinkers increases the level of covalent bonding and hence results in a decrease of hydrogen bond formation and segment ordering. Furthermore, the degree of mixing of the segments

formed by the polyol and isocyanate-crosslinker increases.[46,59,89] This behavior also takes place with chain extenders with high steric hindrance.[60,90]

The most common chain extenders are ethylene glycol, 1,3-propanediol, 1,4-butanediol, 1,6-hexanediol, 1,2-ethylene diamine and 1,6-hexamethylene diamine. Among crosslinkers, glycerol and trimethylol propane are the most employed.

The use of chain extenders and crosslinkers from renewable sources is also gaining attention. Biomass wastes are the main source for the obtaining of these reactants. In this way, the most employed biobased chain extenders are D-isosorbide (obtained from polysaccharides),[91] 1,3-propanediol which can be based on corn sugar[29,91] and also from succinic acid[92,93] and 1,4-butanediol which can be also obtained from succinic acid.[92,93] Among biobased crosslinkers glycerol is the most used which is derived from the saponification of fatty acids and from biodiesel production wastes.[94,95]

Regarding polyurethane foams, chain extenders and crosslinkers are used as reactive modifiers, i.e. as chain extending and crosslinking agents. In this way the density of the foam could be modified and hence flexibility or rigidity.

The most common chain extenders used in polyurethane foams are ethylene glycol, diethylene glycol, 1,3 -propylene glycol and 1,4-butanediol; while among crosslinkers glycerol and trimethylol propane are the most used.[46,47]

1.2.3.4 Main additives in polyurethane foams

- Catalysts

Catalysts are used to promote both isocyanate-polyol (gelling) and isocyanate-water (blowing) reactions. Especially tin compounds catalysts are used to promote mainly the isocyanate-hydroxyl reactions and they are considered "gelling catalysts", being the most common dibutiltyn dilaurate. In contrast, the

isocyanate-water reaction is principally accelerated by employing tertiary amine catalysts and they are known as "blowing catalysts." These catalysts are used in order to balance gelling and blowing reactions, since a greater amount of blowing results in collapsed foams, while a greater amount of gelling results in closed cell foams, resulting in shrinkage.[47]

- Blowing agents

The main function of blowing agents is to form gas bubbles during polymerization process. They can be either chemical or physical. The most common chemical blowing agent is water. Physical blowing agents are liquids that have low boiling points and nonreactivity to isocyanate groups; they vaporize by the exotherm of foaming reaction. Among this kind of blowing agents C5-hydrocarbons, azeotropes with or without halogen, and liquefied carbon dioxide are the most remarkable.[46,47]

- Surfactants

Surfactants help in mixing incompatible components of the reaction.[46] They also contribute to the nucleation of the blowing agent bubbles and stabilize the cell structure, obtaining a foam with high air permeability.[46,96] In this way, the choice of the surfactant depends on the desired final properties, in flexible foams they stabilize the open celled structure, whereas surfactants for rigid foams have a greater surface activity to avoid cell opening due to they increase the incompatibility between components. Moreover, in rigid foams the use of surfactants increases the insulation property of resultant foams.[47] The most used surfactants are based on organosiloxanes or silicon-based surfactants.

1.2.4 Applications of polyurethanes

As previously mentioned, polyurethanes with tailored properties can be obtained just by varying the choice of the reactants. Therefore, these materials

can find applications in different industries due to their versatility. They found applications such as insulating material,[4] aircraft structures, adhesives, coatings, sealants,[97] sports equipment, protective sportswear,[46] vascular grafts, heart valves and so on.[98,99]

Furthermore, polyurethanes can also behave as smart material, thus the development of shape-memory polyurethanes has drawn increasing attention in the last years. The interest that these smart polymers arouse is due to the wide range of applications they can found in different industries.[4,21–27,100]

1.3   Shape-memory polymers

Shape-memory polymers (SMPs) are a type of polymeric smart materials which are able to remember their original shape after being deformed, and recover it as a response to an external stimulus. Heat is one of the most common stimulus, although SMPs could be also triggered by applying an magnetic or electric field, light and moisture, among others.[22,28,101–103]

Shape-memory property is not an intrinsic property, meaning that polymers do not have this effect by themselves. Shape-memory results from a combination of polymer morphology and specific processing.[104] Generally, thermally-activated SMPs consist of two phases, the permanent phase and the thermally reversible phase. The permanent phase, obtained by physical or chemical crosslinks, is the responsible for memorizing the shape. The thermally reversible phase exhibits a phase transition temperature (T_{trans}), which can either be a glass transition or a melting temperature, acting as a molecular switch and also enabling the fixation of the temporary shape.[25,28,105] A scheme of the shape-memory process is shown in Figure 1.4.
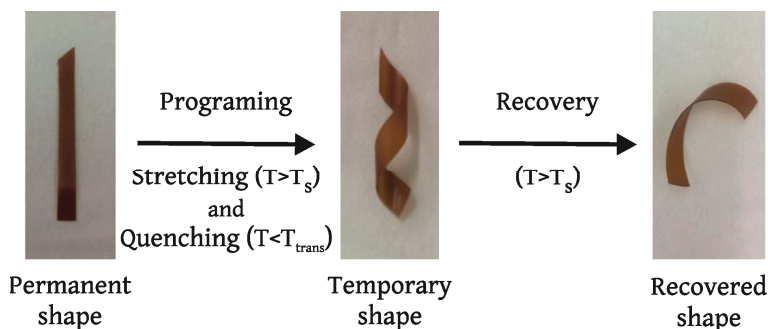
Figure 1.4. Scheme of the shape-memory process.

As can be observed, during the shape-memory process the material is heated and deformed at a temperature above the T_{trans}, named as switching temperature (T_s), and it is subsequently quenched at a temperature below T_{trans} in order to fix the shape. Once the sample is reheated above T_{trans} its original shape is restored.[106]

In fact shape-memory effect is an entropic phenomenon; at the permanent shape the molecular chains adopt conformations with the highest entropic state. During the stretching process, as the molecular chains are heated above their T_{trans}, which activates the mobility thereof, the chains conformation change to a lower entropy state adopting the temporary shape. When the sample is subsequently quenched at a temperature below T_{trans}, as molecular chain segments are frozen, this entropy state is kinetically trapped. Once the polymer is reheated above its T_{trans}, the molecular mobility is re-activated, which allows the chains to return to their highest entropic state, recovering the permanent shape.[102,107] Therefore, the increase of the crystallinity or the crosslink density of the polymer also increases the capability of the polymer to restore its original shape, since these linkages are the responsible for recovering the shape, as mentioned before.[104,106,108] In this way, shape-memory properties are strongly dependent on the nature of the segments, their composition and phase separation.[7,31,104,109]

In addition, the conditions at which the tests were carried out also have a key role on shape-memory properties. The increase of the maximum strain applied during stretching process decreases the capability of the material to recover its original shape.[107,110] A higher strain implies that a greater plastic deformation is taking place and hence greater amount of linkages are broken during the process, which are in fact the responsible to restore the shape. The chosen T_s also influence on shape-properties, if T_s in not high enough the motion of the chains cannot re-activate and hence the material is not able to restore its original shape.[28,107,108]

Moreover, in materials with a broad thermal transition the so-called temperature-memory effect (TME) takes place. This effect refers to the ability of the SMP to memorize the temperature at which the deformation is applied, which is within the range of the thermal transition.[111–117] This effect allows to program multiple temporary shapes at different temperatures.[116,118,119]

Among SMPs segmented polyurethanes, both crosslinked and thermoplastics, are one of the most noteworthy materials.[7,22,25,29,107,120,121] As previously mentioned, they are constituted by different segments. The segment with the lowest transition temperature acts as the switching segment and governs the shape fixity. Whereas the segment with the highest transition temperature, which has physical crosslinks in thermoplastics and also chemical crosslinks in crosslinked polymers, is the responsible for restoring the shape.

Although shape-memory polymers have found diverse applications as thermally responsive materials, they have not fully reached their technological potential, since they show lower stiffness than metals and ceramics materials with shape-memory properties and hence smaller recovery stresses/forces.[122–124] Therefore shape-memory properties of polymeric materials can be enhanced by loading different nanoentities.[30,31,35,102,121] Moreover, the addition of electroconductive or magnetic nanoparticles allows the possibility of activate shape recovery by

applying an electric (if electroconductive nanoentities are added)[125–127] or a magnetic field (in the case of magnetic nanoentities).[22,128,129]

1.4   Polyurethane nanocomposites

Nanocomposites are composed by a disperse phase (nanoentity) homogeneously distributed in a continuous phase (matrix). In the case of polyurethane nanocomposites, the polymer is the matrix. Regarding nanoentities, they have at least one dimension in the nanometric scale and they usually enhance the mechanical properties,[30,32,130,131] as well as thermal stability, and extends the rubbery plateau region.[132,133] Besides, due to the wide range of nanoentities available they can provide the matrix with different properties such as electric,[125,126] magnetic[22,128,129,134] or antimicrobial properties,[135–137] among others. The high interfacial area available between nanoentities and the matrix, promotes the creation of strong interactions between nanoentities and the matrix. In this way, the properties of the matrix are enhanced just by using a small quantity of nanoentities. This behavior is in opposite to conventional composites in which high amount of filler it is necessary to obtain the desired properties. The most important factor for the preparation of nanocomposites is the obtaining of a good dispersion of the nanoentities in the matrix. Polymer matrixes are in general hydrophobic, and if nanoentities have a hydrophilic nature, the incompatibility between them tend to create nanoentity aggregates.[133,138]

As far as the preparation of the nanocomposites is concerned, different preparation processes can be used such as solvent casting,[35,42,139–141] melt belding[142,143] and *in situ* polymerization.[30,32,126,144]

In this work different bionanocomposites based on a thermoplastic biobased polyurethane matrix and chitin nanocrystals, cellulose nanocrystals and magnetite nanoparticles were prepared by solvent casting procedure.

1.4.1 Chitin nanocrystals

Chitin is the second most abundant natural biopolymer derived from exoskeletons of crustaceans and also from cell walls of fungi and insects.[145–147] Chitin is extracted from living animals (especially shells) after demineralization and deproteinization processes.[145,148–150] These processes can be conducted by chemical (using acids and bases) or by biological (employing microorganism) methods.[145,146,148–151] After that chitin fibers are subjected to an acid hydrolysis process to isolate the chitin nanocrystals by removing the amorphous part. The chemical structure of chitin nanofibers and nanocrystals are shown in Figure 1.5.
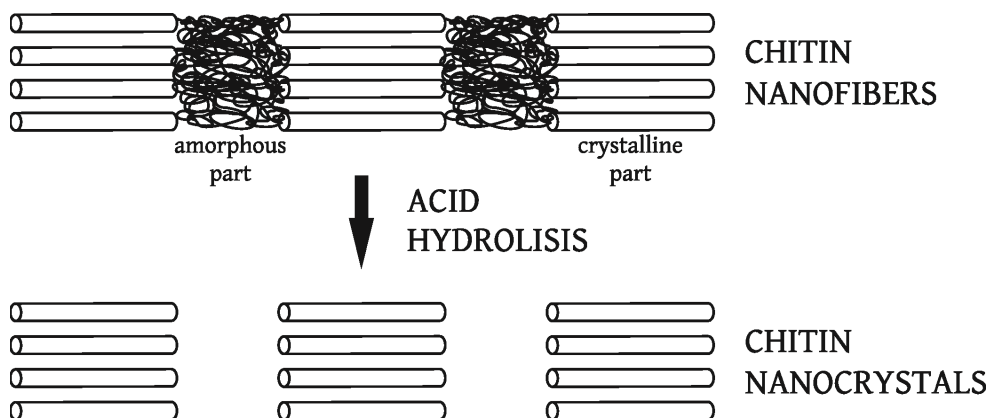
Figure 1.5. Chemical structure of chitin nanofibers (up) and nanocrystals (down).

The addition of chitin nanocrystals is gaining attention due to their light weight, inherent renewability and sustainability, high elastic modulus and tensile strength, non-toxic and antibacterial properties and biocompatibility.[130,131,148,152,153]

1.4.2 Cellulose nanocrystals

Cellulose is the most abundant biopolymer which is derived from plants, animals, bacteria and some amoebas.[154,155] Different isolation methods can be used, such as mechanical, chemical or enzymatic. However, one the most

common method is the isolation by acid hydrolysis using sulfuric or hydrochloric acids. As previously mentioned, the amorphous part is removed and cellulose nanocrystals are obtained, whose crystallinity and aspect ratio are strongly dependent to hydrolysis conditions.[156,157]

The use of cellulose nanocrystals in nanocomposites is increasing due to their light weight, inherent renewability, cheapness, low density, high elastic modulus and tensile strength, biocompatibility, biodegradability and availability.[158,159]

1.4.3 Magnetite nanoparticles

The interest of the preparation of nanocomposites based on magnetite (Fe_3O_4) is increasing due to the simplicity of preparing the nanoparticles and their stable storage in the colloidal form. Colloidal suspensions of stabilized magnetic nanoparticles are called ferrofluids and they can interact with a magnetic field.[160,161] However, magnetite nanoparticles tend to agglomerate because of magnetic and van der Waals forces.[162] Therefore, they can be coated with surfactants such as oleic acid to prevent aggregation.[163–165] Furthermore, magnetite nanoparticles have a great chemical stability, biocompatibility and the heating ability in presence of a magnetic field.[166–168]

Different methods have been developed to synthesize magnetite nanoparticles such as co-precipitation, microemulsion, sputtering and thermal decomposition.[166,169,170] Co-precipitation method is a widely used technique for the synthesis of magnetite nanoparticles which are obtained by precipitating an aqueous solution mixture containing ferric and ferrous salts in the presence of a base.[165,169] In this work magnetite nanoparticles were obtained following this method.

1.5   Biocompatibility

The use of polyurethanes for the design of biomedical devices is gaining attention, due to their excellent mechanical properties, good bio- and blood-compatibility.[5,24,171–173] Therefore, polyurethanes can be used in vascular grafts, heart valves, catheters, as bone regenerating substrate, and so on.[5,98,173,174]

As mentioned before, polyurethanes have extensive structure/property diversity, since their properties can be easily tailored by varying the nature of the reactants and molar composition. Thus, the use of reactants or additive from renewable sources, such as diisocyanates derived from aminoacids or fatty acids, due to its nature could promote the biocompatibility of the polyurethanes.[17,36,40]

1.6   General objectives

The main objective of this work is the increase of the biobased carbon content of porous and different solid (thermoplastic and crosslinked) polyurethanes and bionanocomposites by the incorporation of reactants and nanoentities from renewable sources. To that end different strategies have been followed.

- Incorporate a hydroxylated biobased polyol to the formulation of polyurethane rigid foams and analyzed the effect of the nature of different reactive modifiers and their content on the final properties.

- Synthesize crosslinked biobased polyurethanes with different properties by varying the diisocyanate/crosslinker content, study the influence of the nature of two different biobased diisocyanate and analyze the biocompatibility.

- Synthesize thermoplastic biobased polyurethanes by varying the diisocyanate/chain extender content, analyze the effect of the nature of

biobased diisocyanates and chain extenders on the final properties and study the biocompatibility.

- Study the influence of the shape-memory testing conditions on shape recovery and shape fixity of thermoplastic and crosslinked polyurethanes.

- Prepare polyurethane bionanocomposites to enhance the final properties and shape-memory properties of the matrix, by incorporating chitin and cellulose nanocrystals, as well as magnetite nanoparticles.

1.7   References

1.   U.S. Energy Information Administration (EIA). "International energy outlook 2016". www.eia.gov.

2.   X.S. Sun. "Chapter 1. Overview of plant polymers: resources demands, and sustainability". In: Bio-based polymers and composites. Ed. R.P. Wool, X.S. Sun. Elsevier Academic Press, 2005.

3.   A. Shirke, B. Dholakiya, K. Kuperkar. "Novel applications of castor oil based polyurethanes: a short review". Polym. Sci. Ser. B. 2015. 57: 292–297.

4.   X.Y. Zhang, G.H. Wang, D. Liu, Y. Wang. "Applications of rigid polyurethane foam insulation materials in architectural energy conservation". Adv. Mater. Res. 2013. 608–609: 1783–1785.

5.   A. Burke, N. Hasirci. "Polyurethanes in biomedical applications". In: Biomaterials: from molecules to engineered tissues. Eds. N. Hasirci, V. Hasirci. Kluwer Academic/Plenum Publishers, 2004.

6.   C. Zhang, S.A. Madbouly, M.R. Kessler. "Biobased polyurethanes prepared

from different vegetable oils". ACS Appl. Mater. Interfaces 2015. 7: 1226–1233.

7. M.A. Corcuera, A. Saralegi, B. Fernandez-d'Arlas, I. Mondragon, A. Eceiza. "Shape memory polyurethanes based on polyols derived from renewable resources". Macromol. Symp. 2012. 321–322: 197–201.

8. S. Dworakowska, D. Bogdal, A. Prociak. "Microwave-assisted synthesis of polyols from rapeseed oil and properties of flexible polyurethane foams". Polymers 2012. 4: 1462–1477.

9. S. Dworakowska, D. Bogdał, F. Zaccheria, N. Ravasio. "The role of catalysis in the synthesis of polyurethane foams based on renewable raw materials". Catal. Today 2014. 223: 148–156.

10. L. Ugarte, B. Fernández-d'Arlas, A. Valea, M.L. González, M.A. Corcuera, A. Eceiza. "Morphology-properties relationship in high-renewable content polyurethanes". Polym. Eng. Sci. 2014. 54: 2282–2291.

11. L. Ugarte, A. Saralegi, R. Fernández, L. Martín, M.A. Corcuera, A. Eceiza. "Flexible polyurethane foams based on 100% renewably sourced polyols". Ind. Crops Prod. 2014. 62: 545–551.

12. M.A. Corcuera, L. Rueda, B. Fernandez-d'Arlas, A. Arbelaiz, C. Marieta, I. Mondragon, A. Eceiza. "Microstructure and properties of polyurethanes derived from castor oil". Polym. Degrad. Stab. 2010. 95: 2175–2184.

13. A. Saralegi, L. Rueda, B. Fernández-d'Arlas, I. Mondragon, A. Eceiza, M.A. Corcuera. "Thermoplastic polyurethanes from renewable resources: effect of soft segment chemical structure and molecular weight on morphology and final properties". Polym. Int. 2013. 62: 106–115.

14. Z. Wang, L. Yu, M. Ding, H. Tan, J. Li, Q. Fu. "Preparation and rapid

degradation of nontoxic biodegradable polyurethanes based on poly(lactic acid)-poly(ethylene glycol)-poly(lactic acid) and L-lysine diisocyanate". Polym. Chem. 2011. 2: 601–607.

15.   N. Yamamoto, A. Nakayama, M. Oshima, N. Kawasaki, S. Aiba. "Enzymatic hydrolysis of lysine diisocyanate based polyurethanes and segmented polyurethane ureas by various proteases". React. Funct. Polym. 2007. 67: 1338–1345.

16.   G.A. Skarja, K.A. Woodhouse. "Structure-property relationships of degradable polyurethane elastomers containing an amino acid-based chain extender". J. Appl. Polym. Sci. 2000. 75: 1522–1534.

17.   S.A. Guelcher, K.M. Gallagher, J.E. Didier, D.B. Klinedinst, J.S. Doctor, A.S. Goldstein, G.L. Wilkes, E.J. Beckman, J.O. Hollinger. "Synthesis of biocompatible segmented polyurethanes from aliphatic diisocyanates and diurea diol chain extenders". Acta Biomater. 2005. 1: 471–484.

18.   M. Charlon, B. Heinrich, Y. Matter, E. Couzigné, B. Donnio, L. Avérous. "Synthesis, structure and properties of fully biobased thermoplastic polyurethanes, obtained from a diisocyanate based on modified dimer fatty acids, and different renewable diols". Eur. Polym. J. 2014. 61: 197–205.

19.   Y. Li, B.A.J. Noordover, R.A.T.M. van Benthem, C.E. Koning. "Property profile of poly(urethane urea) dispersions containing dimer fatty acid-, sugar- and amino acid-based building blocks". Eur. Polym. J. 2014. 59: 8–18.

20.   Y. Li, B.A.J. Noordover, R.A.T.M. van Benthem, C.E. Koning. "Chain extension of dimer fatty acid- and sugar-based polyurethanes in aqueous dispersions". Eur. Polym. J. 2014. 52: 12–22.

21. T. Pretsch, M. Ecker, M. Schildhauer, M. Maskos. "Switchable information carriers based on shape memory polymer". J. Mater. Chem. 2012. 22: 7757.

22. J. Leng, X. Lan, Y. Liu, S. Du. "Shape-memory polymers and their composites: stimulus methods and applications". Prog. Mater. Sci. 2011. 56: 1077–1135.

23. D. Ratna, J. Karger-Kocsis. "Recent advances in shape memory polymers and composites: a review". J. Mater. Sci. 2008. 43: 254–269.

24. P. Singhal, W. Small, E. Cosgriff-Hernandez, D.J. Maitland, T.S. Wilson. "Low density biodegradable shape memory polyurethane foams for embolic biomedical applications". Acta Biomater. 2014. 10: 67–76.

25. P.T. Mather, X. Luo, I.A. Rousseau. "Shape memory polymer research". Annu. Rev. Mater. Res. 2009. 39: 445–471.

26. S. Imai, K. Sakurai. "An actuator of two-way behavior by using two kinds of shape memory polymers with different Tgs". Precis. Eng. 2013. 37: 572–579.

27. N. Fritzsche, T. Pretsch. "Programming of temperature-memory onsets in a semicrystalline polyurethane elastomer". Macromolecules 2014. 47: 5952–5959.

28. A. Lendlein, S. Kelch. "Shape-memory polymers". Angew. Chem. Int. Ed. 2002. 41: 2034–2057.

29. A. Saralegi, E.J. Foster, C. Weder, A. Eceiza, M.A. Corcuera. "Thermoplastic shape-memory polyurethanes based on natural oils". Smart Mater. Struct. 2014. 23: 025033 (9pp).

30. A. Saralegi, S.C.M. Fernandes, A. Alonso-Varona, T. Palomares, E.J. Foster,

C. Weder, A. Eceiza, M.A. Corcuera. "Shape-memory bionanocomposites based on chitin nanocrystals and thermoplastic polyurethane with a highly crystalline soft segment". Biomacromolecules 2013. 14: 4475–4482.

31.   A. Saralegi, M.L. Gonzalez, A. Valea, A. Eceiza, M.A. Corcuera. "The role of cellulose nanocrystals in the improvement of the shape-memory properties of castor oil-based segmented thermoplastic poyurethanes". Compos. Sci. Technol. 2014. 92: 27–33.

32.   L. Rueda, A. Saralegi, B. Fernández-d'Arlas, Q. Zhou, A. Alonso-Varona, L.A. Berglund, I. Mondragon, M.A. Corcuera, A. Eceiza. "In situ polymerization and characterization of elastomeric polyurethane-cellulose nanocrystal nanocomposites. Cell response evaluation". Cellulose 2013. 20: 1819–1828.

33.   K.M. Zia, M. Zuber, M. Barikani, A. Jabbar, M.K. Khosa. "XRD pattern of chitin based polyurethane bio-nanocomposites". Carbohydr. Polym. 2010. 80: 539–543.

34.   Y.C. Chung, J.W. Choi, M.W. Choi, B.C. Chun. "Characterization of flexibly linked shape memory polyurethane composite with magnetic property". J. Thermoplast. Compos. Mater. 2011. 25: 283–303.

35.   H. Zou, C. Weder, Y.C. Simon. "Shape-memory polyurethane nanocomposites with single layer or bilayer oleic acid-coated Fe_3O_4 nanoparticles". Macromol. Mater. Eng. 2015. 300: 885–892.

36.   A. Basterretxea, Y. Haga, A. Sanchez-Sanchez, M. Isik, L. Irusta, M. Tanaka, K. Fukushima, H. Sardon. "Biocompatibility and hemocompatibility evaluation of polyether urethanes synthesized using DBU organocatalyst". Eur. Polym. J. 2016. 84: 750–758.

37.   P. Bruin, J. Smedinga, A.J. Pennings, M.F. Jonkman. "Biodegradable lysine

diisocyanate-based poly(glycolide-co-ε-caprolactone)-urethane network in artificial skin". Biomaterials 1990. 11: 291–295.

38.   P. Bruin, G.J. Veenstra, A.J. Nijenhuis, A.J. Pennings. "Design and synthesis of biodegradable poly(ester-urethane) elastomer networks composed of non-toxic building blocks". Makromoleculare Chemie, Rapid Commun. 1988. 9: 589–594.

39.   S.A. Guelcher, V. Patel, K.M. Gallagher, S. Connolly, J.E. Didier, J.S. Doctor, J.O. Hollinger. "Synthesis and in vitro biocompatibility of injectable polyurethane foam scaffolds". Tissue Eng. 2006. 12: 1247–1259.

40.   K.M. Zia, M. Zuber, I.A. Bhatti, M. Barikani, M.A. Sheikh. "Evaluation of biocompatibility and mechanical behavior of chitin-based polyurethane elastomers. Part-II: effect of diisocyanate structure". Int. J. Biol. Macromol. 2009. 44: 23–28.

41.   K. Gorna, S. Gogolewski. "Biodegradable porous polyurethane scaffolds for tissue repair and regeneration". J. Biomed. Mater. Res. - Part A. 2006. 79: 128–138.

42.   D.K. Chattopadhyay, K.V.S.N. Raju. "Structural engineering of polyurethane coatings for high performance applications". Prog. Polym. Sci. 2007. 32: 352–418.

43.   B. Dahlke, H. Larbig, H.D. Scherzer, R. Poltrock. "Natural fiber reinforced foams based on renewable resources for automotive interior applications". J. Cell. Plast. 1998. 34: 361–379.

44.   X. He, Z. Zhai, Y. Wang, G. Wu, Z. Zheng, Q. Wang, G. Wu, Z. Zheng, Q. Wang, Y. Liu. "New method for coupling collagen on biodegradable polyurethane for biomedical applications". J. Appl. Polym. Sci. 2012. 126: E353–E360.

45.   L. Zhou, D. Liang, X. He, J. Li, H. Tan, J. Li, Q. Fu, Q. Gu. "The degradation and biocompatibility of pH-sensitive biodegradable polyurethanes for intracellular multifunctional antitumor drug delivery". Biomaterials 2012. 33: 2734–2745.

46.   G. Woods. "The ICI polyrethanes book". 2nd ed. ICI Polyurethanes and John Wiley & Sons, 1990.

47.   K. Ashida. "Thermosetting foams". In: Handbook of plastic foams. Ed. A. H. Landrock. Noyes, 1994.

48.   G. Oertel. Polyurethane handbook. Hanser Publications, Munich, Germany, 1994.

49.   M.S. Sánchez-Adsuar, E. Papon, J.J. Villenave. "Influence of the synthesis conditions on the properties of thermoplastic polyurethane elastomers". J. Appl. Polym. Sci. 2000. 76: 1590–1595.

50.   M.S. Sánchez-Adsuar, E. Papon, J.J. Villenave. "Influence of the composition on the crystallinity and adhesion properties of thermoplastic polyurethane elastomers. Part II. Relationship between the prepolymer and polyurethane properties". J. Appl. Polym. Sci. 2000. 76: 1602–1607.

51.   M.S. Sánchez-Adsuar, E. Papon, J.J. Villenave. "Influence of the prepolymerization on the properties of thermoplastic polyurethane elastomers. Part I. Prepolymer characterization". J. Appl. Polym. Sci. 2000. 76: 1596–1601.

52.   J.M. Castro, F. Lopez-Serrano, R.E. Camargo, C.W. Macosko, M. Tirrell. "Onset of phase separation in segmented urethane polymerization". J. Appl. Polym. Sci. 1981. 26: 2067–2076.

53. L.M. Leung, J.T. Koberstein. "DSC annealing study of microphase separation and multiple endothermic behavior in polyether-based polyurethane block copolymers". Macromolecules 1986. 19: 706–713.

54. Z.S. Petrovic, I. Javni. "Effect of soft-segment length and concentration on phase separation in segmented polyurethanes". J. Polym. Sci. Part B Polym. Phys. 1989. 27: 545–560.

55. L. Rueda-Larraz, B. Fernández-d'Arlas, A. Tercjak, A. Ribes, I. Mondragon, A. Eceiza. "Synthesis and microstructure-mechanical property relationships of segmented polyurethanes based on a PCL-PTHF-PCL block copolymer as soft segment". Eur. Polym. J. 2009. 45: 2096–2109.

56. C.S. Wang, D.J. Kenney. "Effect of hard segments on morphology and properties of thermoplastic polyurethanes". J. Elastomers Plast. 1995. 27: 182–199.

57. H. Do Kim, T.J. Lee, J.H. Huh, D.J. Lee. "Preparation and properties of segmented thermoplastic polyurethane elastomers with two different soft segments". J. Appl. Polym. Sci. 1999. 73: 345–352.

58. R.W. Seymour, G.M. Estes, S.L. Cooper. "Hydrogen bonding in segmented polyurethane elastomers". Polym. Prepr. 1970. 11: 867–874.

59. Y.M. Tsai, T.L. Yu, Y.H. Tseng. "Physical properties of crosslinked polyurethane". Polym. Int. 1998. 47: 445–450.

60. E. Cognet-Georjon, F. Mechin, J.P. Pascault. "New polyurethanes based on 4,4'-diphenylmethane diisocyanate and 1,4:3,6 dianhydrosorbitol. 2. Synthesis and properties of segmented polyurethane elastomers". Macromol. Chem. Phys. 1996. 197: 3593–3612.

61. M. Hassan, K.A. Mauritz, R.F. Storey, J.S. Wiggins. "Biodegradable

aliphatic thermoplastic polyurethane based on poly(ε-caprolactone) and L-lysine diisocyanate". J. Polym. Sci. Part A Polym. Chem. 2006. 44: 2990–3000.

62. G. Lligadas, J.C. Ronda, M. Galià, V. Cádiz. "Poly(ether urethane) networks from renewable resources as candidate biomaterials: synthesis and characterization". Biomacromolecules 2007. 8: 686–692.

63. U. Biermann, W. Friedt, S. Lang, W. Lühs, G. Machmüller, J.O. Metzger, M. Rüsch, H.J. Schäfer, M.P. Schneider. "New syntheses with oils and fats as renewable raw materials for the chemical industry". Angew. Chem. Int. Ed. 2000. 39: 2206–2224.

64. M. Galià, L.M. de Espinosa, J.C. Ronda, G. Lligadas, V. Cádiz. "Vegetable oil-based thermosetting polymers". Eur. J. Lipid Sci. Technol. 2010. 112: 87–96.

65. L. Hojabri, X. Kong, S.S. Narine. "Fatty acid-derived diisocyanate and biobased polyurethane produced from vegetable oil: synthesis, polymerization, and characterization". Biomacromolecules 2009. 10: 884–891.

66. G. Lligadas, J.C. Ronda, M. Galià, V. Cádiz. "Plant oils as platform chemicals for polyurethane synthesis: current state-of-the-art". Biomacromolecules 2010. 11: 2825–2835.

67. I.A. Mohammed, E.A.J. Al-Mulla, N.K.A. Kadar, M. Ibrahim. "Structure-property studies of thermoplastic and thermosetting polyurethanes using palm and soya oils-based polyols". J. Oleo Sci. 2013. 62: 1059–72.

68. V. Sharma, P.P. Kundu. "Condensation polymers from natural oils". Prog. Polym. Sci. 2008. 33: 1199–1215.

69.   V. Ribeiro Da Silva, M.A. Mosiewicki, M.I. Yoshida, M. Coelho Da Silva, P.M. Stefani, N.E. Marcovich. "Polyurethane foams based on modified tung oil and reinforced with rice husk ash II: mechanical characterization". Polym. Test. 2013. 32: 665–672.

70.   Y.H. Hu, Y. Gao, N. De Wang, C.P. Hu, S. Zu, L. Vanoverloop, D. Randall. "Rigid polyurethane foam prepared from a rape seed oil based polyol". J. Appl. Polym. Sci. 2002. 84: 591–597.

71.   F.S. Güner, Y. Yagci, A.T. Erciyes. "Polymers from triglyceride oils". Prog. Polym. Sci. 2006. 31: 633–670.

72.   R. de Vasconcelos Vieira Lopes, N.P.D. Loureiro, A.P.T. Pezzin, A.C.M. Gomes, I.S. Resck, M.J.A. Sales. "Synthesis of polyols and polyurethanes from vegetable oils-kinetic and characterization". J. Polym. Res. 2013. 20: 238.

73.   T.H. Khoe, F.H. Otey, E.N. Frankel. "Rigid urethane foams from hydroxymethylated linseed oil and polyol esters". J. Am. Oil Chem. Soc. 1972. 49: 615–618.

74.   M.A. Corcuera, L. Rueda, A. Saralegi, M.D. Martín, B. Fernández-d'Arlas, I. Mondragon, A. Eceiza. "Effect of diisocyanate structure on the properties and microstructure of polyurethanes based on polyols derived from renewable resources". J. Appl. Polym. Sci. 2011. 122: 3677–3685.

75.   M. Barikani, M.V. Ebrahimi, S.M.S. Mohaghegh. "Influence of diisocyanate structure on the synthesis and properties of ionic polyurethane dispersions". Polym. Plast. Technol. Eng. 2007. 46: 1087–1092.

76.   P.H. Barbeau, J.F. Gerard, B. Magny, J.P. Pascault. "Effect of the diisocyanate on the structure and properties of polyurethane acrylate

prepolymers". J. Polym. Sci. Part B Polym. Phys. 2000. 38: 2750–2768.

77.   B. Fernández-d'Arlas, A. Alonso-Varona, T. Palomares, M.A. Corcuera, A. Eceiza. "Studies on the morphology, properties and biocompatibility of aliphatic diisocyanate-polycarbonate polyurethanes". Polym. Degrad. Stab. 2015. 122: 153–160.

78.   D.K. Lee, H.B. Tsai. "Properties of segmented polyurethanes derived from different diisocyanates". J. Appl. Polym. Sci. 2000. 75: 167–174.

79.   Y. Li, B.A.J. Noordover, R.A.T.M. van Benthem, C.E. Koning. "Reactivity and regio-selectivity of renewable building blocks for the synthesis of water-dispersible polyurethane prepolymers". ACS Sustain. Chem. Eng. 2014. 2: 788–797.

80.   M.S. Holfincer, A.H. Conner, L.F. Lorenz, C.G. Hill. "Difurfuryl diisocyanates: new adhesives derived from renewable resources". J. Appl. Polym. Sci. 1993. 49: 337–344.

81.   S. Boufi, M.N. Belgacem, J. Quillerou, A. Gandini. "Urethanes and polyurethanes bearing furan moieties. 4. Synthesis, kinetics, and characterization of linear polymers". Macromolecules 1993. 26: 6706–6717.

82.   S. Boufi, A. Gandini, M.N. Belgacem. "Urethanes and polyurethanes bearing furan moieties. 5. Thermoplastic elastomers based on sequenced structures". Polymer 1995. 36: 1689–1696.

83.   J.L. Cawse, J.L. Stanford, R.H. Still. "Polymers from renewable sources. Kinetics and polyurethane formation from furan-based diisocyanates". Makromoleculare Chemie, Rapid Commun. 1984. 185: 709–723.

84.   M.D. Zenner, Y. Xia, J.S. Chen, M.R. Kessler. "Polyurethanes from

isosorbide-based diisocyanates". Chem. Sus. Chem. 2013. 6: 1182–1185.

85. Z. Wirpsza. "Polyurethanes. Chemistry, technology and applications". Ellis Horwood PTR Prentice Hall, 1993.

86. K. Gisselfält, B. Helgee. "Effect of soft segment length and chain extender structure on phase separation and morphology in poly(urethane urea)s". Macromol. Mater. Eng. 2003. 288: 265–271.

87. Y. V Savelyev, E.R. Akhranovich, A.P. Grekov, E.G. Privalko. "Influence of chain extenders and chain end groups on properties of segmented polyurethanes. I. Phase morphology". Polymer 1998. 39: 3425–3429.

88. J. Blackwell, M.R. Nagarajan, T.B. Hoitink. "Structure of polyurethane elastomers: effect of chain extender length on the structure of MDI/diol hard segments". Polymer 1982. 23: 950–956.

89. Z.S. Petrović, I. Javni, V. Divjakovi. "Structure and physical properties of segmented polyurethane elastomers containing chemical crosslinks in the hard segment". J Polym. Sci. B Polym. Phys. 1998. 36: 221–235.

90. E.C. Varkey, K. Sreekumar. "Isosorbide based chiral polyurethanes: optical and thermal studies". J. Mater. Sci. 2010. 45: 1912–1920.

91. K. González, L. Martin, A. González, A. Retegi, A. Eceiza, N. Gabilondo. "D-isosorbide and 1,3-propanediol as plasticizers for starch-based films: characterization and aging study". J. Appl. Polym. Sci. 2017. 134: 1–10.

92. I. Bechthold, K. Bretz, S. Kabasci, R. Kopitzky, A. Springer. "Succinic acid: a new platform chemical for biobased polymers from renewable resources". Chem. Eng. Technol. 2008. 31: 647–654.

93. D. Cimini, O. Argenzio, S. D'Ambrosio, L. Lama, I. Finore, R. Finamore, O. Pepe, C. Faraco, C. Schiraldi. "Production of succinic acid from Basfia

succiniciproducens up to the pilot scale from Arundo donax hydrolysate". Bioresour. Technol. 2016. 222: 355–360.

94. Y. Zhang, M.A. Dubé, D.D. McLean, M. Kates. "Biodiesel production from waste cooking oil. 1. Process design and technological assessment". Bioresour. Technol. 2003. 89: 1–16.

95. A.B. Leoneti, V. Aragão-Leoneti, S.V.W.B. de Oliveira. "Glycerol as a by-product of biodiesel production in Brazil: alternatives for the use of unrefined glycerol". Renew. Energy. 2012. 45: 138–145.

96. S. Gómez-Fernández, L. Ugarte, C. Peña-Rodriguez, M.A. Corcuera, A. Eceiza. "The effect of phosphorus containing polyol and layered double hydroxides on the properties of a castor oil based flexible polyurethane foam". Polym. Degrad. Stab. 2016. 132: 41–51.

97. Meier-Westhues. "Polyurethanes - coatings, adhesives and sealants". Vincentz Network GmbH & Co., Hanover, Germany, 2007.

98. A. Subramaniam, S. Sethuraman. "Biomedical applications of nondegradable polymers". In: Natural and synthetic biomedical polymers. 2014. Pp. 301–308.

99. J.V. Cauich-Rodríguez, L.H. Chan-Chan, F. Hernandez-Sánchez, J.M. Cervantes-Uc. "Degradation of polyurethanes for cardiovascular applications". In: Advances in biomaterials science and biomedical applications. Ed. R. Pignatello. In Tech, 2013. Pp. 51–82.

100. H. Meng, G. Li. "A review of stimuli-responsive shape memory polymer composites". Polymer 2013. 54: 2199–2221.

101. W.M. Huang, B. Yang, Y. Zhao, Z. Ding. "Thermo-moisture responsive polyurethane shape-memory polymer and composites: a review". J.

Mater. Chem. 2010. 20: 3367.

102. T. Xie. "Recent advances in polymer shape memory". Polymer 2011. 52: 4985–5000.

103. D. Habault, H. Zhang, Y. Zhao. "Light-triggered self-healing and shape-memory polymers". Chem. Soc. Rev. 2013. 42: 7244.

104. M. Behl, A. Lendlein. "Shape-memory polymers". Mater. Today 2007. 10: 20–28.

105. G.J. Berg, M.K. McBride, C. Wang, C.N. Bowman. "New directions in the chemistry of shape memory polymers". Polymer 2014. 55: 5849–5872.

106. H.M. Jeong, J.H. Song, K.W. Chi, I. Kim, K.T. Kim. "Shape memory effect of poly(methylene-1,3-cyclopentane) and its copolymer with polyethylene". Polym. Int. 2002. 51: 275–280.

107. J.L. Hu, F.L. Ji, Y.W. Wong. "Dependency of the shape memory properties of a polyurethane upon thermomechanical cyclic conditions". Polym. Int. 2005. 54: 600–605.

108. X.L. Wu, S.F. Kang, X.J. Xu, F. Xiao, X.L. Ge. "Effect of the crosslinking density and programming temperature on the shape fixity and shape recovery in epoxy-anhydride shape-memory polymers". J. Appl. Polym. Sci. 2014. 131: 40559.

109. F.L. Ji, J.L. Hu, S.S.-Y. Chui. "Influences of phase composition and thermomechanical conditions on shape memory properties of segmented polyurethanes with amorphous reversible phase". Polym. Eng. Sci. 2012. 52: 1015–1026.

110. L. Peponi, I. Navarro-Baena, A. Sonseca, E. Gimenez, A. Marcos-Fernandez, J.M. Kenny. "Synthesis and characterization of PCL-PLLA

polyurethane with shape memory behavior". Eur. Polym. J. 2013. 49: 893–903.

111. K. Yu, H.J. Qi. "Temperature memory effect in amorphous shape memory polymers". Soft Matter 2014. 10: 9423–9432.

112. U. Nöchel, C.S. Reddy, K. Wang, J. Cui, I. Zizak, M. Behl, K. Kratz, A. Lendlein. "Nanostructural changes in crystallizable controlling units determine the temperature-memory of polymers". J. Mater. Chem. A. 2015. 3: 8284–8293.

113. P. Miaudet, A. Derré, M. Maugey, C. Zakri, P.M. Piccione, R. Inoubli, P. Poulin. "Shape and temperature memory of nanocomposites with broadened glass transition". Science 2007. 318: 1294–1296.

114. N. Mirtschin, T. Pretsch. "Designing temperature-memory effects in semicrystalline polyurethane". RSC Adv. 2015. 5: 46307–46315.

115. L. Sun, W.M. Huang. "Mechanisms of the multi-shape memory effect and temperature memory effect in shape memory polymers". Soft Matter 2010. 6: 4403.

116. Y. Wang, J. Li, X. Li, Y. Pan, Z. Zheng, X. Ding, Y. Peng. "Relation between temperature memory effect and multiple-shape memory behaviors based on polymer networks". RSC Adv. 2014. 4: 20364–20370.

117. K. Kratz, S.A. Madbouly, W. Wagermaier, A. Lendlein. "Temperature-memory polymer networks with crystallizable controlling units". Adv. Mater. 2011. 23: 4058–4062.

118. C. Samuel, S. Barrau, J. Lefebvre, J. Raquez, P. Dubois. "Designing multiple-shape memory polymers with miscible polymer blends: evidence and origins of a triple-shape memory effect for miscible

PLLA/PMMA blends". Macromolecules 2014. 47: 6791–6803.

119.   R. Xiao, J. Guo, D.L. Safranski, T.D. Nguyen. "Solvent-driven temperature memory and multiple shape memory effects". Soft Matter 2015. 11: 3977–85.

120.   J. Hu, Z. Yang, L. Yeung, F. Ji, Y. Liu. "Crosslinked polyurethanes with shape memory properties". Polym. Int. 2005. 54: 854–859.

121.   M.L. Auad, T. Richardson, M. Hicks, M.A. Mosiewicki, M.I. Aranguren, N.E. Marcovich. "Shape memory segmented polyurethanes: dependence of behavior on nanocellulose addition and testing conditions". Polym. Int. 2012. 61: 321–327.

122.   H. Koerner, G. Price, N.A. Pearce, M. Alexander, R.A. Vaia. "Remotely actuated polymer nanocomposites - stress-recovery of carbon-nanotube-filled thermoplastic elastomers". Nat. Mater. 2004. 3: 115–20.

123.   X. Cao, H. Dong, C.M. Li. "New nanocomposite materials reinforced with cellulose nanocrystals in waterborne polyurethane". Biomacromolecules 2007. 8: 899–904.

124.   J. Xu, W. Shi, W. Pang. "Synthesis and shape memory effects of Si-O-Si cross-linked hybrid polyurethanes". Polymer 2006. 47: 457–465.

125.   J.W. Cho, J.W. Kim, Y.C. Jung, N.S. Goo. "Electroactive shape-memory polyurethane composites incorporating carbon nanotubes". Macromol. Rapid Commun. 2005. 26: 412–416.

126.   N.S. Goo, I.H. Paik, Y.C. Jung, J.W. Cho. "Development and application of conducting shape memory polyurethane actuators". Smart Mater. Struct. 2006. 15: 1476–1482.

127.   Y. Liu, H. Lv, X. Lan, J. Leng, S. Du. "Review of electro-active shape-

memory polymer composite". Compos. Sci. Technol. 2009. 69: 2064–2068.

128. R. Mohr, K. Kratz, T. Weigel, M. Lucka-Gabor, M. Moneke, A. Lendlein. "Initiation of shape-memory effect by inductive heating of magnetic nanoparticles in thermoplastic polymers." Proc. Natl. Acad. Sci. U. S. A. 2006. 103: 3540–3545.

129. U.N. Kumar, K. Kratz, M. Heuchel, M. Behl, A. Lendlein. "Shape-memory nanocomposites with magnetically adjustable apparent switching temperatures". Adv. Mater. 2011. 23: 4157–4162.

130. S. Ifuku, A. Ikuta, T. Hosomi, S. Kanaya, Z. Shervani, M. Morimoto, H. Saimoto. "Preparation of polysilsesquioxane-urethaneacrylate copolymer film reinforced with chitin nanofibers". Carbohydr. Polym. 2012. 89: 865–869.

131. M. Paillet, A. Dufresne. "Chitin whisker reinforced thermoplastic nanocomposites". Macromolecules. 2001. 34: 6527–6530.

132. C.P. Poole, F.J. Owens. Introduction to nanotechnology. Wiley-VCH, London, UK, 2003.

133. J.H. Koo. Polymer nanocomposties. The McGraw-Hill Companies, New York, USA, 2006.

134. C. Meiorin, O.M. Londoño, D. Muraca, L.M. Socolovsky, K.R. Pirota, M.I. Aranguren, M. Knobel, M.A. Mosiewicki. "Magnetism and structure of nanocomposites made from magnetite and vegetable oil based polymeric matrices". Mater. Chem. Phys. 2015. 175: 81–91.

135. P. Sanpui, A. Murugadoss, P.V.D. Prasad, S.S. Ghosh, A. Chattopadhyay. "The antibacterial properties of a novel chitosan-Ag-nanoparticle composite". Int. J. Food Microbiol. 2008. 124: 142–146.

136. S. Imazato. "Antibacterial properties of resin composites and dentin bonding systems". Dent. Mater. 2003. 19: 449–457.

137. Y. Liu, X. Wang, F. Yang, X. Yang. "Excellent antimicrobial properties of mesoporous anatase TiO_2 and Ag/TiO_2 composite films". Microporous Mesoporous Mater. 2008. 114: 431–439.

138. J.N. Coleman, U. Khan, Y.K. Gun'ko. "Mechanical reinforcement of polymers using carbon nanotubes". Adv. Mater. 2006. 18: 689–706.

139. K.G. Nair, A. Dufresne. "Crab shell chitin whisker reinforced natural rubber nanocomposites. 1. Processing and swelling behavior". Biomacromolecules 2003. 4: 657–665.

140. A. Saralegi, L. Rueda, L. Martin, A. Arbelaiz, A. Eceiza, M.A. Corcuera. "From elastomeric to rigid polyurethane/cellulose nanocrystal bionanocomposites". Compos. Sci. Technol. 2013. 88: 39–47.

141. B. Fernández-d'Arlas, U. Khan, L. Rueda, L. Martin, J.A. Ramos, J.N. Coleman, M.L. Gonzalez, A. Valea, I. Mondragon, M.A. Corcuera, A. Eceiza. "Study of the mechanical, electrical and morphological properties of PU/MWCNT composites obtained by two different processing routes". Compos. Sci. Technol. 2012. 72: 235–242.

142. M. Valentini, F. Piana, J. Pionteck, F.R. Lamastra, F. Nanni. "Electromagnetic properties and performance of exfoliated graphite (EG) - Thermoplastic polyurethane (TPU) nanocomposites at microwaves". Compos. Sci. Technol. 2015. 114: 26–33.

143. S. Das Ramôa, G.M. Barra, R.V. Oliveira, M.G. De Oliveira, M. Cossa, B.G. Soares. "Electrical, rheological and electromagnetic interference shielding properties of thermoplastic polyurethane/carbon nanotube composites". Polym. Int. 2013. 62: 1477–1484.

144.   A. Santamaria-Echart, L. Ugarte, C. García-Astrain, A. Arbelaiz, M.A. Corcuera, A. Eceiza. "Cellulose nanocrystals reinforced environmentally-friendly waterborne polyurethane nanocomposites". Carbohydr. Polym. 2016. 151: 1203–1209.

145.   C. Peniche, W. Argüelles-Monal, F.M. Goycoolea. "Chitin and chitosan: major sources, properties and applications". In: Monomers, polymers and composites from renewable resources. Eds. N. Belgacem, A. Gandini. Elsevier Ltd, 2008. Pp. 289–304.

146.   J. Zeng, Y. He, S. Li, Y. Wang. "Chitin whiskers: an overview". Biomacromolecules 2012. 12: 1–11.

147.   M.N.V.R. Kumar. "A review of chitin and chitosan applications". React. Funct. Polym. 2000. 46: 1–27.

148.   J.D. Goodrich, W.T. Winter. "α-Chitin nanocrystals prepared from shrimp shells and their specific surface area measurement". Biomacromolecules 2007. 8: 252–257.

149.   R. Jayakumar, D. Menon, K. Manzoor, S. V. Nair, H. Tamura. "Biomedical applications of chitin and chitosan based nanomaterials. A short review". Carbohydr. Polym. 2010. 82: 227–232.

150.   R. Jayakumar, M. Prabaharan, S. V. Nair, H. Tamura. "Novel chitin and chitosan nanofibers in biomedical applications". Biotechnol. Adv. 2010. 28: 142–150.

151.   W. Arbia, L. Arbia, L. Adour, A. Amrane. "Chitin extraction from crustacean shells using biological methods. A review". Food Technol. Biotechnol. 2013. 51: 12–25.

152.   M. Zeng, H. Gao, Y. Wu, L. Fan, A. Li. "Preparation and characterization of

nanocomposite films from chitin whisker and waterborne poly(ester-urethane) with or without ultra-sonification treatment". J. Macromol. Sci. Part A. 2010. 47: 867–876.

153. K.G. Nair, A. Dufresne. "Crab shell chitin whisker reinforced natural rubber nanocomposites. 2. Mechanical behavior". Biomacromolecules 2003. 4: 666–674.

154. D. Klemm, B. Heublein, H.P. Fink, A. Bohn. "Cellulose: fascinating biopolymer and sustainable raw material". Angew. Chemie - Int. Ed. 2005. 44: 3358–3393.

155. S. Pérez, D. Samain. Structure and engineering of celluloses. Adv. Carbhydr. Chem. Biochem. 2010, 64: 26-116

156. X. Dong. "Effect of microcrystallite preparation conditions on the formation of colloid crystals of cellulose". Cellulose 1998. 5: 19–32.

157. H. Kargarzadeh, I. Ahmad, I. Abdullah, A. Dufresne, S.Y. Zainudin, R.M. Sheltami. "Effects of hydrolysis conditions on the morphology, crystallinity, and thermal stability of cellulose nanocrystals extracted from kenaf bast fibers". Cellulose 2012. 19: 855–866.

158. M. Mariano, N. El Kissi, A. Dufresne. "Cellulose nanocrystals and related nanocomposites: review of some properties and challenges". J. Polym. Sci. Part B Polym. Phys. 2014. 52: 791–806.

159. H.J. Kim, S. Park, S.H. Kim, J.H. Kim, H. Yu, H.J. Kim, Y.H. Yang, E. Kan, Y.H. Kim, S.H. Lee. "Biocompatible cellulose nanocrystals as supports to immobilize lipase". J. Mol. Catal. B Enzym. 2015. 122: 170–178.

160. R.A. Bini, R.F.C. Marques, F.J. Santos, J.A. Chaker, M. Jafelicci Jr. "Journal of magnetism and magnetic materials synthesis and functionalization of

magnetite nanoparticles with different amino-functional alkoxysilanes". J. Magn. Magn. Mater. 2012. 324: 534–539.

161.   I.W. Hamley. "Nanotechnology with soft materials". Angew. Chemie. 2003. 42: 1692–1712.

162.   M. Yoonessi, J.A. Peck, J.L. Bail, R.B. Rogers, B.A. Lerch, M.A. Meador. "Transparent large-strain thermoplastic polyurethane magnetoactive nanocomposites". ACS Appl. Mater. Interfaces. 2011. 3: 2686–2693.

163.   L. Zhang, R. He, H.C. Gu. "Oleic acid coating on the monodisperse magnetite nanoparticles". Appl. Surf. Sci. 2006. 253: 2611–2617.

164.   P. Guardia, B. Batlle-Brugal, A.G. Roca, O. Iglesias, M.P. Morales, C.J. Serna, A. Labarta, X. Battle. "Surfactant effects in magnetite nanoparticles of controlled size". J. Magn. Magn. Mater. 2007. 316: 756–759.

165.   C. Meiorin, D. Muraca, K.R. Pirota, M.I. Aranguren, M.A. Mosiewicki. "Nanocomposites with superparamagnetic behavior based on a vegetable oil and magnetite nanoparticles". Eur. Polym. J. 2014. 53: 90–99.

166.   L.A. Cobos Cruz, C.A. Martínez Perez, H.A. Monreal Romero, P.E. García Casillas. "Synthesis of magnetite nanoparticles-β-cyclodextrin complex". J. Alloys Compd. 2008. 466: 330–334.

167.   Y.K. Sun, M. Ma, Y. Zhang, N. Gu. "Synthesis of nanometer-size maghemite particles from magnetite". Colloids Surfaces A Physicochem. Eng. Asp. 2004. 245: 15–19.

168.   J. Sun, S. Zhou, P. Hou, Y. Yang, J. Weng, X. Li, M. Li. "Synthesis and characterization of biocompatible Fe_3O_4". J. Biomed. Mater. Res. Part A. 2007. 80: 333–341.

169.   G. Kandasamy, D. Maity. "Recent advances in superparamagnetic iron oxide nanoparticles (SPIONs) for in vitro and in vivo cancer nanotheranostics". Int. J. Pharm. 2015. 496: 191–218.

170.   P. Majewski, B. Thierry. "Functionalized magnetite nanoparticles - synthesis, properties, and bio-applications". Crit. Rev. Solid State Mater. Sci. 2007. 32: 203–215.

171.   M. Bonfil, A. Sirkecioglu, O. Bingol-Ozakpinar, F. Uras, F.G. Seniha. "Castor oil and PEG-based shape memory polyurethane films for biomedical applications". J. Appl. Polym. Sci. 2014. 131: 40590.

172.   A. Lendlein, R. Langer. "Biodegradable, elastic shape-memory polymers for potential biomedical applications". Science 2002. 296: 1673–1676.

173.   R.J. Zdrahala, I. Zdrahala. "Biomedical applications of polyurethanes: a review of past promises, present realities, and a vibrant future". J. Biomater. Appl. 1999. 14: 67–90.

174.   T.G. Grasel, S.L. Cooper. "Surface properties and blood compatibility of polyurethaneureas". Biomaterials 1986. 7: 315–328.

CHAPTER 2

METHODOLOGY: MATERIALS AND CHARACTERIZATION TECHNIQUES
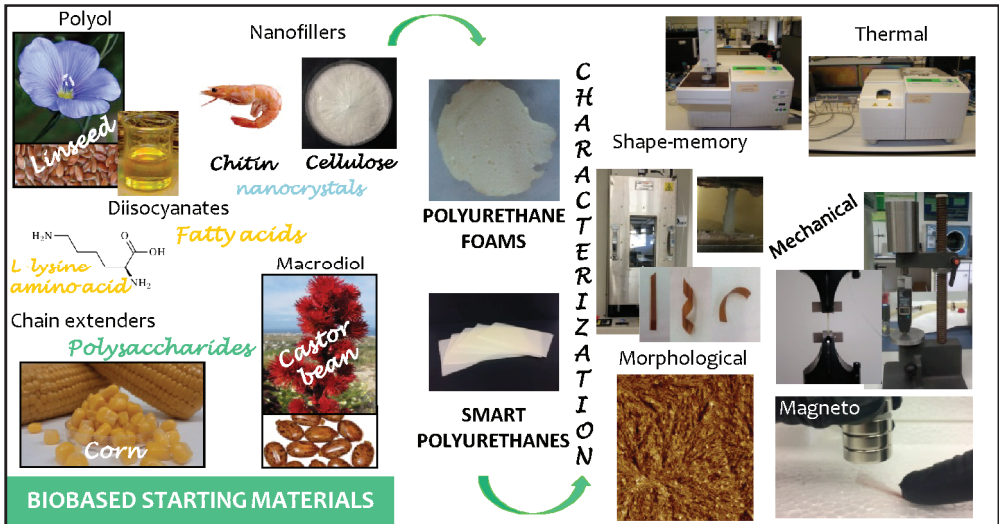
2. METHODOLOGY: MATERIALS AND CHARACTERIZATION TECHNIQUES

2.1 Aim of the chapter

In this chapter, the materials employed for the synthesis of biobased polyurethane rigid foams, crosslinked and thermoplastic biobased polyurethane elastomers and bionanocomposites are described, as well as the characterization techniques and conditions used for the analysis of physicochemical, thermal, mechanical, morphological and surface properties. In the same way, the testing procedure followed for determining the shape-memory behavior of the synthesized thermo-responsive biobased polyurethanes and bionanocomposites is also described. Moreover, the protocol used for the in vitro cell response evaluation is explained.

2.2 Materials

2.2.1 Reactants for the synthesis

2.2.1.1 Biobased rigid polyurethane foams

For the preparation of the polyurethane foams, a linseed oil based polyol (LOP) was used. LOP was obtained from the hydroxylation reaction of linseed oil (LO), supplied by Grainer S.A., with hydrogen peroxide (30 wt%) and formic acid (85 wt%) from Ciccarelli and Biopack, respectively.

Moreover, in the A-side of the formulation of the foams polymeric 4,4-diphenylmethane diisocyanate (pMDI) was used as isocyanate, which was supplied by Huntsman Polyurethanes under Rubinate 5005 trademark. The equivalent weight of this diisocyanate was 131 g eq^{-1}, with an average functionality of 2.7, a viscosity of 170-250 cp and an isocyanate content of 30.2-31.5 wt%. The B-side of the formulation was composed by the mixture of the hydroxylated linseed oil based polyol, whose obtaining is deeply explained in chapter 3 and three different reactive modifiers (Scheme 2.1). The first one was

glycerol (GLY) with an equivalent weight of 30.7 g eq^{-1} and a viscosity of 1.26 cp. The second modifier employed was diethylene glycol (DEG), with an equivalent weight of 53.1 g eq^{-1} and a viscosity of 38 cp. The last modifier was polyethylene glycol (PEG) with a molecular weight of 100 g eq^{-1} and a viscosity of 50 cp. The three reactive modifiers were supplied by Fluka.

a)   b)   c)

$$CH_2-CH-CH_2$$
$$\quad OH \quad OH \quad OH$$

$$CH_2-CH_2$$
$$\quad OH \quad OH$$
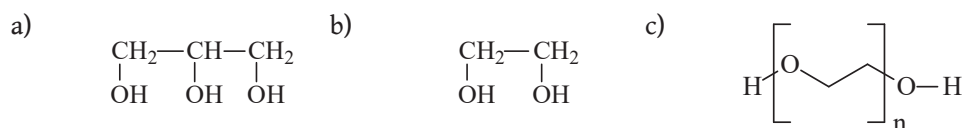
Scheme 2.1. Chemical structure of the employed reactive modifiers a) GLY, b) DEG and c) PEG.

In addition, the following additives were also incorporated. The silicone surfactant agent (Tergostab B8404), supplied by Hunstman Polyurethanes, which as mentioned in the introduction contributes to the nucleation of the blowing agent bubbles and stabilizing the cell structure; the tertiary amine, N,N-dimethyl benzylamine (DMBA), which acts as blowing catalyst and the gelation catalyst dibutyltin dilaureate (DBTDL), both were supplied by Aldrich. Finally, distillate water was employed as blowing agent.

2.2.1.2 Crosslinked and thermoplastic biobased polyurethane elastomers

In order to obtain biobased crosslinked and thermoplastic polyurethane elastomers different precursors were used. All the synthesized polyurethanes contains the same macrodiol derived from castor oil, the poly(butylene sebacate)diol (CO3). This macrodiol was synthesized by copolymerizing sebacic acid with 1,4-butanediol and its chemical structure is shown in Scheme 2.2. The hydroxyl index of the macrodiol was 32.01 mg KOH g^{-1} and it was determined by titration based on ASTM D 4274-88 Test Method A standard, and its number-average molecular weight was 3505 g mol^{-1}. Prior to its use, the macrodiol was dried under vacuum for 6 h at 80 °C.
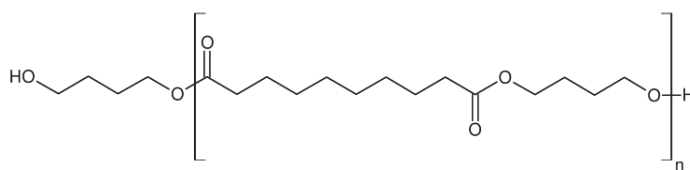
Scheme 2.2 Chemical structure of the employed CO3 macrodiol.

Two different diisocyanates were employed, both derived from renewable sources. The first one was the ethyl ester L-lysine diisocyanate (LDI) with a molecular weight of 226 g mol^{-1} and an isocyanate content of 36.3 wt%, which was supplied by CHEMOS GmBH. It was based on L-lysine amino acid. The second diisocyanate used was the 2-heptyl-3,4-bis(9-isocyanatononyl)-1-pentylcyclohexane (DDI) derived from fatty acids, supplied by GL Syntech, and its molecular weight was 587 g mol^{-1} and the isocyanate content was 13.6–14.3 wt%. The chemical structure of both diisocyanates was previously shown in Table 1.3.

For the synthesis of crosslinked biobased polyurethanes 1,1,1-tris(hydroxymethyl)propane (TMP) crosslinker (134.17 g mol^{-1}) was used, which was supplied by Fluka.

In the case of thermoplastic biobased polyurethane elastomers two chain extenders were employed, the 1,3-propanediol (PD) and dianhydro-D-glucitol, also known as isosorbide (DAS), supplied by Quimidroga and Sigma-Aldrich, respectively. PD was based on corn sugar and its molecular weight was 76 g mol^{-1}, while DAS was derived from polysaccharides and its molecular weight was 146 g mol^{-1}. Prior using PD, it was dehydrated under vacuum for 2 h at 40 °C. Furthermore, DAS was kept in a desiccators due to its hygroscopic behavior.

The chemical structure of both chain extenders and the crosslinker is shown in Scheme 2.3.
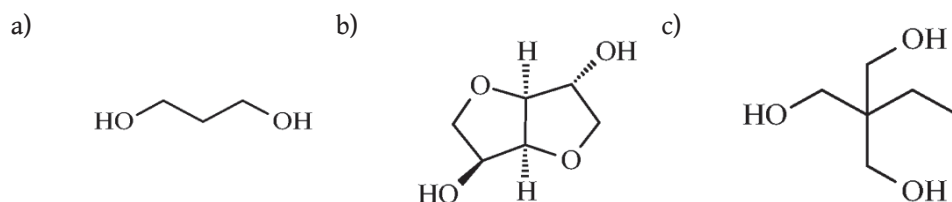
Scheme 2.3. Chemical structure of the chain extenders and crosslinker a) PD, b) DAS and c) TMP.

2.3 Bionanocomposites containing chitin nanocrystals, cellulose nanocrystals and magnetite nanoparticles

Different nanoentities were used in order to prepare biobased polyurethane bionanocomposites.

Chitin nanocrystals (CHNCs) were obtained from the acid hydrolysis of chitin powder obtained from shrimp shells supplied by Sigma. Hydrochloric acid (37%) from Panreac was used for the hydrolysis.

Cellulose nanocrystals (CNCs) were obtained from microcrystalline cellulose (MCC) from Aldrich, with a particle size between 100 and 150 μm. Sulphuric acid (96%) from Panreac was used for the hydrolysis of the MCC.

Magnetite nanoparticles (MNPs) were obtained by co-precipitation method. To that end, iron (III) chloride hexahydrate (98%) from Panreac and iron (II) chloride tetrahydrate ($\geq$ 99%) from Sigma-Aldrich were used. Furthermore, ammonium hydroxide (30%) from Panreac was used. In order to coated and stabilize the obtained nanoparticles, oleic acid (90%) from Fluka was used. The organic solvents n-heptane (anhydrous 99%) and tetrahydrofuran (THF) (HPLC grade) were supplied by Sigma-Aldrich and Macron Fine Chemicals, respectively.

2.4 Characterization techniques

2.4.1 Physicochemical characterization

2.4.1.1 Gel permeation chromatography

Weight and number average molecular weights, $\overline{M}_w$ and $\overline{M}_n$, respectively, and polydispersity index (PI) of the synthesized biopolyurethanes were determined by gel permeation chromatography (GPC) using a Thermo Scientific chromatograph, equipped with an isocratic Dionex UltiMate 3000 pump and a RefractoMax 521 refractive index detector. The separation was carried out at 30 °C within four Phenogel GPC columns from Phenomenex, with 5 μm particle size and 10^5, 10^3, 100 and 50 Å porosities, respectively, located in an UltiMate 3000 Thermostated Colum Compartment. THF was used as mobile phase at a flow rate of 1 mL min^{-1}. For the preparation of the samples, the synthesized thermoplastic biobased polyurethanes were dissolved in THF at 1 wt% and filtered by using nylon filters with 2 μm pore size. $\overline{M}_w$, $\overline{M}_n$ and PI of the synthesized biobased polyurethanes were reported as weight average polystyrene standards.

2.4.1.2 Fourier transform infrared spectroscopy

The characteristic functional groups of the synthesized biobased materials were identified by means of Fourier transform infrared spectroscopy (FTIR) using a Nicolet Nexus FTIR spectrometer, equipped with a MKII Golden Gate accessory with diamond crystal at a nominal incident angle of 45° and a ZnSe lens. In the case of polyurethane rigid foams, a Thermo Scientific Nicolet 6700 FTIR spectrometer was used in attenuated total reflectance (ATR) mode. The spectra were obtained after 32 scans in the range between 4000 and 650 cm^{-1} with a resolution of 4 cm^{-1}. In the case of linseed oil and linseed oil based polyol the range of the spectra is between 4000 and 500 cm^{-1}. Magnetite nanoparticles were analyzed by using KBr pellets and the spectra was obtained after 64 scans in the range of 4000-400 cm^{-1} with a resolution of 4 cm^{-1}.

Moreover, kinetic measurement of the first step of polymerization was also performed, using a temperature chamber and controller (Specac). Reactant were placed above a KBr pellet in the temperature chamber, and sample spectra were recorded every 2 min averaging 34 scans in the range of 4000-650 cm^{-1} with a resolution of 4 cm^{-1}. Absorbance changes were related to conversion by measuring the height of isocyanate group stretching vibration band (H_{NCO}) at 2270 cm^{-1} and normalizing with the height of C-H bond symmetric stretching vibration band at 2860 cm^{-1}, which was taken as reference (H_{ref}). Isocyanate conversion (α) was calculated from equation 2.1, measuring H_{NCO} and H_{ref} at reaction time, t, and at the beginning, 0.[1] During kinetic measurements, relative changes in molar absorptivity for isocyanate and reference bands were considered to be equal.

$$\alpha = 1 - \frac{[H_{NCO}/H_{ref}]_t}{[H_{NCO}/H_{ref}]_0} \tag{2.1}$$

2.4.1.3 Proton nuclear magnetic resonance spectroscopy

Proton nuclear magnetic resonance (H^1NMR) spectra of linseed oil and linseed oil based polyol were recorded on a Bruker AM500 spectrometer (500 MHz) using deuterated acetone and deuterated dimethylsulfoxide as solvents, respectively.

2.4.1.4 Determination of biobased carbon content

The biobased carbon content (BCC) of the starting commercial materials was determined by the ASTM D 6866-12 (0.98) Method B (AMS) standard procedure.[2]

The biobased carbon content of the employed starting materials in the synthesis of crosslinked and thermoplastic biobased polyurethanes are listed in Table 2.1.

Table 2.1. Biobased carbon content of the starting materials employed.

Starting material		BCC (%)
Macrodiol	CO3	72
Diisocyanate	LDI	81
	DDI	98
Chain extender	PD	100
	DAS	100
Crosslinker	TMP	0

The estimation of the biobased carbon content in the final biobased polyurethanes (BCC_{PU}) was calculated by using equation 2.2, where the molar ratio and the biobased carbon content of each component in the final formulation was taken into account.

$$BCC_{PU} \, (\%) = \frac{m_{CB}}{m_C} \cdot 100 = \frac{(m_{C_{mac}} \cdot BCC_{mac}) + (m_{C_{diis}} \cdot BCC_{diis}) + (m_{C_{c.e./cr}} \cdot BCC_{c.e./cr})}{m_{C_{mac}} + m_{C_{diis}} + m_{C_{c.e./cr}}} \quad (2.2)$$

where m_{CB} is the total biobased carbon weight (g), m_C is the total carbon weight (g), $m_{C_{mac}}$ is the carbon weight in the macrodiol (g), $m_{C_{diis}}$ is the carbon weight in the diisocyanate (g), $m_{C_{c.e./cr}}$ is the carbon weigh in the chain extender or crosslinker (g), BCC_{mac} is the renewable carbon content of the macrodiol (%), BCC_{diis} is the renewable carbon content of the diisocyanate (%) and $BCC_{c.e./cr}$ is the renewable carbon content of the chain extender or crosslinker (%).

2.4.1.5 Determination of iodine and hydroxyl values

The iodine value of LO and LOP was determined according to ASTM D 5554.[3] Moreover, the hydroxyl value was determined by an acetylation method with acetic anhydride in pyridine solution, according to ASTM D 4274-05.[4]

2.4.1.6   Density measurement

The density of the foams was obtained as the ratio between the weight and volume of a cylindrical specimen (28 mm diameter x 30 mm height), and values were averaged for five specimens.

2.4.1.7   Elemental analysis

Elemental analysis of chitin nanocrystals was performed in a Euro EA Elemental Analyzer equipment. The nitrogen content in chitin nanocrystals was determined by analyzing the combustion products of the sample in a chromatographic column. A detector of thermal conductivity gave a signal related with nitrogen and the percentages were calculated.

2.4.1.8   X-ray diffraction

The polymorphism of the employed nanoentities and prepared bionanocomposites was determined by performing X-ray diffraction (XRD) studies. The XRD patterns were collected by using a Philips X'pert PRO automatic diffractometer operating at 40 kV and 40 mA, in theta-theta configuration, secondary monochromator with Cu-Kα radiation (λ = 1.5418 Å) and a PIXcel solid state detector (active length in 2θ = 3.347°). A fixed divergence and antiscattering slit giving a constant volume of sample illumination were used.

2.4.2   Thermal characterization

2.4.2.1   Differential scanning calorimetry

Thermal properties were analyzed by means of differential scanning calorimetry (DSC) using a Mettler Toledo DSC822e equipment, provided with a robotic arm and an electric intracooler as a refrigeration unit. Samples with a weight between 5 and 10 mg were sealed in aluminum pans and heated from -75

to 150 °C at a scanning rate of 20 °C min^{-1}, using N_2 as a purge gas (20 mL min^{-1}). The crystallization process was also followed by cooling the samples from 150 to -75 °C at a scanning rate of 10 °C min^{-1}. A second heating run were also performed. The inflexion point of the heat capacity change observed was chosen to evaluate the glass transition temperature, T_g, and melting temperature (T_m) was settled as the maximum of endothermic peak taking the area under the peak as melting enthalpy (ΔH_m). Crystallization temperature (T_c) was taken as the minimum of the exothermic peak observed in the cooling scan and the crystallization enthalpy (ΔH_c) as the peak area. The ΔH_m and ΔH_c values were referred to total sample weight.

Taking into account the melting or crystallization enthalpy values and based on equations 2.3 and 2.4, the relative crystallinity of the biobased polyurethanes (χ_c) (crystallinity of the phase to the crystallinity of the neat phase) were measured in the first heating ($\chi_{c\,heating}$) and cooling ($\chi_{c\,cooling}$) scans:[5]

$$\chi_c = \frac{\Delta H_e}{\Delta H_t} \tag{2.3}$$

$$\Delta H_t = \Delta H_p \cdot \omega \tag{2.4}$$

where ΔH_e is the experimental melting or crystallization enthalpy value and ΔH_t is the theoretical value calculated by equation 2.4, where ΔH_p is the melting or crystallization enthalpy value of the corresponding neat phase and ω is the weight fraction of that phase.

2.4.2.2 Dynamic mechanical analysis

The dynamic mechanical behavior of the biobased polyurethanes was analyzed by dynamic mechanical analysis (DMA) in tensile mode on an Eplexor 100N analyzer from Gabo, using a static strain of 0.10%. The temperature was varied from -100 to 100 °C at a scanning rate of 2 °C min^{-1} and at a fixed operation frequency of 10 Hz. Samples were cut in strips of 22 mm in length, 5 mm in

width and 1.5 mm in thickness. Moreover, crosslink density (ν_e) and molecular weight between crosslinks ($\overline{M}_c$)[6–8] values of the synthesized crosslinked biobased polyurethane were determined by equations 2.5 and 2.6 respectively.

$$\nu_e = \frac{E'}{3RT} \tag{2.5}$$

$$\overline{M}_c = \frac{\rho}{\nu_e} \tag{2.6}$$

where E' is the storage modulus at temperature above T (in the rubbery region at T_g + 85 °C), R is the universal constant of gases (8.314 J mol^{-1} K^{-1}), T is the temperature in Kelvin and ρ is the density of the biobased polyurethane (1.1 g cm^{-3}).[9]

In the case of biobased polyurethane foams measurements were performed using an Anton Paar, Physica MCR 301 rheometer. Torsion geometry was used with solid rectangular samples with dimensions of 30 x 10 x 3 mm³. Measurements were carried out as temperature sweeps in the range from -20 to 225 °C at a heating rate of 10 °C min^{-1}. The frequency was kept in 1 Hz and the applied deformation was 0.5%.

2.4.2.3 Thermogravimetric analysis

The thermal stability of foams was analysed in a Mettler Toledo TGA/SDTA851 thermogravimetric analyzer. Samples with a weight of 2 mg were scanned from room temperature to 600 °C at a heating rate of 10 °C min^{-1}, under nitrogen atmosphere.

2.4.3 Mechanical characterization

2.4.3.1 Tensile testing

Mechanical testing was carried out at room temperature using a Universal Testing Machine (MTS Insight 10) with a load cell of 10 kN and pneumatic grips.

Samples were cut into dog-bone shape according to ASTM D1708-13 standard procedure.[10] Tests were performed with a crosshead rate of 50 mm min^{-1}. Elastic modulus (E), yield strength (σ_y), tensile strength at break (σ_b), yield elongation (ε_y) and elongation at break (ε_b) were averaged from at least five test specimen data.

2.4.3.2 Compression testing

For the compression testing of biobased polyurethane foams, cylindrical specimens of 28 mm diameter x 30 mm height were cut from the upper side of foams, and tested at room temperature in an INSTRON 8501 Universal testing machine. The compression force was applied in the foam rise direction. Samples were compressed a fixed length of 22 mm at a crosshead speed of 10 mm min^{-1}. The average values of compression modulus (calculated as the slope of the stress-strain curve at low deformations), compressive strength (which in accordance to ASTM D1621-16,[11] was taken as the stress reached at the compressive yield point that occurred below 10% deformation for all samples) and densification strain (taken as the strain at the intersection point between the stress plateau and a line extrapolated from the densification line) were calculated from these tests. Compression values were averaged for five specimens.

After compression, the samples were unloaded and allowed to recover for 1 min and 24 h. The length reached after the recovery time (l_r) was compared to the initial specimen height (l_i) and used to calculate the recovery ratio (Rr), as indicated in equation 2.7:

$$Rr = \frac{l_r}{l_i} \cdot 100 \qquad\qquad (2.7)$$

2.4.3.3 Shore D hardness testing

Shore D hardness measurements of biobased crosslinked and thermoplastic polyurethanes were performed at room temperature with a MD-202 DuroTECH digital hardness testing device following ASTM D2240-15 standard procedure.[12] Results were averaged from at least five values measured in different zones of the sample.

2.4.4 Shape-memory characterization

The thermally-activated shape-memory properties of the synthesized thermo-responsive crosslinked and thermoplastic biobased polyurethanes were studied in the strain-controlled mode using the MTS Insight 10 equipment with a temperature chamber (Thermcraft). Strip shape samples (22 mm in length, 5mm in width and a thickness of 1.5 mm for biobased polyurethanes and 0.2 mm for bionanocomposites) were heated at the switching temperature (T_s) for 10 min. Thereafter, samples were stretched up to a maximum elongation, which was different depending on the testing biobased polyurethane properties, at a rate of 5 mm min^{-1}. Once the goal elongation was reached, samples were cooled down below transition temperature (T_{trans}) to fix the temporary shape, and the applied stress was removed. The permanent shape was recovered upon heating the samples up to the switching temperature for 10 min. Five thermo-mechanical cyclic tensile tests were consecutively performed. Thermally-activated shape-memory behavior was quantified taking into account the commonly used parameters, i.e. shape fixity (R_f) and shape recovery (R_r) values, which can be calculated using equations 2.8 and 2.9, respectively.

$$R_f(N) = \frac{\varepsilon_u(N)}{\varepsilon_m(N)} \cdot 100 \qquad (2.8)$$

$$R_r(N) = \frac{\varepsilon_m(N) - \varepsilon_p(N)}{\varepsilon_m(N) - \varepsilon_p(N\text{-}1)} \cdot 100 \qquad (2.9)$$

where ε_m is the maximum strain in the tensile test, ε_u is the residual strain obtained after unloading and after cooling below T_{trans}, ε_p is the residual strain after the shape recovery, and N is the number of cycles.
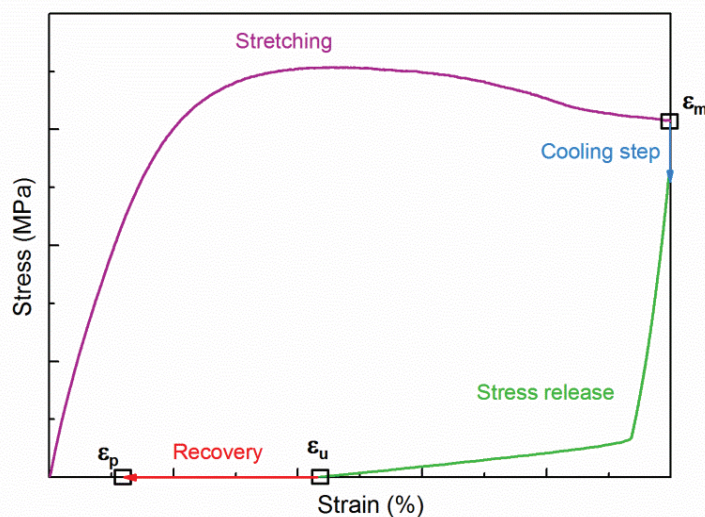
Figure 2.1. Stress-strain diagram for a thermo-responsive material, showing the different steps followed in the thermo-mechanical cycle.

2.4.5 Morphological characterization

2.4.5.1 Atomic force microscopy

Atomic force microscopy (AFM) was used to characterize biopolyurethanes morphology by imaging the cross-sections of the samples cut with a Leica EM FC6 cryo-ultramicrotome equipped with a diamond knife and operated at -120 °C (biobased polyurethanes of chapter 5 with LDI) and at -140 °C (biobased polyurethanes of chapter 5 with DDI). These temperatures were chosen in order to attempt to cut the samples in the glassy state, to obtain an adequate surface. Images of the biobased polyurethanes with LDI were obtained in tapping mode at room temperature with a Nanoscope IIIa scanning probe microscope (Multimode™ Digital Instruments), using an integrated force generated by cantilever/silicon probes, applying a resonance frequency of 180 kHz. The

cantilever was 125 µm long, with a tip radius of 5-10 nm. Images of the biobased polyurethane with DDI were obtained in tapping mode at room temperature with a Bruker Dimension ICON scanning probe microscope equipped with a Nanoscope V Controller. Samples morphology was examined using TESP-V2 type silicon tips having a nominal resonance frequency of 320 kHz and a cantilever spring constant about 42 N m^{-1}.

Furthermore, the morphology of chitin and cellulose nanocrystals was also analyzed by AFM. The images were obtained in tapping mode with a Nanoscope IIIa scanning probe microscope. Suspensions of chitin and cellulose nanocrystals were prepared with a concentration of 0.1 wt%. The prepared suspensions were sonicated for 1 h and a drop was placed on a mica substrate. Samples were prepared by spin coating technique at 1200 rpm for 120 s.

2.4.5.2   Scanning electron microscopy

Scanning electron microscopy (SEM) was use in order to analyze the cell morphology of the prepared foams. Small specimens were cut on a plane parallel to the foam rise direction. A scanning electron microscope Philips model SEM 505 was used to obtain images of the surfaces. Specimens were coated with gold to provide conductivity prior to the microscopy observation.

2.4.5.3   Transmission electron microscopy

Transmission electron microscopy (TEM) was used to analyze the morphology of magnetite nanoparticles. An accelerated electron beam is transmitted through a thin sample and the analysis of the transmitted and dispersed electrons allows obtaining an image of the sample. Measurements were carried out on a Philips SuperTwin CM200 operated at 200 kV and equipped with LaB$_6$ filament and EDAX EDS microanalysis system.

For samples preparation, magnetite nanoparticles were dispersed in THF solvent for 5 min in an ultrasonic bath. Subsequently a drop of suspension was spread onto a TEM copper grid (300 Mesh) covered by a carbon film followed by drying under vacuum.

2.4.6 Surface characterization

2.4.6.1 Water contact angle

The surface properties of synthesized polyurethanes were evaluated measuring the water contact angle (WCA) in a Dataphysics OCA20 equipment. Five measurements of each sample were carried out with a deionised water drop method (2 μL) at 26 °C. The surface tension between the surface of the material and water was calculated using Neumann's Equation of State (2.10), which is based on the equilibrium of forces at the edge of a resting drop, as proposed by Young.

$$\gamma_{PU} = \frac{1}{4} \gamma_{H_2O} \left(1 + \cos\phi\right)^2 \qquad\qquad (2.10)$$

where γ_{PU} is the surface tension of the biopolyurethane, γ_{H_2O} is the water surface tension and ϕ is the angle between water drop and biopolyurethane surface.

2.4.7 *In vitro* cell response evaluation

2.4.7.1 Short-term cytotoxicity test

Biocompatibility of the polyurethanes was analyzed by evaluating the short-term cytotoxicity, cell viability and proliferation. The evaluation of short-term cytotoxicity was carried out using L-929 murine fibroblasts cells, following ISO 10993 standard part 5 guidelines.[13] To prepare extracts of test materials, samples with an area of 6 cm^2 were rinsed with Mili-Q water, sterilized in 70% ethanol for 2 h and washed three times in sterile phosphate buffered saline

(PBS) (Sigma-Aldrich) for 10 min. Sterilized film samples were incubated separately in complete cell culture medium (Dulbecco's modified Eagle's medium [Sigma Chemicals Co] plus 10% fetal calf serum [Gibco] and supplemented with antibiotic-antimycotic solution [Sigma]) at 37 °C for 24 h to obtain the extracted culture medium. In addition, L-929 murine fibroblasts were firstly seeded and allowed to grow in 96-well microplates at a density of 4×10^3 cells/well in the presence of standard culture medium for 24 h before the experiments. In the cytotoxicity test, cultures were treated for 24 and 48 h with the extracted media. As controls, standard culture media (control) were used, high-density polyethylene (negative control, USP Rockville), and polyvinyl chloride (positive control, Portex).

To evaluate cell viability and proliferation, metabolic activity of viable cells was determined using the colorimetric assay MTT (Cell Proliferation Kit I MTT, Roche). This test is based on reduction of 3-(4,5-dimethyltriazol-2yl)-2,5 diphenyltetrazolium bromide on formazan in the mitochondria of living cells. The cell number per well was proportional to the amount of formazan crystals and was determined by measuring the absorbance at 540 nm using a microplate reader (ELISA). Viability (%) was calculated from equation 2.11:

$$\text{Viability (\%)} = \frac{[A]_{\text{test}}}{[A]_{\text{control}}} \cdot 100 \tag{2.11}$$

where $[A]_{\text{test}}$ is the absorbance of the sample cells and $[A]_{\text{control}}$ is the absorbance of the negative control cells, in this case high-density polyethylene. All assays were conducted in triplicate and average values and their standard deviations were estimated.

2.4.7.2 Live/Dead assay

The analysis of cell long term adhesion was carried out by performing Live/Dead assays. First, murine L-929 fibroblasts were cultured in MEM medium

(Gibco) supplemented with 1 mM sodium pyruvate (Gibco), 1% nonessential amino acids (Gibco), 1% penicillin-streptomycin (Lonza), and 10% fetal bovine serum (Biochrom AG) (complete medium). Samples of 0.5 cm^2 were place in 24-well ultralow attachment culture plates (Corning) and sterilized in 70% ethanol for 2 h and washed three times in sterile phosphate buffered saline (Sigma-Aldrich) for 10 min. The sterilized samples were prewetted in complete medium for 24 h at 37 °C. Aliquots containing 5 x 10^4 L-929 fibroblasts were then seeded onto the samples and left for 1.5 h to be adhere. After that PBS was added in the surrounding wells and finally 0.5 mL of complete medium were added. The Live/Dead assays were performed after 7 and 14 days culture. The complete medium was removed and samples were rinsed with PBS twice. Afterwards, they were incubated in darkness with a mix of 4 μM calcein-AM (Sigma-Aldrich) and 5 μM ethidium homodimer-1 (Molecular Probes) in PBS for 20 min at 37 °C. Each sample was examined under a confocal microscope (Olympus LV500) to visualize adhered viable cells (green fluorescence; λ_{ex-em} = 490–515 nm) and dead cells (red fluorescence; λ_{ex-em} = 490–630 nm). Bright-field and fluorescence micrographs were recorded on each sample.

2.5   References

1.   B. Fernandez d'Arlas, L. Rueda, P.M. Stefani, K. de la Caba, I. Mondragon, A. Eceiza. "Kinetic and thermodynamic studies of the formation of a polyurethane based on 1,6-hexamethylene diisocyanate and poly(carbonate-co-ester)diol". Thermochim. Acta 2007. 459: 94–103.

2.   ASTM D6866-12. "Standard test method for determining the biobased content of natural range materials using radiocarbon and isotope ratio mass spectrometry analysis." ASTM International. West Conshohocken, PA, 2012.

3.   ASTM D5554-15. "Standard test method for determination of the iodine

value of fats and oils". ASTM International. West Conshohocken, PA, 2015.

4.   ASTM D4274-16. "Standard test methods for testing polyurethane raw materials: determination of hydroxyl numbers of polyols". ASTM International. West Conshohocken, PA, 2016.

5.   B. Wunderlinch. Thermal analysis of polymeric materials. Springer, Berlin, 2005.

6.   L. Song, Q. Ye, X. Ge, A. Misra, J.S. Laurence, C.L. Berrie, P. Spencer. "Synthesis and evaluation of novel dental monomer with branched aromatic carboxylic acid group". J. Biomed. Mater. Res. B. Appl. Biomater. 2014. 102B: 1473–1484.

7.   J.M. Chenal, L. Chazeau, L. Guy, Y. Bomal, C. Gauthier. "Molecular weight between physical entanglements in natural rubber: a critical parameter during strain-induced crystallization". Polymer 2007. 48: 1042–1046.

8.   G.R. Palmese, R.L. McCullough. "Effect of epoxy-amine stoichiometry on cured resin material properties". J. Appl. Polym. Sci. 1992. 46: 1863–1873.

9.   B. Fernández-d'Arlas, U. Khan, L. Rueda, L. Martin, J.A. Ramos, J.N. Coleman, M.L González, A. Valea, I. Mondragon, M.A. Corcuera, A. Eceiza. "Study of the mechanical, electrical and morphological properties of PU/MWCNT composites obtained by two different processing routes". Compos. Sci. Technol. 2012. 72: 235–242.

10.   ASTM D1708-13. "Standard test method for tensile properties of plastics by use of microtensile specimens". ASTM International. West Conshohocken, PA, 2013.

11.   ASTM D1621-16. "Standard test method for compressive properties of

rigid cellular plastics". ASTM International. West Conshohocken, PA, 2016.

12.   ASTM D2240-15. "Standard test method for rubber property-durometer hardness". ASTM International. West Conshohocken, PA, 2015.

13.   ISO 10993-5. Biological evaluation of medical devices. Test for in vitro cytotoxicity. International Organization for Standardization. Geneve, Switzerland, 2009.

POLYURETHANE RIGID FOAMS FROM A LINSEED OIL BASED POLYOL
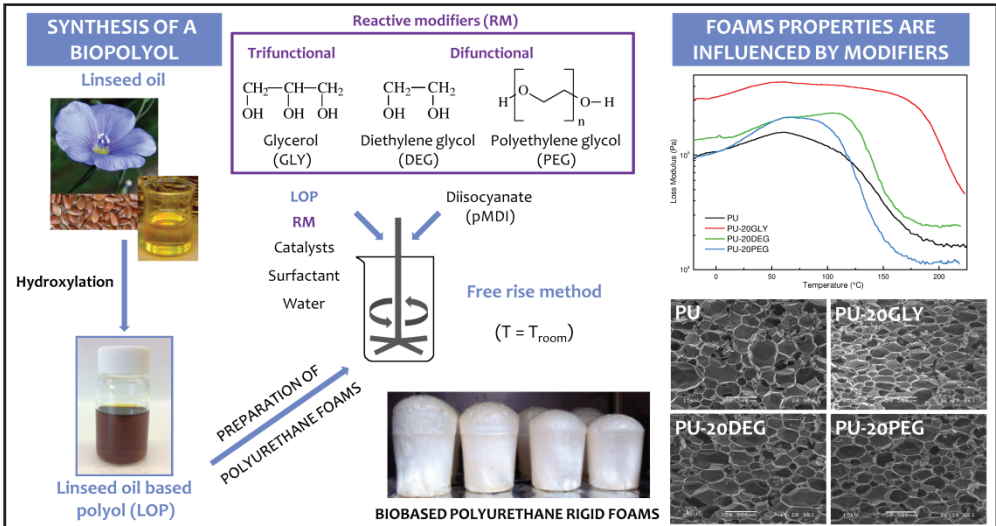
3. POLYURETHANE RIGID FOAMS FROM A LINSEED OIL BASED POLYOL

3.1 Aim of the chapter

This chapter aimed to synthesize a fully biobased polyol in order to prepare biobased rigid polyurethane foams incorporating it to the formulation. To this end, a commercial linseed oil was hydroxylated to obtain the fully biobased polyol. The obtained hydroxylated polyol was characterized by determining the iodine and hydroxyl values, and also by Fourier transform infrared spectroscopy and proton nuclear magnetic resonance spectroscopy (H[1] NMR) techniques.

Moreover, the effect of varying the content and the functionality of different reactive modifiers on physical, chemical and mechanical properties of the foam was studied. Reactive modifiers with different functionality were employed: difunctional DEG and PEG, and trifunctional GLY which acts as a crosslinker. Moreover, the pMDI was used as diisocyanate, Tergostab B8404 surfactant and DMBA and DBTDL catalysts were also used. Finally, water was used as blowing agent, which eliminates the need to add volatile organic compounds and also offers the additional advantage of accelerating the reaction, decreasing the amount of catalyst.

Biobased polyurethane rigid foams were obtained by the free rise method at room temperature. Physical properties were studied by calculating foams density and determining cream, end of rise and tack free times. The physicochemical properties and morphology were analyzed by means of Fourier transform infrared spectroscopy and scanning electron microscopy, respectively. The dynamic mechanical behavior was also studied and mechanical properties were analyzed by performing compression tests. Finally, thermogravimetric analysis was performed in order to study the thermal stability of the foams.

3.2   Hydroxylation of the linseed oil

Linseed oil based polyol (LOP) was obtained by hydroxylation reaction as illustrated in Scheme 3.1.
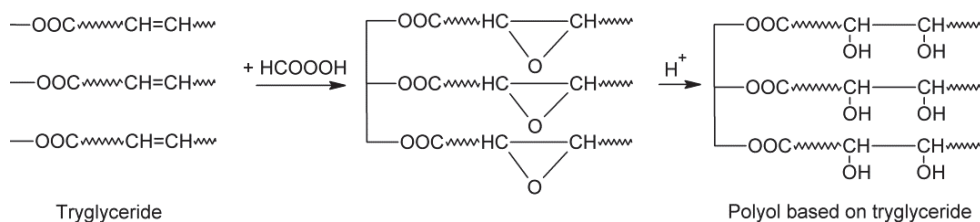
Scheme 3.1. General scheme of hydroxylation of unsaturated oil.

Hydrogen peroxide and formic acid were added in a reactor with mechanical stirrer at 40 °C for 5 min. During that step, the hydrogen peroxide reacted with the formic acid to form performic acid (HCOOOH), and then linseed oil (LO) was added dropwise. Once the LO was incorporated, the reactor temperature was raised to 50 °C and it underwent an intermediate process of epoxidation. The epoxide group is unstable under the strong acid conditions, therefore it opens to form hydroxyl groups.[1] The reaction was continued for 3.5 h. The $C=C/H_2O_2$ and $H_2O_2/HCOOH$ molar ratios were 1/1 and 1/1.4, respectively.

The product was allowed to lie overnight at room temperature and became separated in two layers. Distillated water was added to the product and mixed slowly. Once two layers reappeared, the bottom layer was removed. This process was repeated three times in order to eliminate, as much as possible, the acids from the upper layer. Finally, the upper layer was recovered and distilled under vacuum (70-80 °C at 100 mbar) to eliminate the remaining water and acids, to obtain the hydroxylated LO.

3.3   Characterization of the linseed oil and derived polyol

3.3.1   Determination of iodine and hydroxyl values

The iodine value of LO and LOP was determined following the ASTM D5554-15 standard test method.[2] The iodine value of LO and LOP was 132.2 and 56.5 g I 100 g^{-1}, respectively. As can be observed the iodine value is lower for the LOP, since C=C bonds in the vegetal oil were replaced by hydroxyl groups in LOP. However, not all C=C bonds were reacted in the hydroxylation reaction, since the final iodine value is not null.

The hydroxyl (OH) value of the LOP was determined by an acetylation method with acetic anhydride in pyridine solution according to ASTM D4274-16.[3] The OH value of the LOP was 216.4 mg KOH g^{-1}; this value can be considered high enough for the preparation of rigid and semirigid foams. Therefore a further alcoholysis was not needed.

3.3.2 Fourier transform infrared spectroscopy

The FTIR spectra of LO and LOP are shown in Figure 3.1. The spectrum of the LO shows a broad but shallow band at 2500-3500 cm^{-1} related to the stretching vibration of the hydroxyl group (O-H) of the carboxylic acids, which probably are formed by the hydrolysis of the triglyceride during storage.[4] In addition, the stretching vibration of the carbonyl group of the carboxylic acids is also observed at 1710 cm^{-1}.[4] Moreover, in the carbonyl stretching region the band related to the carbonyl of the ester groups from the triglycerides can be observed at 1741 cm^{-1}.[5] The band at 3010 cm^{-1} and the small peak at 1650 cm^{-1} can be attributed to the stretching vibration of =C-H and C=C groups, respectively, and are related to the triglyceride unsaturations.[5] The main differences observed in LOP spectrum after hydroxylation are the broad and more intense band of hydroxyl group at 3500 cm^{-1} and the decrease of the stretching bands at 3010 and 1650 cm^{-1} due to the attachment of hydroxyl groups to C=C bonds by means of nucleophilic addition reaction.[4] These results agree with the reduction of the iodine value and, correspondingly, increased

hydroxyl value. In the carbonyl stretching region only the band attributed to carbonyl ester group can be observed.
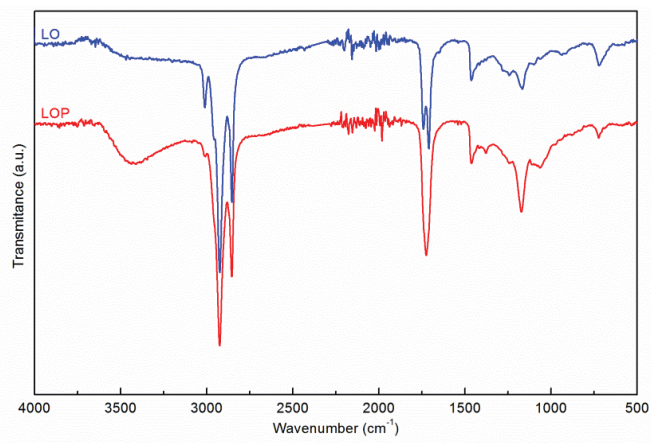

Figure 3.1. FTIR spectra of LO and LOP.

3.3.3 Proton nuclear magnetic resonance spectroscopy

The chemical structure of LO and LOP was analyzed by H^1 NMR and Figure 3.2 shows the H^1 NMR spectra of LO and LOP.
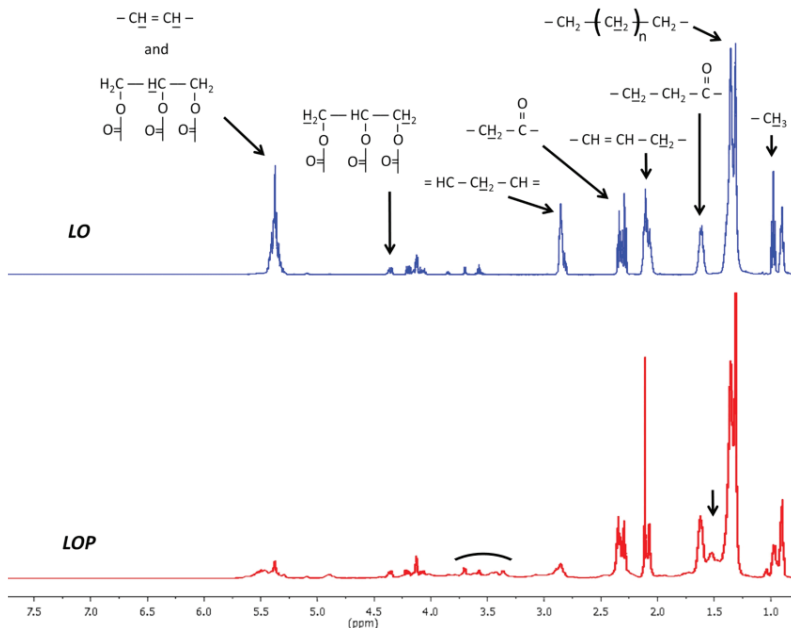
Figure 3.2. H^1 NMR spectra of LO and LOP.

The peaks have been assigned according to the following[4,6,7]

- 0.9 ppm, methyl protons at the end of the fatty acid chains
- 1.3–1.4 and 1.6 ppm, olefinic protons separated by at least one carbon from the ester groups and at least one carbon from the unsaturations
- 2.3 ppm, protons in the methylene groups close to the carbon-carbon insaturations
- 2.3-2.4 ppm (multiplets), methylene neighbour to the carboxylic groups in the triglycerides
- 2.8-2.9 ppm, CH_2 protons between two C=C
- 4.2-4.3 ppm, protons in the methylene groups of the glycerol fragment
- 5.2-5.5 ppm, vinylic protons

The comparison of both spectra shows clear differences between LO and LOP structures. The LOP spectrum suggests the presence of a very low amount of carbon-carbon double bonds as the resonance peaks are much reduced after the hydroxylation reaction (5.35 ppm). Additionally, there is a new peak centered at 1.5 ppm which is due to hydrogen that are neighboring -COH groups in the LOP[8] and that originally belonged to methylene groups neighbors to double bonds (2.3 and 2.8-2.9 ppm). Furthermore, changes can be observed in the region of 3.5-4.0 ppm that is also reported as chemical shifts for protons in carbons linked to hydroxyl groups.[9,10]

These last two observations are relevant to indicate the disappearance of the carbon-carbon double bonds and the appearance of OH containing groups.

3.4 Preparation of the biobased polyurethanes rigid foams

Foams were prepared at room temperature following one-step reaction process by reacting A-side with B-side. First, the B-side: LOP, reactive modifiers (GLY, DEG or PEG), blowing agent (distilled water), surfactant (Tergostab B8404) and catalysts (DMBA and DBTDL) was mechanically premixed for 20 s in a container

and then the A-side (pMDI) was added. The system was further mixed for 20 s and then the foam was allowed to freely rise. Prior their use, LOP and glycerol were dehydrated at 80 °C for 6 h under vacuum. DEG and PEG were not dehydrated, but its water content was taken into account in the formulation, being their water content 0.2 and 0.5 wt% for DEG and PEG, respectively, according to supplier data sheet.

The isocyanate index (moles of NCO groups/moles of OH groups) was adjusted at 1.1 for all the systems. The contributions of LOP, reactive modifiers (GLY/DEG/PEG) and water were taken into consideration in the index calculation. All the mentioned percentages were calculated with respect to the weight of LOP.

The formulation and designation of the polyurethane rigid foams are summarized in Table 3.1. Samples have been designated as PU-xy, where x is the weight percentage of reactive modifier with respect to the weight of LOP and y is the abbreviation of the reactive modifier.

Table 3.1. Designation, formulation for polyurethane rigid foams.

Designation	GLY (wt%)	DEG (wt%)	PEG (wt%)	pMDI (wt%)
PU	-	-	-	44.82
PU–5GLY	5	-	-	49.46
PU–10GLY	10	-	-	53.26
PU–15GLY	15	-	-	56.08
PU–20GLY	20	-	-	58.50
PU–5DEG	-	5	-	47.11
PU–10DEG	-	10	-	49.14
PU–15DEG	-	15	-	50.87
PU–20DEG	-	20	-	52.35
PU–20PEG	-	-	20	47.66

The amount of additives added to the formulation with respect to the weight of LOP was 2 wt% of distilled water, 1.5 wt% of surfactant and 3 wt% of each catalysts (DMBA and DBTDL). A digital image of some of the synthesized biobased polyurethane rigid foams is shown in Figure 3.3.

Figure 3.3. Digital image of the prepared biobased polyurethane rigid foams.

3.5 Characterization of the synthesized biobased polyurethanes rigid foams

3.5.1 Density

The apparent density of the prepared biobased polyurethane rigid foams was measured and the results are shown in Table 3.2.

Table 3.2. Apparent densities for the prepared biobased polyurethane rigid foams.

Sample	ρ (kg m^{-3})
PU	41.01 ± 0.70
PU–5GLY	45.54 ± 0.97
PU–10GLY	45.38 ± 1.34
PU–15GLY	51.56 ± 1.08
PU–20GLY	55.47 ± 0.76
PU–5DEG	43.75 ± 0.63
PU–10DEG	39.05 ± 0.62
PU–15DEG	40.18 ± 0.22
PU–20DEG	40.76 ± 0.92
PU–20PEG	43.86 ± 0.82

As can be observed, density values are higher for the modified biobased foams with the trifunctional GLY. The density increases as GLY content increases due to the decrease of chain length between crosslinking points. Similarly, in foams containing DEG the density also increases with the increase of DEG content except for PU-5DEG. However, if compared with the GLY analogous foams, the DEG series have lower density, which is probably related to the lower pMDI wt% in foams with DEG. This fact decreases allophanate and biuret crosslinking reactions and hence viscosity decreases favoring the blowing efficiency, obtaining lower density values.[11,12] This is also observed for the PU-20PEG that shows lower density than the GLY modified foam.

3.5.2   Morphology

Scanning electron microscopy images of the morphology of the foams analyzed on a plane parallel to the foam rise direction are shown in Figure 3.4. As can be observed non-uniform cell structures with large and small polygonal shaped cells have formed. The irregular distribution of cell sizes observed in reference foam can be related to different structural factors. It must be taken into account that linseed oil is a heterogeneous triglyceride containing different fatty acid chains. Moreover, after the hydroxylation of linseed oil double bonds, OH groups could be in different positions along the chain.[13] Comparing the cell sizes distribution of reference foam and PU-20PEG, more uniform cell sizes can be distinguished in PU-20PEG foam, probably because the addition of an oligomer with a molecular weight similar to the equivalent weight of LOP contributes to reduce the overall chain sizes polydispersity in the polyol mixture. The foams with different amount of GLY and DEG show that cell structure becomes more uniform as reactive modifiers content increases. PU-DEG series shows larger cell sizes than PU-GLY series, due to trifunctional GLY allows reaching higher crosslinking density and hence lower expansion of the cells volume.[11,12] The result of the increased crosslinking density and reduced overall cell size, agrees

with the higher density values measured for this foam series. As can be observed in the micrographs, cell sizes decrease as GLY content increases, in agreement to the observed density increase. This effect is in agreement with the results of other authors that worked with soybean based polyols of different hydroxyl values and found that cell size was smaller in the foams prepared with the polyol of higher OH value.[6] Moreover, as GLY content increases, higher anisotropy can be observed, since the rigidity of the formed network restricts the expansion of the cells during foaming.
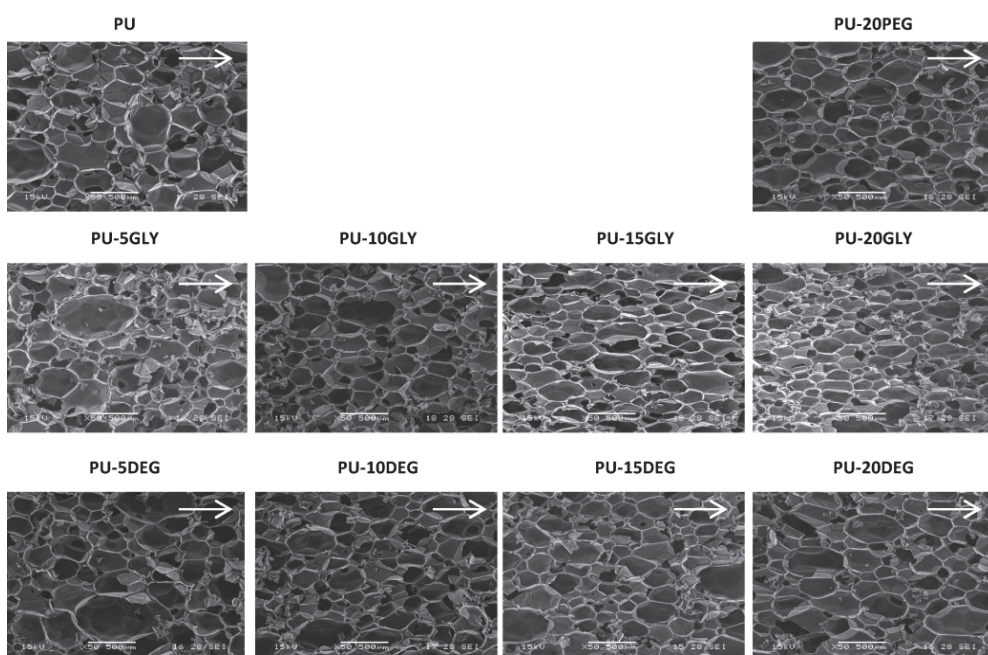
Figure 3.4. SEM images of synthesized foams. Arrows denote the rise direction of the foams.

3.5.3 Cream, end of rise and tack free times

During the reaction, the cream, end of rise and tack free times of foams PU-20GLY, PU-20DEG, PU-20PEG and PU were measured with a digital stopwatch, in order to assess the kinetics of foaming. Cream time is defined as the point where bubble rise starts and the color of the mixture changes from dark brown to cream. Gel time corresponds to stable network formation at the end of rising.

At the tack free time, the outer surface of the foam loses the stickiness and can be removed from the mold.[14] In Table 3.3 the measured characteristic times are shown.

Table 3.3. Foaming characteristic times of foams.

Sample	Cream time (s)	End of rise time (s)	Tack free time (s)
PU	40	160	215
PU-20GLY	42	88	92
PU-20DEG	31	84	90
PU-20PEG	45	117	122

These foams were prepared adding 20 wt% of the three different reactive modifiers with respect to the high-functional polyol derived from linseed oil. The reference foam was the one prepared with linseed oil derived polyol as the only source of hydroxyls. The more clear differences can be established between the end of rise and tack free times of the unmodified PU foam and those of the modified ones. The last ones show shorter characteristic times, this fact is correlated with a higher reactivity of the OH of the smaller molecules and with the higher viscosity of LOP that inhibits a rapid expansion of the foam.[1,11,15] It is reasonable that the reactivity of the OH groups of LOP should be lower because of the internal location of the OH (in the middle of LOP chain) than those present in the lower molecular weight glycerol or the primary OH in the short diols.

Moreover, the addition of 20 wt% of DEG leads to the foam with the lowest characteristic times of the study, which could be related to the combined effects of increased concentration of primary hydroxyl groups in the mixture and viscosity reduction contributed by the low molecular weight DEG.

3.5.4 Fourier transform infrared spectroscopy

The spectra for the synthesized foams containing 0 and 20 wt% of GLY, DEG and PEG together with the spectra of pMDI and neat LOP are shown in Figure 3.5a. All the prepared foams show typical polyurethane foam spectra, confirming that urethane bonds were formed during reaction.[11,15] The spectra of polyurethane foams are similar and the stretching vibrations of the isocyanate group (N=C=O) of pMDI at 2270 cm^{-1} and the hydroxyl group (O-H) of LOP centered at 3500 cm^{-1} are not observed, which confirms that reaction proceeded successfully. Moreover, a broad band at 3200-3400 cm^{-1}, characteristic of the stretching vibration of the urea and urethane N-H bond,[16,17] can be observed in the spectra of all the polyurethane foams.
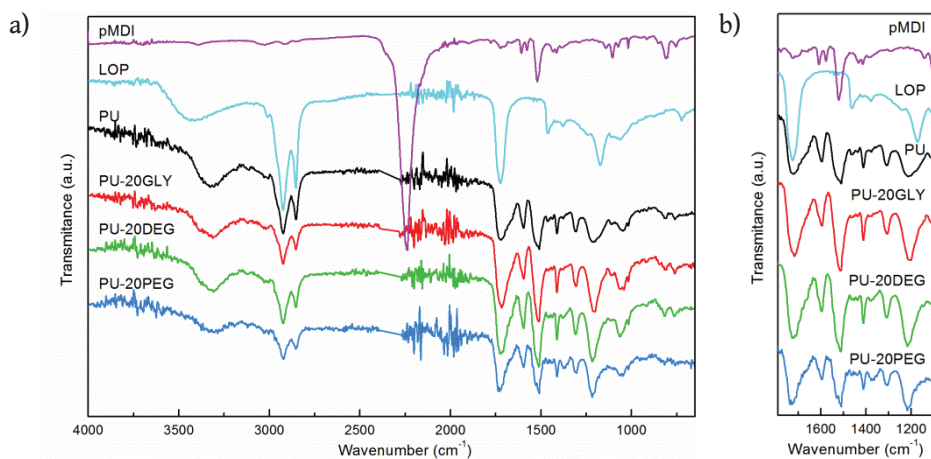
Figure 3.5. a) FTIR spectra of PU, PU-20GLY, PU-20DEG, PU-20PEG foams, as well as neat pMDI and LOP and b) magnification from 1800 to 1100 cm^{-1}.

On the other hand, in Figure 3.5b a magnification of the FTIR spectra is shown from 1800 to 1100 cm^{-1}. As can be observed in the carbonyl stretching region (1630-1730 cm^{-1}), in addition to the carbonyl group stretching vibration at 1740 cm^{-1}, corresponding to the LOP ester group, a shoulder at lower wavenumber related to the carbonyl group stretching vibration of urethane and urea groups (amide-I band) can be observed.[18–21] At 1535 cm^{-1} the amide-II band related to

bending vibration of N-H combined with stretching vibration of C-N can be also seen. Besides, at 1221 cm^{-1} the stretching vibrations of C-N can be observed.[20–22]

3.5.5   Dynamic mechanical analysis

The dynamic mechanical behavior of the foams prepared with different amount of GLY was analyzed studying the evolution of storage modulus and loss modulus with temperature, Figures 3.6a and 3.6b, respectively.

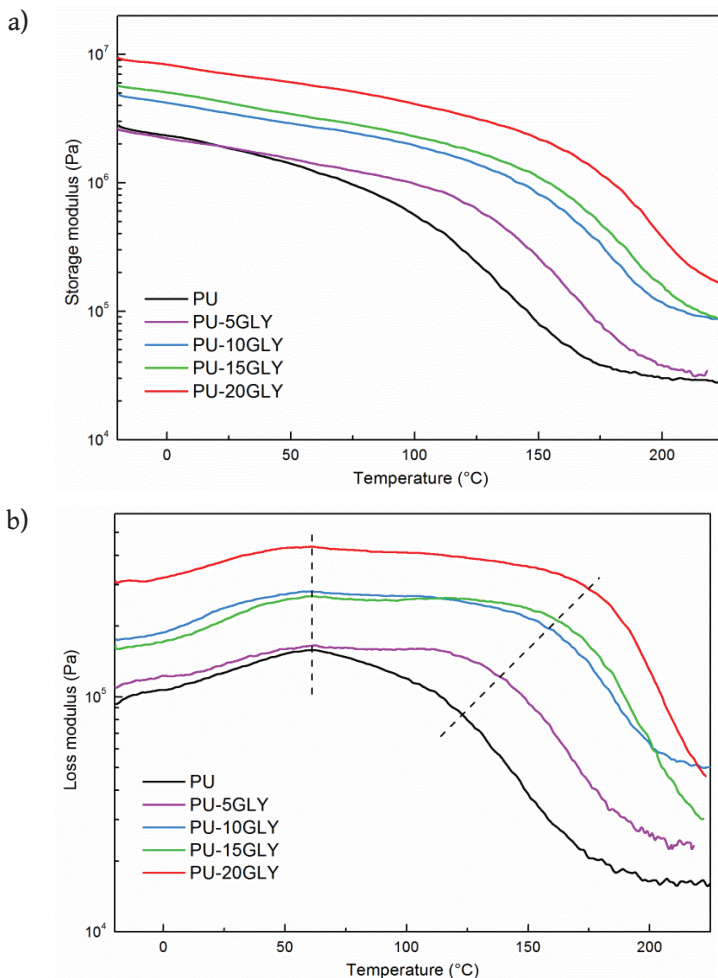**Figure 3.6.** a) Storage modulus of the series of foams prepared with GLY and b) loss modulus of the series of foams prepared with GLY. In both sets of curves, the one corresponding to the PU is added for comparison.

As can be observed, storage modulus at room temperature of the samples increases as the concentration of GLY in the formulation increases. This feature is result of different contributing effects. On the one hand, the higher amount of GLY increases the crosslinking density of the foam since GLY is a trifunctional small molecule. On the other hand, because of the low equivalent weight of the GLY, the higher the GLY concentration, the higher the pMDI percentage in the formulation (in order to maintain constant the NCO:OH molar ratio). The higher crosslinking density improves the cohesive density of the material and the incorporation of increasing amounts of the aromatic and polyfunctional isocyanate also contributes to increase the rigidity of the polymer. These effects are also observed in the rubbery region of these materials, although in some cases the expected rubbery plateau would be fully developed at temperatures above those used in the tests.

The glass-rubber transition is wide for all the foams, and shifts towards higher temperatures as GLY content increases in the initial formulation, in perfect agreement with the effects already discussed for the storage modulus.

The maximum observed in the loss modulus is related with the thermal transition. As can be observed, the transition from glass to rubber is wide and it is the sum of two overlapping events. There is a low temperature transition occurring around 50 °C that does not suffers shift although the composition of the material changes. This transition could corresponded to the relaxation of the dangling chains that are formed when the hydroxylated oil reacts. On the other hand, the higher temperature relaxation, which is related to the glass transition temperature of the polyurethane network, varies with GLY concentration (shown with dashed lines in figure 3.6b). This is in agreement with the increased crosslinking density of the material.

Similar effects can be observed in storage modulus and loss modulus curves of the DEG containing samples, Figure 3.7a and 3.7b, respectively. However,

variations on the storage modulus are much more moderate and the T_g are lower than observed in the glycerol containing samples, due to DEG contributes to the formation of longer chains increasing the mobility of the network.[23]

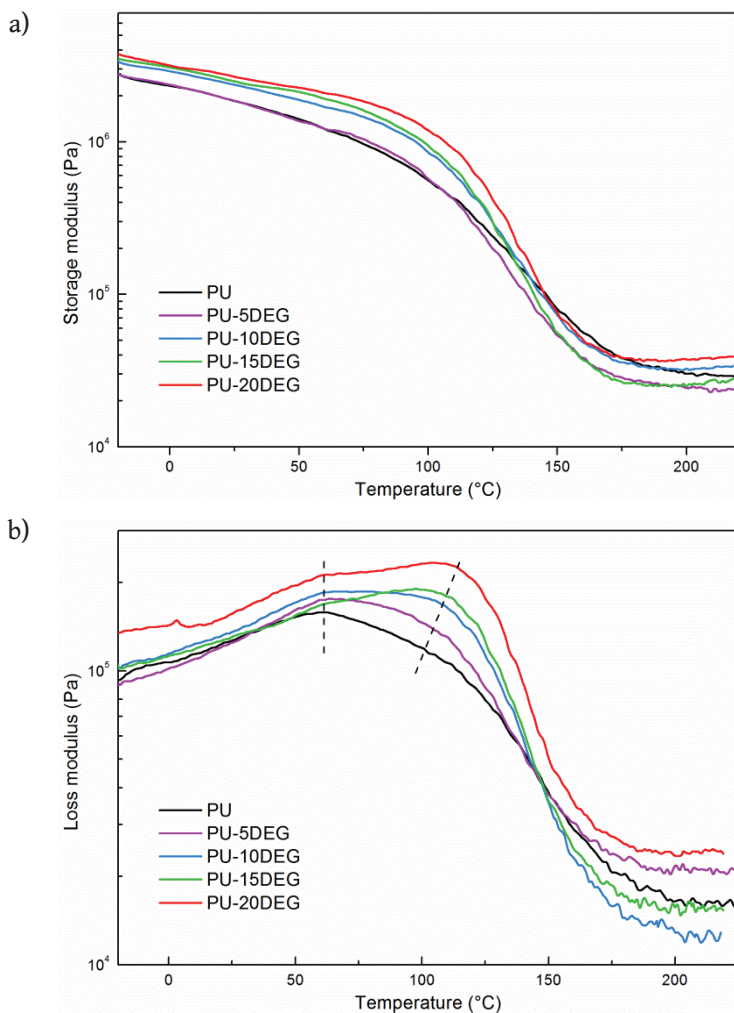**Figure 3.7.** a) Storage modulus of the series of foams prepared with DEG and b) loss modulus of the series of foams prepared with DEG. In both sets of curves, the one corresponding to the PU is added for comparison.

The comparison of the loss modulus of materials prepared with 20 wt% of the three different reactive modifiers and the unmodified linseed oil based biopolyol is presented in Figure 3.8.
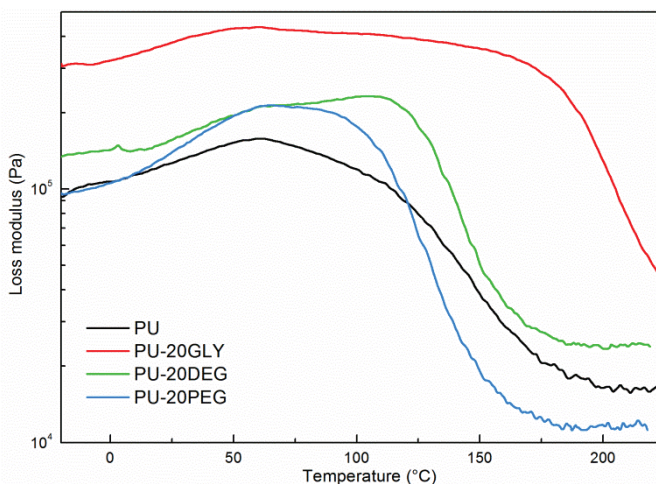
Figure 3.8. Loss modulus of foams prepared with 20% replacement of LOP by other reactive modifiers and PU reference foam.

As can be observed, PU-20GLY foam shows a broader and higher temperature transition than the other formulations. Instead, the incorporation of the diols led to narrower transitions than those measured for GLY containing samples or even the linseed oil based foams. PEG containing foam shows the lowest T_g, because the diol does not contribute to crosslinking and the longer chains of PEG adds mobility to the network.[23] It must be noticed also that the pMDI wt% is also the lowest in this sample (Table 3.1), which also contributes to higher chain mobility.

3.5.6   Compression properties

The mechanical behavior of the synthesized biobased polyurethane rigid foams was studied by performing compression tests. In Figure 3.9 the compressive stress-strain curves for the GLY set of samples is shown. As can be observed the samples showed the typical compression behavior. There is an initial linear elastic response of stress vs. strain, followed by an extended plateau (in certain cases preceded by a local maximum at the yield point) and a final region of increasing stress.[24–26] Initial bending and buckling occurs on the cell walls as compression is applied, but some cracking initiates at the yield point and the

plateau is the result of progressive brittle crushing of the cells under the compressive loads. In the final region, densification of the foam is controlling the material behavior that becomes closer to that of a non-foamed one.

Moreover, as can be seen the concentration of GLY leads to the increase of the modulus and the stress value of the stress plateau, while overall reducing the deformation at the yield point (linseed oil PU does not follow the trend) and that of the deformation at which densification settles down. The increased fragility and higher rigidity of the cell walls due to increased crosslinking density and isocyanate concentration leads to the observed trend on the two critical compression strains.[11,26]
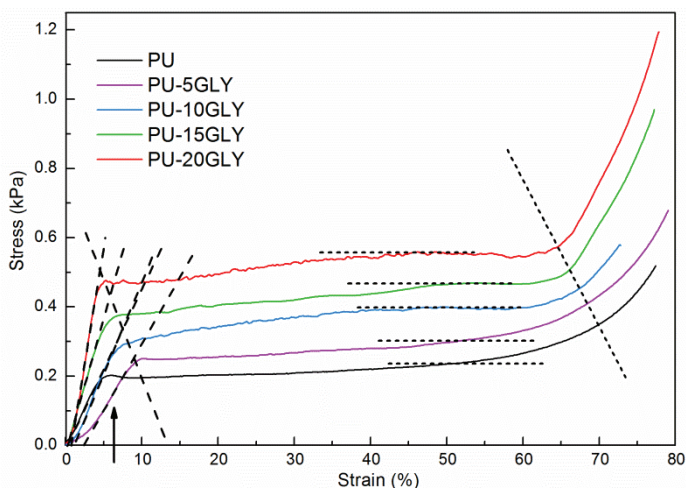
Figure 3.9. Stress-strain curves of reference foam and GLY containing foam series.

The compression properties of all the prepared foams are summarized in Table 3.4. The deformation at which densification appears is in the range of 62-69% strain for all the foams, with the lowest value occurring for the unmodified foam, closely followed by the PU-20PEG sample. This could be related to the similar equivalent weight of LOP and PEG as well as similar initial concentration of pMDI in the formulation. On the other hand, the smallest modifier, DEG, leads to the highest values for the deformation at the densification point ($\varepsilon_{densification}$).

Recovery ratio refers to the ability of the material to recover its original shape after being deformed and thus relates to resilience. A greater recovery ratio indicates a greater degree of rebound of a material after being compressed.[26] The large difference between the instantaneous recovery (Rr_1) and that measured after 24 hours (Rr_{24}) indicates that these foams are viscoelastic materials with long relaxation times. This behavior denotes that samples are not elastic bodies, since the recovery ratio is far from 100%, and hence they show a low resilience. The highest recovery was reached for the reference foam due to the nature of the biopolyol that presents alkyd chains and relatively long pendant chains that add mobility to the structure. Additionally, a functionality per molecule higher than three (it acts as a crosslinker) and a high relatively equivalent weight allows achieving a highly crosslinked structure with high capability for deformation recovery.

Table 3.4. Compression properties of foams.

Sample	E (kPa)	σ_y (kPa)	ε_y (%)	$\varepsilon_{densification}$ (%)	Rr_1 (%)	Rr_{24} (%)
PU	4.2 ± 0.6	0.20 ± 0.01	5.3 ± 0.8	62.7 ± 2.4	59.5 ± 2.6	81.8 ± 2.0
PU–5GLY	3.5 ± 0.6	0.24 ± 0.02	8.8 ± 1.4	64.1 ± 0.6	58.2 ± 1.8	75.5 ± 1.4
PU–10GLY	7.4 ± 2.4	0.30 ± 0.01	5.3 ± 1.2	65.7 ± 0.9	58.3 ± 2.7	74.7 ± 2.6
PU–15GLY	10.7 ± 2.2	0.40 ± 0.02	4.6 ± 1.0	66.3 ± 0.5	54.2 ± 2.7	70.8 ± 3.2
PU–20GLY	12.7 ± 3.0	0.47 ± 0.02	4.7 ± 0.9	66.4 ± 0.3	54.4 ± 0.6	71.1 ± 1.9
PU–5DEG	3.9 ± 0.2	0.22 ± 0.01	6.5 ± 0.9	68.5 ± 1.7	57.5 ± 2.4	74.6 ± 2.9
PU–10DEG	4.7 ± 0.5	0.21 ± 0.01	5.4 ± 0.2	67.2 ± 0.9	56.4 ± 1.9	71.2 ± 1.9
PU–15DEG	5.4 ± 0.5	0.24 ± 0.01	5.0 ± 0.5	64.5 ± 0.4	54.6 ± 1.0	66.5 ± 0.2
PU–20DEG	6.0 ± 0.4	0.26 ± 0.02	5.0 ± 0.3	65.1 ± 1.6	55.0 ± 0.8	66.3 ± 0.2
PU–20PEG	5.7 ± 0.3	0.23 ± 0.01	4.7 ± 0.3	63.1 ± 1.8	55.2 ± 0.4	67.2 ± 0.5

The analysis of the mechanical properties highlights the effect of the foam density and the chemistry of the formulation.[27] Changing the nature of the polyol mixture used, changes the amount of pMDI added to maintain constant (and equal to 1.1) the NCO:OH molar ratio, which in turn changes the

crosslinking density and the rigidity of the polymer chains that form the network. For these reasons, the results were further analyzed by comparing the specific modulus (modulus/foam density) and specific stress at yield (yield stress/foam density) vs pMDI wt% in Figures 3.10a and 3.10b. The lines are included to facilitate the analysis.
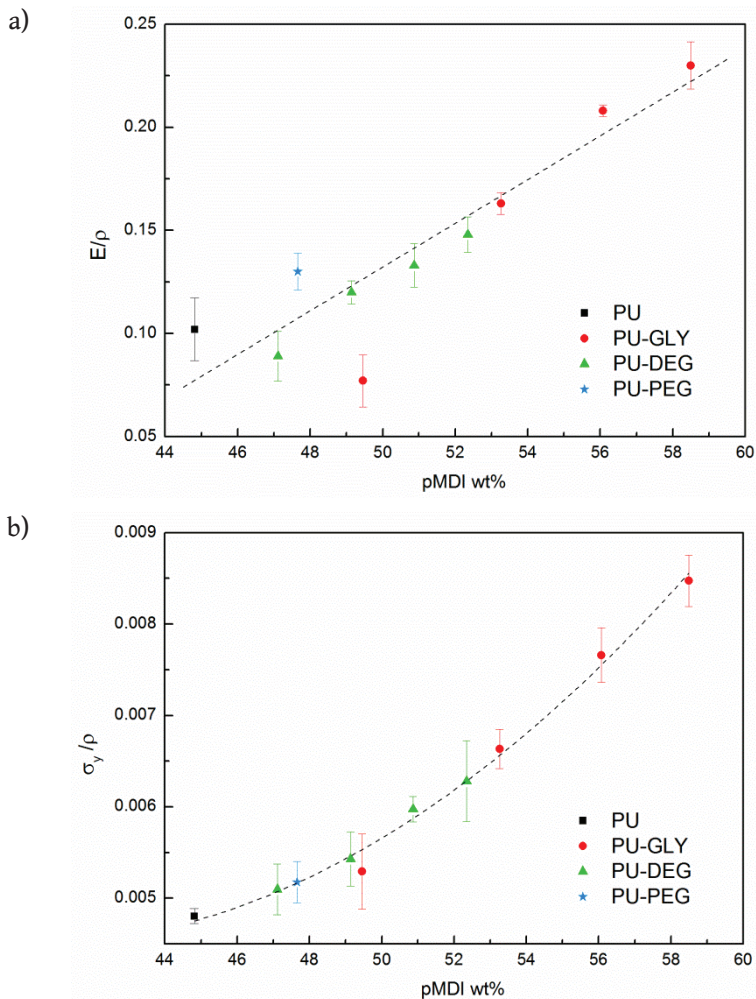

Figure 3.10. a) Specific modulus and b) specific yield stress as function of the percentage of pMDI in the initial formulation for all foams prepared.

As can be observed, it appears that density and isocyanate concentration in the initial formulation are the controlling factors that lead to the observed behavior

of the samples. In particular, the specific yield stress shows the collapse of the results of all the samples in a single curve that also includes the sample made from LOP without additional OH components.

3.5.7 Thermal stability

The thermal stability of PU, PU-20GLY, PU-20DEG and PU-20PEG foams was analyzed by thermogravimetric analysis and their thermograms are shown in Figure 3.11. As can be seen the degradation profiles of the samples is similar. The thermal stability of polyurethane foams depends on the crosslink density, cure conditions and the structure of the network.

As observed in Figure 3.11, PU-20GLY foam is more stable than the rest of the foams (degradation beginning about 15 °C above that of the unmodified foam). This can be due to the higher functionality of GLY (trifunctional) with respect to DEG and PEG (difunctional), resulting in a more crosslinked network and hence higher activation energies would be needed to start thermal degradation.[11] For all foams, two degradation steps can be distinguished. The first one, in the temperature range of 250-335 °C, corresponds to urethane bond degradation.[28,29] Since degradation starts at urethane groups, once that they are broken the foams prepared with low molecular weight modifiers will release volatile compounds with higher probability. Thus, PU-20DEG shows the largest mass loss, followed by PU-20PEG, PU-20GLY and PU.

In the temperature range of 370-500 °C, the residues formed during the first degradation step further degrade to form char residue. Moreover, it can be noted that the char residue of PU-20GLY, about 550 °C, is higher than that of the rest of the systems (26%), which can be related to the high content of pMDI in the initial formulation of the PU-20GLY system (see Table 3.1). On the other hand, the reference foam presents the lowest char value (14%), probably also related to the lowest aromatic isocyanate content in the formulation.[30]
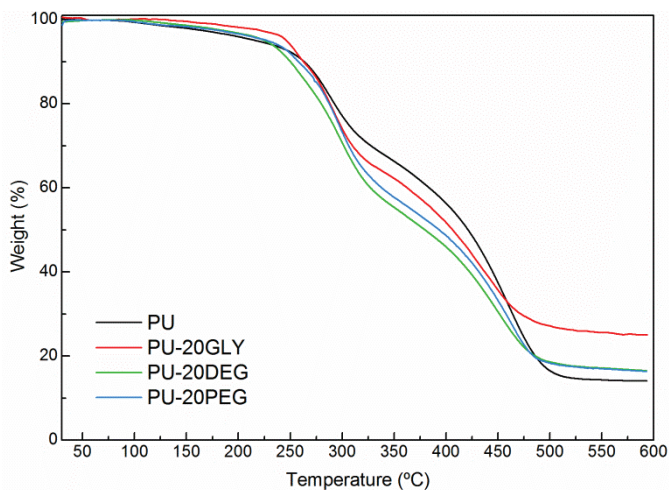
Figure 3.11. Thermogravimetric behavior of PU, PU-20GLY, PU-20DEG and PU-20PEG foams.

3.6 Conclusions

Biobased rigid polyurethane foams were prepared using a polyol derived from linseed oil. The replacement of the linseed oil polyol by hydroxyl-containing modifiers of lower molecular weight in concentrations between 0 and 20 wt% change the reactivity of the system and directly affected the final properties of the foams.

The modified foams showed shorter characteristic times that the reference foam, which was related to a higher reactivity of the OH groups of the modifiers and the lower initial viscosity of the modified systems.

The dynamic mechanical tests showed an increase on the glass transition of the glycerol modified foam, which also showed the highest storage modulus among the different series. This modification also leads to higher compression properties. The analysis of the compression results highlighted the importance of the concentration of the polymeric isocyanate in the initial formulation. The pMDI concentration also played a rol in the char formation of the foams according to thermogravimetric analysis. The higher density of crosslinking of

the GLY modified foam resulted in a better thermal stability among the different foams.

3.7   References

1.   Y.H. Hu, Y. Gao, N. De Wang, C.P. Hu, S. Zu, L. Vanoverloop, D. Randall. "Rigid polyurethane foam prepared from a rape seed oil based polyol". J. Appl. Polym. Sci. 2002. 84: 591–597.

2.   ASTM D5554-15. "Standard test method for determination of the iodine value of fats and oils". ASTM International. West Conshohocken, PA, 2015.

3.   ASTM D4274-16. "Standard test methods for testing polyurethane raw materials: determination of hydroxyl numbers of polyols". ASTM International. West Conshohocken, PA, 2016.

4.   M. Mosiewicki, M.I. Aranguren, J. Borrajo. "Mechanical properties of linseed oil monoglyceride maleate/styrene copolymers". J. Appl. Polym. Sci. 2005. 97: 825–836.

5.   M. Lazzari, O. Chiantore. "Drying and oxidative degradation of linseed oil". Polym. Degrad. Stab. 1999. 65: 303–313.

6.   R. Gu, S. Konar, M. Sain. "Preparation and characterization of sustainable polyurethane foams from soybean oils". J. Am. Oil Chem. Soc. 2012. 89: 2103–2111.

7.   A. Spyros, D. Anglos. "Studies of organic paint binders by NMR spectroscopy". Appl. Phys. A Mater. Sci. Process. 2006. 83: 705–708.

8.   G. López Téllez, E. Vigueras-Santiago, S. Hernández-López. "Characterization of linseed oil epoxidized at different percentages". Superf. y Vacío. 2009. 22: 5–10.

9. S. Caillol, M. Desroches, G. Boutevin, C. Loubat, R. Auvergne, B. Boutevin. "Synthesis of new polyester polyols from epoxidized vegetable oils and biobased acids". Eur. J. Lipid Sci. Technol. 2012. 114: 1447–1459.

10. J. Zhang, Y.J. Zhao, Z.G. Su, G.H. Ma. "Sythesis of monomethoxy poly(ethylene glycol) without diol poly(ethylene glycol)". J. Appl. Polym. Sci. 2007. 105: 3780–3786.

11. L. Ugarte, S. Gómez-Fernández, C. Peña-Rodríguez, A. Prociak, M.A. Corcuera, A. Eceiza. "Tailoring mechanical properties of rigid polyurethane foams by sorbitol and corn derived biopolyol mixtures". ACS Sustain. Chem. Eng. 2015. 12: 3382–3387.

12. H. Lim, S.H. Kim, B.K. Kim. "Effects of the hydroxyl value of polyol in rigid polyurethane foams". Polym. Adv. Technol. 2008. 19: 1729–1734.

13. M. Heinen, A.E. Gerbase, C.L. Petzhold. "Vegetable oil-based rigid polyurethanes and phosphorylated flame-retardants derived from epoxydized soybean oil". Polym. Degrad. Stab. 2014. 108: 76–86.

14. K. Ashida. Polyurethane foams in polyurethane and related foams: chemistry and technology. CRC Press, Boca Raton, FL, 2007.

15. A.A. Septevani, D.A.C. Evans, C. Chaleat, D.J. Martin, P.K. Annamalai. "A systematic study substituting polyether polyol with palm kernel oil based polyester polyol in rigid polyurethane foam". Ind. Crops Prod. 2015. 66: 16–26.

16. J.L. Rivera-Armenta, T. Heinze, A.M. Mendoza-Martínez. "New polyurethane foams modified with cellulose derivatives". Eur. Polym. J. 2004. 40: 2803–2812.

17. S.S. Narine, X. Kong, L. Bouzidi, P. Sporns. "Physical properties of

polyurethanes produced from polyols from seed oils. II. Foams". J. Am. Oil Chem. Soc. 2007. 84: 65–72.

18. M.J. Elwell, A.J. Ryan, H.J.M. Grunbauer, H.C. VanLieshout. "In-situ studies of structure development during the reactive processing of model flexible polyurethane foam systems using FT-IR spectroscopy, synchrotron SAXS, and rheology". Macromolecules 1996. 29: 2960–2968.

19. A.M. Heintz, D.J. Duffy, C.M. Nelson, Y. Hua, S.L. Hsu, C.W. Paul. "A spectroscopic analysis of the phase evolution in polyurethane foams". Macromolecules 2005. 38: 9192–9199.

20. P. Singhal, W. Small, E. Cosgriff-Hernandez, D.J. Maitland, T.S. Wilson. "Low density biodegradable shape memory polyurethane foams for embolic biomedical applications". Acta Biomater. 2014. 10: 67–76.

21. L. Ugarte, A. Saralegi, R. Fernández, L. Martín, M.A. Corcuera, A. Eceiza. "Flexible polyurethane foams based on 100% renewably sourced polyols". Ind. Crops Prod. 2014. 62: 545–551.

22. A.A. Abdel Hakim, M. Nassar, A. Emam, M. Sultan. "Preparation and characterization of rigid polyurethane foam prepared from sugar-cane bagasse polyol". Mater. Chem. Phys. 2011. 129: 301–307.

23. K.I. Suresh. "Rigid polyurethane foams from cardanol: synthesis, structural characterization, and evaluation of polyol and foam properties". ACS Sustain. Chem. Eng. 2013. 1: 232–242.

24. G. Tondi, V. Fierro, A. Pizzi, A. Celzard. "Tannin-based carbon foams". Carbon 2009. 47: 1480–1492.

25. M.F. Ashby. "The properties of foams and lattices". Philos. Trans. A. Math. Phys. Eng. Sci. 2006. 364: 15–30.

26. V. Ribeiro Da Silva, M.A. Mosiewicki, M.I. Yoshida, M. Coelho Da Silva, P.M. Stefani, N.E. Marcovich. "Polyurethane foams based on modified tung oil and reinforced with rice husk ash II: mechanical characterization". Polym. Test. 2013. 32: 665–672.

27. Y.C. Tu, P. Kiatsimkul, G. Suppes, F.H. Hsieh. "Physical properties of water-blown rigid polyurethane foams from vegetable oil-based polyols". J. Appl. Polym. Sci. 2007. 105: 453–459.

28. S. Gómez-Fernández, L. Ugarte, C. Peña-Rodriguez, M.A. Corcuera, A. Eceiza. "The effect of phosphorus containing polyol and layered double hydroxides on the properties of a castor oil based flexible polyurethane foam". Polym. Degrad. Stab. 2016. 132: 41–51.

29. J. Lefebvre, M. Le Bras, B. Bastin, R. Paleja, R. Delobel. "Flexible polyurethane foams: Flammability". J. Fire Sci. 2003. 21: 343–367.

30. S. Wang, H. Chen, L. Zhang. "Thermal decomposition kinetics of rigid polyurethane foam and ignition risk by a hot particle". J. Appl. Polym. Sci. 2014. 131: 39359.

CHAPTER 4

CROSSLINKED BIOBASED POLYURETHANES
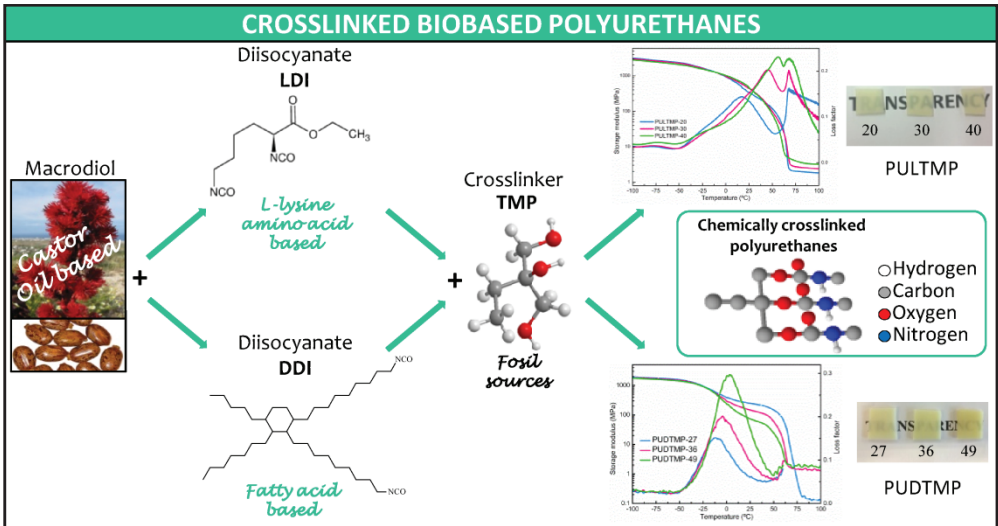
4. CROSSLINKED BIOBASED POLYURETHANES

4.1 Aim of the chapter

The aim of this chapter was to synthesize and characterize two series of crosslinked biobased polyurethanes. For this purpose two different diisocyanates derived from renewable sources were used: ethyl ester L-lysine diisocyanate (LDI), based on L-lysine amino acid, and 2-heptyl-3,4-bis(9-isocyanatononyl)-1-pentylcyclohexane (DDI), obtained from fatty acids. In both crosslinked polyurethane series the same macrodiol and crosslinker were used. As macrodiol poly(butylene sebacate)diol (CO3) derived from castor and as crosslinker 1,1,1-tris-(hydroxymethyl)propane (TMP) with primary hydroxyl groups were used. The influence of the molar ratio of the components, the nature of the diisocyanate and crosslink density on the final properties was analyzed.

First, a kinetic study was performed to establish the polymerization conditions. The crosslinked biobased polyurethanes were synthesized by a two-steps bulk polymerization process, varying the molar ratio of diisocyanate/crosslinker. The thermal behavior was analyzed by means of differential scanning calorimetry and dynamic mechanical analysis. The physicochemical characterization was performed by FTIR, while mechanical behavior was analyzed performing tensile and Shore D hardness tests. The morphology of the synthesized biobased polyurethanes was also analyzed by atomic force microscopy. Finally, the surface behavior by measuring water contact angle and the biocompatibility of the materials was studied.

4.2 Kinetic study

The reaction between the macrodiol and the different diisocyanates was followed by FTIR spectroscopy, as explained in chapter 2. In this way, since conversion is related with absorbance changes, it was possible to determine the

conversion rate of the polymerization by measuring the peak height of N-C=O group (2270 cm^{-1}) and C-H bond (2870 cm^{-1}) and applying equation 2.1.

4.2.1 Crosslinked biobased polyurethanes from LDI

Figure 4.1 shows a series of spectra between 3600 and 1600 cm^{-1} obtained during the polymerization reaction of CO3 and LDI in stoichiometric ratio at 100 °C. Isocyanate group peak height at 2270 cm^{-1} decreases with time as a consequence of the reaction between hydroxyl and isocyanate groups to form urethane groups. Therefore, a small new peak related to stretching vibration of N-H bond of urethane group appears at 3365 cm^{-1}. In the inset, reaction conversion is shown as function of time. The reaction was considered to be ended when the peak at 2270 cm^{-1} disappeared or when the conversion values (α), was close to 1. Therefore, the first step of polymerization was established as 5 h at 100 °C for all the synthesized biobased polyurethanes from LDI.

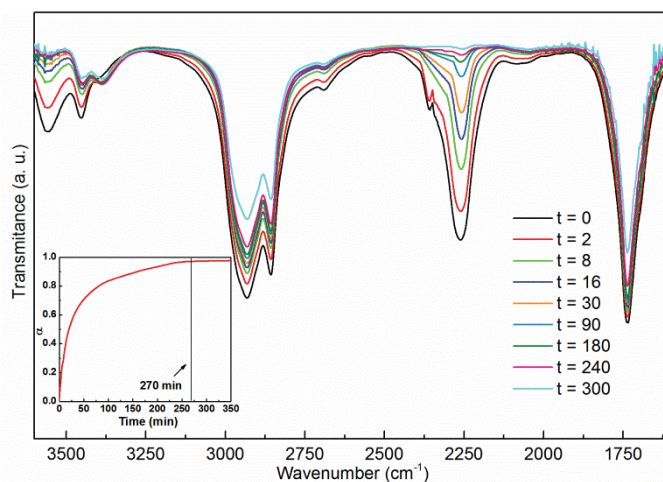**Figure 4.1.** FTIR spectra of the reaction between CO3 and LDI in stoichiometric ratio followed at 100 °C. Inset: reaction conversion as function of time.

4.2.2 Crosslinked biobased polyurethanes from DDI

The evolution of the polymerization reaction when DDI was employed as diisocyanate was also followed by FTIR, as can be observed in Figure 4.2. A lower

polymerization temperature was used, 80°C, if compared with LDI, since it was seen at 100 °C that the polymerization reaction was considerably faster. The results obtained indicate that the reaction conversion was stabilized at its maximum value after 190 min of reaction. Therefore, taking into account the obtained results, the first step of polymerization was established as 4 h at 80 °C for all biobased polyurethanes with DDI.
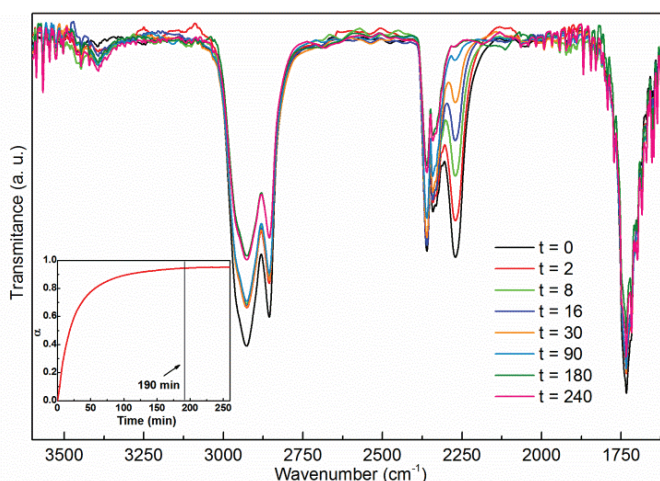

Figure 4.2. FTIR spectra of the reaction between CO3 and DDI in stoichiometric ratio at 80 °C. Inset: reaction conversion as function of time.

4.3 Synthesis of the crosslinked polyurethanes

Biobased crosslinked polyurethanes were synthesized in bulk and without catalyst, by a two-step bulk polymerization procedure. The reaction was carried out in a 250 mL five-neck round-bottom flask equipped with a mechanical stirrer and a dry nitrogen inlet. Firstly, the dried macrodiol (CO3) and diisocyanate (LDI or DDI) were placed in the flask and heated in a thermo-regulated silicon bath stabilized at the reaction conditions, in order to obtain the prepolymer during 5 h at 100 °C for CO3/LDI and 4 h at 80 °C for CO3/DDI series. Then, the crosslinker (TMP) was added to the prepolymer at the same temperature while stirring vigorously for 10-15 min to homogenize the mixture. Finally, the resulting viscous liquid was quickly poured between two Teflon®

coated metal plates separated by 1.5 mm. Subsequently, several compression-decompression cycles were applied in order to remove the stuck air bubbles within the polyurethane and then it was pressed at 100 °C under 50 bar for 10 h. The biobased polyurethane was left to cool down to room temperature inside the mold. The cooling process was controlled for all material by controlling the air flow rate and the pressure (50 bar). The NCO to OH group molar ratio of all biobased polyurethanes was kept constant at 1.01. In addition, pure diisocyanate/TMP biobased polyurethanes were synthesized for comparison, PULTMP-100 (from LDI) and PUDTMP-100 (from DDI). The CO3/diisocyanate/TMP molar ratios and diisocyanate/TMP content (calculated as weight percentage of diisocyanate and TMP respect to total biobased polyurethane weight) are shown in Table 4.1. Sample code is expressed as PUxTMP-y, where x is the first letter of the abbreviation of the diisocyanate name L (for LDI) or D (for DDI), and y is the diisocyanate/TMP content (wt%).

Table 4.1. Designation, molar ratio and diisocyanate/TMP content of the crosslinked biobased polyurethanes.

Sample designation	Molar ratio			Diisocyante/TMP (wt%)
	CO3	Diisocyanate	TMP	
PULTMP-20	1	2.02	1	20
PULTMP-30	1	3.03	2	30
PULTMP-40	1	8.08	7	40
PULTMP-100	0	1.00	1	100
PUDTMP-27	1	2.02	1	27
PUDTMP-36	1	3.03	2	36
PUDTMP-49	1	5.05	4	49
PUDTMP-100	0	1.00	1	100

4.4 Characterization of the synthesized crosslinked biobased polyurethanes from LDI

4.4.1 Biobased carbon content

The biobased carbon content of the starting materials was determined by the ASTM-D6866-12 (0.98) Method B (AMS) standard procedure.[1] The macrodiol has a 72% biobased carbon content and LDI a 81% biobased carbon content, and since TMP is a petroleum derived reactant, its biobased carbon content is 0%. In order to estimate the biobased carbon content of the final polyurethanes, the equation 2.2 was used where the molar ratio and the biobased carbon content of each component in the final formulation was taken into account. The estimated biobased carbon content of the synthesized polyurethanes is shown in Table 4.2.

Table 4.2. Biobased carbon content of the synthesized PULTMP crosslinked polyurethanes.

Sample	Biobased carbon content (%)
PULTMP-20	69
PULTMP-30	67
PULTMP-40	64
PULTMP-100	51

As can be observe as LDI/TMP content increases the biobased carbon content of the material decreases according to the lower amount of macrodiol biobased carbons. Nevertheless, the contribution of biobased CO3 and LDI is high enough to be able to obtain crosslinked polyurethanes with biobased carbon content higher than 50%.

4.4.2 Fourier transform infrared spectroscopy

The characteristic functional groups of the synthesized polyurethanes were analyzed by means of FTIR.

In Figure 4.3 the infrared spectra of the polyurethanes, as well as pure CO3 macrodiol and neat LDI spectra are shown.
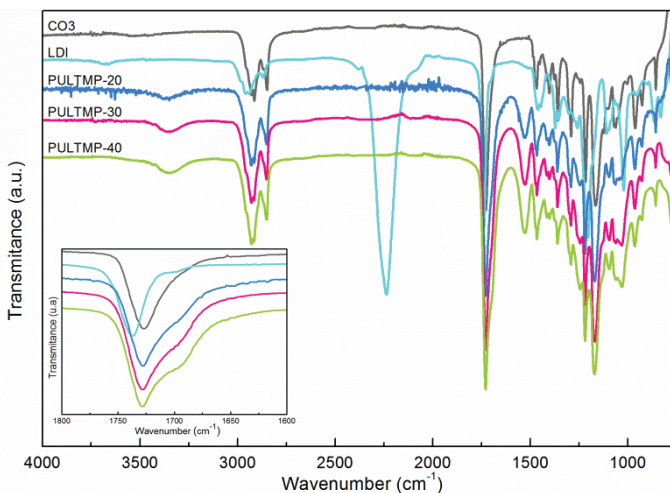

Figure 4.3. FTIR spectra of the synthesized PULTMP biobased polyurethane series, CO3 and LDI. Inset: carbonyl group stretching region.

As can be observed, PULTMP polyurethane series does not show the band associated with N=C=O group stretching vibration at 2270 cm^{-1}, meaning that all the isocyanate groups have reacted during the polymerization. Furthermore, all of them show a broad band centered at 3350 cm^{-1}, ascribed to the N-H stretching vibration of urethane groups.[2,3] In the same way, at 1528 cm^{-1} a band associated to N-H out-of-plane bending combined to C-N stretching vibration can be seen.[4,5] Both bands become more intense as isocyanate content increases due to a higher content of urethane groups. As can be observed in the inset, where the carbonyl group stretching region is shown, the macrodiol and the LDI present a band at 1728 and 1738 cm^{-1} respectively, associated to carbonyl stretching vibration in ester groups.[6] Regarding the synthesized polyurethanes, all of them show a broad band at 1728 cm^{-1}, encompassing the carbonyl groups of CO3 and LDI. Moreover, it is well known that the infrared absorbance of C=O (amide I band) and N-H groups in polyurethanes shifts to different wavenumbers depending on whether they are free or hydrogen bonded.[7,8] In the case of

carbonyl groups, non-bonded (free) carbonyl groups appear at 1718-1730 cm^{-1}, while hydrogen bonded carbonyl groups in disordered (amorphous) conformations can be observed at 1708-1715 cm^{-1} and hydrogen bonded carbonyl groups in ordered (crystalline) domains are also observed at 1680-1700 cm^{-1}.[8,9] Regarding N-H groups, the peaks related to the stretching vibration of non-bonded N-H groups appear at around 3450-3390 cm^{-1}, while the hydrogen bonded N-H groups appears around 3330 cm^{-1}.[9–11] Therefore, the band centered at 1728 cm^{-1} also encompasses the C=O stretching vibration of free urethane groups. Furthermore, this band shows a shoulder around 1698 cm^{-1} attributed to hydrogen bonded C=O urethanes groups stretching vibration,[12] which becomes more noticeable as LDI/TMP content increases.

Furthermore, in order to a deeper analysis of the influence of LDI/TMP content in hydrogen-bonding, the baseline corrected amide I region was deconvoluted, by means of Gaussian curve-fitting method in OriginPro 8.6 software. The peaks resolved into Gaussian curves are shown in Figure 4.4. The area of hydrogen-bonded urethane carbonyl groups band (II) respect to total area (%) was calculated.[8]
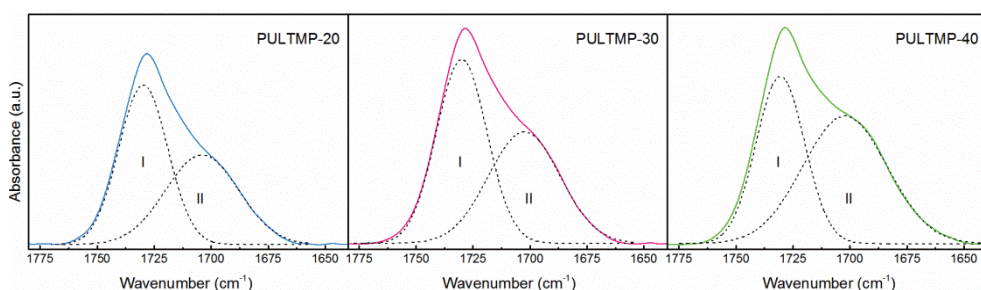

Figure 4.4. Peak deconvolution (dot lines) of baseline corrected C=O stretching bands of the synthesized PULTMP biobased polyurethane series, C=O free stretching (I) and C=O hydrogen-bonded stretching (II) bands.

The obtained areas were 45.5, 46.2 and 57.1% for PULTMP-20, PULTMP-30 and PULTMP-40, respectively. The increase of the area of the band II as LDI/TMP content increases denotes a higher amount of hydrogen-bonded urethane

carbonyl groups. This fact could be attributed to a higher amount of urethane groups per unit volume as mentioned before.

4.4.3   Differential scanning calorimetry

The DSC thermograms of the synthesized polyurethanes, together with the thermograms of pure CO3 and neat LDI/TMP are shown in Figure 4.5a. The thermal behavior was analyzed by DSC and the thermal transitions are listed in Table 4.3.
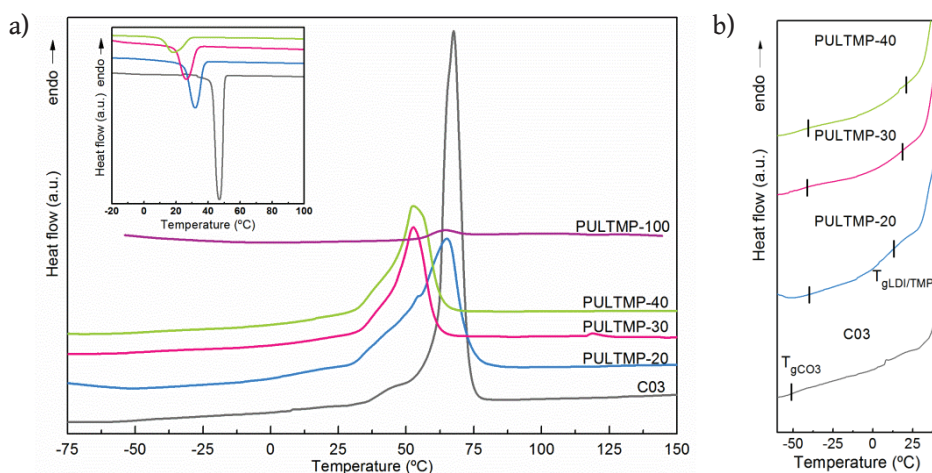

Figure 4.5. a) Heating DSC thermograms of CO3, LDI/TMP and the synthesized PULTMP biobased polyurethane series and b) magnification of the low temperature region. Inset: cooling DSC thermograms.

Table 4.3. Thermal transitions of macrodiol and the synthesized PULTMP polyurethane series.

Sample	T_{gCO3} (°C)	T_m (°C)	ΔH_m (J g^{-1})	$T_{gLDI/TMP}$ (°C)	T_c (°C)	ΔH_c (J g^{-1})	χ_c heating	χ_c cooling
CO3	-52.0	70.0	142.0	–	46.3	-93.1	1	1
PULTMP-20	-40.0	65.0	77.8	13.6	32.1	-51.0	0.7	0.7
PULTMP-30	-41.1	52.8	54.2	19.1	20.9	-36.5	0.5	0.6
PULTMP-40	-40.6	52.2	52.7	22.6	18.4	-24.9	0.6	0.5
PULTMP-100	–	–	–	59.3	–	–	–	–

The semicrystalline CO3 shows a T_g at -52 °C and an endothermic peak associated to crystals melting centered at 70 °C. However, the amorphous LDI/TMP shows a T_g at 59 °C.

Regarding the synthesized polyurethanes, all of them show several thermal transitions related to those observed for the macrodiol and the neat LDI/TMP. The T_g is an indicator of the relative purity of the phases. The miscibility between domains depends on their respective lengths, the affinity between them, and the ability of segments to crystallize.[13–15] At low temperatures, in the interval of -60 °C and -40 °C, polyurethanes show a glass transition (T_{gCO3}) (Figure 4.5b), which is slightly higher than T_g of the neat CO3 and remains nearly constant as LDI/TMP content increases and thus independent, suggesting a microphase separated microstructure, despite a small amount of covalently bonded LDI/TMP could be mixed within the macrodiol rich domain.[16–18] Moreover, all the polyurethanes show a broad endothermic peak associated to the melting temperature of ordered domains mainly formed by the macrodiol. As LDI/TMP content increases the melting enthalpy (ΔH_m) and temperature (T_m) decrease, due to the lower amount of crystallizable macrodiol fraction and also due to the chemically crosslinked LDI/TMP fractions, which inhibits the mobility of chains, hindering the crystallization.[19–21] As can be seen in Table 4.3, the relative crystallinity values decrease with the increase of LDI/TMP content. Moreover, the cooling scans (inset) show a similar behavior, as LDI/TMP content increases crystallization temperature (T_c) and enthalpy (ΔH_c) also decrease. The relative crystallinity values are similar to those determined in the heating scan. All the polyurethanes show a second glass transition ($T_{gLDI/TMP}$), associated to the domain mainly formed by LDI/TMP, between the T_{gCO3} and T_m of the macrodiol rich domain, which increases as LDI/TMP content increases, becoming closer to the T_g of neat LDI/TMP, due to the formation of more crosslinked structure. Since all polyurethanes show two separated glass transition temperatures and the one associated to $T_{gLDI/TMP}$ becomes closer to the

T_g of PULTMP-100 as LDI/TMP content increases, the polyurethanes presents a phase separated microstructure,[16–18,22,23] which degree is enhanced as LDI/TMP content increases.

Moreover, as can be observed due to the aliphatic and nonsymmetrical chemical structure of LDI, results in the formation of amorphous urethane-based domains with low glass transition temperatures. Therefore, the use of CO3 as macrodiol, which shows a melting temperature much higher than room temperature, yields polyurethanes showing behavior different from that of common polyurethanes where the role of segments is inverted.[15,18,24,25]

4.4.4 Dynamical mechanical behavior

The dynamical mechanical behavior of the synthesized crosslinked polyurethanes from LDI was analyzed in order to follow the changes in the viscoelastic properties and also to determine the crosslink density. The temperature dependence of the storage modulus (E') and loss factor (tanδ) for the synthesized polyurethanes is shown in Figure 4.6. As can be seen, as CO3 content increases, the storage modulus values in the glassy state slightly increase, due to the crystallinity of this domain.[14,26]
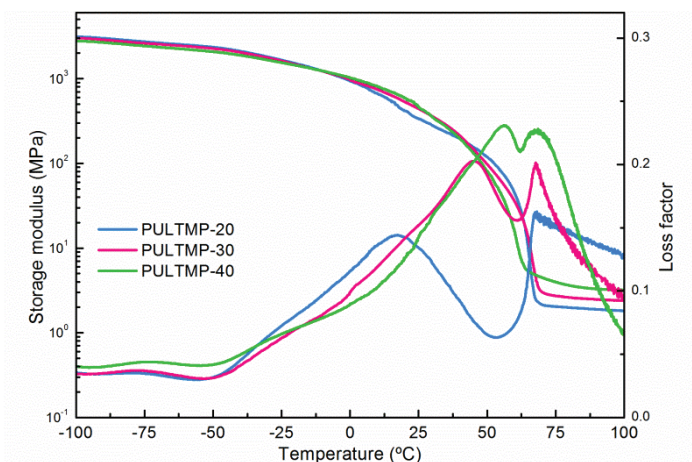

Figure 4.6. Storage modulus and loss factor of the synthesized PULTMP biobased polyurethane series.

Above -50 °C, a slight decrease in E' can be observed, as well as a shoulder in tanδ at low temperatures, which is related with the T_g of the CO3 rich domain[14] (T_{gCO3}) as previously observed by DSC. At higher temperatures a broad E' decrease can be seen, associated with the glass transition temperature of the LDI/TMP rich domain and melting temperature of the macrodiol rich domain. The decrease occurs at lower temperature as LDI/TMP content increases in accordance with the lower T_m values of DSC. After the decrease of E', the material reaches the rubbery plateau, where the storage modulus value increases with the increase of LDI/TMP content, according to a more crosslinked structure which provides significant structural reinforcement and a higher elastic recovery force at high temperature.[14,20]

Regarding tanδ curve a maximum can be observed, which is related with the mechanical relaxation (α)[15,27] of the LDI/TMP rich domain (T_α), which increases as LDI/TMP content increases as can be observed in Table 4.4, and it is in accordance to DSC results.

Moreover, crosslink density (ν_e) values and average molecular weight between crosslinks ($\bar{M}_c$) were calculated following the equation 2.5 and 2.6. As can be observed in Table 4.4, ν_e increases with the increase of LDI/TMP and hence $\bar{M}_c$ decreases, meaning that chain segments will be more closely restricted by net points which inhibit the mobility of the chains.[28–31]

Table 4.4. α temperature, crosslink density and average molecular weight between crosslinks of the synthesized biobased PULTMP polyurethanes.

Sample	T_α (°C)	ν_e (mol cm^{-3})	$\bar{M}_c$ (g mol^{-1})
PULTMP-20	16.9	201	6000
PULTMP-30	44.9	241	4900
PULTMP-40	55.8	313	3800

4.4.5 Mechanical properties

Tensile and Shore D hardness test were carried out in order to analyze the mechanical properties of the material. As can be observed in Figure 4.7, where stress-strain curves of the synthesized polyurethanes are shown, the material behaves as elastomers does.
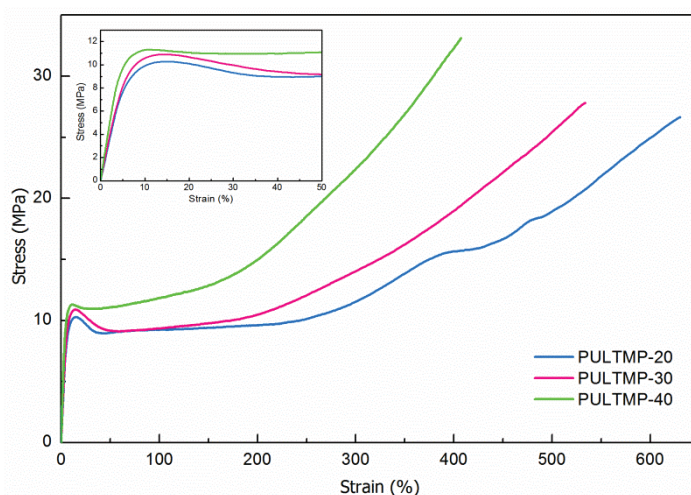

Figure 4.7. Stress-strain curves of the synthesized PULTMP biobased polyurethane series. Inset: magnification from 0 to 50% of elongation.

Moreover, in Table 4.5 the modulus, stress at break, stress at yield point and strain at break values obtained from stress-strain curves are displayed, together with Shore D hardness values.

Table 4.5. Mechanical properties of the biobased crosslinked polyurethanes.

Sample	E (MPa)	σ_y (MPa)	σ_b (MPa)	ε_b (%)	Shore D
PULTMP-20	169 ± 9	9.9 ± 0.1	27.5 ± 1.2	629 ± 11	54.0 ± 0.4
PULTMP-30	179 ± 7	10.7 ± 0.2	29.1 ± 1.0	560 ± 30	57.0 ± 0.5
PULTMP-40	245 ± 3	12.4 ± 1.0	32.0 ± 1.6	399 ± 15	58.6 ± 0.5

As can be observed as LDI/TMP content increases the material withstands higher elastic modulus and stresses at yield and at break, while elongation

decreases. This fact is due to the three-dimensional structure formed through covalent bonds, where net points together with crystalline domains are the responsible for carrying the load, restricting chains slipping.[30,32] As LDI/TMP content increases the crosslink density increases and hence the distance between net points become smaller, resulting in an increase in the elastic modulus and a decrease in elongation.[30] Moreover, the higher crosslinked structure enhances the hardness of the material.

In the stress-strain curves it can be seen, that the material shows different behaviors. Once the yield point is exceeded, it can be observed a plateau, where stress does not significantly change with strain. At elongations higher than 150%, strain-hardening phenomenon takes place due to the orientation of the chains during tensile tests leading a high strength at break. Similar behavior was reported by Ju et al. for poly(ε-caprolactone) based polyurethane.[33]

4.4.6 Water contact angle

The water contact angle of the synthesized crosslinked polyurethanes was analyzed, since contact angle analysis provides information of the surface hydrophobicity or hydrophilicity, and of the molecular mobility at the air-water-solid interface.[25,34] In Table 4.6 the contact angle and surface tension values of the synthesized polyurethanes are gathered.

Table 4.6. Contact angles and surface tension values of synthesized PULTMP crosslinked biobased polyurethane series.

Sample	Contact angle (°)	Surface tension (mN m^{-1})
PULTMP-20	78.8 ± 0.7	30.6
PULTMP-30	79.7 ± 0.2	25.3
PULTMP-40	83.6 ± 0.5	22.5

Usually in thermoplastic polyurethanes, as urethanes group density increases, the hydrophobicity decreases, showing lower water contact angle values.[8,25]

However, in the synthesized crosslinked polyurethanes the opposite behavior can be observed, which can be attributed to a higher crosslink density.[35]

4.5 Characterization of the synthesized crosslinked biobased polyurethanes from DDI

4.5.1 Biobased carbon content

The same procedure followed to estimate the biobased carbon content of the synthesized PULTMP biobased polyurethane series was used in order to estimate the biobased carbon content of the synthesized PUDTMP polyurethane series. As mentioned before CO3 has a 72% biobased carbon content and TMP was derived from fossil sources. The biobased carbon content of DDI diisocyanate is 98%, which is higher than LDI ones. The estimated biobased carbon content of the synthesized biobased polyurethanes is shown in Table 4.7.

Table 4.7. Biobased carbon content of the synthesized PUDTMP crosslinked biobased polyurethanes.

Sample	Biobased carbon content (%)
PUDTMP-27	78
PUDTMP-36	79
PUDTMP-49	80
PUDTMP-100	84

Unlike the obtained results for PULTMP, as DDI/TMP content increases the biobased carbon content also increases, which could be related with the fact that DDI has a higher amount of carbons (36 carbons) and higher biobased carbon content if compared with LDI, therefore its contribution to the total biobased carbon content would be higher. This being so, the use of a crosslinker derived from fossil sources hardly influences on the biobased carbon content of

the material when DDI is used as diisocyanate, obtaining crosslinked polyurethanes with high biobased carbon content.

4.5.2 Fourier transform infrared spectroscopy

FTIR was used to analyze the characteristic groups of the PUDTMP biobased polyurethane series. The infrared spectra of the synthesized crosslinked biobased polyurethanes, CO3 and neat DDI spectra are shown in Figure 4.8. The isocyanate group stretching vibration band was not found at 2270 cm^{-1}, indicating that complete polymerization took place. The synthesized biobased polyurethanes show the typical bands associated to polyurethanes, at 3365 cm^{-1} the band associated with the N-H stretching vibration of the urethane group[2] and at 1530 cm^{-1} a band ascribed to N-H out-of-plane bending combined to the C-N stretching vibration can be observed.[4]
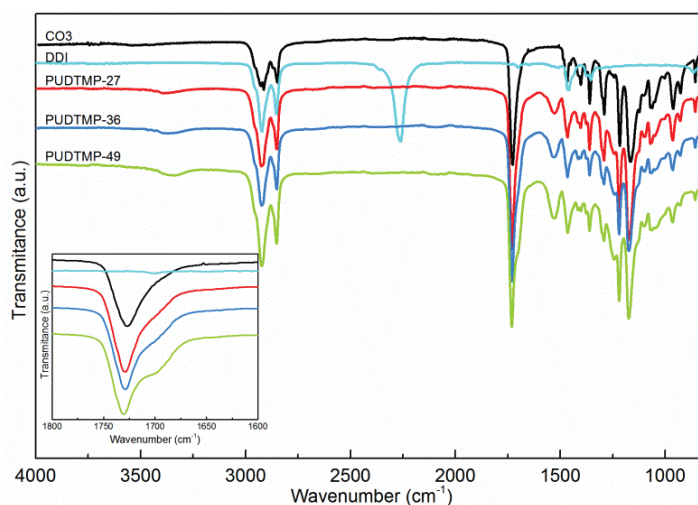
Figure 4.8. FTIR spectra of CO3, DDI and the synthesized PUDTMP biobased polyurethane series. Inset: carbonyl group stretching vibration region.

Similarly to PULTMP biobased polyurethanes, as DDI/TMP content increases the intensity of both bands increases according of a higher content of urethane groups. Furthermore, in the inset the carbonyl group stretching vibration region is shown, where CO3 presents a band at 1728 cm^{-1} associated with

carbonyl stretching in ester group.[6] As can be observed, the synthesized biobased polyurethanes show a broad band at 1728 cm^{-1}, which encompasses the infrared absorbance of C=O group of CO3 and free urethane C=O group. Moreover, this band shows a shoulder between 1680 and 1713 cm^{-1} attributed to the hydrogen-bonded carbonyl of urethane group,[12] which increases in intensity with DDI/TMP content. This fact could be attributed to a higher amount of urethane groups per unit volume. Furthermore, in Figure 4.9 the peak deconvolution of baseline corrected C=O stretching bands of the synthesized PUDTMP biobased polyurethanes is shown. The area of hydrogen-bonded urethane carbonyl groups band (II) respect to total area (%) was calculated.[8] The obtained areas were 31.0, 38.5 and 50.4% for PUDTMP-27, PUDTMP-36 and PUDTMP-49. As can be observed the area of the peak related with hydrogen-bonded urethane carbonyl group (II) increases with the increase of DDI/TMP content. Similar behavior was also observed in PULTMP biobased polyurethane series. However the areas for PUDTMP series are slightly lower if compared with PULTMP series with a similar content of LDI/TMP, suggesting that DDI/TMP segments have a lower tendency to associate in domains.
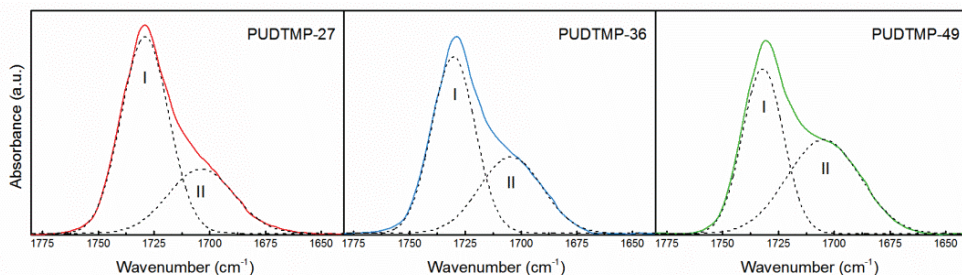

Figure 4.9. Peak deconvolution (dot lines) of baseline corrected C=O stretching bands of the synthesized PUDTMP polyurethane series, C=O free stretching (I) and C=O hydrogen-bonded stretching (II) bands.

4.5.3 Differential scanning calorimetry

The thermal behavior of the synthesized biobased polyurethanes was also analyzed. Figure 4.10 shows the DSC heating and cooling thermograms for the

synthesized biobased polyurethane series together with pure CO3 and neat DDI/TMP. The thermal transitions are listed in Table 4.8.
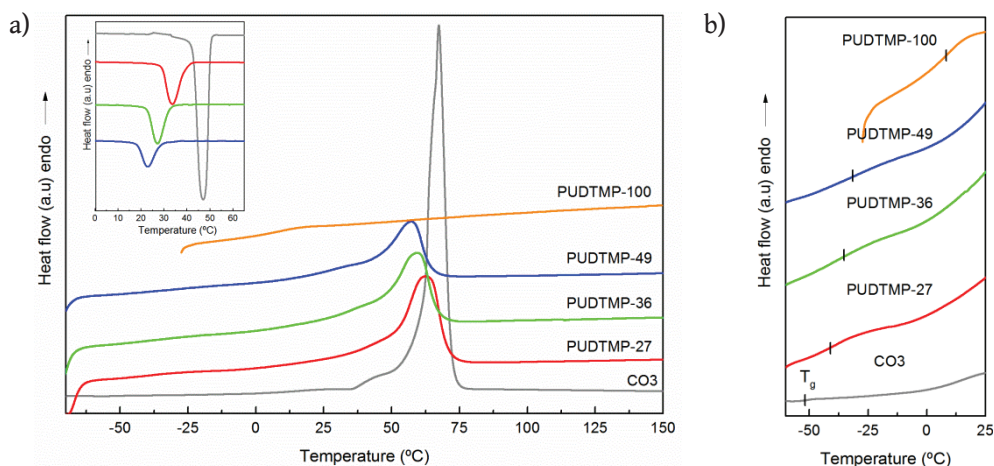

Figure 4.10. a) Heating DSC thermograms of CO3, DDI/TMP and the synthesized PUDTMP biobased polyurethanes series and b) magnification of the low temperature region. Inset: cooling DSC thermograms.

Table 4.8. Thermal transition values of CO3 and the synthesized PUDTMP biobased polyurethane series.

Sample	T_g (°C)	T_m (°C)	ΔH_m (J g^{-1})	T_c (°C)	ΔH_c (J g^{-1})	χ_c heating	χ_c cooling
CO3	–52.0	70.0	142.0	46.3	–93.1	1.0	1.0
PUDTMP-27	–41.2	62.3	63.2	33.6	–60.2	0.6	0.9
PUDTMP-36	–36.5	59.4	52.6	27.2	–50.6	0.6	0.9
PUDTMP-49	–31.7	57.3	43.0	23.0	–37.1	0.6	0.8
PUDTMP-100	9.3	–	–	–	–	–	–

The semicrystalline CO3 shows a T_g at –52 °C and an endothermic peak associated with crystals melting at 70 °C, as it was previously observed. With regard to neat DDI/TMP biobased crosslinked polyurethane, PUDTMP-100 shows a T_g around 9 °C. Moreover, PUDTMP-100 is not able to crystallize, due to its branched structure. In addition the formation of a crosslinked structure inhibits chain motion for crystallization.[20] The use of DDI as the diisocyanate results in low T_g values. Its branched aliphatic structure hinders the association

by hydrogen bonding and leads to flexible chains. This behavior was also observed in the crosslinked PULTMP earlier explained in this chapter. Similarly to DDI, the side chain of the aliphatic LDI inhibited the crystallization of neat LDI/TMP crosslinked biobased polyurethanes. However, because the LDI molecule is smaller, the resultant chains were stiffer and a T_g value of 59 °C was obtained.

Regarding the synthesized crosslinked biobased polyurethanes with different DDI/TMP content, all of them present several thermal transitions related to those observed for neat blocks. At low temperatures, the T_g of the polyurethanes is higher than the T_g of CO3 and increases with the increase of DDI/TMP content. As mentioned before, the T_g is an indicator of the relative purity of the phases. Due to the chemical structure of DDI, a fraction of DDI/TMP can be mixed within the amorphous macrodiol. This behavior differs from the previously observed for PULTMP biobased polyurethane series, which showed lower T_{gCO3} values. This behavior denotes that biobased polyurethanes with DDI show a higher affinity with the amorphous phase of CO3.[27] In addition, CO3 and DDI show close solubility parameters (δ) (calculated by Hoy method),[36] δ_{CO3} = 20.07 $J^{1/2}$ cm$^{-3/2}$ and δ_{DDI} = 18.83 $J^{1/2}$ cm$^{-3/2}$. However, the solubility parameter of LDI (δ_{LDI} = 26.46 $J^{1/2}$ cm$^{-3/2}$) differs in a great extent respect to δ_{CO3}, thus resulting to a more phase separated microstructure. Moreover, between 30 and 70 °C the crosslinked polyurethanes show an endothermic peak with a shoulder. As DDI/TMP content increases, the intensity of the observed endothermic peak decreases, according to a lower content of the CO3 crystallizable rich microdomain. Moreover, the synthesized biobased polyurethanes show a lower relative crystallinity if compared with CO3, which is independent to DDI/TMP content. Furthermore, the cooling scans (inset in Figure 4.10) show a similar behavior, but as the DDI/TMP content increases, the crystallization temperature and enthalpy also decrease. Regarding relative crystallinity of the cooling scan

the biobased polyurethanes show lower values if compared with CO3, denoting that crystallinity of the macrodiol is hindered by the presence of DDI/TMP.

4.5.4 Dynamic mechanical analysis

The dynamic mechanical behavior of the synthesized crosslinked biobased polyurethanes with DDI was analyzed by means of DMA. The temperature dependence of the storage modulus and loss factor is shown in Figure 4.11.
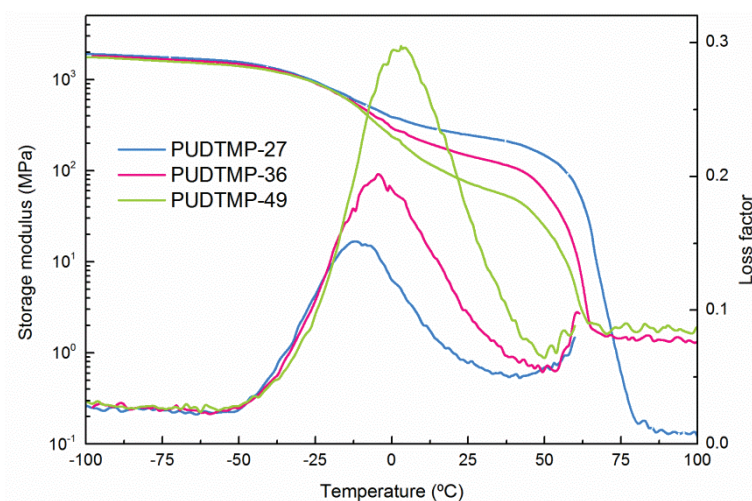

Figure 4.11. Storage modulus and loss factor of the synthesized PUDTMP polyurethane series.

As can be observed, as the CO3 content increases, the storage modulus values in the glassy state are slightly higher, because of the higher crystallinity[20], as previously observed for LDI based polyurethane series. At higher temperatures, the materials show a decrease in E' associated with the T_g. In addition, after the decrease in the E', biobased polyurethanes reach a plateau, where the E' value decreases with the increase in the DDI/TMP content, due to less content of the semicrystalline CO3, which provides significant structural reinforcement.[14,20] Finally, at higher temperatures E' decreases owing to the disruption of ordered domains formed by the CO3. It occurs at lower temperature as DDI/TMP content increases, according to DSC results. Due to the crosslinked structure of the

synthesized polyurethanes, the material does not flow after the disruption of the ordered domains and reaches a second plateau, where the storage modulus value increases with the increase of DDI/TMP content, suggesting a more crosslinked structure.[14,20] ν_e and $\overline{M}_c$ were estimated to quantify the degree of crosslinking (Table 4.9), following equations 2.5 and 2.6.

Table 4.9. α temperature, crosslink density and average molecular weight between crosslinks of the synthesized PUDTMP biobased polyurethane series.

Sample	T_α (°C)	ν_e (mol cm^{-3})	$\overline{M}_c$ (g mol^{-1})
PUDTMP-27	-13.2	17	69000
PUDTMP-36	-3.4	157	7600
PUDTMP-49	3.1	195	6100

As can be observed, the increase in the DDI/TMP content increases ν_e of the biobased polyurethanes, meaning that net points are closer to each other and thus $\overline{M}_c$ decreases. Nevertheless, PUDTMP-27 shows considerably low ν_e, and hence a high $\overline{M}_c$ value; this could be due to the fact that the amount of crosslink agent is not sufficiently large to build a crosslinked structure with net points close to each other. Regarding to the tanδ curve, a wide peak with a maximum can be observed, which is mainly related to the mechanical transition (α) of the DDI/TMP rich domain,[15] because the intensity and temperature increase as the DDI/TMP rich domain content increases. The increase observed in T_α (Table 4.9) as DDI/TMP content increases could be related to a higher ν_e which inhibits the mobility of the chains. Furthermore, a single tanδ peak was observed (there was not observed the shoulder seen in PULTMP series), denoting a mixing between phases as previously observed by DSC.[27] This behavior differs from the previously observed for the biobased polyurethanes with LDI, whose tanδ peak encompasses two T_gs, the one associated to CO3 rich domain and the one correspondent to LDI/TMP rich domain. Thus PULTMP biobased polyurethane

series showed a microphase separate structure. Moreover, PULTMP polyurethane series showed higher v_e and thus lower $\overline{M}_c$. This fact is due to LDI molecule is smaller and hence chains segments were more closely restricted, since net points were closer from each other. In this way, phase separation was more feasible. In addition, polyurethanes based on LDI showed higher T_α values according to a higher crosslinked structure. The increase of intermolecular distance between chains would decrease steric hindrance and other chain interaction, and hence reduce the resistance to place change and rotation of molecular segments.[27,37] Therefore, the mobility of PUDTMP biobased polyurethane series is less restricted due to its lower crosslink density.

4.5.5 Mechanical properties

The mechanical behavior of the synthesized crosslinked biobased polyurethanes was also studied. The stress-strain curves are shown in Figure 4.12 and elastic modulus, stress at yield and at break and strain at break values obtained from them together with hardness Shore D values are listed in Table 4.10.
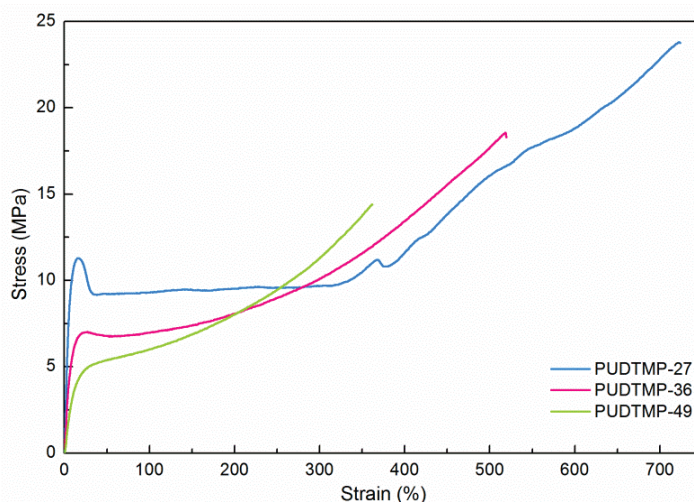
Figure 4.12. Stress-strain curves of the synthesized PUDTMP biobased polyurethane series.

Table 4.10. Mechanical properties of the synthesized PUDTMP biobased polyurethane series.

Sample	E (MPa)	σ_y (MPa)	σ_b (MPa)	ε_b (%)	Shore D
PUDTMP-27	163 ± 8	11.0 ± 0.8	24.4 ± 1.9	760 ± 33	57.2 ± 0.5
PUDTMP-36	82 ± 5	6.9 ± 0.9	15.8 ± 1.9	514 ± 6	56.5 ± 0.9
PUDTMP-49	37 ± 4	4.9 ± 0.3	13.9 ± 1.7	364 ± 23	50.4 ± 0.9

As can be seen, the synthesized crosslinked biobased polyurethanes show lower elastic modulus, stress at break and at yield and strain at break as DDI/TMP content increases. This fact denotes that mechanical properties are governed by the crystallizable CO3 rich domain, as well as crosslink density. Unlikely to the results obtained for PULTMP crosslinked biobased polyurethane series, the increase of crosslink density do not enhance the mechanical properties, which could be attributed to the chemical structure of DDI. Although crosslink density increases, due to the long chain of DDI the distance between net points is large and therefore net points are not effective carrying the load.

Regarding hardness of the synthesized materials, as the DDI/TMP content increases, hardness values decrease according to a lower crystallinity and crosslink density of the material. This fact suggests that hardness is also directly related to the overall crystallinity and crosslink density of the material.

4.5.6 Atomic force microscopy

The morphology of the synthesized crosslinked polyurethanes was analyzed by AFM. Phase AFM images are shown in Figure 4.13. The biobased polyurethanes present a microstructure in which different domains can be distinguished. The lighter regions correspond to the crystalline domains and the darker ones to amorphous domains. The frequency of these dark regions increases as the DDI/TMP content increases, according to a lower overall crystallinity of the material.
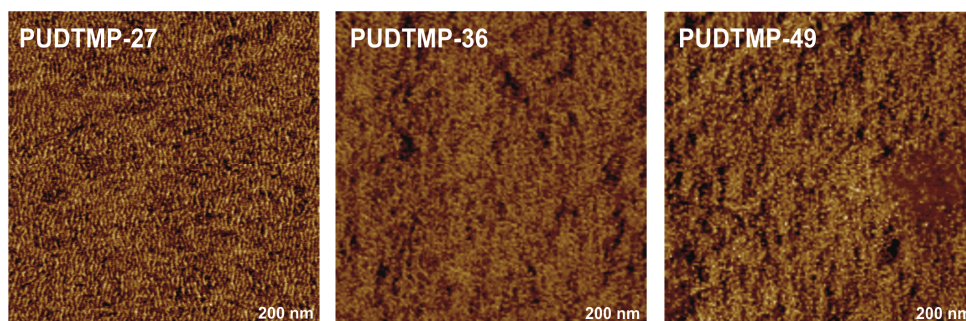
Figure 4.13. Phase AFM images of the synthesized crosslinked biobased polyurethanes (size: 1 x 1 μm^2).

4.5.7 Water contact angle

Water contact angle and surface tension values are listed in Table 4.11. Since fatty acid groups have hydrophobic properties,[38] the synthesized crosslinked biobased polyurethanes show a considerably high water contact angle. As previously observed for PULTMP polyurethanes the hydrophobicity of the material increased with the increase of v_e. However, contact angle values of PUDTMP series barely change as DDI/TMP content increases, denoting that v_e is not high enough to influence on the hydrophobicity of the polyurethane.

Table 4.11. Contact angles and surface tension values of synthesized PUDTMP biobased polyurethanes.

Sample	Contact angle (°)	Surface tension (mN m^{-1})
PUDTMP-27	100.0 ± 0.7	12.5
PUDTMP-36	100.1 ± 0.8	12.4
PUDTMP-49	101.8 ± 0.5	11.5

4.6 Biocompatibility of the synthesized crosslinked biobased polyurethanes

The potential of the synthesized crosslinked biobased polyurethanes to be used in biomedical applications was studied by analyzing the cell viability, cell proliferation and long term cell adhesion.

4.6.1 Cell viability and proliferation of crosslinked biobased polyurethanes

The quantification of the cytotoxicity response for both positive (PVC) and negative (HDPE) controls, as well as for PULTMP-30 and PUDTMP-27 are showed Figure 4.14.
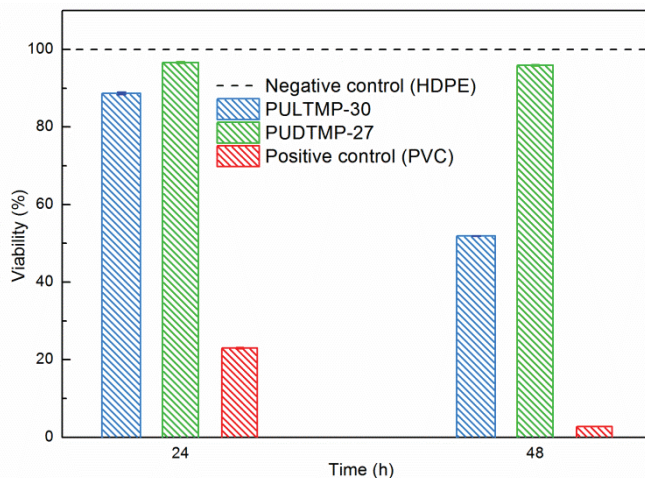
Figure 4.14. Viability of L-929 murine fibroblast cells in extracted media at 24 and 48 h in negative control (HDPE), PULTMP-30 and PUDTMP-27 biobased polyurethanes and positive control (PVC).

The viability analysis performed in the first 24 h showed that both PULTMP-30 and PUDTMP-27 have a non-toxic behavior, since cell viability value is around 90% and 95% of the value of negative control, for PUTMP-30 and PUDTMP-27, respectively. These values are higher than the acceptance limit of 70%, as established by ISO 10993-12 standard.[39] Therefore, the synthesized biobased polyurethanes have the potential to be exploited in biomedicine. As can be observed, the crosslinked biobased polyurethane with DDI promotes the proliferation of fibroblast more than the biobased polyurethane with LDI, which could be related with the nature of the diisocyanate that favors the growing of the cells. The biocompatibility of LDI diisocyanate was also reported in

literature by other authors,[40–43] however for DDI not results were found in literature.

4.6.2 Cell adhesion of crosslinked biobased polyurethanes

Cell long term adhesion of the synthesized crosslinked biobased polyurethanes was carried out by performing Live/Dead assays. In Figure 4.15 the fluorescence confocal microscope images of PULTMP-30 and PUDTMP-27 at 7 and 14 days are shown.
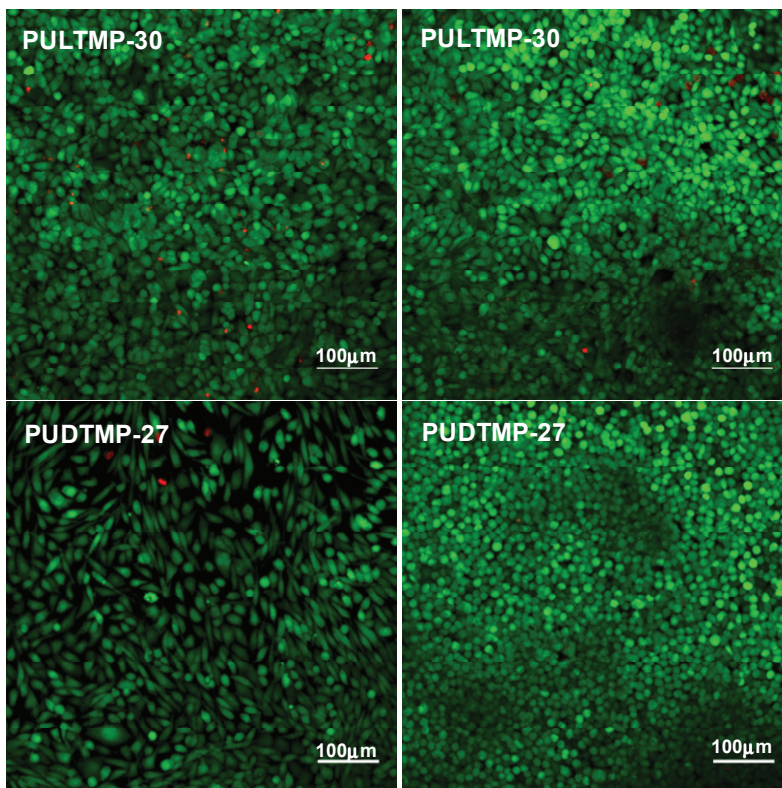
Figure 4.15. Fluorescence confocal microscope images recorded from Live/Dead assays of cells grown in direct contract with PULTMP-30 and PUDTMP-27 biobased polyurethanes for 7 (left) and 14 (right) days.

As can be observed at day 7 (fluorescence micrographs on the left), cells growth on both biobased polyurethanes and were metabolically active (green), and only a few dead cells (red) were observed on each material. At day 14 (fluorescence

micrographs on the right), cell density became significantly higher, especially in PUDTMP-27, which corroborates the better biocompatibility of the biobased polyurethanes based on DDI previously observed.

4.7 Conclusions

Crosslinked biobased polyurethanes with high biobased carbon content were synthesized successfully by a catalyst free two-step bulk polymerization process using a macrodiol based on castor oil and two different diisocyanates, one based on L-lysine amino acid and the other on fatty acids.

It was seen that the use of this kind of diisocyanates with side chains (LDI) or branched structures (DDI), results in biobased polyurethanes with low T_g and their structure inhibits the crystallization of the domain rich in diisocyanate. Therefore, only the macrodiol rich domain was able to crystallize. PULTMP polyurethanes despite of the small phase mixing showed a greater microphase separated morphology, since all biobased polyurethanes showed two well defined T_g associated to CO3 and LDI/TMP rich domains. However, PUDTMP showed a single T_g which slightly increases as DDI/TMP content increases, suggesting a mixing of DDI/TMP with the amorphous phase of the macrodiol. Due to the chemical structure of DDI the diisocyanate tend to mix with the amorphous part of the CO3 resulting in a higher mixing degree of the phases. The dynamic mechanical behavior of the synthesized polyurethanes revealed that PULTMP biobased polyurethanes were higher crosslinked and thus showed lower average molecular weight between crosslinks. This fact was related with the smaller size of LDI molecule which allowed net points to be closer, increasing the crosslink density and α transition temperature. The mechanical properties of both biobased polyurethane series were tightly dependent on the overall crystallinity and crosslink density. When LDI was used as diisocyanate, in addition to crystallinity, crosslink density had also a key role. In this way the variation of crystallinity and crosslink density allows the possibility of

synthesizing crosslinked biobased polyurethanes with tailored mechanical properties.

In addition, all synthesized crosslinked biobased polyurethanes showed non-toxic behavior and it was seen that DDI promoted the proliferation of cells in a higher extent. Moreover, crosslinked polyurethanes showed metabolically active cells after 7 days and only a few dead cells. Besides, in both samples after 14 days cell density increased. Therefore, the synthesized crosslinked biobased polyurethanes showed its potential to be used for biomedical applications.

4.8   References

1.   ASTM D6866-12. "Standard test method for determining the biobased content of natural range materials using radiocarbon and isotope ratio mass spectrometry analysis." ASTM International. West Conshohocken, PA, 2012.

2.   Z. Wang, L. Yu, M. Ding, H. Tan, J. Li, Q. Fu. "Preparation and rapid degradation of nontoxic biodegradable polyurethanes based on poly(lactic acid)-poly(ethylene glycol)-poly(lactic acid) and L-lysine diisocyanate". Polym. Chem. 2011. 2: 601–607.

3.   Y.M. Tsai, T.L. Yu, Y.H. Tseng. "Physical properties of crosslinked polyurethane". Polym. Int. 1998. 47: 445–450.

4.   M.A. Corcuera, L. Rueda, B. Fernandez-d'Arlas, A. Arbelaiz, C. Marieta, I. Mondragon, A. Eceiza. "Microstructure and properties of polyurethanes derived from castor oil". Polym. Degrad. Stab. 2010. 95: 2175–2184.

5.   L. Peponi, I. Navarro-Baena, A. Sonseca, E. Gimenez, A. Marcos-Fernandez, J.M. Kenny. "Synthesis and characterization of PCL-PLLA polyurethane with shape memory behavior". Eur. Polym. J. 2013. 49: 893–903.

6. B. Fernández-d'Arlas, J.A. Ramos, A. Saralegi, M. Corcuera, I. Mondragon, A. Eceiza. "Molecular engineering of elastic and strong supertough polyurethanes". Macromolecules 2012. 45: 3436–3443.

7. A. Santamaria-Echart, A. Arbelaiz, A. Saralegi, B. Fernández-d'Arlas, A. Eceiza, M.A. Corcuera. "Relationship between reagents molar ratio and dispersion stability and film properties of waterborne polyurethanes". Colloids Surfaces A Physicochem. Eng. Asp. 2015. 482: 554–561.

8. L. Rueda-Larraz, B. Fernández-d'Arlas, A. Tercjak, A. Ribes, I. Mondragon, A. Eceiza. "Synthesis and microstructure-mechanical property relationships of segmented polyurethanes based on a PCL-PTHF-PCL block copolymer as soft segment". Eur. Polym. J. 2009. 45: 2096–2109.

9. B. Fernández-d'Arlas, A. Eceiza. "Structure-property relationship in high urethane density polyurethanes". J. Polym. Sci. Part B Polym. Phys. 2016. 54: 739–746.

10. F. Shokrolahi, H. Yeganeh. "Soft segment composition and its influence on phase-separated morphology of PCL/PEG-based poly(urethane urea)s". Iran. Polym. J. (English Ed) 2014. 23: 505–512.

11. J. Mattia, P. Painter. "A comparison of hydrogen bonding and order in a polyurethane and poly(urethane-urea) and their blends with poly(ethylene glycol)". Macromolecules 2007. 40: 1546–1554.

12. L. Ugarte, B. Fernández-d'Arlas, A. Valea, M.L. González, M.A. Corcuera, A. Eceiza. "Morphology-properties relationship in high-renewable content polyurethanes". Polym. Eng. Sci. 2014. 54: 2282–2291.

13. Z.S. Petrovic, I. Javni. "Effect of soft-segment length and concentration on phase separation in segmented polyurethanes". J. Polym. Sci. Part B Polym. Phys. 1989. 27: 545–560.

14. A. Saralegi, L. Rueda, B. Fernández-d'Arlas, I. Mondragon, A. Eceiza, M.A. Corcuera. "Thermoplastic polyurethanes from renewable resources: effect of soft segment chemical structure and molecular weight on morphology and final properties". Polym. Int. 2013. 62: 106–115.

15. E. Cognet-Georjon, F. Mechin, J.P. Pascault. "New polyurethanes based on 4,4'-diphenylmethane diisocyanate and 1,4:3,6 dianhydrosorbitol. 2. Synthesis and properties of segmented polyurethane elastomers". Macromol. Chem. Phys. 1996. 197: 3593–3612.

16. J.M. Castro, F. Lopez-Serrano, R.E. Camargo, C.W. Macosko, M. Tirrell. "Onset of phase separation in segmented urethane polymerization". J. Appl. Polym. Sci. 1981. 26: 2067–2076.

17. L.M. Leung, J.T. Koberstein. "DSC annealing study of microphase separation and multiple endothermic behavior in polyether-based polyurethane block copolymers". Macromolecules 1986. 19: 706–713.

18. J.T. Koberstein, R.S. Stein. "Small-angle X-ray scattering studies of microdomain structure in segmented polyurethane elastomers". J. Polym. Sci. Part B Polym. Phys. 1983. 21: 1439–1472.

19. Z.S. Petrović, I. Javni, V. Divjakovi. "Structure and physical properties of segmented polyurethane elastomers containing chemical crosslinks in the hard segment". J Polym Sci B Polym Phys. 1998. 36: 221–235.

20. D. Ratna, J. Karger-Kocsis. "Recent advances in shape memory polymers and composites: a review". J. Mater. Sci. 2008. 43: 254–269.

21. I. Kaur, P. Ray. "Broader spectrum: Examples". In: Polymer grafting and crosslinking. Eds. A. Bhattacharya, J.W. Rawlins, P. Ray. John Wiley & Sons, Inc., Hoboken, NJ, USA, 2008.

22.   S. Velankar, S.L. Cooper. "Microphase separation and rheological properties of polyurethane melts. 1. Effect of block length". Macromolecules 1998. 31: 9181–9192.

23.   A. Lendlein, R. Langer. "Biodegradable, elastic shape-memory polymers for potential biomedical applications". Science 2002. 296: 1673–1676.

24.   D. Rosu, N. Tudorachi, L. Rosu. "Investigations on the thermal stability of a MDI based polyurethane elastomer". J. Anal. Appl. Pyrolysis 2010. 89: 152–158.

25.   M.A. Corcuera, L. Rueda, A. Saralegi, M.D. Martín, B. Fernández-d'Arlas, I. Mondragon, A. Eceiza. "Effect of diisocyanate structure on the properties and microstructure of polyurethanes based on polyols derived from renewable resources". J. Appl. Polym. Sci. 2011. 122: 3677–3685.

26.   H. Tan, M. Guo, R.N. Du, X.Y. Xie, J.H. Li, Y.P. Zhong, Q. Fu. "The effect of fluorinated side chain attached on hard segment on the phase separation and surface topography of polyurethanes". Polymer 2004. 45: 1647–1657.

27.   H. Ishida, D.J. Allen. "Mechanical characterization of copolymers based on benzoxazine and epoxy". Polymer 1996. 37: 4487–4495.

28.   H. Jiang, W. Su, P.T. Mather, T.J. Bunning. "Rheology of highly swollen chitosan/polyacrylate hydrogels". Polymer 1999. 40: 4593–4602.

29.   J. Hu, Z. Yang, L. Yeung, F. Ji, Y. Liu. "Crosslinked polyurethanes with shape memory properties". Polym. Int. 2005. 54: 854–859.

30.   X.L. Wu, S.F. Kang, X.J. Xu, F. Xiao, X.L. Ge. "Effect of the crosslinking density and programming temperature on the shape fixity and shape recovery in epoxy-anhydride shape-memory polymers". J. Appl. Polym. Sci. 2014. 131: 40559.

31. B.K. Kim, S.Y. Lee, M. Xu. "Polyurethanes having shape memory effects". Polymer 1996. 37: 5781–5793.

32. A. Lendlein, S. Kelch. "Shape-memory polymers". Angew. Chem. Int. Ed. 2002. 41: 2034–2057.

33. D. Ju, L. Han, Z. Guo, J. Bian, F. Li, S. Chen, L. Dong. "Effect of diameter of poly(lactic acid) fiber on the physical properties of poly(ε-caprolactone)". Int. J. Biol. Macromol. 2015. 76: 49–57.

34. H. Yeganeh, M.M. Lakouraj, S. Jamshidi. "Synthesis and characterization of novel biodegradable epoxy-modified polyurethane elastomers". J. Polym. Sci. Part A Polym. Chem. 2005. 43: 2985–2996.

35. S. Oprea. "Effect of the long chain extender on the properties of linear and castor oil cross-linked PEG-based polyurethane elastomers". J. Mater. Sci. 2011. 46: 2251–2258.

36. D.W. van Krevelen. "Properties of polymers". Elsevier Scientific Publising Co., Amsterdam, 1990. Pp. 189-225.

37. M. Zeng, H. Gao, Y. Wu, L. Fan, A. Li. "Preparation and characterization of nanocomposite films from chitin whisker and waterborne poly(ester-urethane) with or without ultra-sonification treatment". J. Macromol. Sci. Part A. 2010. 47: 867–876.

38. A. Sirkecioglu, H.B. Mutlu, C. Citak, A. Koc, F.S. Güner. "Physical and surface properties of polyurethane hydrogels in relation with their chemical structure". Polym. Eng. Sci. 2014. 54: 1182–1191.

39. ISO 10993-5. Biological evaluation of medical devices. Test for in vitro cytotoxicity. International Organization for Standardization. Geneve, Switzerland, 2009.

40. S.A. Guelcher, V. Patel, K.M. Gallagher, S. Connolly, J.E. Didier, J.S. Doctor, J.O. Hollinger. "Synthesis and in vitro biocompatibility of injectable polyurethane foam scaffolds". Tissue Eng. 2006. 12: 1247–1259.

41. A. Basterretxea, Y. Haga, A. Sanchez-Sanchez, M. Isik, L. Irusta, M. Tanaka, K. Fukushima, H. Sardon. "Biocompatibility and hemocompatibility evaluation of polyether urethanes synthesized using DBU organocatalyst". Eur. Polym. J. 2016. 84: 750–758.

42. K.M. Zia, M. Zuber, I.A. Bhatti, M. Barikani, M.A. Sheikh. "Evaluation of biocompatibility and mechanical behavior of chitin-based polyurethane elastomers. Part-II: effect of diisocyanate structure". Int. J. Biol. Macromol. 2009. 44: 23–28.

43. S.A. Guelcher, K.M. Gallagher, J.E. Didier, D.B. Klinedinst, J.S. Doctor, A.S. Goldstein, G.L. Wilkes, E.J. Beckman, J.O. Hollinger. "Synthesis of biocompatible segmented polyurethanes from aliphatic diisocyanates and diurea diol chain extenders". Acta Biomater. 2005. 1: 471–484.

CHAPTER 5

THERMOPLASTIC BIOBASED POLYURETHANES
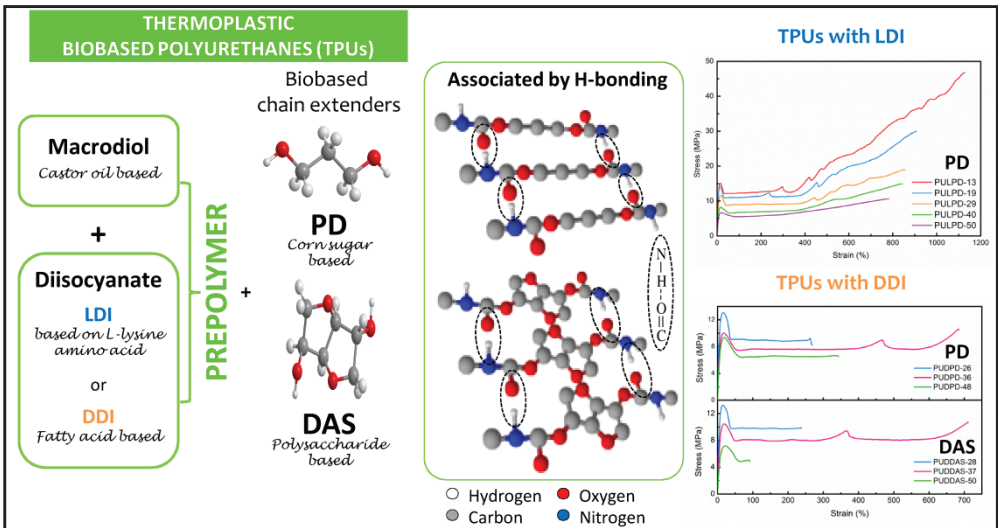
5. THERMOPLASTIC BIOBASED POLYURETHANES

5.1   Aim of the chapter

The main objective of this chapter was to synthesize and characterize thermoplastic biobased polyurethanes using different biobased diisocyanates and chain extenders. On the one hand, a series of segmented thermoplastic biobased polyurethane was synthesized using the same castor oil based macrodiol employed in chapter 4, LDI and 1,3-propanediol (PD), which is derived from corn sugar. On the other hand, two different thermoplastic biobased polyurethane series were synthesized using the same macrodiol and DDI. However, in this case two different chain extenders were used: PD and dianhydro-D-glucitol (DAS), which is obtained from polysaccharides.

The thermoplastic biobased polyurethanes were synthesized by two-steps bulk polymerization process, varying the molar ratio of diisocyanate/chain extender. The thermal properties were measured by means of differential scanning calorimetry and dynamic mechanical analysis. Physicochemical properties were analyzed by using Fourier transform infrared spectroscopy and gel permeation chromatography, while mechanical properties by performing tensile and Shore D hardness tests. The morphology of the synthesized biobased polyurethanes was also analyzed by atomic force microscopy. Finally, surface properties were analyzed by measuring water contact angle and the biocompatibility of the synthesized thermoplastic polyurethanes was also studied.

5.2   Synthesis of thermoplastic biobased polyurethanes

In order to synthesize the thermoplastic biobased polyurethanes from LDI and DDI, the same catalyst free two-step bulk polymerization procedure employed in chapter 4 was followed. Briefly, the dried CO3 and diisocyanate were placed in the flask and heated at 100 °C for 5 h, when LDI was used, and at 80 °C for 4 h when DDI was used. After that, the chain extender (dry PD or DAS) was added at

the same temperature and the mixture was rapidly stirred for 10-15 min. Finally the resulting viscous liquid was quickly poured between two Teflon® coated metal plates. After performing several compression-decompression cycles, the sample was pressed at 100 °C under 50 bar for 10 h. Then, the biobased polyurethane was left to cool down to room temperature at constant pressure and controlling the air flow. The NCO to OH group molar ratio was kept constant at 1.01. CO3/diisocyanate/chain extender molar ratios and diisocyanate/chain extender content (calculated as weight percentage of diisocyanate and chain extender respect to total biobased polyurethane weight) are shown in Table 5.1.

Table 5.1. Designation, molar ratio and diisocyanate/chain extender content of thermoplastic biobased polyurethanes.

Sample	Molar ratio			Diisocyanate/chain extender (wt%)
	CO3	Diisocyanate	Chain extender	
PULPD-13	1	2.02	1	13
PULPD-19	1	3.03	2	19
PULPD-29	1	5.05	4	29
PULPD-40	1	8.08	7	40
PULPD-50	1	12.12	11	50
PULPD-100	0	1.00	1	100
PUDPD-26	1	2.02	1	26
PUDPD-36	1	3.03	2	36
PUDPD-48	1	5.05	4	48
PUDPD-100	0	1.00	1	100
PUDDAS-28	1	2.02	1	28
PUDDAS-37	1	3.03	2	37
PUDDAS-50	1	5.05	4	50
PUDDAS-100	0	1.00	1	100

Sample code is expressed as PUxy-z, where x is the first letter of the abbreviation of the diisocyanate name (L or D), y is the abbreviation of the chain extender (PD or DAS), and z is the diisocyanate/chain extender content (wt%). In addition, pure diisocyanate/chain extender biobased polyurethanes were also synthesized for comparison, PULPD-100, PUDPD-100 and PUDDAS-100.

5.3   Characterization of the synthesized thermoplastic biobased polyurethanes from LDI

5.3.1 Biobased carbon content

As mentioned in chapter 4, the biobased carbon content of the starting materials was determined by the ASTM-D6866-12 (0.98) Method B (AMS) standard procedure,[1] having the macrodiol and LDI 72 and 81% biobased carbon content, respectively. In the case of PD chain extender, it has a 100% biobased carbon content. The estimation of the biobased carbon content of the final polyurethanes was done taken into account the molar ratio and the biobased carbon content of each component in the final formulation (equation 2.2). In Table 5.2 the biobased carbon content of the synthesized biobased polyurethanes are shown.

Table 5.2. Biobased carbon content of the synthesized PULPD biobased polyurethane series.

Sample	Biobased carbon content (%)
PULPD-13	73
PULPD-19	74
PULPD-29	75
PULPD-40	77
PULPD-50	78
PULPD-100	85

As can be observed polyurethanes with a considerable high amount of biobased carbon content were synthesized, ranged from 73 to 85% biobased carbon content. The increase of LDI/PD content leads to the obtaining of thermoplastic biobased polyurethanes with higher biobased carbon content, due to LDI and PD are composed by a higher amount of biobased carbon.

5.3.2 Gel permeation chromatography

Polymer properties depend strongly on their molecular weight. Therefore, the average molecular weight and polydispersity index of the synthesized biobased polyurethanes were measured by GPC. Weight ($\bar{M}_w$) and number ($\bar{M}_n$) average molecular weight and polydispersity index (PI) are shown in Table 5.3.

Table 5.3. Weight and number average molecular weight and polydispersity index of the synthesized PULPD biobased polyurethane series.

Sample	$\bar{M}_w$ (g mol^{-1})	$\bar{M}_n$ (g mol^{-1})	PI
PULPD-13	190000	95000	2.0
PULPD-19	150000	76000	2.0
PULPD-29	100000	40000	2.5
PULPD-40	101000	33000	3.2
PULPD-50	87000	22000	3.9

The obtained $\bar{M}_w$ and $\bar{M}_n$ values indicate that the synthesis resulted in high molecular weight biobased polyurethanes. It was seen that $\bar{M}_w$ and $\bar{M}_n$ decreased with the increase of LDI/PD content, due to the lower proportion of CO3 (the reactant with the higher molar mass) involved in the synthesis of the biobased polyurethanes with higher LDI/PD content.[2,3] As can be observed PI increases due to chain extension is more hindered as diisocyanate/chain extender content increases. In any case, the variations in molecular weight and polydispersity index could be ascribed to segment architecture.[4]

5.3.3 Fourier transform infrared spectroscopy

FTIR was used to analyze the characteristic functional groups of the synthesized biobased polyurethanes. In Figure 5.1 the infrared spectra of the synthesized thermoplastic biobased polyurethanes from LDI and also of the neat CO3 and LDI are shown.
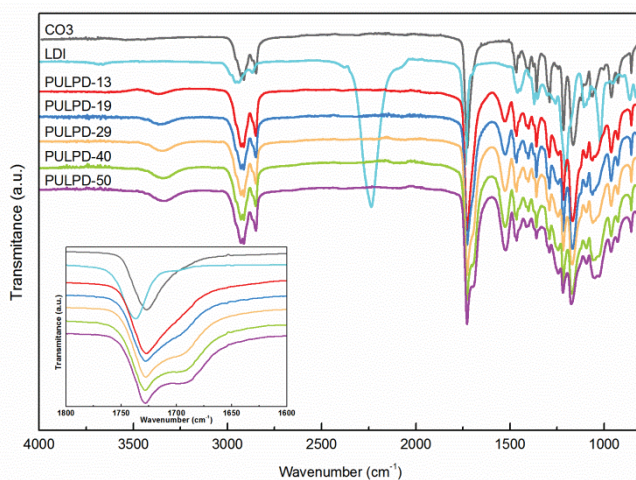
Figure 5.1. FTIR spectra of the synthesized PULPD biobased polyurethane series, CO3 and LDI. Inset: carbonyl group stretching region.

None of the synthesized biobased polyurethanes show the band at 2270 cm^{-1}, associated with the N=C=O group stretching vibration, indicating that all isocyanate groups have reacted during the polymerization. Moreover, a broad band centered at 3338 cm^{-1} appears, associated with the N-H stretching vibration of urethane groups, becoming more intense as isocyanate content increases, due to a higher formation of urethane groups.[5,6] Moreover, it appears at lower wavenumber than in PULTMP, which denotes that it could be more associated by hydrogen bonding, since associated N-H stretching vibration bands appears at lower wavenumber.[7,8] In amide II region, at 1528 cm^{-1}, the band assigned to N-H out-of-plane bending combined with C-N stretching vibration appears.[9,10] This band also becomes more intense with the increase of diisocyanate content, owing to a higher contribution of urethane groups. As can

be observed in the inset, where the infrared spectra related to amide I region (1800-1600 cm^{-1}) is shown, CO3 and LDI present a peak at 1728 and 1738 cm^{-1}, respectively, attributed to the carbonyl stretching vibration in the ester groups.[4] Besides, biobased polyurethanes show a band around 1728 cm^{-1} which encompasses LDI and CO3 carbonyl groups, as well as free carbonyl of urethane groups. In the same way, a shoulder ascribed to the hydrogen bonded carbonyl of urethane group was seen between 1705 and 1682 cm^{-1}, which becomes more intense as diisocyanate content increases, due to a higher amount of urethane groups.[2] In Figure 5.2 the peak deconvolution of baseline corrected C=O stretching vibration bands of the synthesized PULPD-13, PULPD-29 and PULPD-50 biobased polyurethanes is shown. The area of hydrogen bonded urethane carbonyl band (II) respect to total area (%) was calculated.[8] The ratios of band II are 65.9, 71.3 and 73.4% for PULPD-13, PULPD-29 and PULPD-50, respectively. The area of the peak related with hydrogen bonded carbonyl group increases with the increase of LDI/PD content. Furthermore, the obtained areas are higher than those previously calculated for PULTMP biobased polyurethane series, denoting a higher degree of hydrogen bonding association due to the absence of restriction induces by crosslink density. These results are in agreement with the decrease of the wavenumber of N-H stretching vibration band observed in PULPD series if compared to PULTMP series.
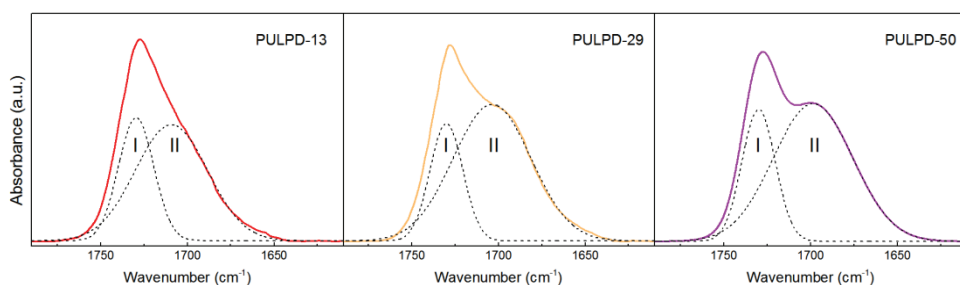
Figure 5.2. Peak deconvolution (dot lines) of baseline corrected C=O stretching bands of the synthesized PULPD biobased polyurethane series, C=O free stretching (I) and C=O hydrogen bonded stretching (II) bands.

5.3.4 Differential scanning calorimetry

The thermal behavior of the synthesized thermoplastic biobased polyurethanes was studied by means of DSC. Figure 5.3 shows the heating DSC thermograms for the synthesized biobased polyurethanes series, together with CO3 and pure LDI/PD. Furthermore, in Table 5.4 the thermal transitions values of CO3 and the synthesized thermoplastic biobased polyurethanes are listed.
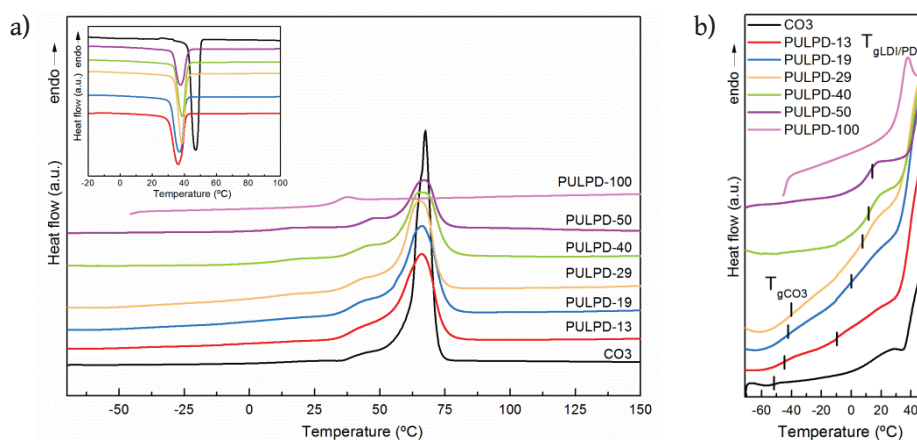
Figure 5.3. a) Heating DSC thermograms of CO3, pure LDI/PD and PULPD biobased polyurethane series and b) magnification of low temperature region. Inset: cooling DSC thermograms.

Table 5.4. Thermal transitions values of macrodiol and the synthesized PULPD biobased polyurethane series.

Sample	T_{gCO3} (°C)	T_m (°C)	ΔH_m (J g^{-1})	$T_{gLDI/PD}$ (°C)	T_c (°C)	ΔH_c (J g^{-1})	χ_c heating	χ_c cooling
CO3	–52.0	70.0	142.0	–	46.3	–93.1	1.0	1.0
PULPD-13	–44.6	66.1	97.2	–8.1	36.1	–58.1	0.8	0.7
PULPD-19	–43.4	66.1	92.0	–0.8	37.1	–57.3	0.8	0.8
PULPD-29	–41.8	65.4	88.3	9.2	38.5	–55.3	0.9	0.8
PULPD-40	–	65.5	73.1	11.7	38.9	–45.5	0.9	0.8
PULPD-50	–	66.9	57.1	12.7	37.6	–37.0	0.8	0.8
PULPD-100	–	–	–	32.7	–	–	–	–

As can be observed CO3 presents a glass transition at -52 °C and an endothermic peak associated with crystals melting at 70 °C, characteristic of a semicrystalline material. Pure LDI/PD polyurethane only shows a glass transition around 33 °C, due to the side chain of LDI inhibits to pack efficiently to form crystalline domains with a high T_m likes in conventional polyurethanes formed by MDI or HDI diisocyanates.[11-13] Similar behavior was previously also observed for PULTMP100 biobased polyurethane. However, T_g of PULTMP100 was higher due to the crosslinked structure hinders the motion of the chains.[14,15]

Regarding the synthesized biobased polyurethanes, all of them present several thermal transitions related to those observed for pure segments. As previously mentioned, T_g is an indicator of the relative purity of the phases and the miscibility between domains depends on their respective lengths, the affinity between them, and the ability of segments to crystallize.[16,12,17] The biobased polyurethanes show a glass transition at low temperatures (T_{gCO3}), which are higher than the ones observed for CO3. However, they remain almost independent to LDI/PD content and the increase could attribute to restriction of the mobility imposed by the covalently bonded LDI/PD.[18,19] Furthermore, this behavior suggests that despite a small amount of covalently bonded LDI/PD could be mixed within the CO3 rich domains, a microphase separated microstructure is developed.[9] This fact is in agreement with the differences between the theoretically determined solubility parameters of CO3 and LDI/PD (δ_{CO3} = 20.07 J$^{1/2}$ cm$^{-3/2}$ and $\delta_{LDI/PD}$ = 24.28 J$^{1/2}$ cm$^{-3/2}$), which suggest that both domains do not tend to be mixed. The obtained T_{gCO3} values are lower than those obtained for LDI based crosslinked biobased polyurethanes, which could be due to the lower motion restriction impose by the linear PD chain extender and favoring in this way higher phase separation, in agreement with FTIR results.[15] Around 70 °C, it can be observed an endothermic peak with a shoulder, associated with the melting temperature of an ordered microdomain mainly formed by CO3. The melting behavior depends on the distribution of crystallite sizes, the presence

of different crystal forms and different degrees of order in the crystalline structure,[9,20] and that is why the small shoulder appears. Although T_m remains nearly constant and independent of the LDI/PD content, ΔH_m decreases as LDI/PD content increases, due to the lower crystallizable CO3 fraction. As can be observed in Table 5.4, for the synthesized biobased polyurethanes, the relative crystallinity values of the CO3 rich domain decreased with respect to pure CO3 relative crystallinity values, due to covalently bonded LDI/PD domains that could inhibit the crystallization of the domain rich in CO3. Nevertheless, relative crystallinity values kept nearly constant and independent to the increase of LDI/PD content. This behavior differs to the observed in PULTMP series, where crystallinity decreased as LDI/TMP increased. Besides, as can be observed in the cooling scans (inset of Figure 5.3), the crystallization temperature also shows an independent behavior with respect to LDI/PD content, as it remains almost constant with the increase of LDI/PD content. This behavior is also in opposite to the previously observed for PULTMP biobased polyurethane series, suggesting that phase separation is less hindered in linear systems.

In addition, all the biobased polyurethanes show a second glass transition ($T_{gLDI/PD}$) between the T_{gCO3} and T_m of CO3 rich domain. This transition is associated with the LDI/PD domain, and increases as LDI/PD content increases, becoming closer to the value given by the neat LDI/PD, due to the formation of longer chains and showing a higher ability to join through interurethane interactions.[9] The observation of two separated glass transitions in all biobased polyurethanes suggests a microseparated phase morphology.[21,22,18,23,24]

5.3.5 Dynamic mechanical analysis

The dynamic mechanical behavior of the biobased polyurethanes was also analyzed. The DMA technique is one of the most sensitive method for following the changes in the viscoelastic properties. The temperature dependence of the

storage modulus (E') and loss factor (tanδ) for the synthesized biobased polyurethanes is shown in Figure 5.4. As can be seen, as LDI/PD content increases, the storage modulus values in the glassy state slightly increase, which could be related with the higher phase separation previously observed.[25] At lower temperatures, a broad E' decrease can be observed which encompasses both microdomains T_gs. Regarding tanδ curve a wide peak with a maximum can be observed, which is mainly related with the mechanical transition (α) of the LDI/PD,[15,17,26] since increases in intensity and temperature as LDI/PD content increases (Table 5.5).
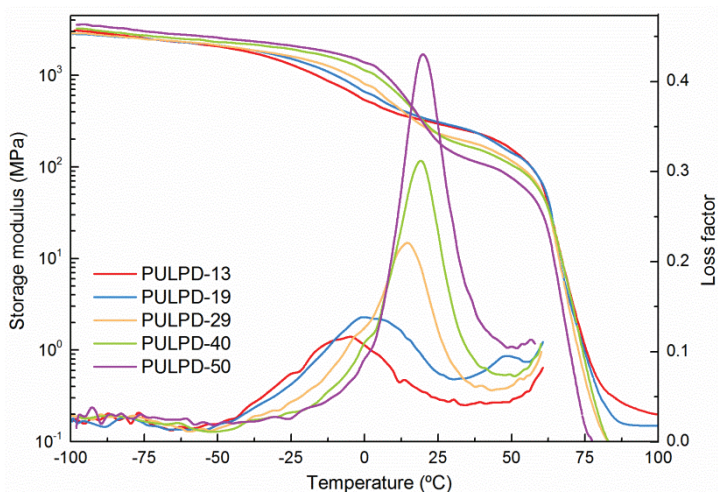
Figure 5.4. Storage modulus and loss factor of PULPD biobased polyurethane series.

Table 5.5. α transition temperature of the synthesized PULPD biobased polyurethane series.

Sample	T_α (°C)
PULPD-13	–5.0
PULPD-19	2.5
PULPD-29	14.4
PULPD-40	19.7
PULPD-50	20.1

The broadening of tanδ peak observed for PULPD-13 and PULPD-19 samples, mainly towards low temperatures, can be attributed to the amorphous phase of the CO3. In accordance with DSC results, T_α shifts to higher temperature as LDI/PD content increases.

At higher temperatures, after the decrease in E' value, the material reaches the rubbery plateau, where the elastic modulus value in the rubbery state increases with the increase of CO3 content, due to the formation of ordered domains by semicrystalline CO3, providing significant structural reinforcement and a higher elastic recovery at high temperature.[12,27] Finally, at higher temperatures, E' values suffer a marked decrease associated with the melting temperature of the CO3, as observed also before by DSC, where a disruption of crystalline domains occurs.

5.3.6   Atomic force microscopy

The morphology of the synthesized biobased polyurethanes was analyzed by AFM, and as shown in the micrographs of PULPD-19 and PULPD-40 (Figure 5.5), the synthesized biobased polyurethanes present a phase separated microstructure. The light regions in height images correspond to the crystalline phase of the CO3. In PULPD-19 sample, almost all the surface is covered by crystalline structures, according to the high crystallinity value observed for this sample by DSC. The observed small dark regions are related to amorphous domains, which became bigger and more heterogeneous for the biobased polyurethane synthesized with higher LDI/PD content. PULPD-19 dark regions are ranged from 250 to 340 nm, while for PULPD-40 are ranged from 370 nm to 1.5 μm.
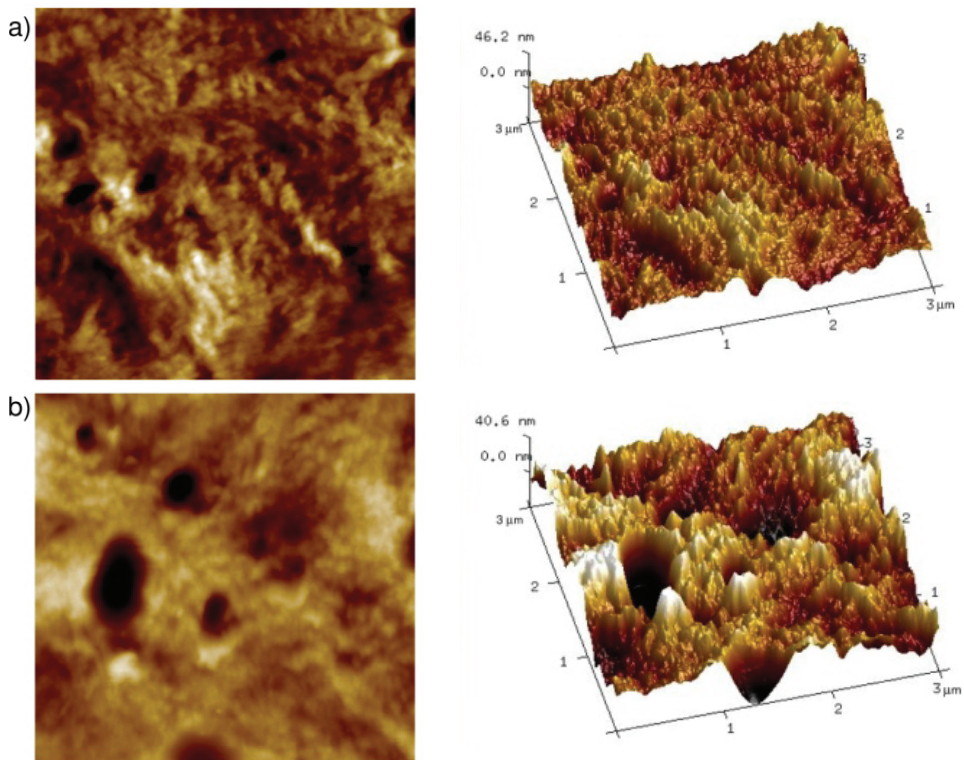
Figure 5.5. Height (left) and three-dimensional (right) AFM images of a) PULPD-19 and b) PULPD-40 (size: 3 x 3 μm²).

5.3.7 Mechanical properties

Figure 5.6 shows stress-strain curves of the synthesized biobased polyurethanes. The characteristic values derived from stress-strain curves and the Shore D hardness values are displayed in Table 5.6.

As can be observed with the increase of LDI/PD content, the material withstands lower strains and stresses. The increase in tensile properties observed with increasing CO3 content can be due to the crystallization of the CO3, which acts as a reinforcing filler. As LDI/PD content increases, according to DSC results, biobased polyurethane crystallinity decreases, and therefore, hardness values also decrease, as they are directly related to the overall crystallinity of the material. Taking into account the results obtained by mechanical tests, it was

found that the tensile properties and hardness of the synthesized biobased polyurethanes are mainly governed by CO_3 content and crystallinity.
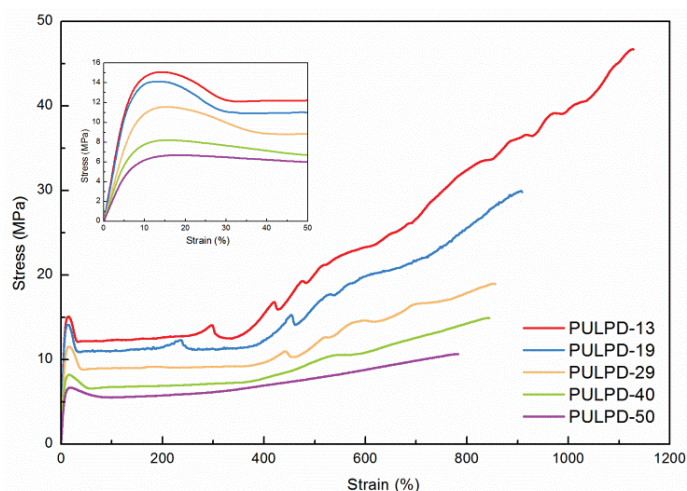
Figure 5.6. Stress-strain curves of the synthesized PULPD biobased polyurethane series.

Table 5.6. Mechanical properties of the synthesized PULPD biobased polyurethane series.

Sample	E (MPa)	σ_y (MPa)	σ_b (MPa)	ε (%)	Shore D
PULPD-13	223 ± 4	14.3 ± 0.8	43.7 ± 3.1	1075 ± 52	49.8 ± 0.8
PULPD-19	206 ± 9	13.5 ± 0.9	28.4 ± 1.1	864 ± 33	47.7 ± 0.6
PULPD-29	143 ± 4	11.2 ± 0.3	18.5 ± 1.0	849 ± 31	45.9 ± 0.5
PULPD-40	128 ± 6	8.5 ± 0.7	14.9 ± 0.6	834 ± 10	42.3 ± 0.4
PULPD-50	89 ± 12	6.4 ± 0.6	10.6 ± 0.5	785 ± 18	36.9 ± 0.3

During the stretching process some jumps can be observed in the stress-strain curves, which are attributed to the formation of necking points during the tensile tests, as can be observe in Figure 5.7, and to the disruption of the crystalline domains. Thus, as CO_3 content decreases, fewer jumps can be observed in the curves, owing to a lower amount of crystals.
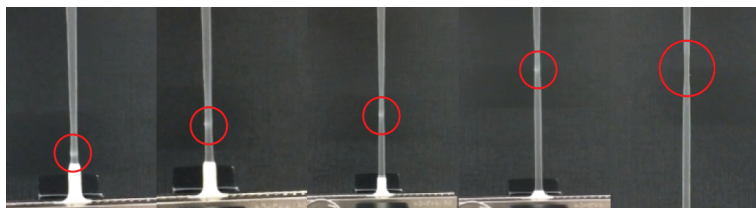
Figure 5.7. Sequence of digital images of the evolution of necking points during the tensile test.

5.3.8 Water contact angle

As chemical nature and domains arrangement could influence on surface properties of biobased polyurethanes, such as hydrophilic character, wettability and surface tension, the contact angle of the synthesized biobased polyurethanes was analyzed. Contact angle analysis provides information of the surface hydrophobicity or hydrophilicity, and of the molecular mobility at the air-water-solid interface.[11,28] Contact angle and surface tension values of the synthesized biobased polyurethanes are given in Table 5.7.

Table 5.7. Contact angle and surface tension values of synthesized PULPD biobased polyurethane series.

Sample	Contact angle (°)	Surface tension (mN m^{-1})
PULPD-13	81.1 ± 0.4	24.3
PULPD-19	79.3 ± 0.3	25.6
PULPD-29	78.4 ± 0.4	26.3
PULPD-40	77.0 ± 0.2	27.3
PULPD-50	74.0 ± 0.4	29.6

As LDI/PD content increases, the contact angle value decreases and surface tension increases, thus the material becomes more hydrophilic, as in conventional polyurethanes.[28] In opposite to PULTMP series, water contact angle values decrease as CO3 content decreases, corroborating that contact angle is dependent not only in the urethane density but also in crosslink density.

5.4 Characterization of the synthesized thermoplastic biobased polyurethanes from DDI

5.4.1 Biobased carbon content

As mentioned before the biobased carbon content of the starting materials was determined by the ASTM-D6866-12 (0.98) Method B (AMS) standard procedure.[1] CO3 has a 72% biobased carbon content, DDI a 98% biobased carbon content and PD and DAS have a 100% biobased carbon content. The biobased carbon content of the final polyurethanes was estimated by taking into account the molar ratio and the biobased carbon content of each component in the final formulation (equation 2.2). The biobased carbon content of the synthesized biobased polyurethanes are shown in Table 5.8.

Table 5.8. Biobased carbon content of the synthesized PUDPD and PUDDAS biobased polyurethane series.

Sample	Biobased carbon content (%)
PUDPD-26	80
PUDPD-36	83
PUDPD-48	86
PUDPD-100	98
PUDDAS-28	80
PUDDAS-37	83
PUDDAS-50	86
PUDDAS-100	98

Results indicate that thermoplastic polyurethanes with high biobased carbon content were synthesized. As DDI/chain extender content increases the biobased carbon content also increases, because of the high biobased carbon content of DDI and chain extenders. This trend was also observed for PULPD series. If comparing PULPD and PUDPD thermoplastic series, it can be seen that

PUDPD biobased polyurethane system shows higher biobased carbon content due to the higher carbon contribution of DDI, 36 carbons, while the carbon contribution of LDI is 10 carbons.

5.4.2 Gel permeation chromatography

As mentioned before polymer properties are strongly dependent on their molecular weight, therefore the average molecular weight and polydispersity index of the synthesized biobased thermoplastic polyurethanes have been measured by GPC and the values are listed in Table 5.9.

Table 5.9. Weight and number average molecular weight and polydispersity index of the synthesized PUDPD and PUDDAS biobased polyurethane series.

Sample	$\overline{M}_w$ (g mol^{-1})	$\overline{M}_n$ (g mol^{-1})	PI
PUDPD-26	78000	33000	2.4
PUDPD-36	75000	27000	2.8
PUDPD-48	74000	25000	3.0
PUDDAS-28	87000	36000	2.4
PUDDAS-37	80000	34000	2.4
PUDDAS-50	47000	21000	2.2

It can be seen that $\overline{M}_w$ and $\overline{M}_n$ values for both series are similar except for PUDDAS-50, which could be due to it was difficult to filtrate and hence some chains could be retained in the filter. The slightly higher values determined for PUDDAS-28 and PUDDAS-37 respect to PUDPD-26 and PUDPD-36 biobased polyurethanes, could be attributed to a higher molar mass of DAS. In the same way, $\overline{M}_w$ and $\overline{M}_n$ in both systems decrease as DDI/chain extender content increases, which could be attributed to the larger amount of DDI and chain extender, which have a lower molecular weight.[3] In any case, similar to PULPD series, the variations in molecular weight can be also ascribed to segment

architecture.[4] As previously observed for PULPD, PI increases as DDI/chain extender content increases.

5.4.3 Fourier transform infrared spectroscopy

FTIR was used to analyze the characteristic groups of the biobased polyurethanes. All the compositions in each series show the same bands in despite of the differences in intensity, which are related with the variation of the molar ratio of components. Similarly to previous systems, it was not observed the isocyanate group stretching vibration at 2270 cm^{-1}, indicating that complete polymerization took place. Therefore, the free catalyst synthesis method was suitable, as previously observed for PUDTMP series. In order to analyze the effect of chain extender structure, the infrared spectra of PUDPD-48, PUDDAS-50, neat CO3 and DDI spectra are compared in Figure 5.8.
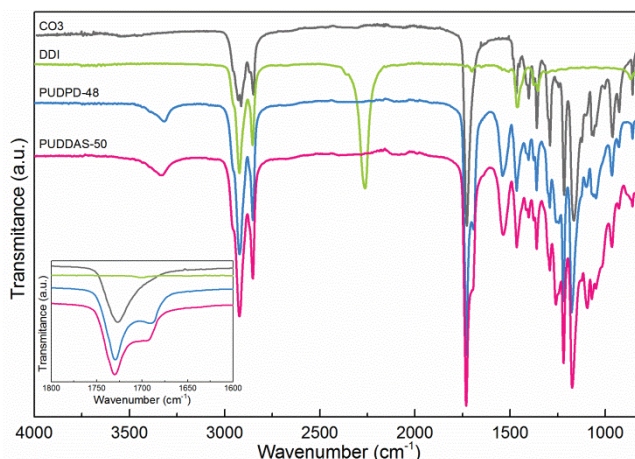
Figure 5.8. FTIR spectra of CO3, DDI and the synthesized PUDPD-48 and PUDDAS-50 biobased polyurethane series. Inset: carbonyl group stretching region.

PUDPD-48 and PUDDAS-50 biobased polyurethanes show a band associated with the N-H stretching vibration of the urethane group[6] at 3314 and 3331 cm^{-1}, respectively. The band ascribed to the N-H out-of-plane bending combined with C-N stretching vibration appears at 1530 cm^{-1}.[9] Furthermore, the carbonyl group stretching region is shown in the inset, where CO3 presents a band at 1728 cm^{-1}

associated with carbonyl stretching in the ester group.[4] As can be observed, the synthesized biobased polyurethanes show a band at 1728 cm^{-1}, which encompasses the infrared absorbance of ester C=O group of CO3 and the free urethane C=O group. Regarding the urethane hydrogen bonded C=O group, PUDPD-48 and PUDDAS-50 present a peak at 1689 and 1692 cm^{-1}, respectively. In addition to the lower wavenumber, the peak is more intense in PUDPD-48, which could be related to the lower steric hindrance due to the linear aliphatic structure of PD, allowing an easier chain association by hydrogen bonding. In the same way, the peak ascribed to the N-H stretching vibration of urethane groups in PUDPD-48 polyurethane appears at a lower wavenumber according to a higher level of association by hydrogen bonding,[7,8] corroborating the behavior observed in the carbonyl group stretching region.

5.4.4   Differential scanning calorimetry

The thermal behavior of the synthesized thermoplastic biobased polyurethanes was also analyzed. Figure 5.9 shows the DSC heating and cooling thermograms for the synthesized PUDPD and PUDDAS series together with CO3. Moreover, the thermal transitions are listed in Table 5.10.
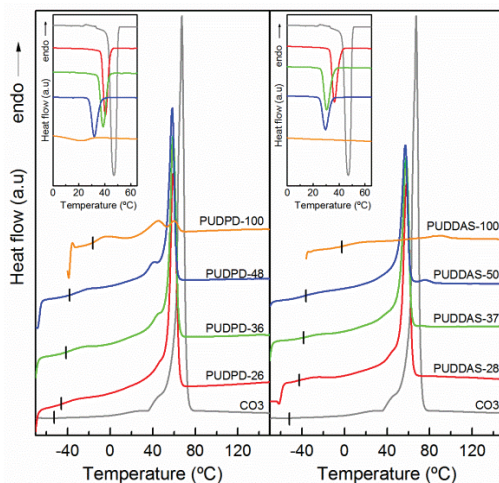
Figure 5.9. Heating and cooling (inset) DSC thermograms of the synthesized biobased polyurethanes PUDPD (left) and PUDDAS (right), together with CO3.

Table 5.10. Thermal transition of CO3 and the synthesized PUDPD and PUDDAS biobased polyurethane series.

Sample	T_g (°C)	T_m (°C)	ΔH_m (J g^{-1})	T_c (°C)	ΔH_c (J g^{-1})
CO3	−52.0	70.0	142.0	46.3	−93.1
PUDPD-26	−45.6	59.1	73.7	40.5	−69.5
PUDPD-36	−41.6	45.79 / 59.0	67.7	38.7	−64.5
PUDPD-48	−39.1	41.35 / 58.3	56.0	31.9	−50.5
PUDPD-100	−14.4	44.9 / 60.1	13.8	21.2	−8.2
PUDDAS-28	−43.0	58.6	76.7	36.4	−63.9
PUDDAS-37	−38.8	57.9	60.6	30.5	−57.1
PUDDAS-50	−36.2	57.2 / 75.9	45.4 / 0.8	29.5	−43.6
PUDDAS-100	−1.1	89.6	5.3	−	−

As mentioned before CO3 is semicrystalline with a T_g at −52 °C and an endothermic peak associated with crystals melting at 70 °C. Regarding neat DDI/chain extender biobased polyurethanes, PUDPD-100 shows a T_g around −14 °C and two endothermic peaks at 45 and 60 °C, while neat PUDDAS-100, besides the T_g at −1 °C, shows an endothermic peak at a temperature higher than that of PUDPD-100, at 89 °C, due to its bicyclic structure. If compared the thermal transitions of the synthesized thermoplastic PUDPD-100 and PUDDAS-100 with the crosslinked PUDTMP-100 (Table 4.8), it can be observed that the T_g of PUDTMP-100 is higher than the T_g of PUDPD-100 and PUDDAS-100, around 23 and 9 °C, respectively, because the net points hinder chain mobility, resulting in a higher T_g.[14,15,26] As can be seen in PUDPD-100 and PUDDAS-100, the use of DDI as diisocyanate results in biobased polyurethanes with low T_g and T_m values, due to its branched aliphatic structure hinders the association by hydrogen bonding and leads to flexible chains. This behavior was also observed in the synthesized crosslinked biobased polyurethane series with TMP (PULTMP and PUDTMP) in chapter 4 and also early in this chapter when thermoplastic biobased polyurethanes were synthesized using LDI as diisocyanate (PULPD). Like DDI,

the side chain of the aliphatic LDI inhibited the crystallization of neat LDI/PD and LDI/TMP biobased polyurethanes. However, because the LDI molecule is smaller, the resultant chains were stiffer and T_g values of 33 and 59 °C were obtained for LDI/PD and LDI/TMP, respectively. Nevertheless, the thermal behavior of polyurethanes with DDI or LDI differs from that reported in the literature when classical diisocyanates like aromatic MDI or aliphatic HDI are employed. For instance, Cognet-Georjon et al.[29] reported a stiff polyurethane formed by MDI/DAS with a T_g of 187 °C and a T_m of 235 °C. In the same way, Saralegi et al.[12] synthesized a HDI/PD polyurethane with a T_g of 60 °C and a T_m higher than 160 °C. Similarly, Ugarte et al.[2] synthesized a MDI/PD polyurethane with a T_g of 109 °C.

Regarding the synthesized PUDPD and PUDDAS thermoplastic biobased polyurethanes with different DDI/chain extender content, all of them present several thermal transitions related to those observed for neat blocks. At low temperatures, both thermoplastic biobased polyurethanes series show a T_g that increases as DDI/PD and DDI/DAS contents increase. Due to the chemical structure of DDI, a fraction of DDI/chain extender is mixed with the amorphous macrodiol. Both CO3 and DDI/PD or DAS domains have similar solubility parameters (δ_{CO3} = 20.07 $J^{1/2}$ $cm^{-3/2}$; $\delta_{DDI/PD}$ = 20.03 $J^{1/2}$ $cm^{-3/2}$ and $\delta_{DDI/DAS}$ = 20.46 $J^{1/2}$ $cm^{-3/2}$), which favors their miscibility. In this way, as the DDI/chain extender content increases T_g also increases according to the miscibility between amorphous blocks. Similar behavior was observed in PUDTMP polyurethane series; as DDI/TMP content increased, T_g also increased. However, higher T_g values were obtain in PUDTMP polyurethane series, due to the restrictions in chain mobility imposed by crosslinks. In contrast, different behaviors were observed when more classical diisocyanates were used. Cognet-Georjon et al.[17] reported a polyurethane system containing a 35 and 48 wt% MDI/DAS segment and a polyether polyol (2000 g mol^{-1} molecular weight), with a T_g slightly higher than the T_g of neat polyol (11-13 °C), almost independent of

hard segment content. This slight increase was attributed to restrictions of the mobility of soft segments and not to the dissolved hard segment.[18,19] Moreover, Saralegi et al.[12] synthesized polyurethanes with HDI and the same CO3 and PD, founding T_g values around -50 °C, which were also independent of the hard segment content and showed a higher degree of phase separation. Similarly, when the trans-trans isomer content of 4,4'-dicyclohexylmethane diisocyanate ($H_{12}MDI$) was increased from 45 to 98 % (determined by ^{13}C NMR),[30] a decrease in T_g was observed and it becomes closer to the macrodiol T_g, suggesting an increase in the soft segment purity and hence the formation of ordered hard domains that contributed to better phase separation.

Moreover, in PUDPD polyurethanes, between 30 and 70 °C, an endothermic peak with a shoulder can be seen. As mentioned before, PUDPD-100 show two peaks at similar temperatures, meaning that the endothermic peak observed encompasses the melting enthalpy of both CO3 and DDI/PD rich domains. However, as the DDI/PD content increases, the enthalpy of the peak (58 °C) decreases while the shoulder at 45 °C increases, becoming a peak. Therefore, the peak could be mainly associated with the crystalline microdomain formed by macrodiol and the shoulder with that formed by ordered structure of DDI/PD. Regarding PUDDAS, as DDI/DAS content increases, the intensity of the overal endothermic peak observed decreases, according to a lower content of the CO3 rich microdomain. Nevertheless, as the DDI/DAS content increases, a second endothermic peak appears around 75 °C, which could be associated with the melting of crystals formed by the DDI/DAS rich microdomain. Melting enthalpy values for PUDPD thermoplastic biobased polyurethanes are higher than those of PUDDAS because PD is an aliphatic linear small molecule with a lower steric hindrance, which facilitates the efficient packaging of macrodiol chains to form crystals and is also due to the contribution of the melting of DDI/PD crystals. Furthermore, the cooling scans of both PUDPD and PUDDAS series (inset on the left of each figure in Figure 5.9) show a similar behavior, but as the DDI/chain

extender content increases, the crystallization temperature and enthalpy also decrease, in opposite to the observed for PULPD series where T_c remained nearly constant and independent to LDI/PD in accordance to a more microphase separated morphology.

5.4.5 Dynamic mechanical analysis

The dynamic mechanical behavior of the synthesized thermoplastic biobased polyurethanes was analyzed by means of DMA (Figure 5.10).
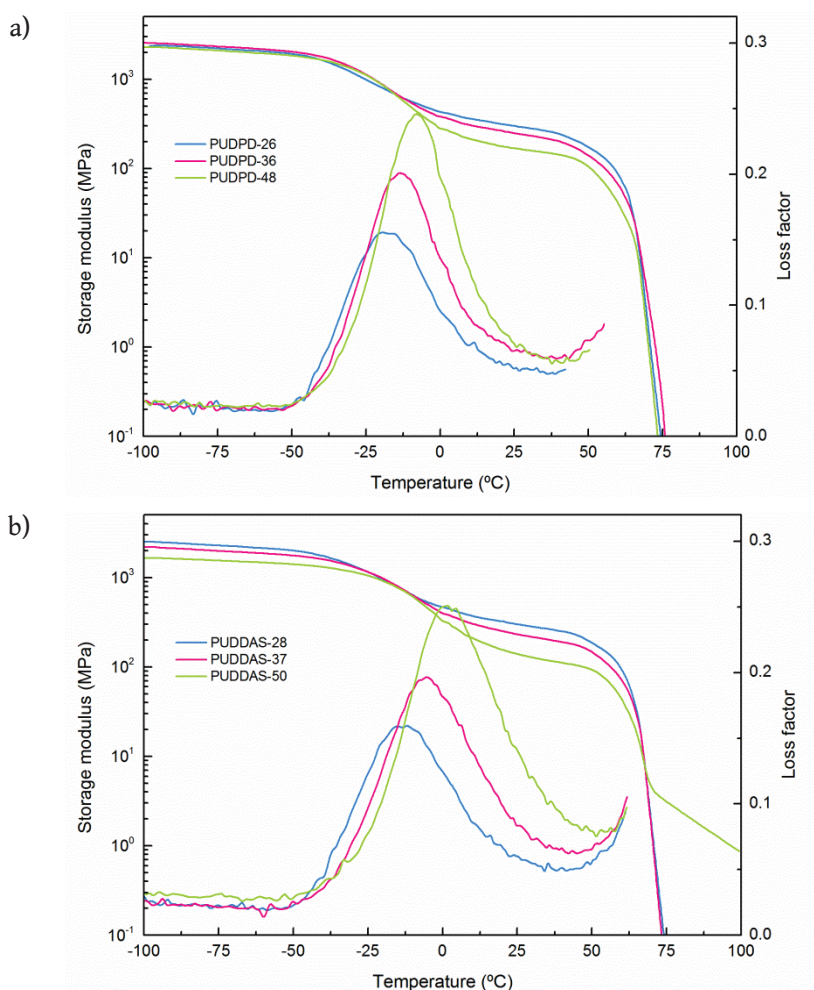
Figure 5.10. Storage modulus and loss factor of the synthesized biobased polyurethanes series a) PUDPD and b) PUDDAS.

As can be observed PUDPD and PUDDAS, show a similar behavior. As the CO3 content increases, the E' values in the glassy state are slightly higher, due to the higher crystallinity.[27] At higher temperatures, the materials show a decrease in E' associated with the T_g. In addition, after the decrease in the E', biobased polyurethanes reach a plateau, where the E' value decreases with an increase in the DDI/chain extender content, due to less ordered domains related with semicrystalline CO3, which provides significant structural reinforcement.[12,27] In the same way, E' values are higher for PUDPD biobased polyurethanes because of the higher crystallinity of the material, which is in accordance with the results observed in DSC. Finally, at higher temperatures E' decreases due to the disruption of ordered domains formed by the CO3. For PUDDAS-50, the decrease in E' is less abrupt due to the crystals formed by DDI/DAS domain that exhibit higher T_m, as revealed by DSC, which contributes to the physical crosslink.

With regard to the tanδ curve, a wide peak with a maximum can be observed, which is related to the mechanical transition (α) of the amorphous domains formed mainly by DDI/chain extender,[17] because the intensity and temperature increase as the DDI/chain extender rich domain content increases. The contribution of amorphous CO3 domain is very low due to its high crystallinity. The T_α of the synthesized biobased polyurethanes are listed in Table 5.11.

Table 5.11. α temperature of the synthesized PUDPD and PUDDAS biobased polyurethane series.

Sample	T_α (°C)
PUDPD-26	-17.9
PUDPD-36	-13.3
PUDPD-48	-8.0
PUDDAS-28	-13.5
PUDDAS-37	-5.5
PUDDAS-50	1.6

As can be observed PUDDAS biobased polyurethanes show a T_α higher than those of PUDPD because of the higher steric hindrance of DAS that inhibits the mobility of the chains. This behavior is in agreement with T_g values measured by DSC.

5.4.6 Mechanical properties

The stress-strain curves are shown in Figure 5.11 and the values derived from them together with hardness Shore D values are listed in Table 5.11.
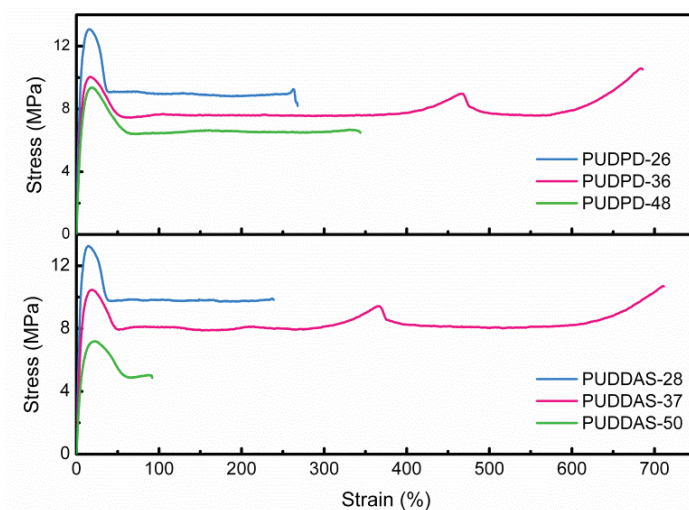
Figure 5.11. Stress-strain curves of the synthesized PUDPD and PUDDAS biobased polyurethane series.

Table 5.12. Mechanical properties of the synthesized PUDPD and PUDDAS biobased polyurethane series.

Sample	E (MPa)	σ_y (MPa)	σ_b (MPa)	ε_b (%)	Shore D
PUDPD-26	243 ± 16	13.8 ± 0.6	13.7 ± 0.7	272 ± 28	55.7 ± 0.8
PUDPD-36	167 ± 8	11.1 ± 0.2	10.8 ± 1.0	691 ± 9	51.4 ± 0.6
PUDPD-48	135 ± 5	9.4 ± 0.2	9.7 ± 0.4	346 ± 18	50.0 ± 0.7
PUDDAS-28	226 ± 9	13.0 ± 0.6	13.0 ± 0.6	262 ± 29	57.3 ± 0.5
PUDDAS-37	150 ± 6	10.3 ± 0.1	10.9 ± 0.4	715 ± 6	51.0 ± 0.7
PUDDAS-50	107 ± 2	7.3 ± 0.1	7.3 ± 0.1	87 ± 8	55.2 ± 0.6

For both polyurethane series, the elastic modulus, stress at break and at yield increase as the CO3 content increases due to the higher crystallinity of the material that acts as reinforcement.[31] Similar trend was also observed in the thermoplastic biobased polyurethanes synthesized earlier in this chapter, PULPD series, where it was seen that mechanical properties were mainly governed by the crystallizable macrodiol rich domain. However, when crystallizable urethane rich domains like HDI/PD[12] were used, also with the same macrodiol (CO3), the stress at break and elastic modulus increased as the HDI/PD content increased, contributing both domains to the observed improvement. With regard to elongation at break of the synthesized thermoplastic biobased polyurethanes, PUDPD-36 and PUDDAS-37 show a significant increase in the elongation. This fact could be related to the formation of crystals composed by DDI/PD and DDI/DAS segments as observed previously by DSC that could be able to absorb more strain energy upon deformation, acting as effective stress-bearing phase during deformation.[32,33] However, for PUDPD-48 and PUDDAS-50 samples the formation of crystals formed by longer DDI/PD and DDI/DAS segments could contribute to the appearance of more breaking points which result in a steep decrease in elongation, being more pronounced in PUDDAS-50, in agreement with the results obtained by DSC and DMA.

Regarding Shore D hardness of the synthesized materials, as the DDI/chain extender content increases, hardness values decrease according to a lower crystallinity of the material. However, PUDDAS-50 shows a higher value. This fact might be due to the presence of DDI/DAS crystals, which have a T_m higher than that of CO3 crystals, providing the material a greater hardness. Similar behavior was found in the literature for crystallizable rich domains[12], as well as for amorphous rich domains in the case of the previously analyzed PULPD polyurethane series.

5.4.7   Atomic force microscopy

In order to a deeper understanding of the final properties of the synthesized materials, the morphology was analyzed by AFM (Figure 5.12).
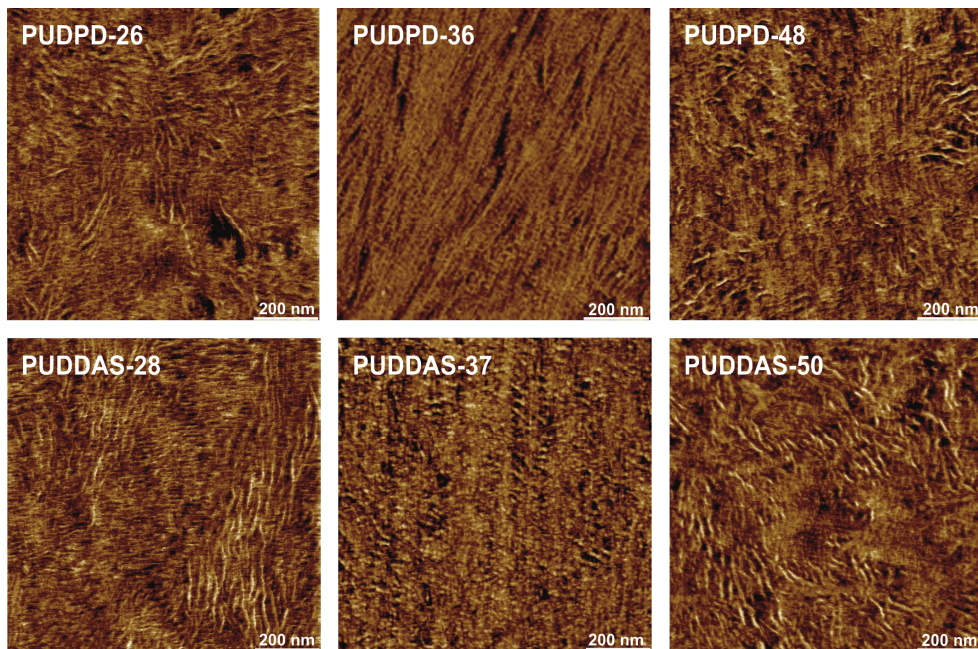
Figure 5.12. Phase AFM images of PUDPD and PUDDAS biobased polyurethane series (size: 1 x 1 μm^2).

As can be observed, both synthesized thermoplastic biobased polyurethanes present a microstructure in which different domains can be distinguished. The lighter regions correspond to the crystalline domains and the darker ones to amorphous domains. The frequency of these dark regions increases as the DDI/chain extender content increases, according to a lower overall crystallinity of the material. With regard to the morphology of PUDPD-36 and PUDDAS-37, it seems more homogeneous and could be the reason for the greater deformability observed for these materials. However, an orientation in the morphology can be observed, especially in PUDPD-36, which could take place during the cryo-cut of the samples due to their higher ductility as also observed in mechanical testing.

5.4.8 Water contact angle

Contact angle and surface tension values are listed in Table 5.13. Since fatty acid groups have hydrophobic properties,[34] the contact angle of all the synthesized thermoplastic biobased polyurethanes increases as the DDI/chain extender content increases, in opposite to the behavior observed in LDI/PD series. And in consequence, the surface tension of the materials decreases with the increase of DDI/chain extender content. PUDPD and PUDDAS thermoplastic biobased polyurethanes show similar values at each DDI/chain extender content, suggesting that contact angle is more influenced by the amount of fatty acid groups instead of the structure of the chain extender.

Table 5.13. Contact angles and surface tension values of synthesized PUDPD and PUDDAS biobased polyurethane series.

Sample	Contact angle (°)	Surface tension (mN m^{-1})
PUDPD-26	88.1 ± 0.6	19.4
PUDPD-36	93.8 ± 1.2	15.9
PUDPD-48	100.2 ± 1.6	12.3
PUDDAS-28	88.0 ± 0.9	19.5
PUDDAS-37	90.4 ± 0.9	17.9
PUDDAS-50	98.3 ± 0.9	13.3

5.5 Biocompatibility of the synthesized thermoplastic biobased polyurethanes

As previously mentioned due to the versatility of polyurethane properties, they can found application in different fields such as in biomedicine. Therefore, in order to evaluate the potential of the synthesized thermoplastic biobased polyurethanes to be used in biomedical applications the biocompatibility of the synthesized biobased polyurethanes was studied by performing short-term cytotoxicity assays and by analyzing the long term cell adhesion.

5.5.1 Cell viability and proliferation of thermoplastic biobased polyurethanes

The viability of the synthesized PULPD-29, PUDPD-26 and PUDDAS-28 biobased polyurethanes, together with, both positive (PVC) and negative (HDPE) controls are shown in Figure 5.13. As can be seen, the cell viability value is above 100 % for PULPD-29 and around 85% for PUDPD-26 and PUDDAS-28 of the value of negative control. These values are higher than the acceptance limit of 70%, as established by ISO 10993-12 standard.[35] Therefore, the synthesized thermoplastic biobased polyurethanes show non-toxic behavior demonstrating the potential of these materials to be used for biomedical applications.
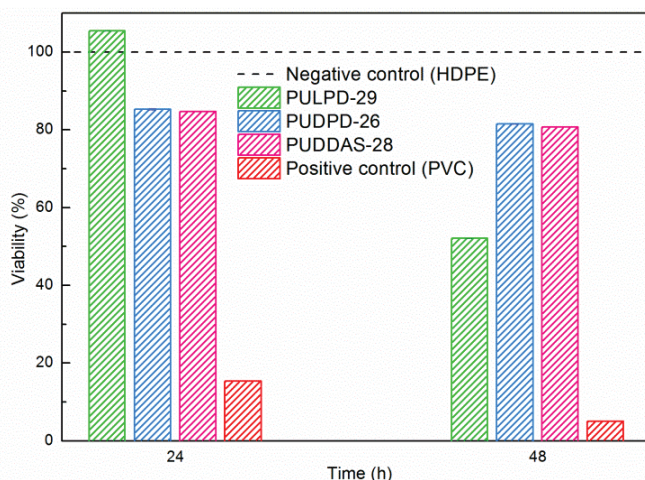
Figure 5.13. Viability of L-929 murine fibroblast cells in extracted media at 24 and 48 h in negative control (HDPE), PULPD-29, PUDPD-26 and PUDDAS-28 biobased polyurethanes and positive control (PVC).

Although at the first 24 h the thermoplastic biobased polyurethane based on LDI show a better biocompatibility behavior, at 48 h its viability decreases, whereas the cell viability of the polyurethanes based on DDI is almost the same. The higher viability of the polyurethanes with DDI was also observed for the homologue crosslinked biobased polyurethane PUDTMP-27, denoting that DDI promotes in a higher extent the proliferation of the cells.

5.5.2 Cell adhesion of thermoplastic biobased polyurethanes

Cell adhesion of the synthesized thermoplastic biobased polyurethanes was analyzed by performing Live/Dead assays. The fluorescence micrographs of PULPD-29, PUDPD-26 and PUDDAS-28 at 7 and 14 days are shown in Figure 5.14.
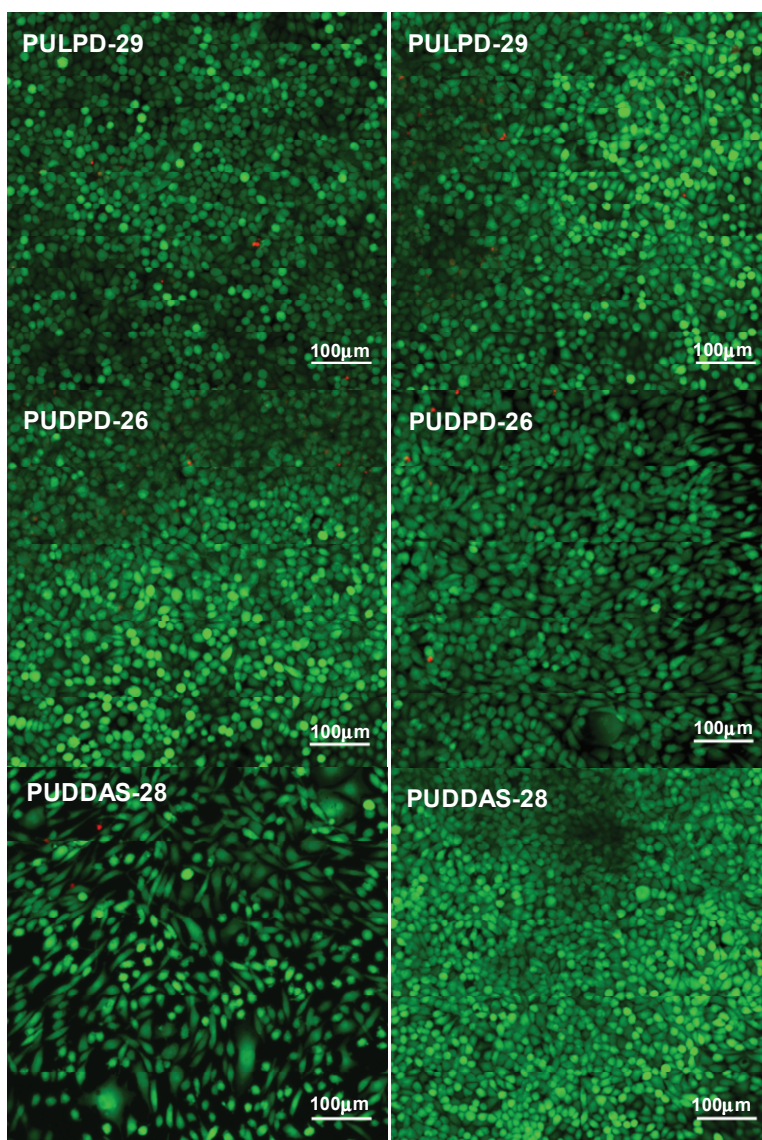
Figure 5.14. Fluorescence confocal microscope images recorded from Live/Dead assays of cells grown in direct contract with PULPD-29, PUDPD-26 and PUDDAS-28 biobased polyurethanes for 7 (left) and 14 (right) days.

Regarding to cell adhesion at 7 days (micrographs on the left) it can be observed that cells grown in all the synthesized polyurethanes and they were metabolically active (green) and only a few dead cells (red) can be observed. Furthermore, at 14 days (microghaps on the right) cell density increased in each materials, especially in PUDDAS-28.

5.6   Conclusions

Thermoplastic biobased polyurethanes with high biobased carbon content were synthesized successfully by a catalyst free two step bulk polymerization process using a macrodiol derived from castor oil and two different biobased diisocyanates, LDI derived from L-lysine amino acid and DDI from fatty acids. In the case of thermoplastic biobased polyurethanes with LDI, PD was used as chain extender, which was derived from corn sugar. When the diisocyanate derived from fatty acids was used, in addition to the corn sugar based PD, DAS derived from polysaccharides was also used as chain extender.

It was seen that the use of an aliphatic with side chain diisocyanate (LDI) or a branched one (DDI) results in thermoplastic polyurethanes with low T_g and their steric hindrance inhibits the crystallization. Synthesized biobased polyurethanes showed different behavior. In the case of PULPD series two T_g were observed suggesting a microphase separated morphology. However in PUDPD an PUDDAS series a single T_g was observed, which increased with DDI/chain extender content, denoting a microphase mixing. Moreover, with PUDPD and PUDDAS polyurethane series the influence of the structure of the chain extender was also seen, as the steric hindrance of the chain extender increased (in the case of DAS chain extender) higher T_g values and lower ability to crystallize were observed. Furthermore, in both PULPD and PUDPD and PUDDAS polyurethane series an inversion of the behavior of the segments was observed, since the crystallizable phase formed by the macrodiol showed a T_m higher than the T_g of LDI/PD and DDI/PD or DDI/DAS, which made the

macrodiol to act as hard phase. These results differed with the observed in the literature when conventional diisocyanates are employed, where segments formed by diisocyanates and chain extender with high T_g and T_m are obtained. It was observed in all the synthesized thermoplastic biobased polyurethane series that mechanical properties were tightly dependent on the overall crystallinity and morphology. As the crystallinity of the material increased mechanical properties improved, which allows the possibility of synthesizing thermoplastic biobased polyurethanes with tailored mechanical properties. Furthermore, the different behavior observed for the synthesized thermoplastic biobased polyurethanes in comparison with the results available in literature allows a deeper understanding of the chemistry and reactants structure, which influence on polyurethane final properties.

In addition, the preliminary *in vitro* cytotoxicity evaluation of the synthesized thermoplastic biobased polyurethanes revealed that all synthesized materials showed non-toxic behavior. Polyurethanes based on DDI promoted the proliferation of fibroblast in a larger extend, which could be attributed to the nature of the diisocyanate. Furthermore, Live/Dead assays showed that cells were metabolically active, only dying a few of them in the first 7 days and at 14 days cell density increases for all synthesized thermoplastic biobased polyurethanes. In this way, the synthesized thermoplastic polyurethanes showed their potential to be used for biomedical applications.

5.7   References

1.   ASTM D6866-12. "Standard test method for determining the biobased content of natural range materials using radiocarbon and isotope ratio mass spectrometry analysis." ASTM International. West Conshohocken, PA, 2012.

2.   L. Ugarte, B. Fernández-d'Arlas, A. Valea, M.L. González, M.A. Corcuera,

A. Eceiza. "Morphology-properties relationship in high-renewable content polyurethanes". Polym. Eng. Sci. 2014. 54: 2282–2291.

3. C. Bueno-Ferrer, E. Hablot, F. Perrin-Sarazin, M.C. Garrigós, A. Jiménez, L. Averous. "Structure and morphology of new bio-based thermoplastic polyurethanes obtained from dimeric fatty acids". Macromol. Mater. Eng. 2012. 297: 777–784.

4. B. Fernández-d'Arlas, J.A. Ramos, A. Saralegi, M.A. Corcuera, I. Mondragon, A. Eceiza. "Molecular engineering of elastic and strong supertough polyurethanes". Macromolecules 2012. 45: 3436–3443.

5. Y.M. Tsai, T.L. Yu, Y.H. Tseng. "Physical properties of crosslinked polyurethane". Polym. Int. 1998. 47: 445–450.

6. Z. Wang, L. Yu, M. Ding, H. Tan, J. Li, Q. Fu. "Preparation and rapid degradation of nontoxic biodegradable polyurethanes based on poly(lactic acid)-poly(ethylene glycol)-poly(lactic acid) and L-lysine diisocyanate". Polym. Chem. 2011. 2: 601–607.

7. A. Santamaria-Echart, A. Arbelaiz, A. Saralegi, B. Fernández-d'Arlas, A. Eceiza, M.A. Corcuera. "Relationship between reagents molar ratio and dispersion stability and film properties of waterborne polyurethanes". Colloids Surfaces A Physicochem. Eng. Asp. 2015. 482: 554–561.

8. L. Rueda-Larraz, B. Fernández-d'Arlas, A. Tercjak, A. Ribes, I. Mondragon, A. Eceiza. "Synthesis and microstructure-mechanical property relationships of segmented polyurethanes based on a PCL-PTHF-PCL block copolymer as soft segment". Eur. Polym. J. 2009. 45: 2096–2109.

9. M.A. Corcuera, L. Rueda, B. Fernandez-d'Arlas, A. Arbelaiz, C. Marieta, I. Mondragon, A. Eceiza. "Microstructure and properties of polyurethanes derived from castor oil". Polym. Degrad. Stab. 2010. 95: 2175–2184.

10.   L. Peponi, I. Navarro-Baena, A. Sonseca, E. Gimenez, A. Marcos-Fernandez, J.M. Kenny. "Synthesis and characterization of PCL-PLLA polyurethane with shape memory behavior". Eur. Polym. J. 2013. 49: 893–903.

11.   M.A. Corcuera, L. Rueda, A. Saralegi, M.D. Martín, B. Fernández-d'Arlas, I. Mondragon, A. Eceiza. "Effect of diisocyanate structure on the properties and microstructure of polyurethanes based on polyols derived from renewable resources". J. Appl. Polym. Sci. 2011. 122: 3677–3685.

12.   A. Saralegi, L. Rueda, B. Fernández-d'Arlas, I. Mondragon, A. Eceiza, M.A. Corcuera. "Thermoplastic polyurethanes from renewable resources: effect of soft segment chemical structure and molecular weight on morphology and final properties". Polym. Int. 2013. 62: 106–115.

13.   L. Tatai, T.G. Moore, R. Adhikari, F. Malherbe, R. Jayasekara, I. Griffiths, P.A. Gunatillake. "Thermoplastic biodegradable polyurethanes: the effect of chain extender structure on properties and in-vitro degradation". Biomaterials 2007. 28: 5407–5417.

14.   X.L. Wu, S.F. Kang, X.J. Xu, F. Xiao, X.L. Ge. "Effect of the crosslinking density and programming temperature on the shape fixity and shape recovery in epoxy-anhydride shape-memory polymers". J. Appl. Polym. Sci. 2014. 131: 40559.

15.   H. Ishida, D.J. Allen. "Mechanical characterization of copolymers based on benzoxazine and epoxy". Polymer 1996. 37: 4487–4495.

16.   Z.S. Petrovic, I. Javni. "Effect of soft-segment length and concentration on phase separation in segmented polyurethanes". J. Polym. Sci. Part B Polym. Phys. 1989. 27: 545–560.

17.   E. Cognet-Georjon, F. Mechin, J.P. Pascault. "New polyurethanes based on

4,4'-diphenylmethane diisocyanate and 1,4:3,6 dianhydrosorbitol. 2. Synthesis and properties of segmented polyurethane elastomers". Macromol. Chem. Phys. 1996. 197: 3593–3612.

18.   J.T. Koberstein, R.S. Stein. "Small-angle X-ray scattering studies of microdomain structure in segmented polyurethane elastomers". J. Polym. Sci. Part B Polym. Phys. 1983. 21: 1439–1472.

19.   Z.S. Chen, W.P. Yang, C.W. Macosko. "Polyurea synthesis and properties as a function of hard segment content". Rubber Chem. Technol. 1988. 61: 86–99.

20.   E. Del Río, G. Lligadas, J.C. Ronda, M. Galià, V. Cádiz. "Biobased polyurethanes from polyether polyols obtained by ionic-coordinative polymerization of epoxidized methyl oleate". Am. Chem. Soc. Polym. Prepr. Div. Polym. Chem. 2008. 49: 487–488.

21.   J.M. Castro, F. Lopez-Serrano, R.E. Camargo, C.W. Macosko, M. Tirrell. "Onset of phase separation in segmented urethane polymerization". J. Appl. Polym. Sci. 1981. 26: 2067–2076.

22.   L.M. Leung, J.T. Koberstein. "DSC annealing study of microphase separation and multiple endothermic behavior in polyether-based polyurethane block copolymers". Macromolecules 1986. 19: 706–713.

23.   S. Velankar, S.L. Cooper. "Microphase separation and rheological properties of polyurethane melts. 1. Effect of block length". Macromolecules 1998. 31: 9181–9192.

24.   A. Lendlein, R. Langer. "Biodegradable, elastic shape-memory polymers for potential biomedical applications". Science 2002. 296: 1673–1676.

25.   B.K. Kim, S.Y. Lee, M. Xu. "Polyurethanes having shape memory effects".

Polymer 1996. 37: 5781–5793.

26.   M. Zeng, H. Gao, Y. Wu, L. Fan, A. Li. "Preparation and characterization of nanocomposite films from chitin whisker and waterborne poly(ester-urethane) with or without ultra-sonification treatment". J. Macromol. Sci. Part A. 2010. 47: 867–876.

27.   D. Ratna, J. Karger-Kocsis. "Recent advances in shape memory polymers and composites: a review". J. Mater. Sci. 2008. 43: 254–269.

28.   H. Yeganeh, M.M. Lakouraj, S. Jamshidi. "Synthesis and characterization of novel biodegradable epoxy-modified polyurethane elastomers". J. Polym. Sci. Part A Polym. Chem. 2005. 43: 2985–2996.

29.   E. Cognet-Georjon, F. Mechin, J.P. Pascault. "New polyurethanes based on diphenylmethane diisocyanate and 1,4:3,6-dianhydrosorbitol. 1. Model kinetic-studies and characterization of the hard segment". Macromol. Chem. Phys. 1995. 196: 3733–3751.

30.   A. Saralegi, A. Etxeberria, B. Fernández-D'Arlas, I. Mondragon, A. Eceiza, M.A. Corcuera. "Effect of $H_{12}MDI$ isomer composition on mechanical and physico-chemical properties of polyurethanes based on amorphous and semicrystalline soft segments". Polym. Bull. 2013. 70: 2193–2210.

31.   G.A. Skarja, K.A. Woodhouse. "Structure-property relationships of degradable polyurethane elastomers containing an amino acid-based chain extender". J. Appl. Polym. Sci. 2000. 75: 1522–1534.

32.   M. Charlon, B. Heinrich, Y. Matter, E. Couzigné, B. Donnio, L. Avérous. "Synthesis, structure and properties of fully biobased thermoplastic polyurethanes, obtained from a diisocyanate based on modified dimer fatty acids, and different renewable diols". Eur. Polym. J. 2014. 61: 197–205.

33. L. Hojabri, X. Kong, S.S. Narine. "Functional thermoplastics from linear diols and diisocyanates produced entirely from renewable lipid sources". Biomacromolecules 2010. 11: 911–918.

34. A. Sirkecioglu, H.B. Mutlu, C. Citak, A. Koc, F.S. Güner. "Physical and surface properties of polyurethane hydrogels in relation with their chemical structure". Polym. Eng. Sci. 2014. 54: 1182–1191.

35. ISO 10993-5. Biological evaluation of medical devices. Test for in vitro cytotoxicity. International Organization for Standardization. Geneve, Switzerland, 2009.

CHAPTER 6

THERMO-RESPONSIVE BIOBASED POLYURETHANES
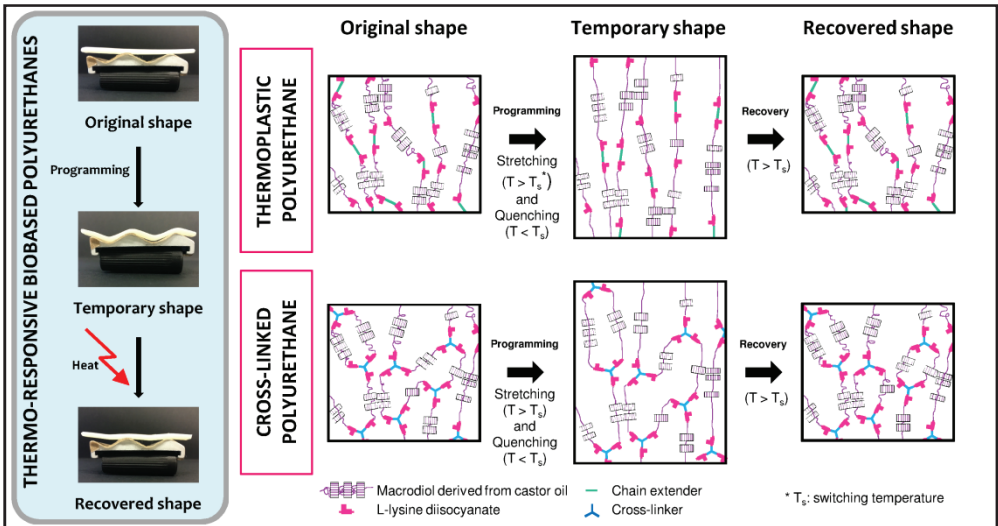
6. THERMO-RESPONSIVE BIOBASED POLYURETHANES

6.1 Aim of the chapter

This chapter aimed to study the thermally-activated shape-memory properties of the crosslinked and thermoplastic biobased polyurethanes synthesized in chapters 4 and 5. To that end, first the thermal and mechanical properties of the biobased polyurethanes were analyzed in deep to understand which of the synthesized materials could show a thermo-responsive behavior, and also to identify which of the phases was responsible for shape fixity and which for the permanent shape. After that, thermo-mechanical cyclic test conditions were established in function of the properties showed by each material. Taking into account the properties of the synthesized biobased polyurethanes, in thermoplastic biobased polyurethanes, the effect of switching temperature on thermally-activate shape-memory properties was studied. For that purpose two different switching temperatures were chosen: 25 and 40 °C. In the case of crosslinked biobased polyurethanes the effect of crosslink density and maximum elongation on shape-memory properties was studied; therefore three different maximum elongations were applied: 50, 100 and 250% at a switch temperature of 40 °C.

6.2 Choice of thermally-responsive biobased polyurethanes and testing conditions

As mentioned in chapter 1, thermally-activated shape-memory polymers are able to remember their original shape after being deformed and recover it as a response to heat.[1,2] In general, the driving force responsible for shape recovery is in fact the residual stress introduced in the sample during the stretching process.[1,3] The residual stress is stored through physical (crystalline segregated domains or entanglements) or chemical crosslinks (covalent bonds).[4,5] While the so-called switching phase acts as a molecular switch and enables the fixation of

the temporary shape[6,7] showing a transition. During the shape-memory test the material is heated and deformed in a temperature above the transition temperature (T_{trans}), switching temperature (T_s), and it is subsequently quenched at a temperature below T_{trans} in order to fix the shape, by frozen the mobility of chains. Once the sample is reheated above T_{trans} its original shape is restored.[8]

Therefore, the thermal transitions of the synthesized materials were studied in order to determine which of the synthesized biobased polyurethanes, both crosslinked and thermoplastic, could be used as thermo-responsible materials.

As it was observed in chapters 4 and 5 the synthesized biobased polyurethanes showed an endothermic peak associated to the melting of crystalline CO3. In thermoplastic polyurethanes once the melting temperature was reached a disruption of the crystalline domain occurred and the material flowed. Moreover, it was seen that biobased polyurethanes with LDI showed two different T_gs due to their microseparated phase morphology. The T_g at the lowest temperature was associated to amorphous CO3 rich domain, which belongs to a low fraction of CO3 since it is mainly crystalline, whereas the second T_g was attributed to LDI/PD or TMP rich domain, being the latter the T_{trans} of the material. In the case of biobased polyurethanes with DDI, they showed a single T_g at low temperatures. Since thermo-responsive polymers had to be quenched down to a temperature below their T_{trans}, the biobased polyurethanes with DDI were excluded to be assessed as thermo-responsive materials since their T_{trans} is far below room temperature.

Shape-memory tests conditions of PULPD and PULTMP series were established taking into account the thermal and mechanical properties of the biobased polyurethanes. Moreover, in order to a better understanding of shape-memory properties of these materials the effect of different factors, such as T_s and maximum elongation (ε_m), was also studied.

The synthesized thermoplastic PULPD series was chosen in order to understand the effect of T_s on the shape-memory properties. To that end, two different temperatures were chosen, 25 and 40 °C, which were within the interval of $T_{gLDI/PD}$ and T_m of CO3 rich domain, as can be observed in Figure 6.1, where DSC heating thermograms of the synthesized PULPD series together with the chosen T_ss (vertical dot lines in Figure 6.1) are shown.
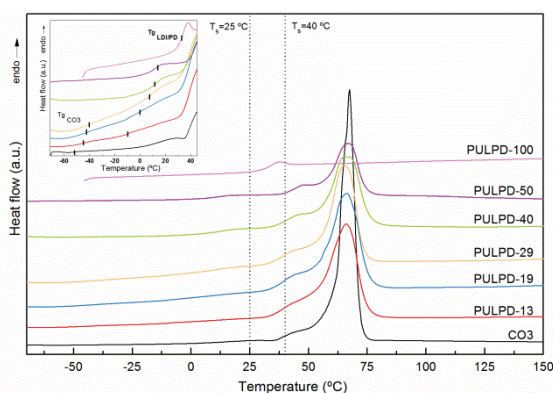
Figure 6.1. The chosen switching temperatures for PULPD polyurethanes.

In addition, as observed in Figure 4.8 PULTMP polyurethanes showed different behaviors during the stretching process. Thus, in order to analyze the effect of ε_m in shape-memory properties, three different ε_m were applied during thermomechanical tensile tests, 50, 100 and 250% (vertical dash lines in Figure 6.2), which were associated to the intervals previously discussed in chapter 4.
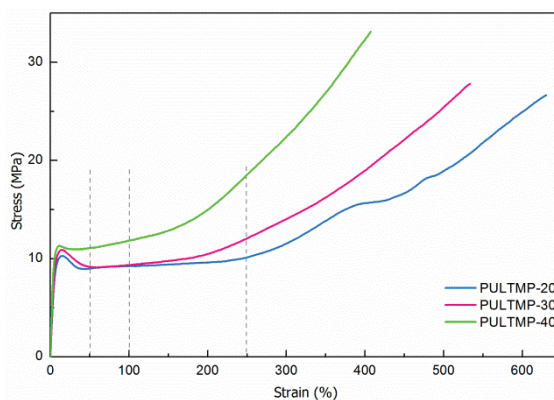
Figure 6.2. Maximum elongation applied for PULTMP polyurethanes.

Regarding T_s, Bruin et al.[9,10] reported that the use of LDI in the synthesis provides the advantage of synthesizing polyurethanes that do not produce adverse tissue reaction and whose degradation products are considered non-toxic. That means that the synthesized biobased polyurethanes would show potential to be used in biomedical applications. Therefore, the chosen T_s was 40 °C, which was within the interval of $T_{gLDI/TMP}$ and T_m of the CO3 rich domain (Table 4.3) and it could be a suitable temperature for further biomedical applications.

The analysis of the dynamic mechanical behavior could help to foreseen the shape-memory behavior of polymers. Polymers with a higher elastic modulus in the glassy state (E_g) show greater shape fixity.[11,12] Therefore, in PULPD series since E_g increases as LDI/PD content increases (Figure 5.4), PULPD-50 would show the highest shape fixity. Moreover the value of the storage modulus in the rubbery state (E_r) of PULPD polyurethane series increased as CO3 content increased providing a higher elastic recovery at high temperature.[13,11] Thus, polyurethanes with lower LDI/PD content would show greater shape recovery values. In addition, a high elasticity ratio (E_g/E_r) allows an easy shaping of the material at $T > T_{trans}$ and a great resistance to the deformation at $T < T_{trans}$,[11] therefore it was expected that PULPD-50 sample would present the best shape-memory properties (Figure 6.3).
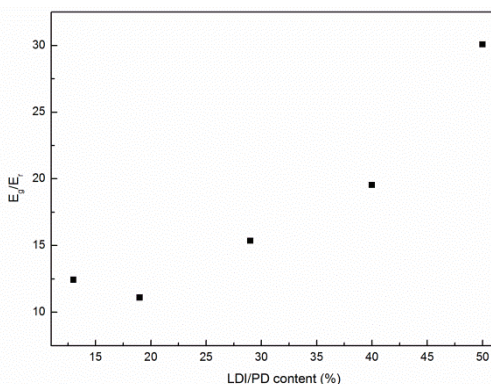
Figure 6.3. Elasticity ratio of synthesized PULPD polyurethane series.

As E_g/E_r values of PULPD-13 and PULPD-19 were similar, 12.4 and 11.1, respectively, shape-memory properties of PULPD-13 sample were not analyzed.

In the case of PULTMP crosslinked biobased polyurethanes, it was expected that PULTMP-20 polyurethane showed a better shape fixation, because of its greater modulus in the glassy state. Regarding shape recovery, since it was not observed the plateau after the transition from glassy to rubbery state, as previously observed for LDI/PD series, the E_g/E_r ratio was not calculated. The elastic modulus decreased gradually due to a progressive disruption of the crystals. Moreover, since in thermoset polymers the shape recovery is given through covalently bonded net points,[1,4,14] it was foreseen that biobased polyurethanes with higher LDI/TMP content would show higher shape recovery.

6.3   Methodology for thermo-mechanical tests

The shape-memory properties of both thermoplastic and crosslinked biobased polyurethanes were studied in the strain-controlled mode. Samples were cut in strips of 22 mm in length, 5 mm in width and 1.5 mm in thickness. First samples were heat at the switching temperature. In the case of PULPD biobased polyurethane series as mentioned before two different T_s were chosen, 25 and 40 °C, while the chosen T_s for PULTMP biobased polyurethane series was 40 °C. The samples were kept at T_s for 10 min. Thereafter, samples were stretched up at a rate of 5 mm min^{-1}. Due to the geometry of the sample, sandpaper pasted into pneumatic grips was used in order to avoid slipping. The thermoplastic PULPD polyurethanes were stretched up to 50%, while PULTMP crosslinked polyurethanes were stretched up to 50, 100 and 250%. Once the maximum elongation was reached, the sample was cooled down below T_{trans} to fix the temporary shape and the applied stress was removed. The permanent shape was recovered upon heating the sample up to switching temperature for 10 min. Five thermo-mechanical cyclic tensile tests were consecutively performed.

Thermally activated shape-memory behavior was quantified following the commonly used parameters, shape fixity and shape recovery values, which were calculated following equations 2.8 and 2.9, respectively.

6.4 Results and discussion

6.4.1 Shape-memory properties of PULPD thermoplastic biobased polyurethanes

In Table 6.1 R_f and R_r values are gathered, whereas the stress-strain curves of thermo-mechanical cycles of PULPD series, taken at 25 and 40 °C, are shown in Figure 6.4.

As can be observed from the results obtained in the first cycle at T_s = 25 °C, R_f values of the biobased polyurethanes range from 78.1 to 93.5%, and R_r values from 95.6 to 90.5% as LDI/PD content increases.

Table 6.1. R_f and R_r values calculated for each thermo-mechanical cycle at different T_s.

T_s (°C)	Cycle	PULPD-19		PULPD-29		PULPD-40		PULPD-50	
		R_f	R_r	R_f	R_r	R_f	R_r	R_f	R_r
25	1	78.1	95.6	81.0	92.7	90.1	90.5	93.5	91.0
	2	78.7	99.2	81.8	98.3	91.1	98.6	91.9	99.3
	3	79.5	98.2	81.9	99.9	92.1	99.4	91.8	99.7
	4	80.3	99.6	82.3	99.7	92.2	99.8	91.8	99.7
	5	79.8	98.1	82.5	99.9	92.3	99.7	91.7	100.0
40	1	87.1	94.5	89.7	93.9	92.5	91.5	95.5	91.1
	2	86.3	98.5	89.3	99.2	92.1	99.9	94.4	98.8
	3	85.8	99.8	86.9	98.6	91.8	99.8	94.4	99.1
	4	85.8	100.0	87.1	99.6	91.8	99.8	94.4	100.0
	5	85.8	99.8	87.1	99.6	91.8	100.0	94.1	100.0
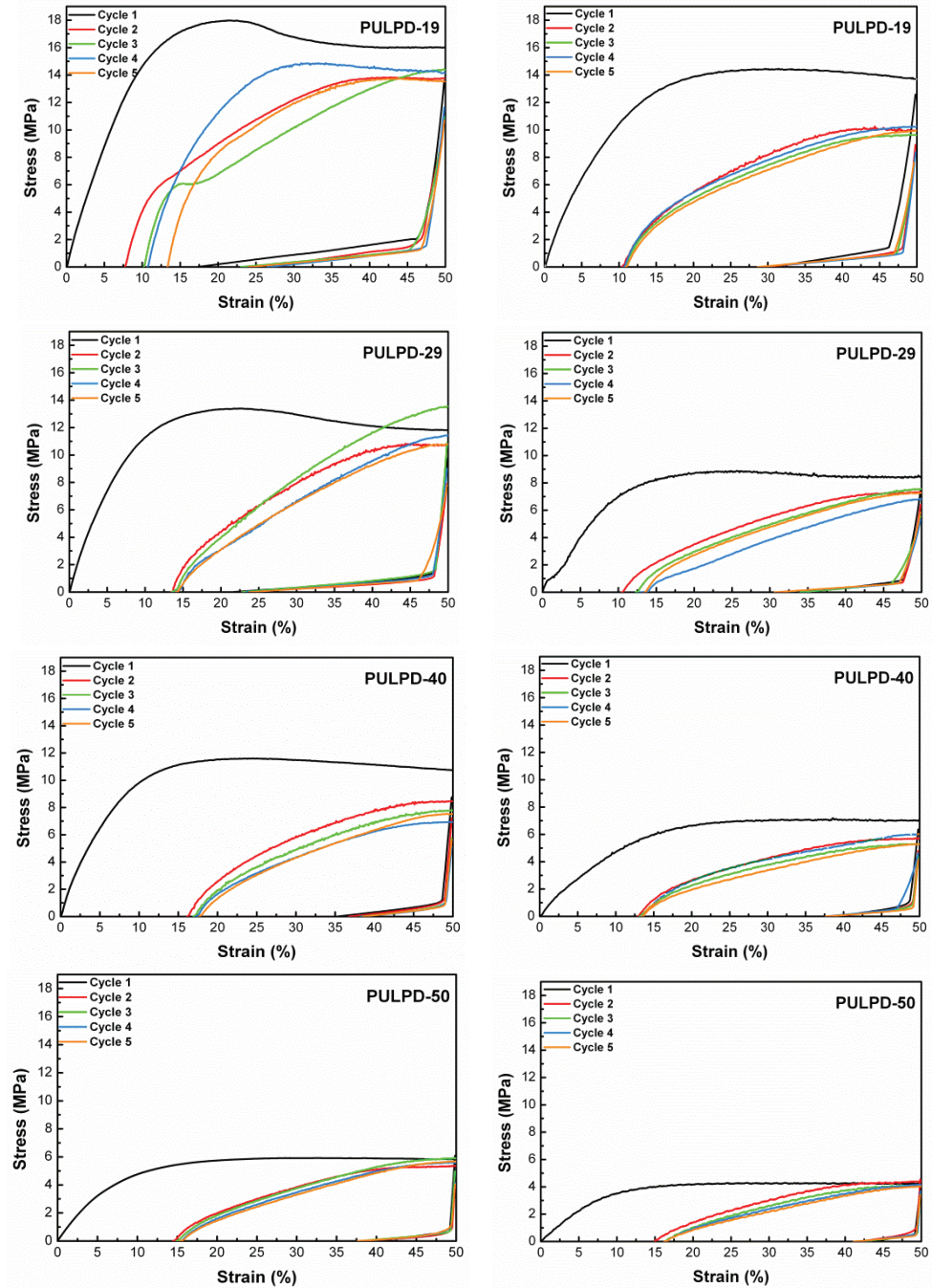
Figure 6.4. Stress-strain curves of thermo-mechanical cycles performed at 25 °C (left) and 40 °C (right) for PULPD polyurethane series.

As can be observed, as LDI/PD content increases R_f values also increase. Shape-memory effect is an entropic phenomenon. At the permanent shape the molecular chains adopt conformations with the highest entropic state. During the stretching process, as the molecular chains are heated above their T_{trans}, which activates the mobility thereof, the chains conformation change to a lower entropy state adopting the temporary shape. When the sample is subsequently quenched at a temperature below T_{trans}, as molecular chain segments are frozen, this entropy state is kinetically trapped.[7,15] Therefore, as LDI/PD content increases the mobility of the chains also increases due to the lower crystallinity of the material, as previously observed by DSC. Furthermore, the increase of LDI/PD content leaded biobased polyurethanes with higher E_g, as observed in Figure 5.4, and a high E_g provides materials with high shape fixity during simultaneous cooling and unloading.[11,12,16,17]

Regarding shape recovery, the molecular mobility is reactivated when the sample is reheated above T_{trans}, which allows the chains to return to their highest entropy state, since the driving force responsible for shape recovery is in fact the residual stress introduced in the sample during the stretching process.[1,3,11,18,19] In this way, the original shape can be restored through crystalline structures.[8] The decrease in R_r values observed when increasing the LDI/PD content of the biobased polyurethanes is associated with the decrease in the amount of crystals (lower degree of crystallinity, as observed by DSC), which are the ones that store the elastic strain energy during the stretching process. [8] Moreover, as all samples were stretched in the first cycle over the yield point, plastic deformation occurs, resulting in the break of some interactions among crystals, which allows the shifting of the chains. Therefore, in the first cycle, the R_r values will not reach 100%, and the original shape cannot be completely restored.[2,11] The residual strain left after the first thermo-mechanical cycle increases with LDI/PD content, according to a lower crystallinity of the biobased polyurethane. This means that the crystalline CO3 is effective acting as a fixed

structure, which memorizes the original shape.[8] Similar results were reported by other authors,[2] where shape fixity values were lower as crystalline domain content decreased, but in that case crystalline domains were formed by a diisocyanate and a chain extender.

When T_s is 40 °C, temperature-memory effect (TME) is taking place due to the overlapping of the deformation temperature with the onset of the melting enthalpy of the CO3.[20–22] This means that the shape-memory is due to a partial thermal transition, besides of the complete ones related to the T_g of the LDI/PD domain. In this way, the CO3 crystals which have a T_m close to the deformation temperature, could contribute to the shape fixation. As can be observe in Figure 6.5, the percentage of the overlapped area increases with the increase of CO3 content (3.02, 2.77, 1.74 and 1.23% for PULPD-19, PULPD-29, PULPD-40 and PULPD-50 respectively).
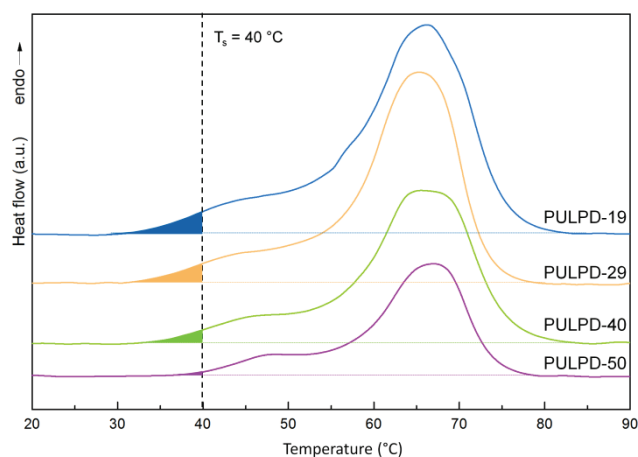
Figure 6.5. Evolution of the overlapped area for PULPD biobased polyurethane series at T_s = 40 °C.

As can be seen in Table 6.1, and comparing the obtained R_f values for each LDI/PD composition at T_s = 25 and 40 °C, it can be observed that R_f values increase when T_s increases. The differences between R_f values at 25 °C and at 40 °C for PULPD-19, PULPD-29, PULPD-40 and PULPD-50 systems are 9.4, 8.7, 2.4

and 2.0, respectively. As can be observed, the difference becomes more pronounced as CO3 content increases. This fact could be attributed to the melted fraction of CO3 crystals, contributing to the rubbery state of the polymer.[20] The difference between R_f values is more marked for PULPD-19 and PULPD-29 samples, probably due to a higher fraction of CO3 is melted, suggesting that TME depends on the CO3 content.

It is noteworthy that when the material is deformed at T_s = 40 °C it withstands lower stress. This could be a result of an easier disentangle of the chains as temperature increases, and also due to the higher fraction of CO3 in the rubbery state at this temperature. Moreover, with increasing temperature, the rubbery modulus values of polymers decrease, making the orientation more feasible.[11] Similar results were found in literature for copolyester-urethanes,[20] where higher shape fixity values were obtained at the highest switching temperatures and shape fixity increased as the content of the block with the highest melting temperature decreased.

The changes between the first and the remaining cycles can be attributed to the history of the sample. During the first cycle, the reorganization of the polymer at molecular scale takes place, involving the redistribution in the direction of the stress.[6,23] As can be seen in Figure 6.4, after several cycles, the thermo-mechanical properties of the material become similar, suggesting that the biobased polyurethanes have stable thermo-mechanical cyclic properties, except in the case of PULPD-19 at 25 °C.

Analyzing the R_r values taken at 25 and 40 °C, the material recovers practically the same, despite the fact that at 40 °C some of the crystals of the CO3 are melted, so both temperatures are high enough to achieve the maximum shape recovery. The effect of T_s in recovery time was also analyzed. To that end, PULPD-29 sample was heated at the employed T_s, 25 and 40 °C, for 10 min. Afterwards, the sample was deformed with a home-made gadget (Figure 6.6)

and kept at T_s for 10 min. Subsequently the sample was quenched to fix the temporary shape. Once the temporary shape was fixed the sample was immersed in a water bath at T_s and the recovery process was recorded.

Figure 6.6. Employed home-made gadget to deform the sample.

Figure 6.7 shows real shape images of PULPD-29 sample, taken along a thermo-mechanical cycle, where recovery times were measured at 25 and 40 °C.

As can be observed, after 74 s, at 40 °C, the maximum recovery that the material was able to withstand was reached, whereas at 25 °C, the material still maintains the deformed shape. The maximum recovery at 25 °C was reached after 195 s. The main difference between both temperatures is the time required to restore the shape, as at higher temperatures chain mobility increases, and it would have influence over shape recovery time. Thus, the higher the recovery temperature is, the faster the shape recovery is.
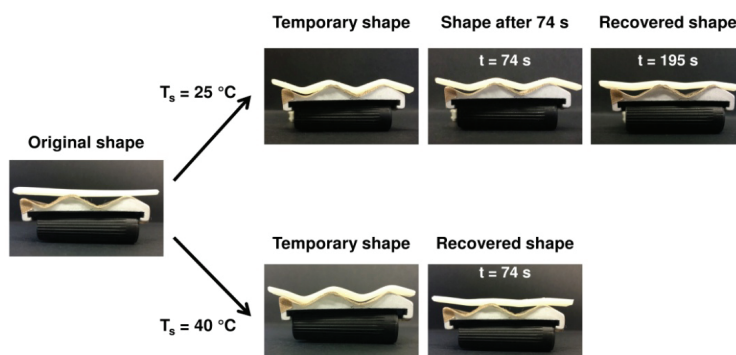
Figure 6.7. Real shape digital images of PULPD-29, taken during a thermo-mechanical cycle, at switching temperature of 25 and 40 °C.

Once five thermo-mechanical cyclic tensile tests were performed, samples were stretched up to ε_m again, cooled down to fix the shape, and kept at 4 °C in a refrigerator. After three months, it was observed that all samples still maintained the fixed shape, and after being heated up to T_s, they restored their original shape. The obtained R_r value was similar to the ones obtained after the last cycle.

6.4.2 Shape-memory properties of crosslinked biobased polyurethanes

As previously mentioned, the effect of maximum elongation in shape-memory properties was also studied. To that end, the crosslinked PULTMP biobased polyurethane series was used. In Figure 6.8, the stress-strain curves for the successive thermo-mechanical cycles are shown.
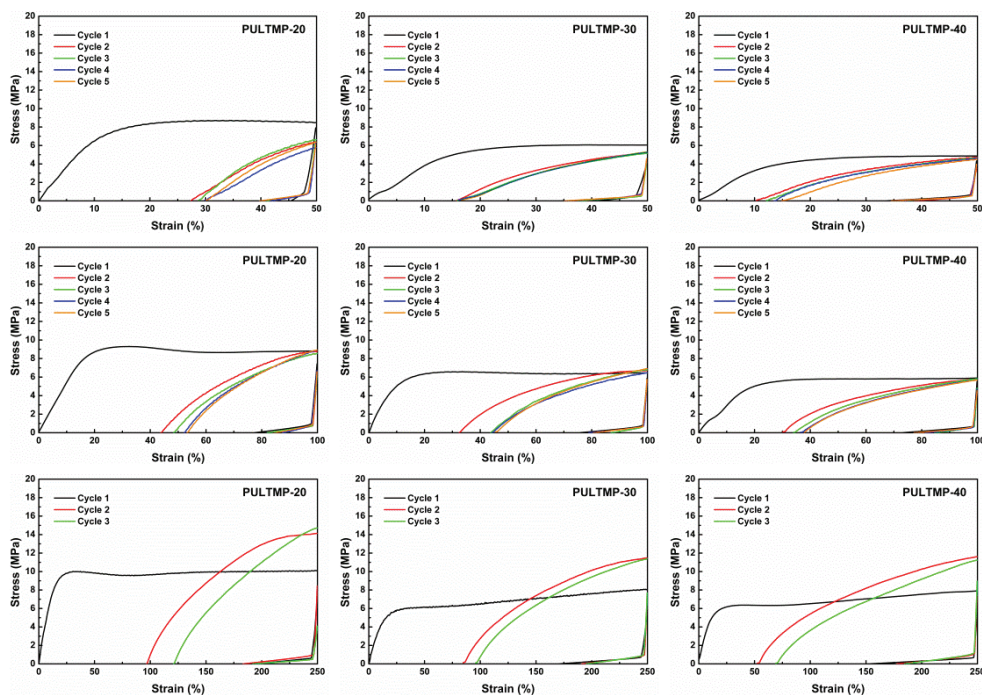
Figure 6.8. Stress-strain curves of thermo-mechanical cycles performed at 50% (up), 100% (centre) and 250% (down) at 40 °C for PULTMP biobased polyurethane series.

In Table 6.2 the R_f and R_r values of the successive thermo-mechanical cycles of PULTMP series at 50, 100 and 250% are summarized. As can be observe in the first cycle at maximum elongation of 50%, R_f values range from 97 to 89%, and R_r values from 82 to 93%. The increase of LDI/TMP content decreases R_f due to in crosslinked polymers chains are more closely restricted and net points provide a greater steric hindrance inhibiting the chains conformations to adopt the lowest entropy state and hence decreases the shape fixation.[7,15] Moreover, as it was observed by DMA in Figure 4.6, the increase of LDI/TMP decreases the elastic modulus in the glassy state and hence shape fixity also decreases.[11,12,16,17]

Table 6.2. R_f and R_r values calculated for each thermo-mechanical cycle at 40 °C and at different maximum stretching elongations for PULTMP biobased polyurethane series.

ε_m (%)	Cycle	PULTMP-20		PULTMP-30		PULTMP-40	
		R_f (%)	R_r (%)	R_f (%)	R_r (%)	R_f (%)	R_r (%)
	1	96.9	81.7	93.9	89.5	88.9	93.1
	2	94.7	98.9	92.0	99.9	92.4	98.7
50	3	93.8	99.1	91.5	99.9	90.6	99.0
	4	94.5	99.8	90.1	99.6	90.1	99.0
	5	93.2	99.8	90.1	99.6	89.7	99.5
	1	88.6	78.1	87.7	83.8	86.4	85.0
	2	91.6	97.1	89.8	93.3	89.1	97.7
100	3	91.0	97.5	93.5	99.6	92.3	98.4
	4	93.7	99.3	89.5	99.2	90.6	99.3
	5	92.3	99.5	90.3	99.6	88.6	100.0
	1	80.0	72.4	77.1	75.8	72.0	84.7
250	2	80.9	90.4	83.1	95.8	79.3	94.8
	3	83.3	99.7	84.3	97.0	74.3	98.3

Regarding shape recovery, as LDI/TMP content increases R_r increases according to a greater crosslink density. Polymers with a high crosslink density have a great elastic strain energy stored, which provides them a higher driving force for subsequent thermally induced shape recovery, due to as mentioned before the driving force responsible for shape recovery is the residual stress

introduced in the sample during the stretching process.[1,3] Furthermore, as all samples were stretched over the yield point in the first cycle, plastic deformation took place, resulting in the break of some chemical and physical bonds, which allows the shifting of the chains. Therefore, in the first cycle, the R_r values will not reach 100%, and the original shape cannot be completely restored.[2,11]

Comparing the obtained shape-memory properties of crosslinked PULTMP biobased polyurethane series, with the thermoplastic PULPD polyurethane series, different trend can be observed. In thermoplastic biobased polyurethanes as LDI/PD content increase R_f also increases, while R_r decreases. The differences on shape fixity are related with the elastic modulus in the glassy state.[11,14,17] As can be seen in Table 6.3, where E_g and R_f values of PULPD and PULTMP biobased polyurethane series are compared, for PULPD polyurethane series both E_g and R_f increase as LDI/PD content increases.

Table 6.3. E_g and R_f of PULPD and PULTMP biobased polyurethane series.

LDI/PD or TMP content (%)	E_g (MPa)		R_f (%)	
	PULPD	PULTMP	PULPD	PULTMP
20	2810	3120	87.1	96.9
30	2870	3005	89.7	93.9
40	3240	2780	92.5	88.9
50	3503	–	95.5	–

Comparing shape recovery ratios, in the case of PULPD biobased polyurethane series R_r decreases as LDI/PD content increases or CO3 content decreases, due to the lower amount of crystals which are the driving force for memorizing the original shape. Whereas in PULTMP biobased polyurethane series, R_r increases as LDI/TMP content increases, due to the higher crosslink density.

As can be observed in both biobased polyurethane series the trends of the variation in R_r and R_f are inverted. In thermoplastic PULPD polyurethane series R_f increases while R_r decreases as LDI/PD content increase. Whereas, in crosslinked PULTMP polyurethane series, R_f decreases while R_r increases as LDI/TMP content increase. Notwithstanding, in both cases shape fixity and recovery are ruled by the same principles. Shape fixity is governed by the higher E_g, whereas the driving force for shape recovery is the residual stress introduced in the sample during the stretching process, which is stored in the case of thermoplastic PULPD series through crystals and in the case of crosslinked PULTMP series in addition to crystals through net points. This behavior suggests that covalent bonds are more effective storing the residual strain than crystals.

Moreover, regarding the so-called temperature-memory effect previously observed in PULPD thermoplastic biobased polyurethanes, since the percentage of overlapped area in PULTMP series is similar for all the compositions (8.16, 8.81, 8.08% for PULTMP-20, PULTMP-30 and PULTMP-40 respectively) the contribution to the rubbery state would be alike for all systems. In Figure 6.9 the evolution of the overlapped area as LDI/TMP increases is shown.
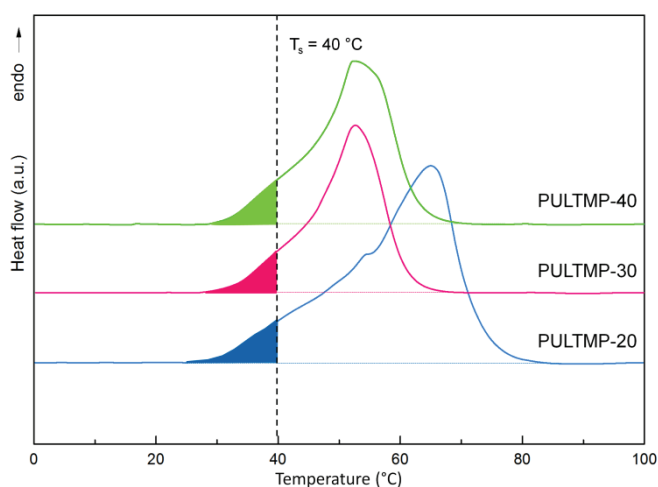
Figure 6.9. Evolution of the overlapped area as LDI/TMP content increases.

In order to understand how the increase of the maximum elongation influences on shape-memory properties, the thermo-mechanical cyclic tensile tests were also carried out at maximum elongation of 100 and 250%. The shape-memory tendency in the first cycle is similar to the one observed at 50%, as LDI/TMP content increases R_f decreases while R_r increases. However, at higher maximum elongations the material withstands a greater plastic deformation and hence a higher amount of physical and chemical bonds are broken and therefore lower R_r values were measured. In the same way, with the increase of the maximum elongation the R_f decreases. When the maximum elongation is 250%, the stress that the polyurethanes withstand increases from one cycle to another (Figure 6.8 down). This behavior is known as "cyclic hardening" and is due to a relaxation of the material in the stretched state which results in a higher orientation and crystallization of the chains, as previously observed in Figure 4.8. In this way, the material is more resistant against the strain from cycle to cycle. [3,6,16,24,25]

Since T_{trans} of the synthesized polyurethanes is bellow or close to room temperature, they should be stored bellow its T_{trans}. Therefore, in order to verify if the material is able to keep the fixed shape over time, once the last thermo-mechanical cyclic tensile test was performed, the sample was stretched up again to each maximum elongation and quenched in order to fix the shape and kept at 4 °C in a refrigerator. After 2 months it was seen that all samples still maintained the fixed shape. Subsequently, the samples were heat up to T_s and they were able to restore their shape obtaining R_r values similar to previous ones.

6.5   Conclusions

The study of thermally-responsive shape-memory properties revealed that the synthesized thermoplastic and crosslinked biobased polyurethanes with LDI in chapters 4 and 5, PULTMP and PULPD series, showed shape-memory properties.

It was analyzed the effect of switching temperature on the thermally-activated shape-memory properties of PULPD biobased polyurethane series. Both switching temperatures were between LDI/PD rich domain glass transition and CO3 rich domain melting temperature. At the lowest switching temperature, the shape-memory behavior of PULPD thermoplastic biobased polyurethane series showed that the shape fixity values increased as LDI/PD content increased. Regarding shape recovery values, in the first thermo-mechanical cycle, R_r values increased as CO3 content increased. After the first cycle, all the polyurethanes presented similar R_r values and were close to 100%, which was attributed to the erase of the thermal history. At the highest switching temperature, as a consequence of being this temperature partially overlapped with the onset of CO3 rich domain melting enthalpy, a TME was observed. It was seen that shape fixity values increased due to the contribution of the melted CO3 crystals to the rubbery state, however, it had no effect on shape recovery.

The effect of the maximum elongation and crosslink density on shape-memory properties of the synthesized PULTMP crosslinked biobased polyurethanes in chapter 4 was analyzed. It was observed that shape-memory properties varied with crosslink density, allowing obtaining biobased polyurethanes with tailored shape-memory properties. As crosslink density increased R_f decreased, according to a higher steric hindrance which inhibited chain conformations to adopt the lowest entropy state. Moreover, R_r increased with the increased of the crosslink density, showing that the net points of the structure contribute also to memorize the shape. It was seen that the highest R_r and R_f values were obtained when the maximum elongation was closer to the yield point.

Nevertheless, it was seen than the shape fixity of both systems was governed by the elastic modulus in the glassy state. Materials with a higher E_g shower higher fixity ratios. While the driving force for shape recovery was the residual stress introduced during stretching processes which was stored by crystalline domains

in PULPD thermoplastic series and by crystalline and net points in PULTMP crosslinked series. It was deduced that net points were more effective for storing the residual stress, since although the decrease of crystallinity as LDI/TMP content increases higher R_r values were obtained.

6.6   References

1.   X.L. Wu, S.F. Kang, X.J. Xu, F. Xiao, X.L. Ge. "Effect of the crosslinking density and programming temperature on the shape fixity and shape recovery in epoxy-anhydride shape-memory polymers". J. Appl. Polym. Sci. 2014. 131: 40559.

2.   A. Saralegi, E. Johan Foster, C. Weder, A. Eceiza, M.A. Corcuera. "Thermoplastic shape-memory polyurethanes based on natural oils". Smart Mater. Struct. 2014. 23: 025033 (9pp).

3.   A. Tcharkhtchi, S. Abdallah-Elhirtsi, K. Ebrahimi, J. Fitoussi, M. Shirinbayan, S. Farzaneh. "Some new concepts of shape memory effect of polymers". Polymers 2014. 6: 1144–1163.

4.   C.P. Buckley, C. Prisacariu, A. Caraculacu. "Novel triol-crosslinked polyurethanes and their thermorheological characterization as shape-memory materials". Polymer 2007. 48: 1388–1396.

5.   C.M. Yakacki, R. Shandas, D. Safranski, A.M. Ortega, K. Sassaman, K. Gall. "Strong, tailored, biocompatible shape-memory polymer networks". Adv. Funct. Mater. 2008. 18: 2428–2435.

6.   A. Lendlein, S. Kelch. "Shape-memory polymers". Angew. Chem. Int. Ed. 2002. 41: 2034–2057.

7.   J.L. Hu, F.L. Ji, Y.W. Wong. "Dependency of the shape memory properties of a polyurethane upon thermomechanical cyclic conditions". Polym. Int.

2005. 54: 600–605.

8. H.M. Jeong, J.H. Song, K.W. Chi, I. Kim, K.T. Kim. "Shape memory effect of poly(methylene-1,3-cyclopentane) and its copolymer with polyethylene". Polym. Int. 2002. 51: 275–280.

9. P. Bruin, J. Smedinga, A.J. Pennings, M.F. Jonkman. "Biodegradable lysine diisocyanate-based poly(glycolide-co-ε-caprolactone)-urethane network in artificial skin". Biomaterials 1990. 11: 291–295.

10. P. Bruin, G.J. Veenstra, A.J. Nijenhuis, A.J. Pennings. "Design and synthesis of biodegradable poly(ester-urethane) elastomer networks composed of non-toxic building blocks". Makromoleculare Chemie, Rapid Commun. 1988. 9: 589–594.

11. D. Ratna, J. Karger-Kocsis. "Recent advances in shape memory polymers and composites: a review". J. Mater. Sci. 2008. 43: 254–269.

12. X. Qiu, X. Xiao, D. Kong, W. Zhang, Z. Ma. "Facile control of high temperature shape memory polymers". J. Appl. Polym. Sci. 2017. 44902: 6–11.

13. A. Saralegi, L. Rueda, B. Fernández-d'Arlas, I. Mondragon, A. Eceiza, M.A. Corcuera. "Thermoplastic polyurethanes from renewable resources: effect of soft segment chemical structure and molecular weight on morphology and final properties". Polym. Int. 2013. 62: 106–115.

14. J. Hu, Z. Yang, L. Yeung, F. Ji, Y. Liu. "Crosslinked polyurethanes with shape memory properties". Polym. Int. 2005. 54: 854–859.

15. T. Xie. "Recent advances in polymer shape memory". Polymer 2011. 52: 4985–5000.

16. B.K. Kim, S.Y. Lee, M. Xu. "Polyurethanes having shape memory effects".

Polymer 1996. 37: 5781–5793.

17. X.L. Lu, W. Cai, Z. Gao, W.J. Tang. "Shape memory effects of poly(L-lactide) and its copolymer with poly(ε-caprolactone)". Polym. Bull. 2007. 58: 381–391.

18. T. Sauter, M. Heuchel, K. Kratz, A. Lendlein. "Quantifying the shape-memory effect of polymers by cyclic thermomechanical tests". Polym. Rev. 2013. 53: 6–40.

19. E. Ghobadi, M. Heuchel, K. Kratz, A. Lendlein. "Simulating the shape-memory behavior of amorphous switching domains of poly(L-lactide) by molecular dynamics". Macromol. Chem. Phys. 2013. 214: 1273–1283.

20. K. Kratz, U. Voigt, A. Lendlein. "Temperature-memory effect of copolyesterurethanes and their application potential in minimally invasive medical technologies". Adv. Funct. Mater. 2012. 22: 3057–3065.

21. C. Samuel, S. Barrau, J. Lefebvre, J. Raquez, P. Dubois. "Designing multiple-shape memory polymers with miscible polymer blends: evidence and origins of a triple-shape memory effect for miscible PLLA/PMMA blends". Macromolecules. 2014. 47: 6791–6803.

22. Y. Wang, J. Li, X. Li, Y. Pan, Z. Zheng, X. Ding, Y. Peng. "Relation between temperature memory effect and multiple-shape memory behaviors based on polymer networks". RSC Adv. 2014. 4: 20364–20370.

23. B. Fernández-d'Arlas, J.A. Ramos, A. Saralegi, M.A. Corcuera, I. Mondragon, A. Eceiza. "Molecular engineering of elastic and strong supertough polyurethanes". Macromolecules 2012. 45: 3436–3443.

24. B. Fernández-d'Arlas, R. Fernández, J. Runt, A. Eceiza. "Polyurethanes containing a crystalline polyol and semiflexible urethane segments". J.

Appl. Polym. Sci. 2015. 132: 41281.

25. H. Tobushi, S. Hayashi, S. Kojima. "Mechanical properties of shape memory polymer of polyurethane series". JSME Int. J. 1992. 35: 296–302.

CHAPTER 7

BIOBASED NANOCRYSTALS AND MAGNETIC NANOPARTICLES

ISOLATION OF CHITIN AND CELLULOSE NANOCRYSTALS

NANOFIBERS

Acid hydrolisis

CHITIN NANOCRYSTALS

CELLULOSE NANOCRYSTALS

SYNTHESIS OF MAGNETITE NANOPARTICLES

NH_4OH Oleic acid

$Fe(aq)^{2+}$
$Fe(aq)^{3+}$

MAGNETITE NANOPARTICLES COATED WITH OLEIC ACID

1 μm   1 μm
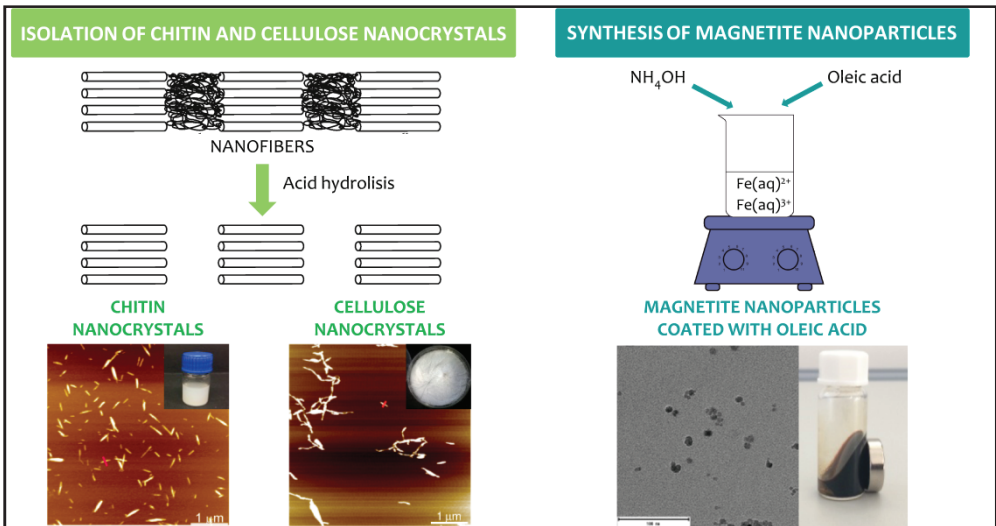
7. BIOBASED NANOCRYSTALS AND MAGNETIC NANOPARTICLES

7.1 Aim of the chapter

The aim of this chapter was to prepare and characterize nanoentities to be used as nanofillers in the preparation of biobased polyurethane nanocomposites. On the one hand, chitin (CHNC) and cellulose (CNC) nanocrystals were isolated by acid hydrolysis. To this end, microcrystalline cellulose (MCC) and chitin powder were acid hydrolyzed using sulfuric (H_2SO_4) and clorhidric (HCl) acids, respectively. On the other hand, magnetic magnetite nanoparticles (MNP) were prepared by co-precipitation method from an aqueous Fe^{3+}/Fe^{2+} solution.

The morphology and dimensions of the nanocrystals were characterized by AFM. Moreover, the acetylation degree of CHNCs was also measured. Similarly, the morphology of the MNP was analyzed by TEM. Furthermore, all nanoentities were characterized by X-ray diffraction in terms of crystallinity, as well as by FTIR for physicochemical characterization.

7.2 Chitin and cellulose nanocrystals

7.2.1 Isolation of nanocrystals

α-Chitin and cellulose nanocrystals were isolated by acid hydrolysis of the amorphous regions of chitin powder and MCC, respectively. Chitin powder was hydrolyzed by using HCl (3M) at 100 °C for 90 min under vigorous stirring and under reflux. The ratio of HCl to chitin powder was kept at a value of 30 mL g^{-1}.[1] While MCC was hydrolyzed in H_2SO_4 (64%) at 45 °C for 30 min under vigorous stirring in a ratio of 8.75 mL g^{-1}. In both cases, after acid hydrolysis the suspensions were diluted 20-fold with distilled water to stop the process and washed by centrifugation until it become turbid, removing the supernatant and replacing by the same amount of distilled water in each centrifugation step. The centrifugation process was carried out at 4000 rmp for 20 min and CHNC or CNC

rich sediment was collected. The pH value was stabilized in 5-6 values by transferring the sediment into dialysis membranes (Spectra Por® 6 MWCO 8000) and performing a dialysis process against deionized water.

Afterward, CHNC suspension in water was solvent exchanged into tetrahydrofuran THF by centrifugation. First the mixture was centrifuged at 4500 rpm for 20 min to remove the excess of water and replaced by the same amount of THF. Then the suspension was centrifuged at 4500 rpm for 10 min, removing the supernatant and replacing by the same amount of THF in each centrifugation, until the supernatant was colorless. In order to breakup any remaining chitin nanocrystal aggregates, the suspension was subjected to sonication treatment in a sonication bath (JP Selecta Ultrasons H-D) with iced water for 2 h. Finally, it was stored in a refrigerator at 4 °C. The concentration of the CHNC in THF was 6.5 g L^{-1}.

In the case of CNC, the obtained suspension was sonicated for 1 h in a sonication bath. Finally, the suspension was freeze-dried and stored in desiccators until it was used.

In Sheme 7.1 the chemical structure of CHNCs and CNCs is shown.
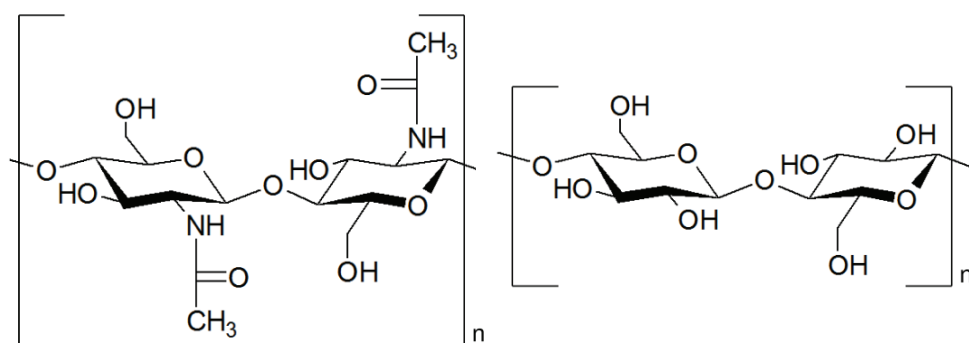
Scheme 7.1. Chemical structure of CHNCs (left) and CNCs (right).

7.2.2 Characterization of nanocrystals

7.2.2.1 Atomic force microscopy

The morphology and the distribution of the CHNCs and CNCs were analyzed by AFM (Figures 7.1).
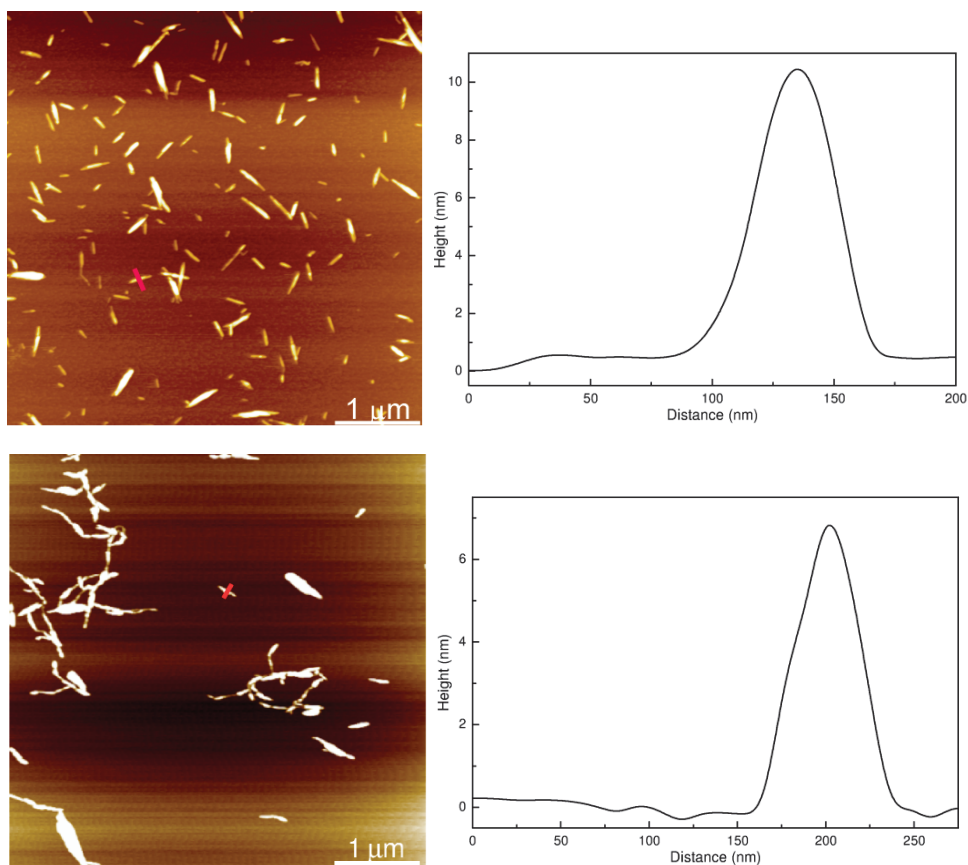
Figure 7.1. AFM height image of nanocrystals (left) and cross sectional profile of the red line (right) of CHNCs (up) and CNCs (down) (size: 5 x 5 μm^2).

Height images of the nanocrystals obtained by AFM reveled that the isolated nanocrystals were rod-like, as can be observed in the images on the left, indicating that the acid hydrolysis was effective in both cases. The aspect ratio of CHNCs and CNCs was calculated by performing 75 measurements. The length of the nanocrystals was calculated from AFM height images. The diameter was

calculated from height profiles. An example of the cross sectional profile calculated along the red line is shown in Figures 7.1 (right). In this way, CHNCs showed an average length of 222 ± 31 nm and an average diameter of 10 ± 1 nm, while CNCs showed an average length and diameter of 146 ± 16 nm and 7 ± 2 nm, respectively. The aspect ratio (L/D) value of CHNCs was 23 ± 5 nm, while the L/D of CNCs was 21 ± 6 nm. These values are in agreement to the reported in the literature.[2–5]

7.2.2.2 X-ray diffraction

XRD was used in order to determine the crystalline polymorphism of the isolated α-chitin (Figure 7.2) and cellulose (Figure 7.3) nanocrystals.

As can be observed in Figure 7.2, XRD pattern of CHNC shows strong peaks at 9.5 and 19.5° and minor peak at 20.9 and 23.6°, which corresponded to (020), (110), (120) and (130) crystallographic planes, respectively, corroborating that the obtained CHNC showed the typical crystal patterns of α-chitin.[6–9]
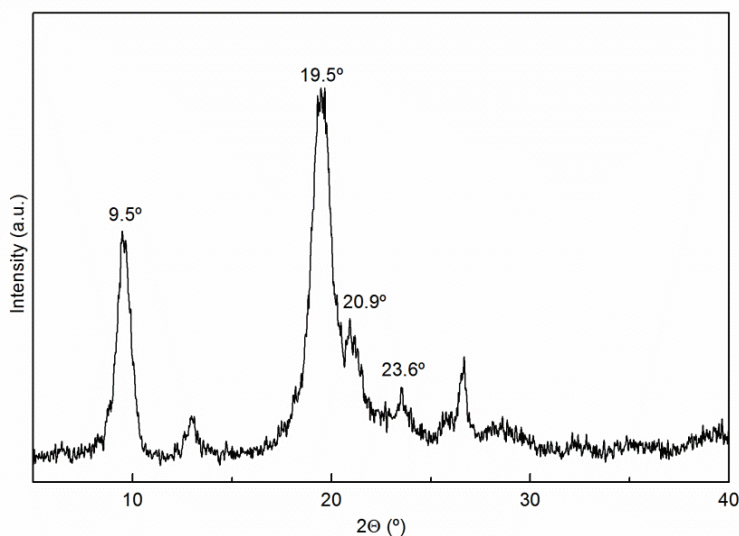
Figure 7.2. X-ray diffractogram of CHNCs.

Regarding to XRD patterns of CNC, at 22.9° a strong peak can be observed and three minor peaks at 15.2, 16.6 and 34.8°, corresponding to (002), (101), (10$\bar{1}$) and (040) crystallographic planes, respectively, which are associated to the typical cellulose I crystalline structure.[4,10,11]
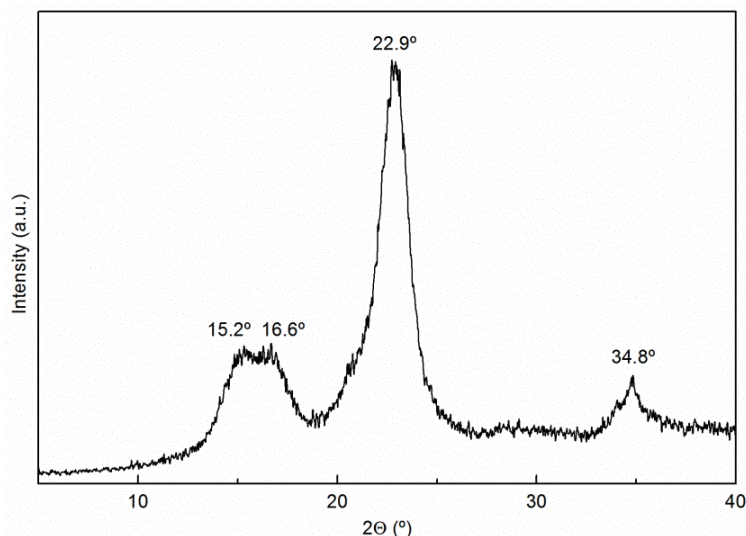
Figure 7.3. X-ray diffractogram of CNCs.

The crystallinity degree (CrI) of the isolated nanocrystals was determined. To that end, the empirical method described in the literature[12–14] was used, following equations 7.1 for CHNC, and 7.2 for CNC:

$$CrI = \frac{I_{110} - I_{am}}{I_{100}} \times 100 \tag{7.1}$$

$$CrI = \frac{I_{002} - I_{am}}{I_{002}} \times 100 \tag{7.2}$$

where I_{110} and I_{002} are the peak intensity of the (110) and (002) crystallographic planes, showed at 19.5 and 22.9° for CHNC and CNC, respectively and I_{am} is the intensity scattered by amorphous part of the sample measured at 16 ° for CHNC and 18 ° for CNC. The crystallinity degree of CHNCs was 93%, while the isolated CNCs showed a crystallinity degree of 85%. Similarly to reported in the literature amorphous domains were not completely removed by hydrolysis.[15]

7.2.2.3 Fourier transform infrared spectroscopy

Figure 7.4 shows the FTIR spectrum of the obtained chitin nanocrystals. As can be observed at 3433 cm^{-1} the peak associated to stretching vibration of O-H groups appears.[1] Furthermore, the bands ascribed to N-H symmetric and asymmetric stretching vibration are centered at 3260 and 3100 cm^{-1}, respectively.[1,16] Similarly, at 2960 and 2920 cm^{-1} the bands attributed to C-H symmetric and asymmetric stretching vibration of CH$_2$ and CH$_3$ groups can be observed, respectively.[16] The peaks associated to C=O stretching vibrations in amide I region can be seen at 1650 and 1620 cm^{-1} and the N-H bending in amide II can be observed at 1550 cm^{-1}.[1,9,17] Moreover, at 1155 cm^{-1} the C-C ring stretching band can be observed. Similarly, at 1110 cm^{-1} the band ascribed to C-O-C glycosidic ether group is observed and at 1068 and 1011 cm^{-1}, the peaks attributed to C-O stretching vibration of the CH$_2$-OH, C-OH and C-O-C groups in the pyranose rings can be observed.[9,17] Finally, at 889 cm^{-1} the band attributed to β-glycosidic linkage appears.
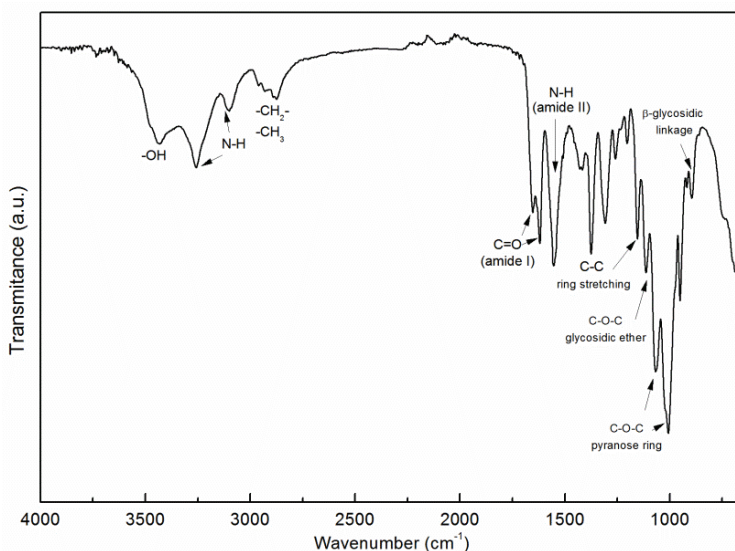
Figure 7.4. FTIR spectrum of CHNCs.

Figure 7.5 shows the FTIR spectrum of the cellulose nanocrystals. The band ascribed to stretching vibration of O-H group is centered at 3340 cm^{-1}. The main characteristic bands of the CNC can be also observed. The C-C ring stretching band can be seen at 1160 cm^{-1}. Moreover, at 1106 cm^{-1} the band ascribed to C-O-C glycosidic ether group is observed and at 1053 and 1027 cm^{-1} the C-O-C pyranose ring stretching vibration bands. Finally, at 892 cm^{-1} the band attributed to cellulosic β-glycosidic linkage can be observed.[18,19]
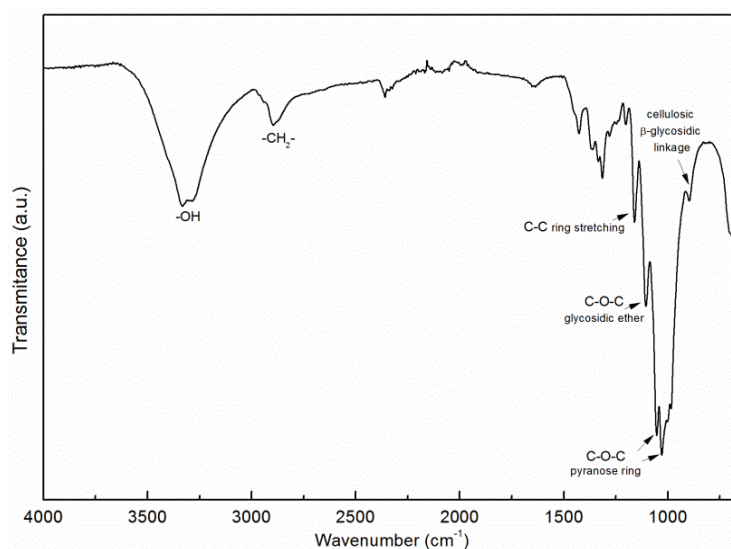
Figure 7.5. FTIR spectrum of CNCs.

7.2.2.4 Elemental analysis

Chitin and cellulose nanocrystals show similar chemical structures. The main difference between their structures is the presence of acetyl groups (-NHCOCH$_3$) in CHNCs. The deacetylation of CHNCs leads to the formation of chitosan, which shows similar structure but completely different properties. That is why, it is important to determine the acetylation degree of the isolated CHNC. To that purpose the elemental analysis of the CHNC was performed. Taking into account the theoretical value of nitrogen for a completely acetylated sample (N = 6.9%), and comparing with the experimental value obtained by elemental analysis (N =

6.83%), results in a degree of acetylation of 98.9%. This value was in accordance to the value found in literature.[6]

7.3   Magnetite nanoparticles

7.3.1   Preparation of magnetite nanoparticles

MNPs were prepared by a co-precipitation method from an aqueous Fe^{3+}/Fe^{2+} solution (molar ratio 3:2) using ammonium hydroxide (30%) in excess. First, 0.09 mol of $FeCl_3 \cdot 6H_2O$ and 0.06 mol of $FeCl_2 \cdot 4H_2O$ were dissolved in 50 mL of distilled water and heated at 70 °C. After that, 40 mL of NH_4OH were added and the formation of a black precipitate was immediately observed. The particles were subsequently coated by adding 0.02 mol of oleic acid and the suspension was heated at 80 °C for 30 min. The obtained oleic acid coated magnetite nanoparticles were washed with distilled water and separated by centrifugation several times until neutral pH was obtained. After that, they were dispersed in n-heptane to form a stable ferrofluids and stored.

 Prior its use the obtained nanoparticles were precipitated in ethanol and recovered with a strong magnet. The n-heptane and ethanol mixture was removed and the same amount of THF was added. Subsequently, the particles were centrifuged at 700 rpm for 10 min. The particles were recovered with the magnet, the supernatant was removed and the same amount of THF was added. This process was repeated three times. Finally, the particles were re-dispersed in THF and stored in a refrigerator at 4 °C.

7.3.2   Characterization of magnetite nanoparticles

7.3.2.1   X-ray diffraction

The polymorphism of the MNP was determined by XRD, Figure 7.6. The obtained magnetite nanoparticles showed peaks at (220), (311), (400), (422), (333) and

(440) crystallographic planes, which agreed with those reported from the standard crystal of magnetite (Fe_3O_4).[20–24]
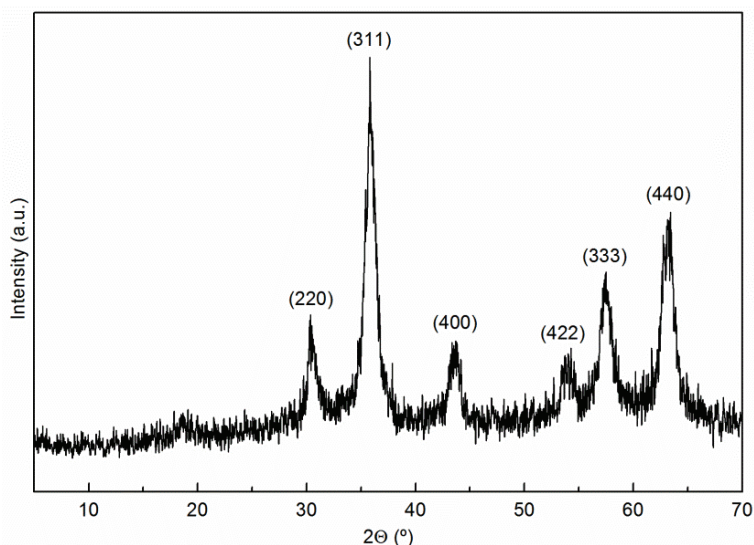
Figure 7.6. X-ray diffractogram of MNPs.

Crystal size (D) could be determine though Scherrer's equation.[25]

$$D = \frac{\kappa \cdot \lambda}{\beta \cdot \cos\theta} \qquad (8.3)$$

where κ is the Scherrer constant (0.9); λ is the radiation wavelength (Cu Kα = 0.15418 nm); β is the width at half height of the selected peak in radians and θ is Bragg angle.

According to this equation, and using the diffraction signal corresponding to the (311) crystallographic plane, the crystal size was calculated as 7 nm. However, the "crystallite size" is not necessarily synonymous with "particle size" and this method is only an estimation of the diameter of the magnetite nanoparticles.[20]

7.3.2.2   Transmission electron microscopy

In Figure 7.7 TEM images obtained of the prepared magnetite nanoparticles are shown. As can be observed the magnetite nanoparticles are spherical and they are well dispersed. The average particle diameter of the MNPs was calculated from TEM images by performing 80 measurements. The obtained average diameter was 8.0 ± 2.2 nm, which is in accordance with the estimated value by Scherre's equation and also with the values reported in literature.[20,24,26]
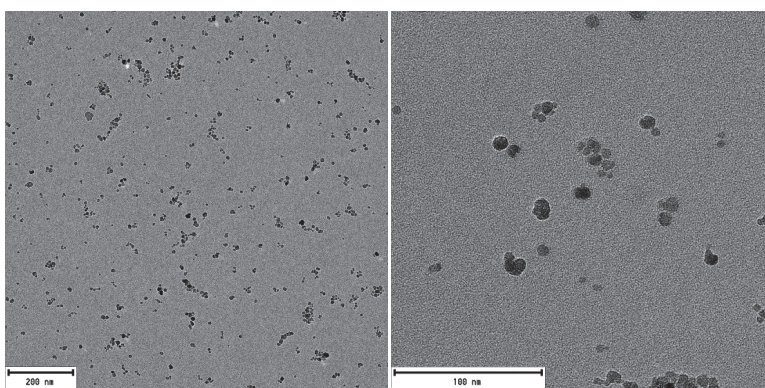
Figure 7.7. TEM image of MNPs at different magnifications.

7.3.2.3   Fourier transform infrared spectroscopy

In Figure 7.8 the FTIR spectrum of MNPs can be observed. The bands associated to asymmetric and symmetric stretching vibration of C-H bonds in methylene groups,[20,27,28] centered at 2921 and 2850 cm^{-1}, respectively, can be observed. At 1622 and 1520 cm^{-1} the bands ascribed to carboxylate (COO-) asymmetric and symmetric stretching vibration bands, respectively, can be observed.[24,27,29,30] At 1415 cm^{-1} the band ascribed to coordinate in-plane deformation of the hydroxyl groups of the carbonyl group, i.e. oleic acid physisorbed on particle surface can be seen.[20,27] Moreover, the band observed at 1050 cm^{-1} is related with C-O single bond stretching vibration originated after adsorption of the oleic acid on the particle surface.[20] Besides, the broad band centered at 582 cm^{-1} corresponds to Fe-O bonds of magnetite.[20,22,23] Finally, The broad band centered at 3420 cm^{-1}

could be attributed to the O-H vibration of adsorbed water on nanoparticles surface.[27]
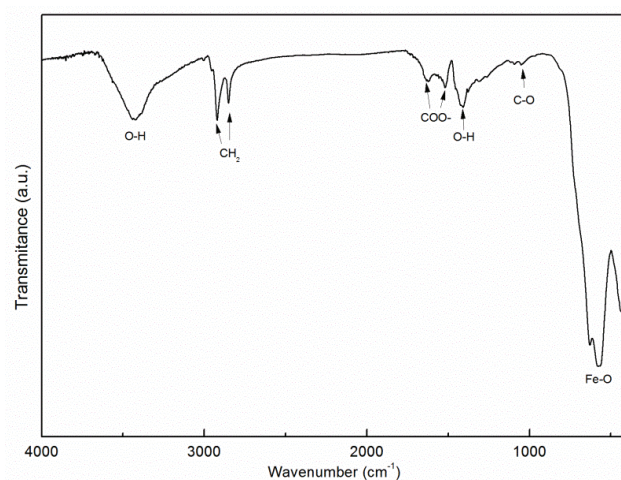
Figure 7.8. FTIR spectrum of MNPs.

The wavenumber separation, Δ, between the asymmetric and symmetric COO- stretching vibration bands can be used to distinguish the type of the interaction between the carboxylate head and the metal atom, which can be monodentate (Δ = 200-300 cm^{-1}), bridging bidentate (Δ = 140-190 cm^{-1}), chelating bidentate (Δ < 100 cm^{-1}) and ionic interaction.[24,29,30] In this work, the Δ (1622 - 1520 = 102 cm^{-1}), is ascribed to chelating bidentate denoting that the interaction between COO- group of oleic acid and the Fe is covalent[24] and thus oleic acid in carboxylate form is chemisorbed on the surface of oxide particles (Scheme 7.2).[27] These results revealed that oleic acid was physic and chemisorbed onto the magnetite nanoparticles as a carboxylate.[20,24]
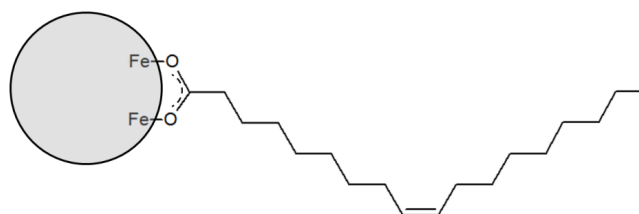
Scheme 7.2. Chelating bidentate interaction between the COO- group of oleic acid and the iron atom.

7.4 Conclusions

Different nanoentities were isolated and synthesized in order to employ them in the preparation of polyurethane bionanocomposites. On the one hand, chitin and cellulose nanocrystals were isolated via acid hydrolysis of chitin powder and microcrystalline cellulose. Chitin nanocrystals show an average length of 222 ± 31 nm and an aspect ratio of 23 ± 5 nm, while cellulose nanocrystals show an average length of 140 ± 20 nm and an aspect ratio of 21 ± 6 nm. The X-ray diffraction and Fourier transform infrared spectroscopy revealed that the isolated chitin and cellulose nanocrystals show a similar polymorphism and chemical groups to the observed in literature. Moreover, the obtained chitin and cellulose nanocrystals showed a high crystallinity degree. On the other hand, magnetite nanoparticles coated with oleic acid were synthesized *via* co-precipitation method. The average diameter of the obtained magnetite nanoparticles was 8 ± 2 nm, which was in accordance with the diameter of other similar magnetite nanoparticles reported in literature. FTIR spectrum revealed that oleic acid was physic and chemisorbed onto particle surface. Furthermore, the polymorphism of the magnetite nanoparticles was similar to the reported in literature.

7.5 References

1. J.D. Goodrich, W.T. Winter. "α-Chitin nanocrystals prepared from shrimp shells and their specific surface area measurement". Biomacromolecules 2007. 8: 252–257.

2. K. Gopalan Nair, A. Dufresne. "Crab shell chitin whisker reinforced natural rubber nanocomposites. 1. Processing and swelling behavior". Biomacromolecules 2003. 4: 657–665.

3. M. Zeng, H. Gao, Y. Wu, L. Fan, A. Li. "Preparation and characterization of nanocomposite films from chitin whisker and waterborne poly(ester-

urethane) with or without ultra-sonification treatment". J. Macromol. Sci. Part A. 2010. 47: 867–876.

4.   K. González, A. Retegi, A. González, A. Eceiza, N. Gabilondo. "Starch and cellulose nanocrystals together into thermoplastic starch bionanocomposites". Carbohydr. Polym. 2015. 117: 83–90.

5.   A. Saralegi, L. Rueda, L. Martin, A. Arbelaiz, A. Eceiza, M.A. Corcuera. "From elastomeric to rigid polyurethane/cellulose nanocrystal bionanocomposites". Compos. Sci. Technol. 2013. 88: 39–47.

6.   S. Liu, J. Sun, L. Yu, C. Zhang, J. Bi, F. Zhu, M. Qu, C. Jiang, Q. Yang. "Extraction and characterization of chitin from the beetle *Holotrichia parallela* Motschulsky". Molecules 2012. 17: 4604–4611.

7.   S. Ifuku, M. Nogi, K. Abe, M. Yoshioka, M. Morimoto, H. Saimoto, H. Yano. "Preparation of chitin nanofibers with a uniform width as α-chitin from crab shells". Biomacromolecules. 2009. 10: 1584–1588.

8.   R. Minke, J. Blackwell. "The structure of α-chitin". J. Mol. Biol. 1978. 120: 167–181.

9.   A.M. Salaberria, J. Labidi, S.C.M. Fernandes. "Chitin nanocrystals and nanofibers as nano-sized fillers into thermoplastic starch-based biocomposites processed by melt-mixing". Chem. Eng. J. 2014. 256: 356–364.

10.   N. Lin, J. Huang, P.R. Chang, L. Feng, J. Yu. "Effect of polysaccharide nanocrystals on structure, properties, and drug release kinetics of alginate-based microspheres". Colloids Surfaces B Biointerfaces 2011. 85: 270–279.

11.   D. Liu, T. Zhong, P.R. Chang, K. Li, Q. Wu. "Starch composites reinforced

by bamboo cellulosic crystals". Bioresour. Technol. 2010. 101: 2529–2536.

12. H. Kargarzadeh, I. Ahmad, I. Abdullah, A. Dufresne, S.Y. Zainudin, R.M. Sheltami. "Effects of hydrolysis conditions on the morphology, crystallinity, and thermal stability of cellulose nanocrystals extracted from kenaf bast fibers". Cellulose 2012. 855–866.

13. L. Segal, J.J. Creely, A.E.J. Martin, C.M. Conrad. "An empirical method for estimating the degree of crystallinity of native cellulose using the X-ray diffractometer". Text. Res. J. 1958. 29: 786–794.

14. Y. Fan, T. Saito, A. Isogai. "Chitin nanocrystals prepared by TEMPO-mediated oxidation of α-chitin". Biomacromolecules 2008. 9: 192–198.

15. N. Lin, J. Huang, A. Dufresne. "Nanoscale preparation, properties and applications of polysaccharide nanocrystals in advanced functional nanomaterials: a review". Nanoscale 2012. 4: 3274–3294.

16. K.M. Zia, M. Barikani, M. Zuber, I.A. Bhatti, M.A. Sheikh. "Molecular engineering of chitin based polyurethane elastomers". Carbohydr. Polym. 2008. 74: 149–158.

17. N. Butchosa, C. Brown, P.T. Larsson, L.A. Berglund, V. Bulone, Q. Zhou. "Nanocomposites of bacterial cellulose nanofibers and chitin nanocrystals: fabrication, characterization and bactericidal activity". Green Chem. 2013. 15: 3404–3413.

18. A. Kumar, Y.S. Negi, V. Choudhary, N.K. Bhardwaj. "Characterization of cellulose nanocrystals produced by acid-hydrolysis from sugarcane bagasse as agro-waste". J. Mater. Phys. Chem. 2014. 2: 1–8.

19. M.L. Nelson, P. Fibers, R.T.O. Connor, S. Regional. "Relation of certain infrared bands to cellulose crystallinity and crystal lattice type. Part I.

Spectra of lattice types I, II, III and of amorphous cellulose". J. Appl. Polym. Sci. 1964. 8: 1311–1324.

20. C. Meiorin, D. Muraca, K.R. Pirota, M.I. Aranguren, M.A. Mosiewicki. "Nanocomposites with superparamagnetic behavior based on a vegetable oil and magnetite nanoparticles". Eur. Polym. J. 2014. 53: 90–99.

21. Z. Es'haghzade, E. Pajootan, H. Bahrami, M. Arami. "Facile synthesis of Fe_3O_4 nanoparticles via aqueous based electro chemical route for heterogeneous electro-Fenton removal of azo dyes". J. Taiwan Inst. Chem. Eng. 2016. 0: 1–15.

22. R.A. Bini, R.F.C. Marques, F.J. Santos, J.A. Chaker, M. Jafelicci Jr. "Journal of magnetism and magnetic materials synthesis and functionalization of magnetite nanoparticles with different amino-functional alkoxysilanes". 2012. J. Magn. Magn. Mater. 324: 534–539.

23. L.A. Cobos Cruz, C.A. Martínez Perez, H.A. Monreal Romero, P.E. García Casillas. "Synthesis of magnetite nanoparticles-β-cyclodextrin complex". J. Alloys Compd. 2008. 466: 330–334.

24. L. Zhang, R. He, H.C. Gu. "Oleic acid coating on the monodisperse magnetite nanoparticles". Appl. Surf. Sci. 2006. 253: 2611–2617.

25. A.L. Patterson. "The Scherrer formula for X-ray particle size determination". Phys. Rev. 1939. 56: 978–982.

26. P. Guardia, B. Batlle-Brugal, A.G. Roca, O. Iglesias, M.P. Morales, C.J. Serna, A. Labarte, X. Battle. "Surfactant effects in magnetite nanoparticles of controlled size". J. Magn. Magn. Mater. 2007. 316: 756–759.

27. M. González, I. Martín-Fabiani, J. Baselga, J. Pozuelo. "Magnetic

nanocomposites based on hydrogenated epoxy resin". Mater. Chem. Phys. 2012. 132: 618–624.

28. D. Maity, S.G. Choo, J. Yi, J. Ding, J.M. Xue. "Synthesis of magnetite nanoparticles via a solvent-free thermal decomposition route". J. Magn. Magn. Mater. 2009. 321: 1256–1259.

29. E. Karaoglu, A. Baykal, M. Senel, H. Sözeri, M.S. Toprak. "Synthesis and characterization of piperidine-4-carboxylic acid functionalized Fe_3O_4 nanoparticles as a magnetic catalyst for Knoevenagel reaction". Mater. Res. Bull. 2012. 47: 2480–2486.

30. H. Erdemi, A. Baykal, E. Karaoglu, M.S. Toprak. "Synthesis and conductivity studies of piperidine-4-carboxylic acid functionalized Fe_3O_4 nanoparticles". Mater. Res. Bull. 2012. 47: 2193–2199.

CHAPTER 8

BIONANOCOMPOSITES WITH
SHAPE-MEMORY PROPERTIES
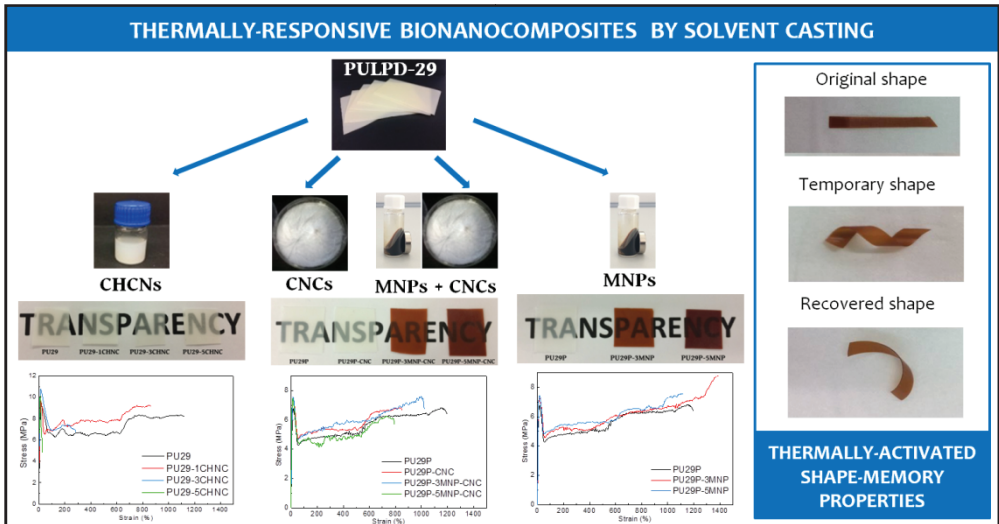
8. BIONANOCOMPOSITES WITH SHAPE-MEMORY PROPERTIES

8.1 Aim of the chapter

The aim of this chapter was to prepare and characterize polyurethane bionanocomposites with shape-memory properties using different nanoentities as reinforcement and varying the nanoentity content. The bionanocomposites were prepared by solvent casting procedure. For this purpose, neat PULPD-29 biobased polyurethane synthesized in chapter 5 and the nanoentities prepared in chapter 7 were used. As it was seen in chapter 6 the synthesized thermoplastic polyurethanes with the highest CO3 and LDI/PD content showed the highest shape recovery and shape fixity values, respectively. Therefore, PULPD-29 thermoplastic biobased polyurethane was chosen as matrix, since in this way it allows an improvement margin of both shape recovery and fixation, as it is an intermediate composition. Thermo-responsive bionanocomposites were prepared with CHNCs, CNCs and MNPs as well as combining CNCs and MNPs.

In order to analyze the influence of the addition of nanoentities (type and content) in final properties, as well as in shape-memory properties, a comprehensive study was carried out from the viewpoint of physicochemical, thermal, dynamic mechanical and mechanical behavior and their influence on shape-memory properties was analyzed. To that end, Fourier transform infrared spectroscopy, differential scanning calorimetry, dynamic mechanical analysis and tensile test and thermo-mechanical cyclic tests were performed.

8.2 Bionanocomposites based on chitin nanocrystals

8.2.1 Preparation of bionanocomposites with CHNCs

Shape-memory bionanocomposites based on chitin and biobased polyurethanes were prepared by solvent casting procedure. First, the biobased polyurethane

was dissolved in THF (25 mg mL^{-1}) and different amounts of CHNC (1, 3 and 5 wt% with respect to the total bionanocomposite mass) was added to the solution, which were previously dispersed in THF as previously mentioned in chapter 8. After that, the mixture was sonicated in a sonication bath with iced water for 1 h. Subsequently, the dispersion was ultrasonicated in order to break up the possible remaining aggregates of CHNCs in an ultrasonic processor (Vibra-cell 75043) with iced water for 30 min at an amplitude of 40%. Finally the dispersion was casted into a petri dish coated with Teflon°. In order to remove the solvent, the dispersion was subjected to a pressure-temperature cycle at 200 mbar and 55 °C for 48 h. Figure 8.1 shows a scheme of bionanocomposites preparation process.
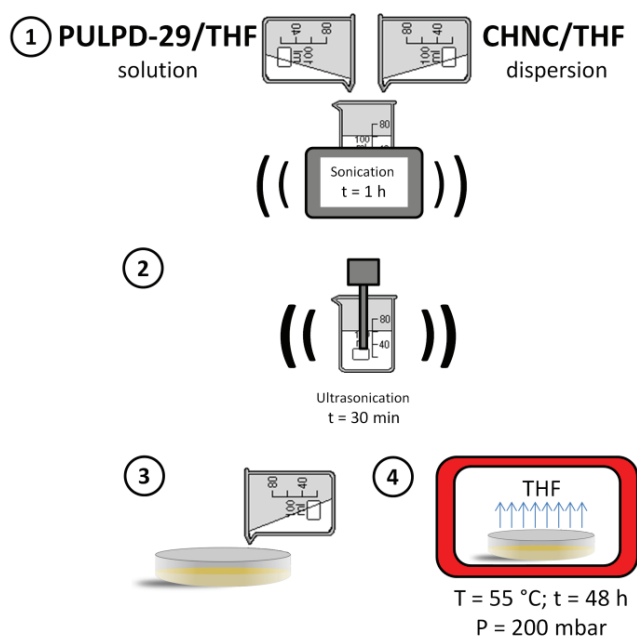
Figure 8.1. Scheme of the followed process for the preparation of bionanocomposites with CHNCs.

Biobased polyurethanes bionanocomposites films containing different amounts of chitin nanocrystals were successfully obtained. All films showed a thickness around 0.2 mm and they were designated as PU29-xCHNC, being x the amount of CHNC (expressed as weight percentage, wt%). As reference, the biobased

polyurethane was also prepared following the same procedure and it was designated as PU29. Figure 8.2 shows digital images of the prepared bionanocomposites with different CHNC content.
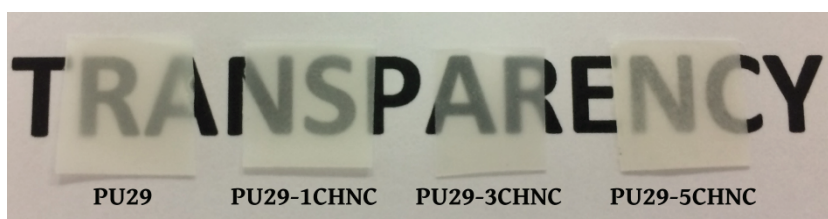
Figure 8.2. Digital images of PU29 biobased polyurethane and PU29-CHNC bionanocomposite series.

8.2.2 Characterization of the bionanocomposites with CHNCs

8.2.2.1 Fourier transform infrared spectroscopy

The characteristic functional groups of the polyurethane bionanocomposites with different CHNC content were analyzed by means of FTIR. As can be seen in Figure 8.3a, where FTIR spectra in N-H region is shown, in addition to the N-H stretching band observed in PU29 three shoulders can be observed: the first one between 3520 and 3400 cm^{-1}, the second between 3290 and 3210 cm^{-1} and the third between 3145 and 3000 cm^{-1}. These peaks are ascribed to CHNCs hydroxyl groups,[1] N-H symmetric and N-H asymmetric groups,[1,2] respectively, as mentioned in chapter 7. These peaks become more intense as CHNC content increases. Moreover, in amide I region (Figure 8.3b) the bands centered at 1655 and 1620 cm^{-1} becomes more intense as CHNC content increases, which are attributed to C=O stretching vibrations ($\nu_{C=O}$) of chitin.[1,3,4] The detection of these bands as CHNCs content increases confirmed the incorporation of the nanocrystals within the biobased polyurethane matrix.[3,4]
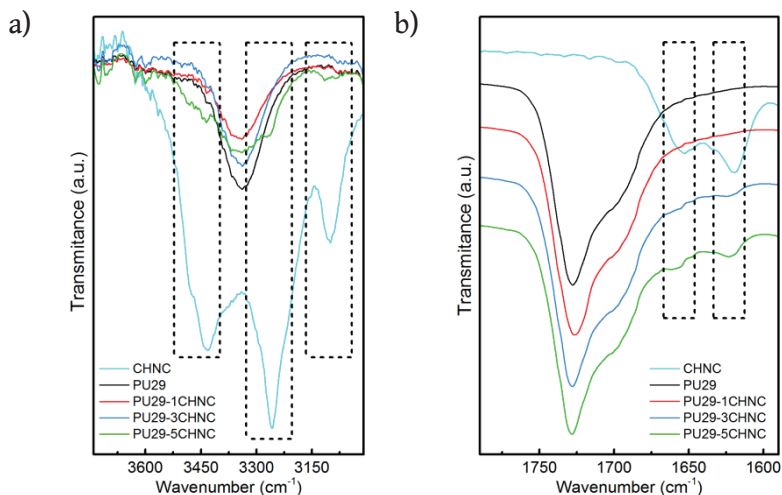
Figure 8.3. FTIR spectra of PU29 biobased polyurethane, CHNCs and PUP29-CHNC bionanocomposite series a) -NH region and b) amide I region.

8.2.2.2   Differential scanning calorimetry

As mentioned in previous chapters, the study of thermal transitions of the domains has a key role to determine the shape-memory test conditions, and also to understand the shape-memory behavior. To that end, thermal properties of the neat biobased polyurethane and bionanocomposites films prepared by solvent casting were analyzed by DSC. In Figure 8.4a the heating thermograms, as well as the cooling thermograms in the crystallization interval (inset), obtained for PU29 and for the corresponding bionanocomposites with different CHNCs contents and in Figure 8.4b a magnification of the heating scan at low temperatures are presented. In addition, Table 8.1 summarizes the principal thermal transitions observed by DSC, as well as the relative crystallinity values (relative crystallinity to the neat biobased polyurethane) calculated by equation 8.1:[5]

$$\chi_c = \frac{\Delta H_{m\,bc}}{\omega \cdot \Delta H_{100}}$$

(8.1)

where $\Delta H_{m\ bc}$ is the experimental melting enthalpy of the corresponding bionanocomposite, ω is the weight fraction of the neat biobased polyurethane in the bionanocomposites and ΔH_{100} is the melting enthalpy of the neat biobased polyurethane.
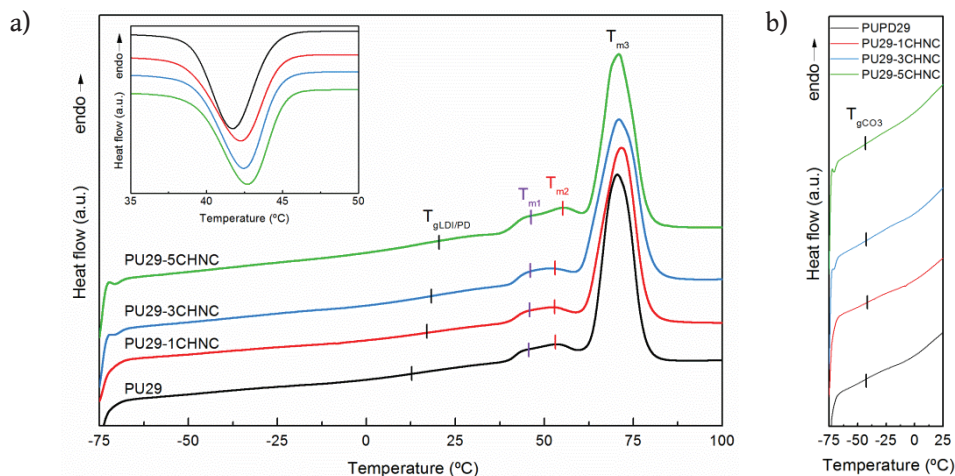
Figure 8.4. a) Heating DSC thermograms of PU29 biobased polyurethane and PU29-CHNC bionanocomposite series and b) magnification of low temperature. Inset: cooling DSC thermograms.

As previously mentioned in chapters 4 and 5, the thermodynamic incompatibility between domains leads to the formation of microphase separated morphology. Therefore, the obtained neat biobased polyurethane and bionanocomposites with CHNCs show several thermal transitions previously associated to neat LDI/PD rich domain and CO3 rich domain in chapter 5. At low temperatures, Figure 8.4b, both neat biobased polyurethane and bionanocomposites show a T_g associated to CO3 (T_{gCO3}), which remains nearly independent to the increase of CHNCs. Nevertheless, the T_g associated to LDI/PD ($T_{gLDI/PD}$) shifts to higher temperature as CHNCs content increases suggesting that CHNCs could interact with LDI/PD segments, hindering chain mobility of this segment.[6] Similar results were found in the literature where CHNC interacted with the domain formed by HDI and PD.[7] Since $T_{gLDI/PD}$ is the T_{trans} for

shape-memory properties, as previously observed in chapter 6 for PULPD biobased polyurethanes, the incorporation of CHNCs also increases T_{trans} and hence the quenching temperature necessary to fix the temporary shape is higher.

Table 8.1. Thermal transitions values of PU29 biobased polyurethane and PU29-CHNC bionanocomposite series.

Sample	T_{gCO3} (°C)	$T_{gLDI/PD}$ (°C)	T_{m1} (°C)	T_{m2} (°C)	T_{m3} (°C)	ΔH_m (J g^{-1})	T_c (°C)	ΔH_c (J g^{-1})	χ_c heating	χ_c cooling
PU29	-42.5	12.5	44.1	52.4	70.6	70.5	41.8	-57.9	1.00	1.00
PU29-1CHNC	-41.3	16.2	44.7	52.4	71.8	70.6	42.3	-58.5	1.01	1.02
PU29-3CHNC	-42.4	18.2	45.3	53.7	71.0	73.8	42.5	-60.3	1.08	1.07
PU29-5CHNC	-42.2	20.2	44.7	55.8	71.0	74.3	42.7	-61.1	1.11	1.11

Regarding melting behavior, both the neat biobased polyurethane and the bionanocomposites show an endothermic peak with three different maximum (T_{m1}, T_{m2} and T_{m3}) resulting from different crystal structures, domain sizes or degrees of order and reorganization in the crystalline structure of CO3 rich domain.[8] As CHNCs content increases bionanocomposites show a higher enthalpy and also χ_c.[9,10] Moreover, although T_{m1} and T_{m3} are almost independent to CHNCs content, T_{m2} shifts to higher temperatures with the increase of CHNCs content. This increase is more evident in PU29-5CHNC bionanocomposite. The increase of melting enthalpy and the shift of T_{m2} to higher temperatures suggest that CHNC could behave also as nucleating agent. Similar behavior was also observed for nanocomposites in literature.[7,11,12] Regarding, the cooling DSC thermograms, inset of Figure 8.4a, bionanocomposites show a slightly higher T_c and ΔH_c, which corroborats the nucleating effect of the CHNCs.

8.2.2.3 Dynamic mechanical analysis

The dynamic mechanical behavior of the neat biobased polyurethane and the bionanocomposites was analyzed by DMA. In Figure 8.5 the temperature

dependence of the storage modulus and loss factor for the biobased polyurethane and bionanocomposites is shown. As can be observed, at low temperatures the E' value in the glassy state of the biobased polyurethane and bionanocomposites is ranged between 2800 and 2950 MPa. As CHNCs content increases E' value also increases according to the reinforcement effect of the CHNCs and crystals. At higher temperatures, E' value of all materials shows a marked decrease associated to the transition from glassy to rubbery state. After the decrease of E' value, the materials reach the rubbery plateau, where the E_r value increases with the increase of CHNCs due to the effective reinforcement of the nanoentities, as well as to the increase of crystallinity. Finally, at a temperature around 60 °C E' of the biobased polyurethane and their bionanocomposites suffer a sharp decrease ascribed to the melting of CO3 rich domain, which was also observed in DSC, and therefore to the disruption of crystalline CO3 domains.
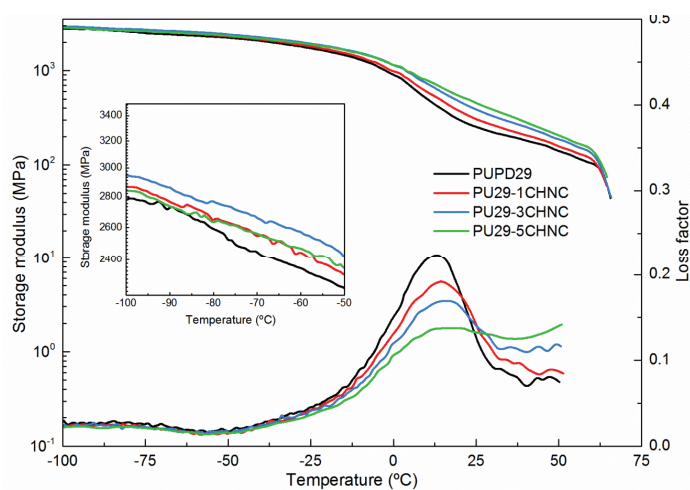
Figure 8.5. Storage modulus and loss factor of PU29 biobased polyurethane and PU29-CHNC bionanocomposite series.

As previously mentioned the maximum observed in tanδ curve is associated to the T_α of the material and provides information about the motion of molecules. As CHNCs content increases T_α shifts to higher temperatures as it can be observed in Table 8.2 where T_α values of the biobased polyurethane and

bionanocomposites are gathered. Since tanδ is the ratio of loss to storage modulus, it can be surmised that the decreasing intensity is associated with restriction in segmental mobility and thus the increase of the content of CHNCs inhibits the motion of the chains and results in a higher T_α.[13]

Table 8.2. α transition temperature of PU29 biobased polyurethane and PU29-CHNC bionanocomposite series.

Sample	T_α (°C)
PU29	13.1
PU29-1CHNC	14.1
PU29-3CHNC	15.7
PU29-5CHNC	18.6

8.2.2.4 X-ray diffraction

The analysis of the polymorphism of the bionanocomposites with a 3 wt% CHNCs was carried out by XRD. In Figure 8.6, the XRD patterns of PU29-3CHNC together with PU29 and CHNC are displayed.
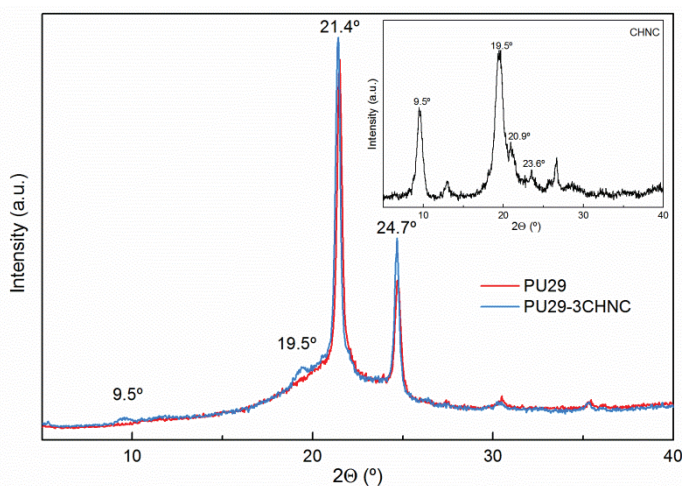
Figure 8.6. X-ray diffraction patterns of PU29 biobased polyurethane and PU29-3CHNC bionanocomposite. Inset: XRD of CHNCs.

XRD pattern of PU29-3CHNC shows strong reflections at 21.4 and 24.7°, which corresponded to the crystals of the CO3 rich domain.[14–17] Moreover, at 9.5 and 19.5° the bionanocomposite show minor peaks, which corresponded to (020) and (110) crystallographic planes of the α-chitin.[3,18–20] Therefore, the presence of CHNCs within the biobased polyurethane matrix was confirmed by XRD, as it was previously supported by FTIR. As can be observed, the intensity of the peaks related with CO3 rich domain increases in the bionanocomposite, which denotes a higher crystallinity of the material and corroborates the nucleating effect of the CHNCs previously observed by DSC.

8.2.2.5   Mechanical properties

Mechanical properties of the bionanocomposites were analyzed by performing tensile tests. The stress-strain curves and the values of E, σ_y, σ_b, strain at yield point (ε_y) and strain at break (ε_b) obtained from these curves are shown in Figure 8.7 and Table 8.3, respectively.
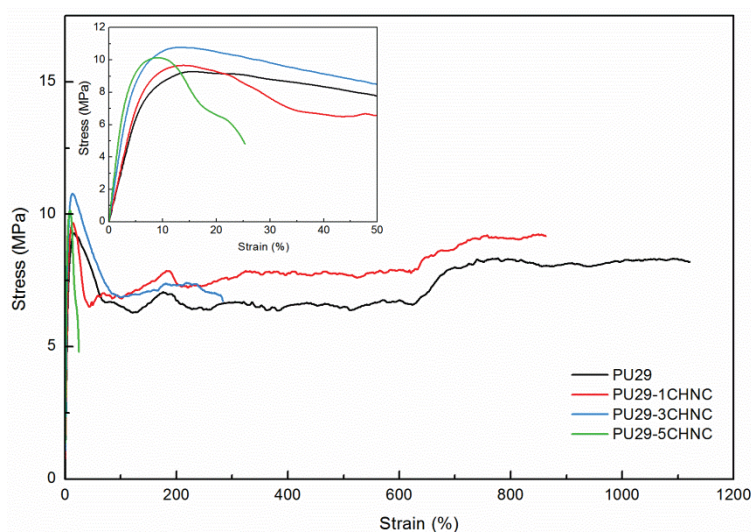
Figure 8.7. Stress-strain curves of PU29 biobased polyurethane and PU29-CHNC bionanocomposite series.

Table 8.3. Mechanical properties of PU29 biobased polyurethane and PU29-CHNC bionanocomposite series.

Sample	E (MPa)	σ_y (MPa)	σ_b (MPa)	ε_y (%)	ε_b (%)
PU29	135 ± 5	9.2 ± 0.3	8.1 ± 0.3	13.6 ± 2.1	1018 ± 100
PU29-1CHNC	152 ± 20	9.6 ± 0.2	8.9 ± 0.4	13.2 ± 1.1	870 ± 59
PU29-3CHNC	220 ± 7	10.8 ± 0.1	7.2 ± 0.5	13.4 ± 0.2	249 ± 48
PU29-5CHNC	256 ± 26	10.3 ± 0.4	6.5 ± 0.5	9.4 ± 0.8	23 ± 2

In almost all polymeric matrices founded in literature, the addition of CHNCs leads to an improvement of stiffness.[7,21–24] This improvement in mechanical properties is attributed to the percolation network formed though the strong hydrogen bonding between chitin nanocrystals.[22]

In the case of the bionanocomposites, the addition of CHNCs improves mechanical properties by increasing elastic modulus and stress at yield, due to the nano-reinforcement effect of the nanocrystals and also to the higher crystallinity as observed in DSC. This behavior corroborates the results observed previously by DMA. Notwithstanding, the strain at break and the stress at break shows a marked decrease as CHNCs content increases, which could be attributed to the higher rigidity of the material formed by nanocrystals and CO3 rich domain crystals.[25]

As mentioned before, a rigid percolated network can be formed through the interaction between nanoparticles, which contribute to the improvement of the mechanical properties for the nanocomposites. The percolation threshold value depends on the aspect ratio (L/D) of rod-like chitin nanocrystals, and can be estimated by following equation 8.2:[26,27]

$$V_{Rc} = \frac{0.7}{(L/D)} \tag{8.2}$$

The theoretically obtained percolation threshold value were 3.26 vol% and 4.29 wt%, taking 1.100 and 1.462 g cm^{-3} for the density of the biobased polyurethane

matrix[28] and crystalline chitin,[1] respectively. However, the increase of CO3 rich domain crystallinity could contribute to the formation of a percolated structure formed by CHNCs interacting with crystalline CO3 rich domains at lower CHNCs contents than the estimated theoretically. Thus, the marked increased of elastic modulus and decrease of strain at break of PU29-3CHNC and PU29-5CHNC bionanocomposites could be attributed to the presence of this three-dimensional network.

8.2.2.6 Shape-memory properties

Since the matrix shows thermally activated shape-memory properties, as previously analyzed in chapter 6, the effect of the addition of CHNCs on shape-memory properties was studied.

In chapter 6 it was seen that the synthesized polyurethanes (PULPD series) showed better shape-memory properties at T_s of 40 °C: higher R_f values were obtained and although R_r values were similar, recovery times were shorter. Therefore, the thermo-mechanical cycles were performed at T_s = 40 °C and ε_m = 50% following the previously employed process for the determination of shape-memory properties of PULPD series. Moreover, since PU29-5CHNC underwent elongations at break lower than ε_m, it was not possible to determine the shape-memory properties of this bionanocomposite at the same conditions.

In Figure 8.8 the stress-strain curves of thermo-mechanical cycles of PU29, PU29-1CHNC and PU29-3CHNC are displayed. Moreover, in Table 8.4 R_f and R_r values are gathered.
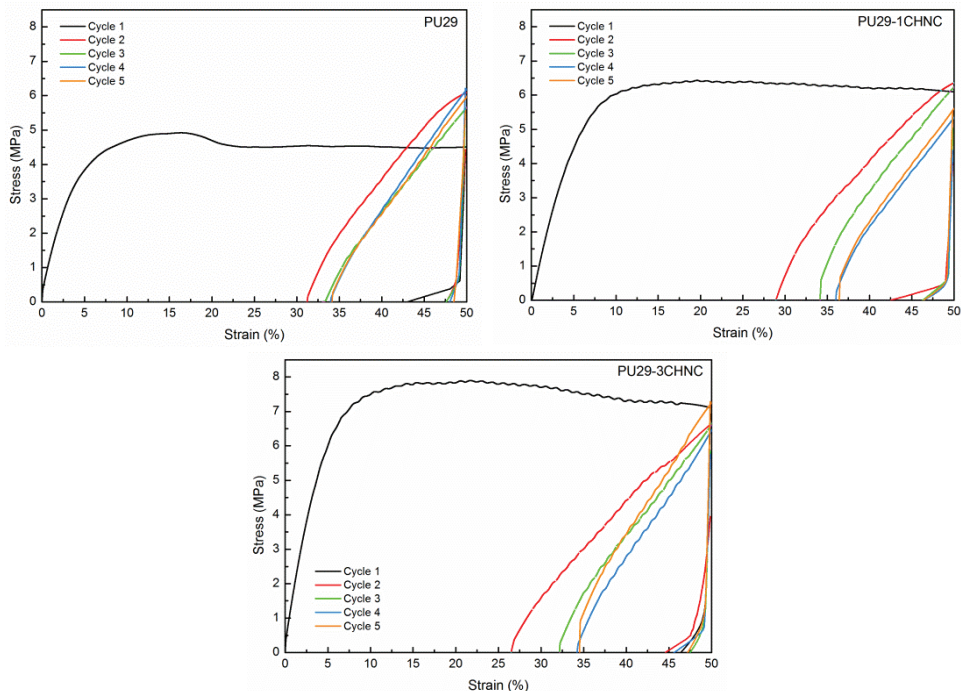
Figure 8.8. Stress-strain curves of thermo-mechanical cycles of PU29 biobased polyurethane and PU29-CHNC bionanocomposite series.

Table 8.4. R_f and R_r values calculated for each thermo-mechanical cycle for PU29 biobased polyurethane and PU29-CHNC bionanocomposite series.

Cycle	PU29		PU29-1CHNC		PU29-3CHNC	
	R_f (%)	R_r (%)	R_f (%)	R_r (%)	R_f (%)	R_r (%)
1	95.3	82.5	94.2	83.8	96.9	85.8
2	97.5	98.5	95.0	95.9	97.6	95.4
3	98.4	99.1	97.5	98.3	98.3	98.1
4	98.7	99.8	97.6	99.6	97.1	99.8
5	99.0	100.0	97.6	100.0	98.1	99.8

Regarding the results obtained in the first cycle at T_s = 40 °C, R_f values of the biobased polyurethane and bionanocomposites range from 94.2 to 96.9%, and R_r values from 82.5 to 85.8%.

As it is known, sample preparation procedure can have influence on thermal transitions and hence on the final properties of the material. Shape-memory properties of the biobased polyurethane obtained by casting, PU29, are different from the biobased polyurethane synthesized by bulk, PULPD-29, which showed R_r and R_f value of 93.9% and 89.7%, respectively. The lower R_r value of PU29 is related with the lower crystallinity of the material (70.5 and 88.3 J g^{-1} for PU29 and PULPD-29, respectively) and also to the higher amount of crystals broken during the stretching processes since the strain at yield point for PU29 was 13.6% while for PULPD-29 was 16.1%. Regarding shape fixation, the higher R_f value observed for PU29 could be related with two factors. On the one hand with the geometry of the sample, PULPD-29 had a thickness of 1.5 mm and PU29 of 0.2 mm, therefore due to its smaller thickness PU29 could be quenched better and hence the shape fixity is higher. On the other hand, with the higher T_g (12.5 and 9.5 °C for PU29 and PULPD-29, respectively), which is related to the temperature necessary to fix the temporary shape.

Regarding the shape-memory properties of the bionanocomposites, as previously observed in chapter 6 section 6.4.1, shape-memory properties of PULPD series depended on transition temperatures and crystallinity of domains, modulus in glassy and rubbery state as well as TME. Therefore, in order to a better understanding of the shape-memory behavior of the bionanocomposites based on PULPD-29 and different contents of CHNCs, those parameters are gathered in Table 8.5, as well as the shape-memory properties of the first cycle.

As can be observed the addition of CHNC influences on shape-memory properties of the biobased materials. On the one hand, as CHNC content increases the shape recovery of the first cycle of the bionanocomposites also increases, suggesting that the addition of CHNCs contribute to shape recovery. This contribution could be ascribed to the higher crystallinity of the material due to the nucleating effect of the CHNCs. As previously observed, shape-

memory polymers can restore their original shape through crystalline structures.[29] Furthermore, none of the bionanocomposites, neither PU29, show a complete shape recovery in the first cycle, due to they were stretched up above their yield point. On the other hand, R_f values of the materials remains nearly constant with the addition of CHNCs, suggesting that the increase observed in T_{trans} does not affect considerably to shape fixity.

Table 8.5. Thermal transition, melting enthalpy, shape-memory properties, elastic moduli in glassy and rubbery state and strain at yield point of PU29 biobased polyurethane and PU29-CHNC bionanocomposites.

Sample	$T_{gLDI/PD}$ (°C)	ΔH_m (J g^{-1})	R_f (%)	E_g (MPa)	R_r (%)	E_r (MPa)	ε_y (%)
PU29	12.5	70.5	95.3	2718	82.5	223	13.6
PU29–1CHNC	16.2	70.6	94.2	2754	83.8	261	13.2
PU29–3CHNC	18.2	73.8	96.9	2846	85.8	315	13.4

Regarding TME, the deformation temperature does not overlap the onset of melting enthalpy, as can be observed in Figure 8.9. Therefore, in the case of bionanocomposites with CHNC, TME was not considered.
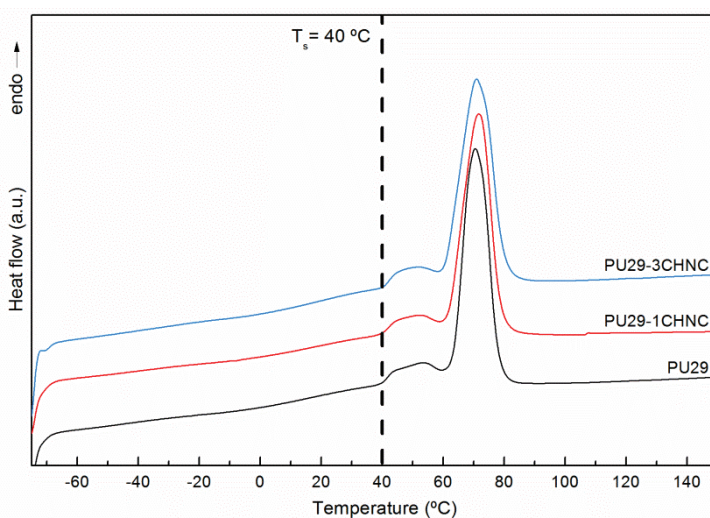
Figure 8.9. The chosen switching temperature for PU29 biobased polyurethane and PU29-CHNC bionanocomposite series.

8.3   Bionanocomposites based on magnetite nanoparticles

8.3.1   Preparation of bionanocomposites with MNPs

Different shape-memory bionanocomposites based on MNP and biobased polyurethanes were prepared by solvent casting procedure. First, the biobased polyurethane was dissolved in THF (50 mg mL^{-1}) and different amount of MNP dispersed in THF (3 and 5 wt% with respect to the total bionanocomposite mass) were added to the solution. Subsequently, the mixture was sonicated in a sonication bath for 1 h with a cold water recirculation system. After that, the dispersion was casted into a Teflon° mold. In order to remove the solvent, the dispersion was placed in an oven at 70 °C for 20 h. Finally, the obtained casted films were subjected to compression molding. In Figure 8.10 a scheme of the preparation process of magnetic bionanocomposites is shown.
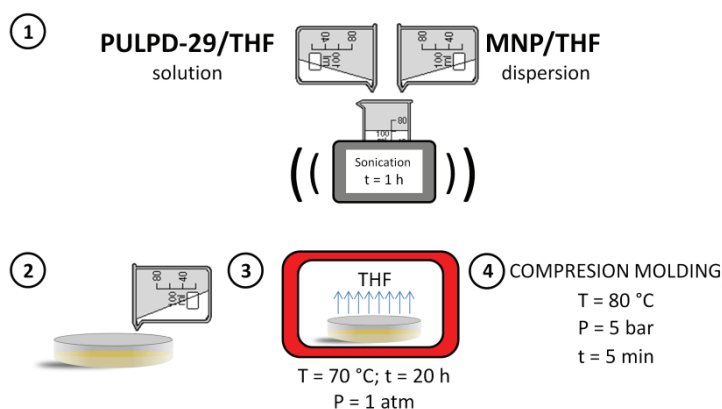
Figure 8.10. Scheme of the followed process for the preparation of bionanocomposites with MNPs.

Bionanocomposites with biobased polyurethane and MNPs were successfully obtained. The obtained bionanocomposites were designated as PU29P-xMNP, being x the amount of MNPs added (expressed as weight percentage, wt%). As reference, biobased polyurethane was also prepared following the same procedure and it was designated as PU29P. In Figure 8.11 digital images of the prepared bionanocomposites are shown.
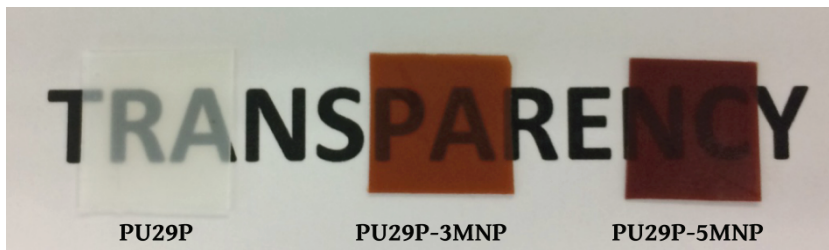
Figure 8.11. Digital images of PU29P biobased polyurethane and PU29P-MNP bionanocomposite series.

Furthermore, the magnetic properties of the bionanocomposites were also checked. To that end, a magnetic field formed by a strong magnet was applied to a strip shape sample. The initial distance left between the sample and magnet was kept around 3 cm and the process was recorded with a digital camera. In Figure 8.12 a sequence of digital images of the recorded video of PU29-5MNP bionanocomposite is shown. As can be observed the bionanocomposite was attracted to the magnet, thus the bionanocomposites show magnetic properties.
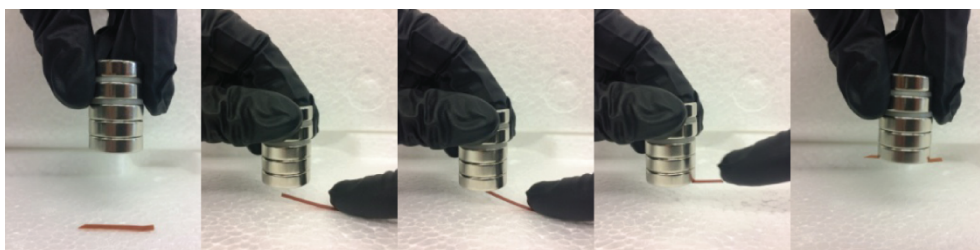
Figure 8.12. Sequence of digital images of the magnetic response of PU29P-5MNP.

8.3.2 Characterization of the magnetic bionanocomposites

8.3.2.1 Differential scanning calorimetry

The analysis of the thermal behavior of the magnetic bionanocomposites was performed by DSC. The heating DSC thermograms and cooling thermograms are showed in Figure 8.13. Furthermore, the thermal transitions, as well as the relative crystallinity values (relative crystallinities to the neat biobased polyurethane) calculated by equation 8.1 are listed in Table 8.6.
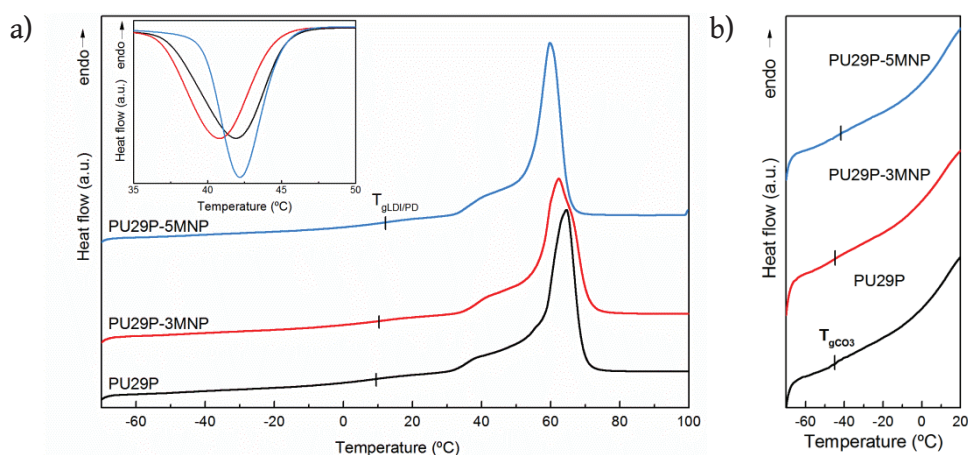
Figure 8.13. a) Heating DSC thermograms of PU29P biobased polyurethane and PU29P-MNP bionanocomposite series and b) magnification of the thermograms at low temperatures. Inset: Cooling DSC thermograms.

Table 8.6. Thermal transition values of PU29P biobased polyurethane and PU29P-MNP bionanocomposite series.

Sample	T_{gCO3} (°C)	$T_{gLDI/PD}$ (°C)	T_m (°C)	ΔH_m (J g^{-1})	T_c (°C)	ΔH_c (J g^{-1})	χ_c heating	χ_c cooling
PU29P	-45.2	13.6	64.6	62.8	41.9	-58.8	1.00	1.00
PU29P-3MNP	-44.6	11.3	62.3	59.1	40.8	-56.1	0.97	0.98
PU29P-5MNP	-41.7	12.0	59.6	58.0	42.2	-54.5	0.97	0.98

As can be observed, similarly to the bionanocomposites with CHNC, the obtained neat biobased polyurethane and magnetic bionanocomposites with MNPs show the thermal transitions associated to neat LDI/PD rich domain and CO3 rich domain, suggesting that the magnetic bionanocomposites show a microphase separated structure. The magnetic bionanocomposites show a T_g at low temperatures, Figure 8.3b, ascribed to T_{gCO3}, which shifts to higher temperatures. As previously mentioned, the T_g is an indicator of the relative purity of the phases.[30–32] The increase of T_{gCO3} value with higher MNP content denotes that MNPs could interact with CO3 rich domain restricting its mobility and hence increasing the T_g.[6] Moreover, at higher temperatures the T_g

associated to LDI/PD reach domain could be observed, which remains almost constant with the increase of MNP content suggesting that MNPs do not interact with LDI/PD rich domain.

In addition, bionanocomposites with MNPs show a lower T_m and ΔH_m values, indicating that the overall crystallinity decreased and crystals of different chains arrangement were formed during the crystallization of the magnetic bionanocomposite. Regarding the crystallizable domain, bionanocomposites show lower $\chi_{c\ heating}$ values, which suggests that the addition of MNPs could decrease the crystallization ability of CO3 rich domain. Similar behavior was observed in the cooling DSC thermograms, inset of Figure 8.13a, where it can be observed that the overall crystallinity and $\chi_{c\ cooling}$ decreases as MNP content increases. Similar results were observed in literature.[33]

From this behavior it can be surmised that MNPs tend to interact with CO3 rich domain, since T_{gCO3} increases and lower T_m, ΔH_m and $\chi_{c\ heating}$ values were obtained with the addition of MNPs. This fact differs from the behavior of CHNCs, which interact with LDI/PD rich domain acting as well as nucleating agent as previously observed. In order to a better understanding of this interactions, the solubility parameters of CO3, LDI/PD, CHNC and oleic acid used for the synthesis of MNPs were calculated by Hoy method.[34] The calculated solubility parameters are gathered in Table 8.7.

Table 8.7. Solubility parameter of CO3 and LDI/PD domains, chitin and oleic acid.

Sample	δ ($J^{1/2}\ cm^{-3/2}$)
CO3	20.07
LDI/PD	24.28
Chitin	29.77
Oleic acid	18.53

Solubility parameters suggest that CHNCs have a higher affinity with LDI/PD rich domain, while the magnetite coated with oleic acid would preferably interact with CO3 rich domain, corroborating the behavior observed by DSC.

8.3.2.2 Dynamic mechanical analysis

DMA was employed in order to analyze the dynamic mechanical behavior of the neat biobased polyurethane prepared by solvent casting and the magnetic bionanocomposites. Figure 8.14 shows the temperature dependence of storage modulus and loss factor for the biobased polyurethane and magnetic bionanocomposites. At low temperatures the magnetic bionanocomposites show higher E' in the glassy state, suggesting that MNPs contribute to the effective reinforcement.[6] At higher temperatures the E' decreases reaching the rubbery plateau, where the E' value in the rubbery state of the bionanocomposites is higher due to the effective reinforcement of the nanoparticles, as observed by other authors.[35] This behavior was also observed when CHNCs were added. At temperatures around 60 °C a sharp decrease of E' occurs, which corresponds to the disruption of the crystalline structure of the material.
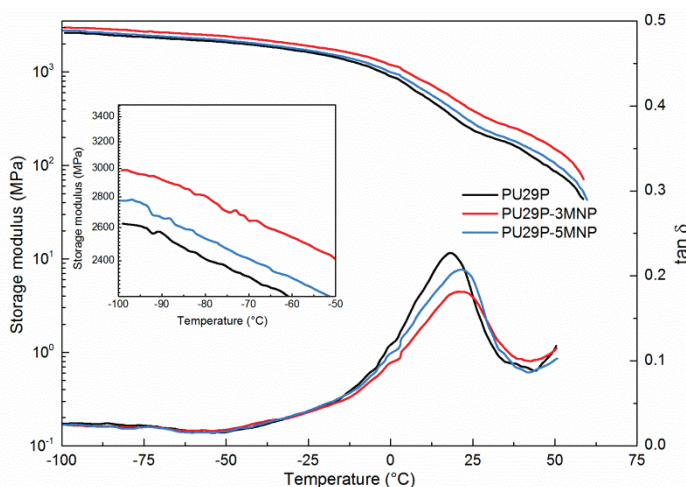
Figure 8.14. Storage modulus and loss factor of PU29P biobased polyurethane and PU29P-MNP bionanocomposite series.

Furthermore, as it can be observed in Figure 8.14 and in Table 8.8, where T_α values of the biobased polyurethane by solvent casting and magnetic bionanocomposites are gathered, T_α seems not to be dependent on MNP content, since similar values were obtained for PU29P-3MNP and PU29P-5MNP.

Table 8.8. α transition temperature of PU29P biobased polyurethane and PU29P-MNP bionanocomposite series.

Sample	T_α (°C)
PU29P	18.9
PU29P-3MNP	21.7
PU29P-5MNP	21.5

8.3.2.3 X-ray diffraction

XRD was used in order to analyze the polymorphism of the magnetic bionanocomposite with a 3 wt% MNP. In Figure 8.15, the XRD patterns of PU29P-3MNP together with PU29P and MNP are shown.
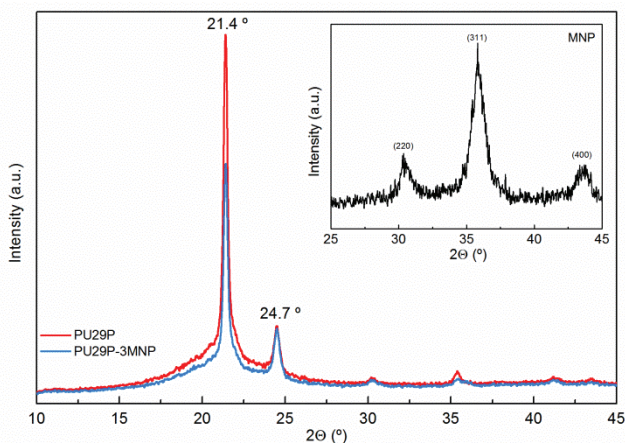
Figure 8.15. XRD patterns of PU29P biobased polyurethane and PU29P-3MNP magnetic bionanocomposite. Inset: XRD pattern of MNPs.

As can be seen, PU29P-3MNP magnetic bionanocomposite shows a different crystallinity if compared with neat biobased polyurethane since the intensity of

the peaks at 2θ = 21.4° decreases considerably, which is related with the biobased polyurethane CO3 rich domain.[15–17] Thus, the lower intensity of the magnetic bionanocomposite denotes that the addition of the spherical MNPs results in different chains arrangements of CO3 rich domain, which is in agreement with the lower T_m and ΔH_m values observed by DSC. Similar results were observed for other authors.[33] Moreover, this behavior differs from the behavior observed in bionanocomposites with rod-like CHNCs, which interact with LDI/PD rich domain and behaving as nucleating agent of CO3 rich domain.

8.3.2.4   Mechanical properties

The effect of the addition of MNPs in mechanical properties of the biobased polyurethane was analyzed by performing tensile tests. The stress-strain curves of the biobased polyurethane and magnetic bionanocomposites prepared by solvent casting are shown in Figure 8.16.
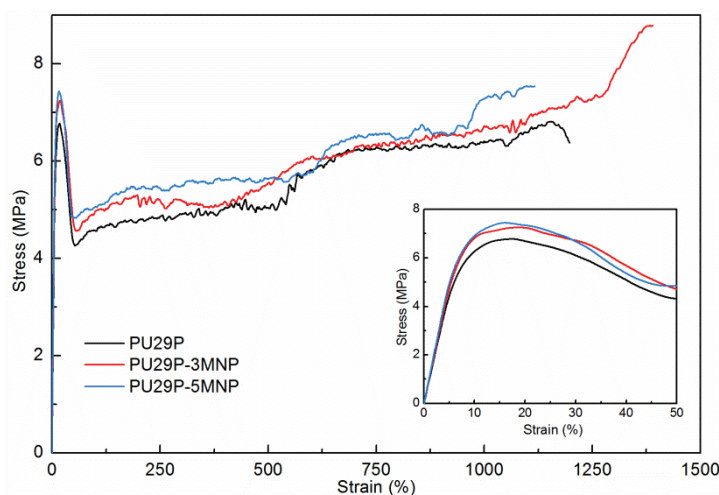
Figure 8.16. Stress-strain curves of PU29P biobased polyurethane and PU29P-MNP bionanocomposite series.

Moreover, in Table 8.9 the characteristic values derived from stress-strain curves are gathered.

Table 8.9. Mechanical properties of PU29P biobased polyurethane and PU29P-MNP bionanocomposite series.

Sample	E (MPa)	σ_y (MPa)	σ_b (MPa)	ε_y (%)	ε_b (%)
PU29P	93 ± 8	6.9 ± 0.2	7.2 ± 0.4	16.9 ± 2.2	1149 ± 153
PU29P-3MNP	98 ± 1	7.1 ± 0.1	8.4 ± 0.8	15.8 ± 2.0	1342 ± 72
PU29P-5MNP	102 ± 4	7.3 ± 0.3	7.7 ± 0.1	16.3 ± 1.4	1105 ± 78

Regarding the magnetic bionanocomposites, as MNP content increases similar mechanical behavior can be observed. As observed in chapter 5, the mechanical properties of PULPD biobased polyurethane series were governed by CO3 rich domain crystallinity. In this way, since MNPs interact with CO3 rich domain and in opposition to CHNCs, they do not show a nucleating effect and they do not form a percolated network which could interfere in the elongation of the bionanocomposite,[22] so that mechanical properties are not greatly affected by the incorporation of the nanoparticles. Furthermore, it could be deduce that MNPs could be able to absorb strain energy upon deformation, acting as effective stress-bearing phase during deformation,[36,37] since elastic modulus, stress at yield and at break are not affected in a great extent although the lower overall crystallinity of the material observed by DSC.

Several differences could be observed when the mechanical properties of PU29P are compared with the previously synthesized PULPD-29 and PU29, which were prepared following different preparation routes. In Table 8.10 the mechanical properties and melting enthalpy of PULPD-29, PU29 and PU29P are gathered.

Table 8.10. Melting enthalpy and mechanical properties of PULPD-29, PU29 and PU29P.

Sample	ΔH_m (J g^{-1})	E (MPa)	σ_b (MPa)	ε_b (%)
PULPD-29	88.3	143 ± 4	18.5 ± 1.0	847 ± 31
PU29	70.5	135 ± 5	9.2 ± 0.3	1018 ± 100
PU29P	62.8	93 ± 8	7.2 ± 0.4	1149 ± 153

As can be observed, PU29P show a lower crystallinity which could be associated to the preparation process, since the cooling process after be compressed at 80 °C was faster. Therefore, due to the faster cooling rate of the material, fewer crystals were formed. Moreover, PU29P biobased polyurethane shows lower E and σ_b due to the mentioned lower crystallinity, and thus PU29P shows the highest strain at break.

8.3.2.5 Shape-memory properties

The influence of the addition of MNPs on shape-memory properties was also studied. For the analysis of these properties the same conditions followed for bionanocomposites with CHNCs were used; five thermo-mechanical cycles at T_s of 40 °C and ε_m of 50%.

The stress-strain curves for the successive thermo-mechanical cycles are shown in Figure 8.17.
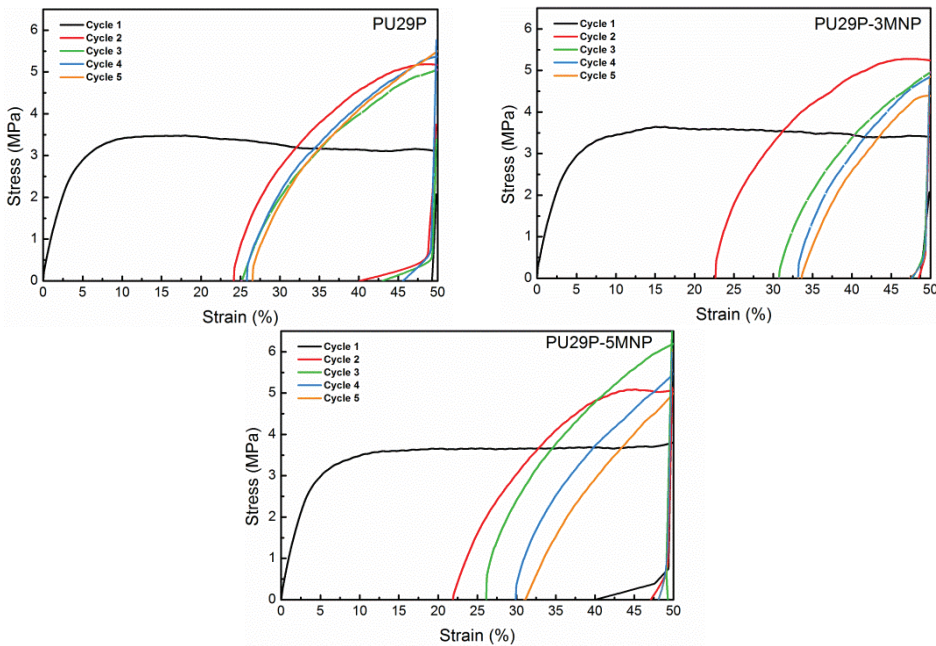
Figure 8.17. Stress-strain curves of thermo-mechanical cycles of PU29P biobased polyurethane and PU29P-MNP bionanocomposite series.

Moreover, in Table 8.11 the R_f and R_r values of the successive thermo-mechanical cycles of the biobased polyurethane as well as magnetic bionanocomposites prepared by solvent casting are shown. As can be observed in the first cycle, R_f values of the prepared materials range from 91.6 to 94.7%, and R_r values from 87.3 to 88.7%.

Table 8.11. R_f and R_r values calculated for each thermo-mechanical cycle for PU29P biobased polyurethane and PU29P-MNP bionanocomposite series.

Cycle	PU29P		PU29P-3MNP		PU29P-5MNP	
	R_f (%)	R_r (%)	R_f (%)	R_r (%)	R_f (%)	R_r (%)
1	91.6	87.3	94.7	88.2	93.3	88.7
2	93.4	99.3	99.0	94.0	98.1	97.0
3	94.8	99.5	98.5	97.9	99.5	97.1
4	96.4	99.5	98.4	99.6	98.7	99.1
5	99.4	100.0	98.2	100.0	98.7	100.0

Furthermore, in order to a better understanding of shape-memory properties and the factors which influence on them, glass transition temperature, melting enthalpies, elastic moduli at glassy and rubbery state, strain at yield point, percentage of overlapped area during deformation process as well as R_f and R_r of the first cycle are gathered in Table 8.12.

Table 8.12. Glass transition temperature, melting enthalpy, shape-memory properties, elastic moduli in glassy and rubbery state, strain at yield point, percentage of the overlapped area of PU29P polyurethane and PU29P-MNP bionanocomposite series.

Sample	$T_{gLDI/PD}$ (°C)	ΔH_m (J g^{-1})	R_f (%)	E_g (MPa)	R_r (%)	E_r (MPa)	ε_y (%)	$A_{overlapped}$ (%)
PU29P	13.6	62.8	91.6	2546	87.3	184	16.9	4.33
PU29P-3MNP	11.3	59.1	94.7	2915	88.2	192	15.8	2.56
PU29P-5MNP	12.0	58.0	93.3	2654	88.7	261	16.3	4.46

As can be observed in Table 8.11 and 8.12 the addition of MNPs results in a higher shape fixity, which could be related with the higher E' in the glassy state,

due to polymers with a higher E' in the glassy state show greater shape fixity, as previously mentioned.[38] The shape fixity of the magnetic bionanocomposites is lower if compared with PU29-CHNC bionanocomposites. This fact could be related with the slightly lower $T_{gLDI/PD}$ of the material.

Regarding shape recovery, since all prepared materials were stretched above their yield point, R_r values are lower than 100% in the first cycle. Moreover, similar R_r values were obtained, despite of the lower crystallinity of bionanocomposites, denoting that the addition of MNPs could contribute to store the residual stress introduced in the sample during the stretching process. This behavior was also observed in mechanical properties where due to the incorporation to MNPs the material was able to absorb more strain energy upon deformation.[36,37]

Moreover, as previously mentioned, when deformation temperature overlaps a transition, in this case the onset of melting enthalpy of CO3 rich domain, TME takes place, which means that shape-memory is also due to a partial thermal transition. In Figure 8.18 it can be observed the evolution of overlapped area as MNP content increases.
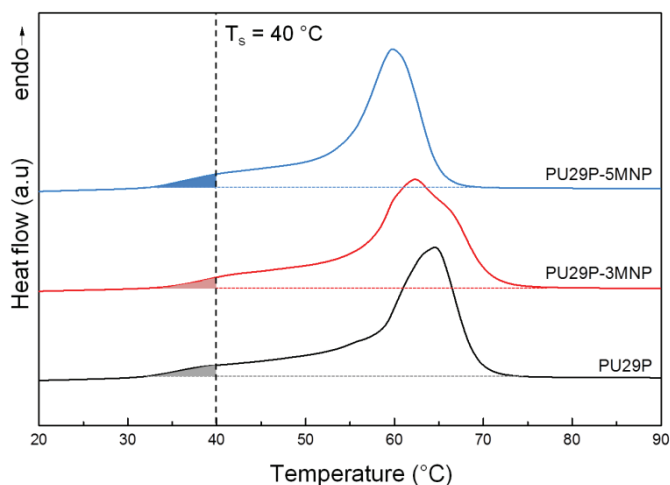
Figure 8.18. Evolution of the overlapped area as MNP content increases.

The overlapped area is similar for PU29P and PU29P-5MNP (Table 8.12) thus the contribution to the rubbery state would be alike. However, PU29P-3MNP shows the highest R_f despite of its smaller overlapped area.

8.4 Bionanocomposites based on the combination of cellulose nanocrystals and magnetite nanoparticles

8.4.1 Preparation of bionanocomposites combining CNCs and MNPs

Different shape-memory bionanocomposites based on biobased polyurethanes containing on the one hand CNCs, and on the other hand CNCs and MNPs were prepared by solvent casting procedure. First, 10 wt% of CNCs (with respect to the total bionanocomposite mass) were dispersed in THF in a sonication bath for 4 h with a cold water recirculation system. The dispersed CNCs were added into previously dispersed MNPs (3 and 5 wt% with respect to the total bionanocomposite mass) in dissolved PULPD-29 in THF (50 mg mL^{-1}). Subsequently, the mixture was sonicated for 30 min. Finally the dispersion was casted into a Teflon® mold. In order to remove the solvent, the dispersion was placed in an oven at 70 °C for 20 h and pressed in a compression press at 80 °C for 5 min at 5 bar. In Figure 8.19a a scheme of the preparation process of magnetic bionanocomposites based on both CNCs and MNPs is shown.

As reference a bionanocomposite with a 10 wt% of CNCs was also prepared, PU29P-CNC (Figure 8.19b). To that end 10 wt% of CNCs were dispersed in THF for 4 h in a sonication bath. The dispersed CNCs were added into PULPD-29 dissolved in THF (50 mg mL^{-1}), subsequently the mixture was sonicated for 30 min and finally casted into a Teflon® mold. After that, the same procedure followed for the preparation of the magnetic bionanocomposites with CNCs and MNPs was followed.
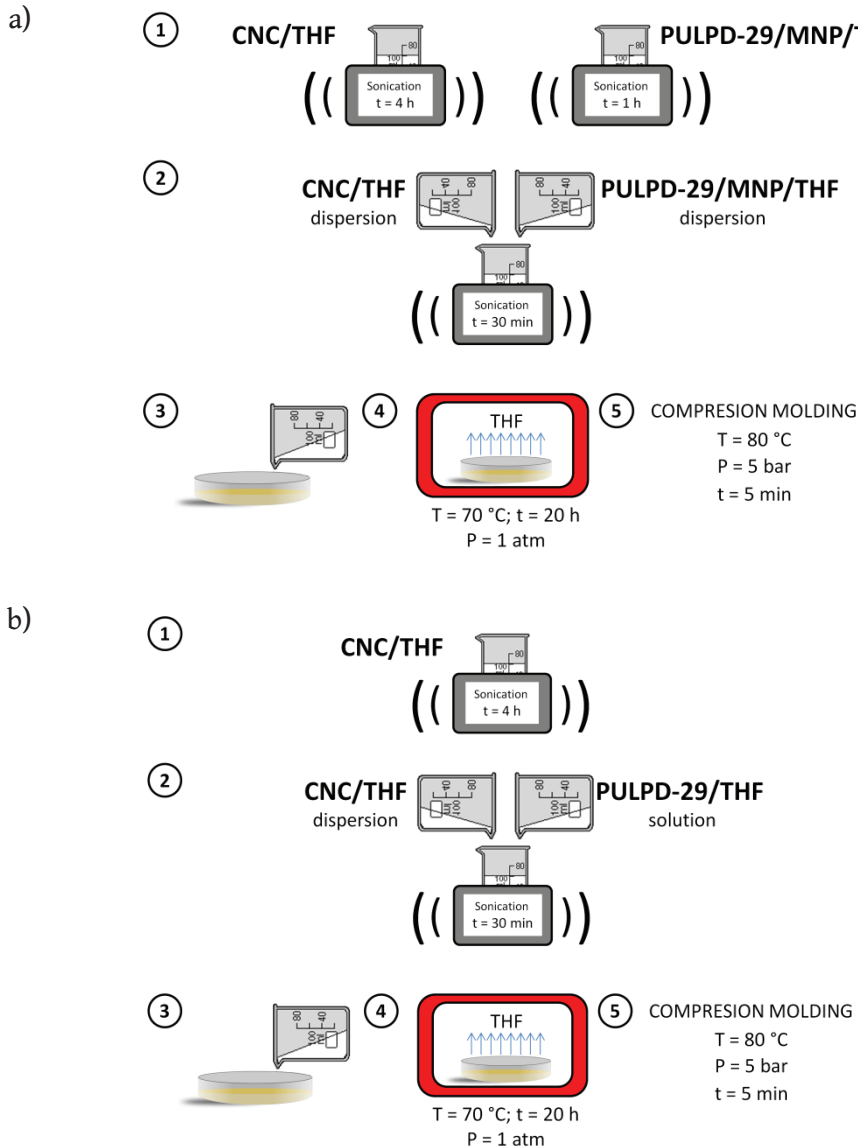
Figure 8.19. Followed process for the preparation of bionanocomposites with a) both CNCs and MNPs and b) CNCs.

Bionanocomposites based on biobased polyurethane with CNCs and MNPs were successfully obtained. The obtained bionanocomposites were designated as PU29P-xMNP-CNC, being x the amount of MNPs added (expressed as weight percentage, wt%). In Figure 8.20 the digital images of the prepared PU29P-CNC bionanocomposite and PU29P-MNP-CNC bionanocomposite series are shown.
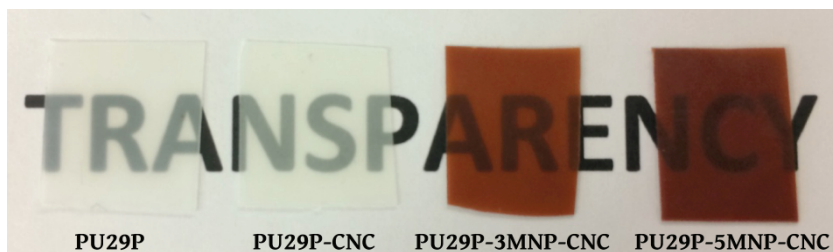
Figure 8.20. Digital images of PU29P biobased polyurethane, PU29P-CNC and PU29P-MNP-CNC bionanocomposite series.

In order to check if the prepared bionanocomposites with both nanoentities show a response to a magnetic field, the same procedure followed for the PU29P-MNP bionanocomposite series was used. In Figure 8.21 a sequence of digital images of the recorded video is shown. As it can be observed, the PU29P-5MNP-CNC show a response when the magnetic field was applied, thus these materials show magnetic properties.
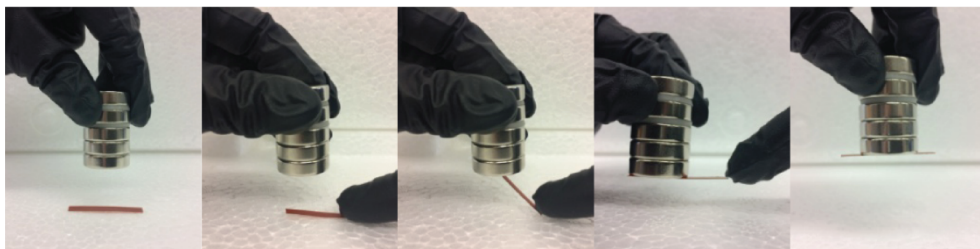
Figure 8.21. Sequence of digital images of the magnetic response of PU29P-5MNP-CNC.

8.4.2 Characterization of the bionanocomposites combining CNCs and MNPs

8.4.2.1 Differential scanning calorimetry

The thermal behavior of the obtained bionanocomposites combining CNCs and MNPs was analyzed by DSC in order to determine the effect of the addition of the nanoentities. The heating thermograms of the neat biobased polyurethane, bionanocomposite based on CNCs, together with magnetic bionanocomposites with both CNCs and MNPs are shown in Figure 8.22.
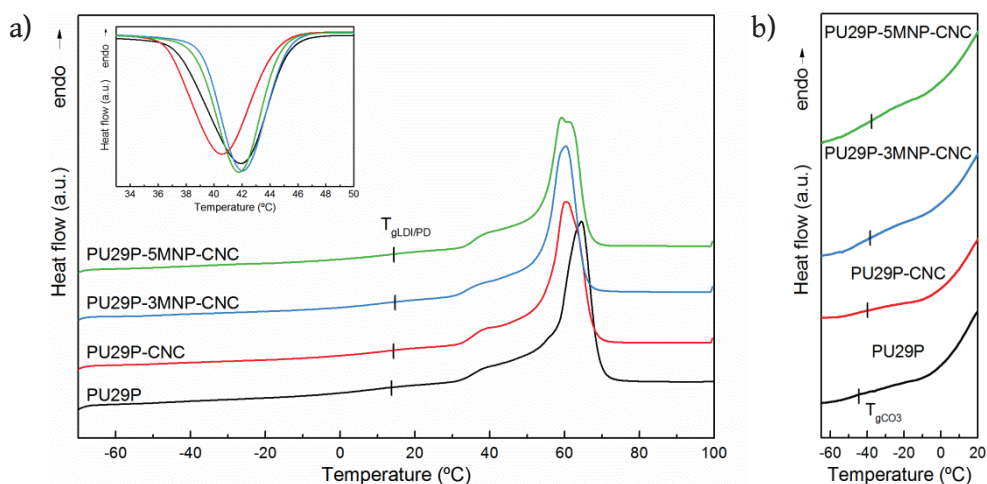
Figure 8.22. a) Heating DSC thermograms of PU29P biobased polyurethane and PU29P-CNC and PU29P-MNP-CNC bionanocomposite series and b) magnification of the thermograms at low temperatures. Inset: Cooling DSC thermograms.

Furthermore, in Table 8.13 the thermal transitions values and the relative crystallinity values (relative crystallinities to the neat biobased polyurethane) calculated by equation 8.1 are gathered.

Table 8.13. Thermal transitions values of PU29P biobased polyurethane and PU29P-CNC and PU29P-MNP-CNC bionanocomposite series.

Sample	T_{gCO3} (°C)	$T_{gLDI/PD}$ (°C)	T_m (°C)	ΔH_m (J g^{-1})	T_c (°C)	ΔH_c (J g^{-1})	χ_c heating	χ_c cooling
PU29P	-45.2	13.6	64.6	62.8	41.9	-58.8	1.00	1.00
PU29P-CNC	-40.4	14.1	60.3	58.2	40.5	-54.2	1.03	1.02
PU29P–3MNP-CNC	-38.9	14.5	60.3	51.3	42.0	-49.8	0.94	0.97
PU29P–5MNP-CNC	-37.6	14.5	59.3	52.4	41.8	-49.0	0.98	0.98

The PU29P-CNC and PU29P-MNP-CNC bionanocomposite series also show several transitions which are associated with CO3 and LDI/PD rich domains, denoting that the obtained bionanocomposites show a microphase separated microstructure. As can be observed, the addition of both nanoentities increases the T_g ascribed to CO3 rich domain, denoting that the mobility of CO3 rich

domain was restricted by the presence of the nanoentities. Similar behavior was observed for bionanocomposites with MNPs. Furthermore, the incorporation of CNCs shifts the T_g of LDI/PD rich domain to higher temperature if compared with the $T_{gLDI/PD}$ of pristine biobased polyurethane. The incorporation of nanoentities results in a lower mobility of the chains and hence in an increase of the $T_{gLDI/PD}$.[6,13] In addition, the bionanocomposites with the combination of CNCs and MNPs show a slightly higher $T_{gLDI/PD}$ if compared with the bionanocomposites with only CNCs, which can be attributed to a higher amount of nanoentities. In order to predict which of the nanoentities interact with each domain, the solubility parameters of cellulose was also estimated by Hoy method.[34] The theoretically calculated solubility parameters for CO3 and LDI/PD domains, oleic acid and cellulose are gathered in Table 8.14. As can be seen, solubility parameters suggest that CNCs would have a higher affinity with LDI/PD rich domain, while the magnetite coated with oleic acid would preferably interact with CO3 rich domain.

Table 8.14. Solubility parameters of CO3 and LDI/PD domains, oleic acid and cellulose.

Sample	δ $(J^{1/2} \, cm^{-3/2})$
CO3	20.07
LDI/PD	24.28
Oleic acid	18.53
Cellulose	31.91

Moreover, all materials show a broad endothermic peak related with the melting of crystalline CO3 rich domain. The bionanocomposites with only CNCs and also with both CNCs and MNPs, show a lower T_m suggesting that during crystallization process crystals with different chain arrangements were formed.[8] In addition, bionanocomposites with CNCs and both CNCs and MNPs show lower ΔH_m, denoting that the overall crystallinity decreases obtaining more amorphous materials. Regarding the relative crystallinity of the

bionanocomposites, the $\chi_{c\ heating}$ of PU29P-CNC is similar to PU29P, while for PU29P-MNP-CNC bionanocomposite series decreases, suggesting that the addition of MNPs decreases the ability of CO3 rich domain to crystallize. This behavior was also observed for PU29P-MNP bionanocomposites. Similar results were observed in the cooling scans, inset of Figure 8.21, where bionanocomposites shows a lower ΔH_c but $\chi_{c\ cooling}$ is similar to PU29P for PU29P-CNC bionanocomposite and lower for PU29P-MNP-CNC bionanocomposites.

The thermal behavior observed suggests that the incorporated nanoentities would interact with both domains, i.e. MNPs tend to interact with CO3 rich domain and CNCs with LDI/PD rich domain, since the addition of CNCs increases the $T_{gLDI/PD}$ and the incorporation of MNPs leads to the obtaining of bionanocomposites with lower T_m and ΔH_m.

8.4.2.2 Dynamic mechanical analysis

As previously observed in chapter 6 and also in PU29-CHNC and PU29P-MNP bionanocomposites, the dynamic mechanical behavior has a key role on shape-memory properties, since the E' in glassy and rubbery state could determine the thermo-responsive shape-memory behavior.[38] Therefore, the dynamic mechanical behavior of the bionanocomposites with CNCs and magnetic bionanocomposites with MNPs and CNCs was studied.

The temperature dependence of storage modulus and loss factor of the bionanocomposites is shown in Figure 8.23. As can be observed at low temperatures the bionanocomposites show a higher E' in the glassy state if compared with pristine biobased polyurethane. At higher temperatures, a decrease in E' happens, which is related with the transition from glassy to rubbery state. After that, the prepared materials reach the rubbery plateau. The bionanocomposites show higher E' in the rubbery state. Furthermore the bionanocomposites with both nanoentities show a higher E' if compared with

PU29P-CNC, which suggests that the addition of MNPs provides to the material a higher structural reinforcement, as previously observed in PU29P-MNP bionanocomposite series. The bionanocomposite with CNCs show a higher E' in rubbery state than PU29P, denoting that CNCs also act as effective nanoreinforcement agent, similarly to CHNCs. Finally, at temperatures around 60 °C the E' suffers a step decrease due to the melting of the crystals of CO3 rich domain.
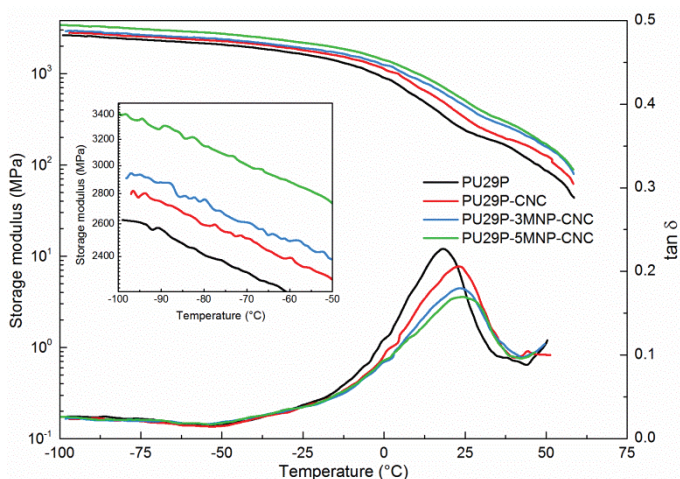
Figure 8.23. Storage modulus and loss factor of PU29P biobased polyurethane and PU29P-CNC and PU29P-MNP-CNC bionanocomposite series.

Furthermore, the tanδ curves of the bionanocomposites show a maximum, which is related with the mechanical relaxation (α) of the LDI/TMP rich domain (T_α).[31] The T_α of the prepared biobased polyurethane and bionanocomposites with CNCs and both CNCs and MNPs are gathered in Table 8.15.

As can be seen the addition of CNCs shifts the T_α to higher temperatures, similarly to observed for CHNCs, which restrings the mobility of the molecular chains and increases T_α.[6,13] However, bionanocomposites with both nanoentities show similar T_α to PU29P-CNC. The incorporation of MNPs seems not to affect to

T_α. This behavior is in accordance with the predicted by the solubility parameters, since MNPs seems to interact preferably with CO3 rich domains.

Table 8.15. α transition temperature of PU29P biobased polyurethane and PU29P-CNC and PU29P-MNP-CNC bionanocomposite series.

Sample	T_α (°C)
PU29P	18.9
PU29P-CNC	23.1
PU29P-3MNP-CNC	23.3
PU29P-5MNP-CNC	23.9

8.4.2.3 X-ray diffraction

The influence of the addition of CNCs and both CNCs and MNPs on the polymorphism of the sample was analyzed by XRD. In Figure 8.24 the XRD patterns of PU29P, PU29P-CNC and PU29P-3MNP-CNC, as well as XRD patterns of pure MNPs and CNCs, are shown.
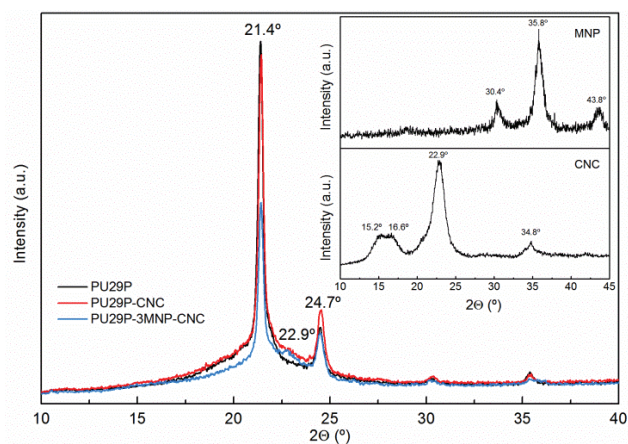
Figure 8.24. XRD patterns of the PU29P biobased polyurethane and PU29P-CNC and PU29P-3MNP-CNC bionanocomposite series. Insets: XRD patterns of MNPs and CNCs.

As can be seen, there is not a remarkably effect on the polymorphism of the sample when only CNCs were incorporated, in agreement with the behavior

observed by DSC. However, when both nanoentities were combined the intensity of the peak decreases, suggesting the presence of different chains arrangement and a lower ability to crystallize of the crystallizable CO3 rich domain, which is in agreement with the lower T_m and ΔH_m observed by DSC, and suggests that MNPs interact with CO3 rich domain. Similar behavior was also observed for PU29P-3MNP bionanocomposite. Furthermore, PU29P-3MNP-CNC show a peak at 22.9°, also observed in the XRD pattern of neat CNCs, which corroborates the presence of CNCs in the material. In this region PU29P-CNC shows a higher intensity if compared with PU29P, which also confirms the presence of CNCs.

8.4.2.4 Mechanical properties

The mechanical properties of the materials were studied by performing tensile tests. In Figure 8.25 the stress-strain curves of the PU29P biobased polyurethane and PU29P-CNC and PU29P-MNP-CNC bionanocomposite series are shown. Moreover, in Table 8.16 the characteristic mechanical properties derived from stress-strain curves are gathered.
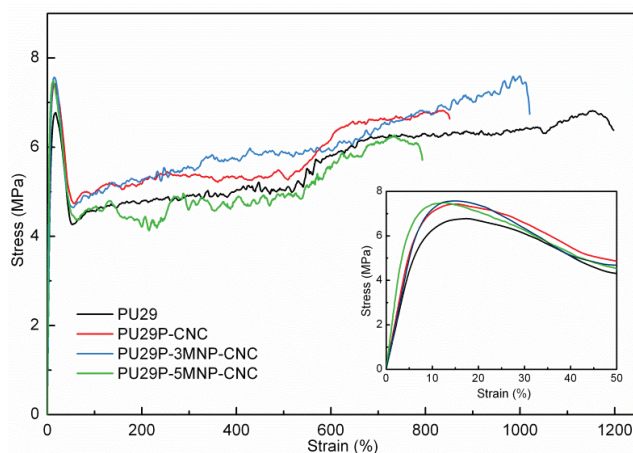
Figure 8.25. Stress-strain curves of PU29P biobased polyurethane and PU29P-CNC and PU29P-MNP-CNC bionanocomposite series.

The incorporation of CNCs results in materials with higher elastic modulus and stress at break. This behavior is in agreement with the results observed in literature where polyurethanes were reinforced with CNCs.[9,15,26,39,40] Regarding bionanocomposites containing both nanoentities, the improvement in mechanical properties could be attributed to the formation of a percolated network of CNCs[22] and also to the reinforcement effect of the MNPs.[41,42] This behavior was also observed separately in the previous analyzed bionanocomposites with CHCNs or MNPs, and also agrees with the results available in literature.[7,21–24]

Table 8.16. Mechanical properties of PU29P biobased polyurethane and PU29P-CNC and PU29P-MNP-CNC bionanocomposite series.

Sample	E (MPa)	σ_y (MPa)	σ_b (MPa)	ε_y (%)	ε_b (%)
PU29P	92.9 ± 7.6	6.9 ± 0.2	7.2 ± 0.4	16.9 ± 2.2	1149 ±153
PU29P-CNC	106.8 ± 2.9	7.4 ± 0.2	7.4 ± 0.1	14.7 ± 0.3	857 ± 11
PU29P-3MNP-CNC	106.4 ± 3.4	7.8 ± 0.2	7.8 ± 0.2	14.3 ± 2.3	1160 ± 83
PU29P-5MNP-CNC	165.8 ± 9.1	7.8 ± 0.3	7.8 ± 0.3	11.7 ± 2.2	779 ± 14

Moreover, the percolation threshold value of CNCs was theoretically estimated following equation 8.2. The obtained values were 3.33 vol% and 4.10 wt%, taking 1.1 and 1.5 g cm^{-3} for the density of the biobased polyurethane matrix[28] and crystalline cellulose,[26] respectively. The three-dimensional network would be formed for all prepared bionanocomposites with CNCs since CNC loading level was higher than the percolation threshold.

Regarding strain at break, PU29P-CNC bionanocomposites withstand higher values than those observed for PU29-CHNC series, which could be attributed to its lower crystallinity. PU29P-MNP-CNC bionanocomposites also show high strain at break values, suggesting that MNPs could be able to absorb strain energy upon deformation, acting as effective stress-bearing phase during deformation,[36,37] in addition to the lower crystallinity of the material. Similar

behavior was observed for PU29P-MNPs bionanocomposites. However, the increase of MNP content decreases strain at break, which might be due to the presence of aggregates at those CNCs and MNPs nanoentity contents.[35] In any case, the combination of CNCs with higher amount of MNPs, leads to the obtaining of a magnetic bionanocomposite with a high elastic modulus without compromise strain at break in a great extent.

8.4.2.5   Shape-memory properties

Since the matrix show thermally-activated shape-memory properties the influence of the addition of CNCs and a combination of CNCs and MNPs to it was analyzed. The conditions previously used for studying the effect of the nanoentities on shape-memory properties of PU29-CHNC and PU29P-MNP bionanocomposites were used. To sum up, five thermo-mechanical cyclic tests were carried out, using 40 °C as T_s and applying a ε_m of 50%.

The R_f and R_r values of the preformed thermo-mechanical cycles of the biobased polyurethane as well as bionanocomposites with CNCs and both CNCs and MNPs are gathered in Table 8.17 and the stress-strain curves of the performed thermo-mechanical cycles are presented in Figure 8.26.

Table 8.17. R_f and R_r values calculated for each thermo-mechanical cycle of PU29P biobased polyurethane and PU29P-CNC and PU29P-MNP-CNC bionanocomposite series.

Cycle	PU29P		PU29P-CNC		PU29P-3MNP-CNC		PU29P-5MNP-CNC	
	R_f (%)	R_r (%)	R_f (%)	R_r (%)	R_f (%)	R_r (%)	R_f (%)	R_r (%)
1	91.6	87.3	96.5	86.2	98.3	86.1	97.0	85.5
2	93.4	99.3	98.7	96.7	98.5	93.8	99.1	97.5
3	94.8	99.5	98.7	97.7	98.8	97.9	99.1	98.7
4	96.4	99.5	98.7	99.4	98.8	99.6	99.2	98.9
5	99.4	100.0	98.9	100.0	99.1	99.1	99.6	100.0
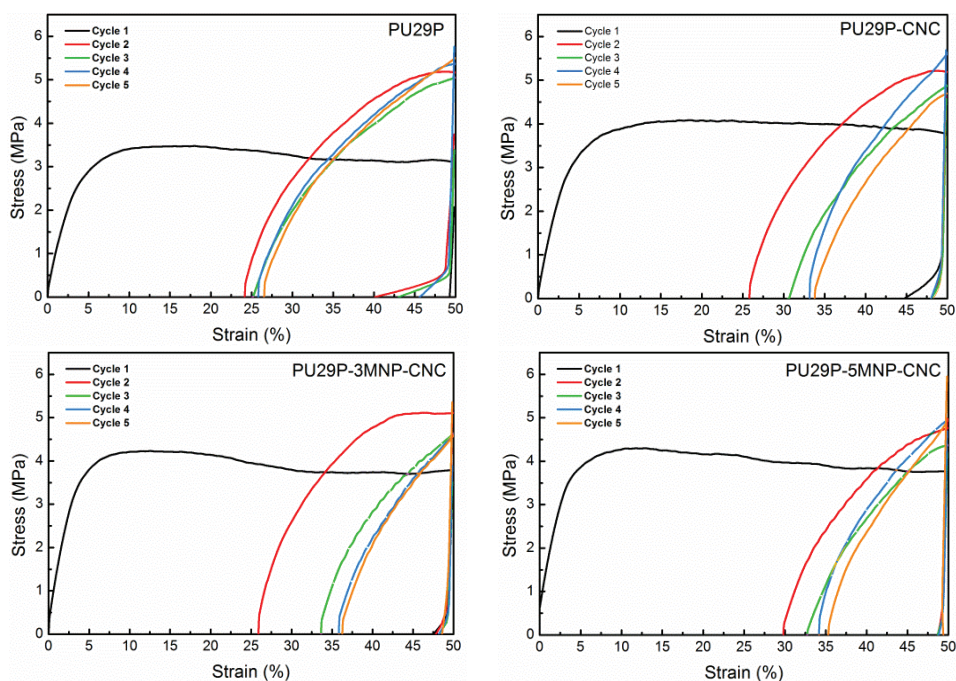
Figure 8.26. Stress-strain curves of thermo-mechanical cycles of PU29P biobased polyurethane and PU29P-CNC and PU29P-MNP-CNC bionanocomposite series.

In addition, glass transition temperature, melting enthalpy, storage moduli at glassy and rubbery state, strain at yield point, percentage of overlapped area during deformation process as well as R_f and R_r of the first cycle are gathered in Table 8.18, in order to a deeper understanding of the shape-memory properties.

Table 8.18. Thermal transition temperature, melting enthalpy, shape-memory properties, storage moduli in glassy and rubbery state, strain at yield point, percentage of the overlapped area of PU29P biobased polyurethane and PU29P-CNC and PU29P-MNP-CNC bionanocomposite series.

Sample	$T_{gLDI/PD}$ °C	ΔH_m (J g^{-1})	R_f (%)	E_g MPa	R_r (%)	E_r MPa	ε_y (%)	$A_{overlapped}$ (%)
PU29P	13.6	62.8	91.6	2546	87.3	143	16.9	4.33
PU29P-CNC	14.1	58.2	96.5	2730	86.2	184	14.7	4.16
PU29P-3MNP-CNC	14.5	51.3	98.3	2877	86.1	241	14.3	5.40
PU29P-5MNP-CNC	14.5	52.4	97.0	3286	85.5	261	11.7	4.36

As it can be observed the R_f and R_r values range from 92 to 98% and from 85 to 87%, respectively. The addition of the nanoentities increases the fixation of the matrix, since all of them show a higher R_f values. As already has been mentioned, those polymers which presents a high E' in the glassy state in general will show a better shape fixity.[38] Therefore, since bionanocomposites show a higher E' in the glassy state shape fixity also increases. The bionanocomposites with both MNPs and CNCs show higher R_f if compared with PU29P-MNP bionanocomposites. Furthermore, according to DSC results, the addition of CNCs and MNPs influence over the overall crystallization of CO3 rich domains, resulting more amorphous bionanocomposites. In this way, since chains are less restricted, due to the lower crystallinity of the material, the material is less hindered to adopt the lowest entropy state and thus shape fixation increases in the bionanocomposites.[43,44]

Regarding shape recovery, it can be seen that the bionanocomposites present similar R_r values, however they show a slight decreasing tendency. This fact could be attributed to the lower crystallinity of the material. As it was previously observed in chapter 6, the original shape could be restored through crystalline structures.[29] Furthermore, since all samples were stretched up above their yield point, plastic deformation occurs and hence the bionanocomposites could not restored their original shape in a 100%. However, after five cycles almost all samples could completely restore their shape. If compared with PU29P-MNP bionanocomposite slightly lower R_r values were obtained due to the lower overall crystallinity.

As previously observed, since deformation temperature overlaps the onset of the melting enthalpy of the CO3 rich domain, TME effect takes place. The evolution of overlapped area is shown in Figure 8.27.

As in can be seen the percentage of the overlapped area was 4.33, 4.16, 5.40 and 4.36% for PU29P, PU29P-CNC, PU29P-3MNP-CNC and PU29P-5MNP-CNC,

respectively. Except for PU29P-3MNP-CNC the percentage of the overlapped area is similar for all bionanocomposites denoting that contribution to the rubbery state would be alike for the bionanocomposites. Moreover, the higher overlapped area for PU29P-3MNP-CNC denotes that higher amount of CO3 crystals were melted and hence its contribution to the rubbery state would be higher and therefore R_f is higher for this magnetic bionanocomposite.
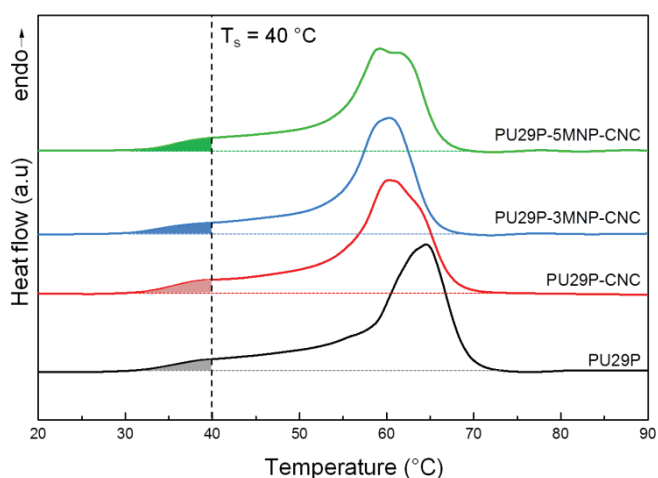
Figure 8.27. Overlapped area in PU29P biobased polyurethane and PU29P-CNC and PU29P-MNP-CNC bionanocomposite series.

8.5 Conclusions

Different thermo-responsive bionanocomposites were prepared and characterized by using the previously synthesized PULPD-29 as matrix and different nanoentities such as chitin and cellulose nanocrystals and magnetite. The effect of varying the content and the nature of the nanoentities on shape-memory properties was analyzed.

In the case of bionanocomposites with CHNC, PU29-CHNC, it was observed that the CHNCs interacted with LDI/PD rich domain and acting as a nucleating agent over CO3 rich domain and thus the crystallinity increased. Moreover due to the formation of a percolated network of CHNCs and crystalline CO3 rich domain

crystals elastic modulus was enhanced. Therefore, bionanocomposites showed low strain at break values at high CHNC contents. The analysis of shape-memory properties revealed that the increase of crystallinity with the addition of CHCNs leaded to a higher shape recovery.

Magnetic bionanocomposites were also prepared by adding MNPs to the matrix. The incorporation of MNPs within the matrix decreases the overall crystallinity leading to more amorphous materials. The increase of T_{gCO3} and the lower χ_c values suggested that MNPs interacted with CO3 rich domain. Furthermore, it was seen that MNPs reinforced the materials, since elastic modulus and stress at break increased as MNP content increased. Regarding shape-memory properties the addition of MNP increased the shape fixation due to the higher E' showed in the glassy state, while shape recovery is similar although their lower crystallinity, suggesting that MNPs were able to absorb strain energy upon deformation contributing to shape recovery. If compared with the shape-memory of PU29-CHNC bionanocomposites, PU29P-MNP bionanocomposites showed higher strain at yield values, thus fewer crystals were broken during stretching process resulting in higher shape recovery values. Furthermore, temperature memory effect took place since the deformation temperature overlapped the onset of the melting temperature. However, it was similar for all bionanocomposites, denoting that the contribution to the rubbery state would be alike.

MNPs tend to interact with CO3 rich domain and CNCs with LDI/PD rich domain, since the addition of CNCs increases the $T_{gLDI/PD}$ and the incorporation of MNPs leads to the obtaining of bionanocomposites with lower T_m and ΔH_m.

Finally, magnetic bionanocomposites combining CNCs and MNPs were prepared. The addition of CNCs increased $T_{gLDI/PD}$ of the bionanocomposites and did not decrease the ability to crystallize of CO3 rich domain, meaning that CNCs interacted with LDI/PD rich domain. Moreover, with the addition of both

nanoentities lower χ_c values were obtained, denoting MNPs interacted with CO3 rich domain hindering the crystallization of CO3 rich domain. The analysis of mechanical properties revealed that stif materials were obtained. Moreover, the combination of CNCs with higher amount of MNPs, leaded to the obtaining of a magnetic bionanocomposite with a high elastic modulus without compromise strain at break in a great extent. According to shape-memory properties, materials with a higher shape fixation and lower shape recovery were obtained due to the lower crystallinity of the material if compared with PU29P-MNP bionanocomposites. This bionanocomposites also showed temperature memory effect and similarly to PU29P-MNP bionanocomposites the percentage of overlapped area was similar, so the contribution to the rubbery state was alike.

Taking into account the overall results of the different obtained bionanocomposites, it was observed that final properties influenced by preparation process. A fast crystallization, leaded to less crystalline materials and that affected on shape-memory properties. Furthermore it was seen that shape-memory properties were determined by the dynamic mechanical behavior of the material and also by the nature of the nanoentities. On the one hand, CHNCs showed a nucleating effect and hence contributed to a higher shape recovery. On the other hand, MNPs absorbed strain energy upon deformation contributing to shape recovery and in this way made up for the lower crystallinity. Finally, CNCs increased $T_{gLDI/PD}$ which contributed to a higher shape fixation of the bionanocomposites.

8.6   References

1.   J.D. Goodrich, W.T. Winter. "α-Chitin nanocrystals prepared from shrimp shells and their specific surface area measurement". Biomacromolecules 2007. 8: 252–257.

2.   K.M. Zia, M. Barikani, M. Zuber, I.A. Bhatti, M.A. Sheikh. "Molecular

engineering of chitin based polyurethane elastomers". Carbohydr. Polym. 2008. 74: 149–158.

3.   A.M. Salaberria, J. Labidi, S.C.M. Fernandes. "Chitin nanocrystals and nanofibers as nano-sized fillers into thermoplastic starch-based biocomposites processed by melt-mixing". Chem. Eng. J. 2014. 256: 356–364.

4.   N. Butchosa, C. Brown, P.T. Larsson, L.A. Berglund, V. Bulone, Q. Zhou. "Nanocomposites of bacterial cellulose nanofibers and chitin nanocrystals: fabrication, characterization and bactericidal activity". Green Chem. 2013. 15: 3404–3413.

5.   B. Wunderlinch. Thermal analysis of polymeric materials. Springer, Berlin, 2005.

6.   X. Yan, Q. He, X. Zhang, H. Gu, H. Chen, Q. Wang, L. Sun, S. Wei, Z. Guo. "Magnetic polystyrene nanocomposites reinforced with magnetite nanoparticles". Macromol. Mater. Eng. 2014. 299: 485–494.

7.   A. Saralegi, S.C.M. Fernandes, A. Alonso-Varona, T. Palomares, E.J. Foster, C. Weder, M.A. Corcuera, A. Eceiza. "Shape-memory bionanocomposites based on chitin nanocrystals and thermoplastic polyurethane with a highly crystalline soft segment". Biomacromolecules 2013. 14: 4475–4482.

8.   L. Rueda-Larraz, B. Fernández-d'Arlas, A. Tercjak, A. Ribes, I. Mondragon, A. Eceiza. "Synthesis and microstructure-mechanical property relationships of segmented polyurethanes based on a PCL-PTHF-PCL block copolymer as soft segment". Eur. Polym. J. 2009. 45: 2096–2109.

9.   A. Santamaria-Echart, L. Ugarte, C. García-Astrain, A. Arbelaiz, M.A. Corcuera, A. Eceiza. "Cellulose nanocrystals reinforced environmentally-friendly waterborne polyurethane nanocomposites". Carbohydr. Polym.

2016. 151: 1203–1209.

10.   L. Rueda, A. Saralegi, B. Fernández-d'Arlas, Q. Zhou, A. Alonso-Varona, L.A. Berglund, I. Mondragon, M.A. Corcuera, A. Eceiza. "In situ polymerization and characterization of elastomeric polyurethane-cellulose nanocrystal nanocomposites. Cell response evaluation". Cellulose 2013. 20: 1819–1828.

11.   G.R. Saad, H.E. Salama, N.A. Mohamed, M.W. Sabaa. "Crystallization and thermal properties of biodegradable polyurethanes based on poly[(R)-3-hydroxybutyrate] and their composites with chitin whiskers". J. Appl. Polym. Sci. 2014. 131: 9395–9407.

12.   A. Pei, Q. Zhou, L.A. Berglund. "Functionalized cellulose nanocrystals as biobased nucleation agents in poly (L -lactide) (PLLA) – crystallization and mechanical property effects". Compos. Sci. Technol. 2010. 70: 815–821.

13.   M. Zeng, H. Gao, Y. Wu, L. Fan, A. Li. "Preparation and characterization of nanocomposite films from chitin whisker and waterborne poly(ester-urethane) with or without ultra-sonification treatment". J. Macromol. Sci. Part A. 2010. 47: 867–876.

14.   A. Saralegi, L. Rueda, B. Fernández-d'Arlas, I. Mondragon, A. Eceiza, M.A. Corcuera. "Thermoplastic polyurethanes from renewable resources: effect of soft segment chemical structure and molecular weight on morphology and final properties". Polym. Int. 2013. 62: 106–115.

15.   M. Auad, V.S. Contos, S. Nutt, M.I. Aranguren, N.E. Marcovich. "Characterization of nanocellulose reinforced shape memory polyurethanes". Polym. Int. 2008. 57: 651–659.

16.   U.M. Casado, R.M. Quintanilla, M.I. Aranguren, N.E. Marcovich.

"Composite films based on shape memory polyurethanes and nanostructured polyaniline or cellulose–polyaniline particles". Synth. Met. 2012. 162: 1654–1664.

17.   S. Thakur, N. Karak. "Castor oil-based hyperbranched polyurethanes as advanced surface coating materials". Prog. Org. Coatings. 2012. 76: 157–164.

18.   S. Ifuku, M. Nogi, K. Abe, M. Yoshioka, M. Morimoto, H. Saimoto, H. Yano. "Preparation of chitin nanofibers with a uniform width as α-chitin from crab shells". Biomacromolecules 2009. 10: 1584–1588.

19.   S. Liu, J. Sun, L. Yu, C. Zhang, J. Bi, F. Zhu, M. Qu, C. Jiang, Q. Yang. "Extraction and characterization of chitin from the beetle *Holotrichia parallela* Motschulsky". Molecules 2012. 17: 4604–4611.

20.   R. Minke, J. Blackwell. "The structure of α-chitin". J. Mol. Biol. 1978. 120: 167–181.

21.   S. Ifuku, A. Ikuta, T. Hosomi, S. Kanaya, Z. Shervani, M. Morimoto, H. Saimoto. "Preparation of polysilsesquioxane-urethaneacrylate copolymer film reinforced with chitin nanofibers". Carbohydr. Polym. 2012. 89: 865–869.

22.   N. Lin, S. Wei, T. Xia, F. Hu, J. Huang, A. Dufresne. "Green bionanocomposites from high-elasticity 'soft' polyurethane and high-crystallinity 'rigid' chitin nanocrystals with controlled surface acetylation". RSC Adv. 2014. 4: 49098–49107.

23.   A. Morin, A. Dufresne. "Nanocomposites of chitin whiskers from Riftia tubes and poly(caprolactone)". Macromolecules 2002. 35: 2190–2199.

24.   M. Paillet, A. Dufresne. "Chitin whisker reinforced thermoplastic

nanocomposites". Macromolecules 2001. 34: 6527–6530.

25.   J. Huang, J.W. Zou, P.R. Chang, J.H. Yu, A. Dufresne. "New waterborne polyurethane-based nanocomposites reinforced with low loading levels of chitin whisker". eXPRESS Polym. Lett. 2011. 5: 362–373.

26.   X. Cao, C. Xu, Y. Wang, Y. Liu, Y. Liu, Y. Chen. "New nanocomposite materials reinforced with cellulose nanocrystals in nitrile rubber". Polym. Test. 2007. 8: 889–904.

27.   Z. Gao, J. Peng, T. Zhong, J. Sun, X. Wang, C. Yue. "Biocompatible elastomer of waterborne polyurethane based on castor oil and polyethylene glycol with cellulose nanocrystals". Carbohydr. Polym. 2012. 87: 2068–2075.

28.   B. Fernández-d'Arlas, U. Khan, L. Rueda, L. Martin, J.A. Ramos, J.N. Coleman, M.L. Gonzalez, A. Valea, I. Mondragon, M.A. Corcuera, A. Eceiza. "Study of the mechanical, electrical and morphological properties of PU/MWCNT composites obtained by two different processing routes". Compos. Sci. Technol. 2012. 72: 235–242.

29.   H.M. Jeong, J.H. Song, K.W. Chi, I. Kim, K.T. Kim. "Shape memory effect of poly(methylene-1,3-cyclopentane) and its copolymer with polyethylene". Polym. Int. 2002. 51: 275–280.

30.   Z.S. Petrovic, I. Javni. "Effect of soft-segment length and concentration on phase separation in segmented polyurethanes". J. Polym. Sci. Part B Polym. Phys. 1989. 27: 545–560.

31.   E. Cognet-Georjon, F. Mechin, J.P. Pascault. "New polyurethanes based on 4,4'-diphenylmethane diisocyanate and 1,4:3,6 dianhydrosorbitol. 2. Synthesis and properties of segmented polyurethane elastomers". Macromol. Chem. Phys. 1996. 197: 3593–3612.

32. A. Saralegi, E. Johan Foster, C. Weder, A. Eceiza, M.A. Corcuera. "Thermoplastic shape-memory polyurethanes based on natural oils". Smart Mater. Struct. 2014. 23: 025033 (9pp).

33. M. Shahrousvand, M.S. Hoseinian, M. Ghollasi, A. Karbalaeimahdi, A. Salimi, F.A. Tabar. "Flexible magnetic polyurethane/Fe_2O_3 nanoparticles as organic-inorganic nanocomposites for biomedical applications: properties and cell behavior". Mater. Sci. Eng. C., 2016. 74: 556–567.

34. D.W. van Krevelen. "Properties of polymers". Elsevier Scientific Publising Co., Amsterdam, 1990. Pp. 189-225.

35. H. Zou, C. Weder, Y.C. Simon. "Shape-memory polyurethane nanocomposites with single layer or bilayer oleic acid-coated Fe_3O_4 nanoparticles". Macromol. Mater. Eng. 2015. 300: 885–892.

36. L. Hojabri, X. Kong, S.S. Narine. "Functional thermoplastics from linear diols and diisocyanates produced entirely from renewable lipid sources". Biomacromolecules 2010. 11: 911–918.

37. M. Charlon, B. Heinrich, Y. Matter, E. Couzigné, B. Donnio, L. Avérous. "Synthesis, structure and properties of fully biobased thermoplastic polyurethanes, obtained from a diisocyanate based on modified dimer fatty acids, and different renewable diols". Eur. Polym. J. 2014. 61: 197–205.

38. D. Ratna, J. Karger-Kocsis. "Recent advances in shape memory polymers and composites: a review". J. Mater. Sci. 2008. 43: 254–269.

39. X. Kong, L. Zhao, J.M. Curtis. "Polyurethane nanocomposites incorporating biobased polyols and reinforced with a low fraction of cellulose nanocrystals". Carbohydr. Polym. 2016. 152: 487–495.

40. J. Sethi, M. Illikainen, M. Sain, K. Oksman. "Polylactic acid/polyurethane blend reinforced with cellulose nanocrystals with semi-interpenetrating polymer network (S-IPN) structure". Eur. Polym. J. 2017. 86: 188–199.

41. W. Guo, H. Kang, Y. Chen, B. Guo, L. Zhang. "Stronger and faster degradable biobased poly(propylene sebacate) as shape memory polymer by incorporating boehmite nanoplatelets". ACS Appl. Mater. Interfaces. 2012. 4: 4006–4014.

42. C. Meiorin, O.M. Londoño, D. Muraca, L.M. Socolovsky, K.R. Pirota, M.I. Aranguren, M. Knobel, M.A. Mosiewicki. "Magnetism and structure of nanocomposites made from magnetite and vegetable oil based polymeric matrices". Mater. Chem. Phys. 2015. 175: 81–91.

43. J.L. Hu, F.L. Ji, Y.W. Wong. "Dependency of the shape memory properties of a polyurethane upon thermomechanical cyclic conditions". Polym. Int. 2005. 54: 600–605.

44. T. Xie. "Recent advances in polymer shape memory". Polymer 2011. 52: 4985–5000.
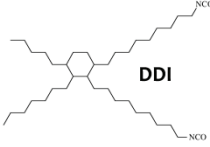
CHAPTER 9
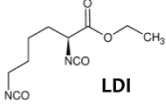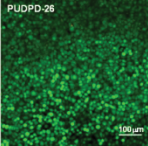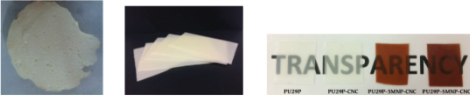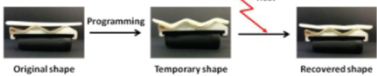
GENERAL CONCLUSIONS, FUTURE WORK AND PUBLICATIONS

9. GENERAL CONCLUSIONS, FUTURE WORK AND PUBLICATIONS

In this chapter the general conclusions drawn from this work are presented. Moreover, the future works suggested to continue with the development of this research line are also gathered. Finally, a list of the publications and conference participations derived from this work is presented.

9.1   General conclusions

In this work polyurethane rigid foams, crosslinked and thermoplastic polyurethanes and bionanocomposites with high biobased carbon content have been synthesized. To this end, different reactants and nanoentities derived from renewable sources have been used. The renewability of polyurethane rigid foams has been increased by incorporating a polyol derived from hydroxylated linseed oil as well as glycerol as hydroxyl-containing reactive modifier and by using water as blowing agent. The renewability of crosslinked and thermoplastic polyurethanes has been enhanced by using a macrodiol derived from castor oil and two different diisocyanates, one based on L-lysine amino acid (LDI) and the other on fatty acids (DDI). Besides, in the case of the thermoplastic polyurethanes two chain extenders have been also employed, one is derived from corn sugar (PD), while the other is based on polysaccharides (DAS). Furthermore, bionanocomposites were prepared adding chitin and cellulose nanocrystals to one of the synthesized thermoplastic biobased polyurethane, specifically the one that has shown interesting properties for shape-memory applications.

Regarding rigid polyurethane foams, the final properties are directly affected by the nature and content of hydroxyl-containing modifiers. The use of glycerol as reactive modifier increases the glass transition temperature, storage modulus, crosslink density and thermal stability. In the same way, the foam density and

concentration of polymeric isocyanate influences on the compression properties of the rigid foam.

As far as crosslinked biobased polyurethanes is concerning the use of biobased diisocyanates with side chains or branched structure results in amorphous urethane-based domains with low glass transition temperature. The affinity of DDI with macrodiol leads to a lower microphase separation degree than in the case of LDI. In addition, the high molecular weight of DDI results in a lower crosslink density. Furthermore, the increase of diisocyanate/crosslinker content in both PULTMP and PUDTMP biobased polyurethane series decreases the overall crystallization of the material. Therefore, mechanical properties are modulated on the one hand by the overall crystallinity and in the other hand by crosslink density, since the semicrystalline rich domain and net points act as reinforcing element.

Regarding the properties of thermoplastic biobased polyurethanes, they are influenced by the nature of the diisocyanate and chain extender. Similarly to crosslinked biobased polyurethanes the use of aliphatic and nonsymmetrical diisocyanates, with side chains or branched, results in the formation of urethane-based domains with low glass transition temperature. The LDI urethane-based domains are not able to crystallize, whereas the one based on DDI does. Due to its chemical structure LDI leads to a higher microphase separation, while polyurethanes with DDI show a higher microphase mixing degree. The overall crystallinity also decreases as diisocyanate/chain extender content increases. DDI/DAS domain shows a higher glass transition temperature and lower crystallinity than DDI/PD domain, due to the higher steric hindrance of DAS. The low glass transition temperature observed for the domain formed by the diisocyanate/chain extender together with the high melting temperature of the macrodiol rich domain, leads to the inversion of the behavior of the segments. In this way the macrodiol acts as hard phase, differing with the

behavior of polyurethanes based on conventional diisocyanates. Moreover, the mechanical properties are governed to the overall crystallinity.

Crosslinked and thermoplastic polyurethanes with high biocompatibility have been synthesized, denoting that these materials can be good candidates for its use in biomedical applications. Biocompatibility is closely related with the nature of the diisocyanate employed, since DDI promotes in a higher extent the proliferation of the cells.

Therefore, crosslinked and thermoplastic polyurethanes with tailored properties can be synthesized by controlling the nature of the reactants, as well as the diisocyanate/chain extender or crosslinker content.

In addition, crosslinked and thermoplastic polyurethanes based on LDI show shape-memory properties, which are strongly dependent to the chosen switching temperature and also to the maximum elongation applied during the shape-memory process. Shape fixity is governed by the elastic modulus in the glassy state, a high modulus results in higher fixity ratios. While the driving force for shape recovery is the residual stress introduced during stretching process which is stored by crystalline domains in thermoplastic polyurethanes or by crystalline domains and net points in crosslinked polyurethanes. In addition, net points are more effective for storing the residual stress. Moreover, temperature memory effect takes place since the deformation temperature overlaps the onset of the melting enthalpy which contributes to the rubbery state increasing the fixation of the material.

Bionanocomposites with shape memory properties have been obtained from the addition of chitin nanocrystals (CHNCs), cellulose nanocrystals (CNCs), magnetite (MNPs) and a combination of CNCs and MNPs to a thermoplastic biobased polyurethane. In bionanocomposites with CHNCs, the nanoentities interact with LDI/PD rich domain having a nucleating effect over the macrodiol

rich domain. Therefore, bionanocomposites with enhanced elastic modulus have been obtained. Furthermore, MNPs interact with macrodiol rich domain decreasing the ability to crystallize of the macrodiol rich domain. CNCs also interact with LDI/PD rich domain and when both MNPs and CNCs are combined MNPs interact with CO3 rich domain, while CNCs with LDI/PS rich domain. The addition of both nanoentities separately, as well as in combination, decrease the overall crystallinity and increase elastic modulus and stress at break, obtaining stiffer materials.

Shape-memory properties of the bionanocomposites are strongly related with dynamic mechanical behavior, crystallinity, the nature of the nanoentity and the preparation process. Since CHNCs show a nucleating effect they contribute to a higher shape recovery. Moreover, MNPs absorb strain energy upon deformation contributing also to shape recovery and in this way make up for the lower overall crystallinity. Finally, the addition of CNCs increased the glass transition of LDI/PD rich domain, which contributes to a higher shape fixation of the bionanocomposites. Therefore, bionanocomposites with only CNCs and also with the combination of both CNCs and MNPs show a higher fixation.

9.2   Future work

With the purpose of giving continuity to the work here performed, different research lines are suggested:

- Taking into account the potential showed for the synthesized solid polyurethanes for biomedical applications it would be interesting to study the behavior of these materials in contact with blood by performing hemocompatibility assays. Similarly, it would be also worthy to analyze the biocompatibility and hemocompatibility of the synthesized bionanocomposites.

- In this work different magnetic bionanocomposites have been prepared

by the addition of magnetite nanoparticles. Therefore, it would be interesting to analyze the potential over magnetic properties of the synthesized nanoparticles. In addition, since shape-memory could be also triggered by applying an alternative magnetic field, it is suggested to analyze the magneto-responsive shape-memory properties of the prepared bionanocomposites containing magnetite nanoparticles and analyze the effect of the presence of cellulose nanocrystals, as well as the different magnetite nanoparticles content on the magneto-responsive shape-memory properties.

9.3   Publications and conferences

9.3.1   List of publications

Authors: Tamara Calvo-Correas, M. Dolores Martin, Nagore Gabilondo, Aloña Retegi, M. Ángeles Corcuera, Arantxa Eceiza.

Title: Synthesis and characterization of polyurethanes with high renewable carbon content and tailored properties.

Journal: ACS Sustainable Chemistry & Engineering

Year: 2016

Impact factor: 5.267 (JCR 2015)

Rank: 4/29 (Green & Sustanaible Chemistry & Technology) (JCR 2015)

Authors: Tamara Calvo-Correas, Nagore Gabilondo, Ana Alonso-Varona, Teodoro Palomares, M. Ángeles Corcuera, Arantxa Eceiza.

Title: Shape-memory properties of crosslinked biobased polyurethanes.

Journal: European Polymer Journal

Year: 2016

Impact factor: 3.485 (JCR 2015)

Rank: 13/85 (Polymer Science) (JCR 2015)

Authors: Tamara Calvo-Correas, Arantzazu Santamaria-Echart, Ainara Saralegi, Loli Martin, Ángel Valea, M. Ángeles Corcuera, Arantxa Eceiza

Title: Thermally-responsive biopolyurethanes from a biobased diisocyanate

Journal: European Polymer Journal

Year: 2015

Impact factor: 3.485 (JCR 2015)

Rank: 13/85 (Polymer Science) (JCR 2015)

Authors: Tamara Calvo-Correas, Mirna A. Mosiewicki, M. Ángeles Corcuera, Arantxa Eceiza, Mirta I. Aranguren

Title: Linseed oil-based polyurethane rigid foams. Synthesis and characterization.

Journal: Journal of Renewable Materials

Year: 2015

Impact factor: 1.263 (JCR 2015)

Rank: 24/29 (Green & Sustanaible Chemistry & Technology) (JCR 2015)
       10/25 (Material Science, Composites) (JCR 2015)
       52/85 (Polymer Science) (JCR 2015)

9.3.2 List of conferences

Authors: T. Calvo-Correas, L. Ugarte, S. Gómez-Fernández, M.A. Corcuera, A. Eceiza.

Title: Shape-memory bionanocomposites based on chitin and fully biobased polyurethanes.

Conference: The 3rd International Conference on Bioinspired and Biobased Chemistry & Materials.

Contribution: Poster

Year: 2016

Place: Nice, France

Authors: T. Calvo-Correas, N. Gabilondo, X. Molina, M.A. Corcuera, A. Eceiza.

Title: Iturri berriztagarrietatik eratorritako poliuretano gurutzatuen forma-oroimen propietateen azterketa.

Conference: Materialen Zientzia eta Teknologia III. Kongresua.

Contribution: Poster

Year: 2016

Place: Markina-Xemein, Spain

Authors: T. Calvo-Correas, A. Saralegi, A. Arbelaiz, M.A. Corcuera, A. Eceiza.

Title: Biopolyurethanes as thermally-activated shape memory polymers.

Conference: II Workshop on Bio-degradable Polymers and Biocomposites. III Workshop BIOPURFIL, Bio-based Polyurethane Composites with Natural Fillers.

Contribution: Keynote

Year: 2015

Place: Buenos Aires, Argentina

Authors: T. Calvo-Correas, A. Santamaria-Echart, N. Gabilondo, M.A. Corcuera, A. Eceiza.

Title: Effect of the chain extender structure on bio-based polyurethane properties.

Conference: 5th International Conference on Biodegradable and Biobased Polymers. BIOPOL 2015.

Contribution: Poster

Year: 2015

Place: Donostia-San Sebastian, Spain

Authors: T. Calvo-Correas, S. Gómez-Fernández, L. Ugarte, M.A. Corcuera, A. Eceiza.

Title: Novel biobased thermally-responsive biopolyurethanes.

Conference: 6th Workshop Green Chemistry and Nanotechnogies in Polymer Chemistry.

Contribution: Oral

Year: 2015

Place: Bragança, Portugal

Authors: T. Calvo-Correas, B. Fernández d'Arlas, L. Martin, M.A. Corcuera, A. Eceiza.

Title: Thermo-responsive biopolyurethanes.

Conference: 5th Workshop Green Chemistry and Nanotechnogies in Polymer Chemistry, ECLIPSE Workshop, BIOPURFIL Workshop.

Contribution: Poster

Year: 2014

Place: Donostia – San Sebastian, Spain

Authors: T. Calvo-Correas, M.I. Aranguren, M.A. Corcuera, A. Eceiza, M.A. Moseiwicki.

Title: Linseed oil-based polyurethane foams: manufacture and characterization.

Conference: 5th Workshop Green Chemistry and Nanotechnogies in Polymer Chemistry, ECLIPSE Workshop, BIOPURFIL Workshop.

Contribution: Poster

Year: 2014

Place: Donostia – San Sebastian, Spain

Authors: T. Calvo-Correas, A. Saralegi, B. Fernández d'Arlas, M.A. Corcuera, A. Eceiza.

Title: Poliuretano termoerantzuleen sintesia eta karakterizazioa.

Conference: Materialen Zientzia eta Teknologia II. Kongresua.

Contribution: Poster

Year: 2014

Place: Donostia – San Sebastian, Spain

Authors: T. Calvo-Correas, A. Retegi, A. Santamaría-Echart, M.A. Corcuera, A. Eceiza.

Title: Shape-memory behaviour of polyurethanes derived from renewable resources.

Conference: 4th Workshop Green Chemistry and Nanotechnogies in Polymer Chemistry, ECLIPSE Workshop, BIOPURFIL Workshop.

Contribution: Poster

Year: 2013

Place: Pisa, Italy

Authors: T. Calvo-Correas, L. Ugarte, L. Martin, M.A. Corcuera, A. Eceiza.

Title: Memoria de forma de poliuretanos con elevado contenido de carbono renovable.

Conference: X Simposio Argentino de Polímeros.

Contribution: Poster

Year: 2013

Place: Buenos Aires, Argentina

ANNEXES

LIST OF TABLES

Chapter 5: Thermoplastic biobased polyurethanes

Chapter 6: Thermo-responsive biobased polyurethanes

Chapter 8: Bionanocomposites with shape-memory properties

Annexes

LIST OF FIGURES

Chapter 1: Introduction

Chapter 2: Methodology: materials and characterization techniques

Chapter 3: Polyurethane rigid foams from a linseed oil based polyol

Chapter 4: Crosslinked biobased polyurethanes

Chapter 7: Biobased nanocrystals and magnetic nanoparticles

Chapter 8: Bionanocomposites with shape-memory properties

LIST OF SCHEMES

LIST OF ABBREVIATIONS

LDI	L-lysine diisocyanate
	Ethyl ester L-lysine diisocyanate
DDI	Dimeryldiisocyanate
	2-Heptyl-3,4-bis(9-isocyanatononyl)-1-pentylcyclohexane
SMP	Shape-memory polymer
MDI	4,4'-Diphenylmethane diisocyanate
HDI	1,6-Hexamethylene diisocyanate
TDI	Toluene diisocyanate
pMDI	Polymeric MDI
EDFI	5,5'-Isopropylidenebis(2-furfuryl isocyanate)
TME	Temperature memory effect
LOP	Linseed oil based polyol
LO	Linseed oil
GLY	Glycerol
DEG	Diethylene glycol
PEG	Polyethylene glycol
DMBA	N,N'-dimethyl benzylamine
DBTDL	Dibutyltin dilaurate
CO3	Poly(butylene sebacate)diol
TMP	1,1,1-Tris(hydroxymethyl)propane
PD	1,3-Propanediol
DAS	Dianhydro-D-glucitol
	Isosorbide
CNC	Cellulose nanocrystal

MCC   Microcrystalline cellulose

CHNC   Chitin nanocrystal

MNP   Magnetic nanoparticle

THF   Tetrahydrofurane

HPLC   High-performance liquid chromatography

PI   Polydispersity index

GPC   Gel permeation chromatography

FTIR   Fourier transform infrared spectroscopy

ATR   Attenuated total reflectance

H^1NMR Proton nuclear magnetic resonance

BCC   Biobased carbon content

XRD   X-ray diffraction

DSC   Differential scanning calorimetry

DMA   Dynamic mechanical analysis

AFM   Atomic force microscopy

SEM   Scanning electron microscopy

TEM   Transmission electron microscopy

WCA   Water contact angle

PBS   Phosphate buffered saline

PVC   Polyvinyl chloride

HDPE   High-density polyethylene

$H_{12}MDI$ 4,4'-Dicyclohexylmethane diisocyanate

^{13}C NMR   Carbon nuclear magnetic resonance

LIST OF SYMBOLS

I_{OH}	Hydroxyl value
T_{trans}	Transition temperature
T_s	Switching temperature
$\overline{M}_w$	Weight average molecular weight
$\overline{M}_n$	Number average molecular weight
H_{NCO}	Height of isocyanate group stretching vibration band
H_{ref}	Height of C–H bond symmetric stretching vibration band
α	Isocyanate conversion
t	Reaction time
BCC_{PU}	Biobased carbon content of the final biobased polyurethane
m_{CB}	Total biobased carbon weight
m_C	Total carbon weight
$m_{C_{mac}}$	Carbon weight in the macrodiol
$m_{C_{diis}}$	Carbon weight in the diisocyanate
$m_{C_{c.e./cr}}$	Carbon weigh in the chain extender or crosslinker
BCC_{mac}	Renewable carbon content of the macrodiol
BCC_{diis}	Renewable carbon content of the diisocyanate
$BCC_{c.e./cr}$	Renewable carbon content of the chain extender or crosslinker
T_g	Glass transition temperature
T_m	Melting temperature
ΔH_m	Melting enthalpy
T_c	Crystallization temperature
ΔH_c	Crystallization enthalpy

χ_c	Relative crystallinity
$\chi_{c\ heating}$	Relative crystallinity in the heating scan
$\chi_{c\ cooling}$	Relative crystallinity in the cooling scan
ΔH_e	Experimental melting or crystallization enthalpy value
ΔH_t	Theoretical melting or crystallization enthalpy value
ΔH_p	Melting or crystallization enthalpy value of the neat phase
ω	Weight fraction
ν_e	Crosslink density
$\overline{M}_c$	Molecular weight between crosslinks
E'	Storage modulus
T	Temperature
ρ	Density
E	Elastic modulus
σ_y	Stress at yield
σ_b	Stress at break
ε_y	Yield elongation
ε_b	Strain at break
l_r	Length reached after the recovery time
l_i	Initial height
Rr	Recovery ratio
R_f	Shape fixity ratio
R_r	Shape recovery ratio
ε_m	Maximum strain
ε_u	Residual strain after unloading

ε_p	Residual strain after the shape recovery
N	Number of cycles
γ_{PU}	Biopolyurethane surface tension
γ_{H_2O}	Water surface tension
ϕ	Angle between water drop and biopolyurethane surface
$[A]_{test}$	Absorbance of the sample cells
$[A]_{control}$	Absorbance of the negative control cells
$\lambda_{ex\text{-}em}$	Excitation emission wavelength
$\varepsilon_{densification}$	Deformation at the densification point
Rr_1	Recovery ratio after 1 min
Rr_{24}	Recovery ratio after 24 h
T_{gCO3}	Glass transition of CO3 rich domain
$T_{gLDI/TMP}$	Glass transition of LDI/TMP rich domain
$\tan\delta$	Loss factor
δ	Solubility parameter
δ_{CO3}	Solubility parameter of CO3
δ_{DDI}	Solubility parameter of DDI
δ_{LDI}	Solubility parameter of LDI
T_α	Temperature of the α transition
$T_{gLDI/PD}$	Glass transition of LDI/PD rich domain
$\delta_{LDI/PD}$	Solubility parameter of LDI/PD rich domain
$\delta_{DDI/PD}$	Solubility parameter of DDI/PD rich domain
$\delta_{DDI/DAS}$	Solubility parameter of DDI/DAS rich domain
E_g	Elastic modulus in the glassy state

E_r	Elastic modulus in the rubbery state
CrI	crystallinity degree
I_{110}	Intensity of the (110) crystallographic plane
I_{002}	Intensity of the (002) crystallographic plane
D	Crystal size
κ	Scherrer constant
λ	Radiation wavelength
β	Width at half height of the peak
θ	Bragg angle
Δ	Wavenumber separation
$\Delta H_{m\,bc}$	Experimental melting enthalpy of bionanocomposite
ΔH_{100}	Melting enthalpy of neat biobased polyurethane
$A_{overlapped}$	Overlapped area

RESUMEN

En este trabajo de tesis se presenta la síntesis y caracterización de biopoliuretanos tanto porosos como sólidos (entrecruzados y termoplásticos) y bionanocomposites, con el principal objetivo de desarrollar materiales con elevado contenido en carbono renovable. Para ello, se han empleado diferentes reactivos y nanoentidades derivados de fuentes renovables.

Los poliuretanos son un material de gran potencial debido a su gran versatilidad, lo que permite su aplicación en sectores tales como la construcción, la automoción, la aeronáutica y la biomedicina. Además, el interés sobre la síntesis de biopoliuretanos derivados de fuentes renovables va en aumento debido a la disminución de las reservas fósiles y a razones económicas, medioambientales y sociales. Generalmente, estos polímeros están constituidos por un macrodiol o poliol que rige las propiedades a bajas temperaturas y por un dominio formado por un isocianato (diisocianato o poliisocianato) y un extendedor de cadena o agente de entrecruzamiento de baja masa molecular, el cual controla las propiedades a altas temperaturas y actúa como refuerzo. En el caso de los poliuretanos porosos (espumas), además de los precursores mencionados, también son necesarios agentes de espumación, catalizadores y surfactantes específicos. El agua es uno de los agentes de espumación más empleado, ya que al reaccionar con un isocianato da lugar a grupos funcionales urea y dióxido de carbono, el cual permite el crecimiento de la espuma.

En esta tesis se han llevado a cabo diferentes estrategias para aumentar el contenido de carbono renovable de los biopoliuretanos sintetizados. Por un lado, se han preparado espumas de poliuretano rígidas incorporando un poliol derivado de aceite de lino mediante reacciones de hidroxilación y glicerol como agente modificador de la reactividad, además de agua como agente de espumación. Por otro lado, el contenido de carbono renovable en poliuretanos termoplásticos y entrecruzados se ha aumentado mediante el empleo de un macrodiol derivado de aceite de ricino (CO3) y dos diisocianatos provenientes de fuentes renovable, uno basado en el aminoácido L-lisina (LDI) y otro derivado de ácidos grasos (DDI). Además, en el caso de los termoplásticos también se han utilizado dos extendedores de cadena de origen renovable, uno proveniente de azúcar de maíz (PD) y otro basado en un polisacárido (DAS). Del mismo modo, el contenido de carbono renovable de los bionanocomposites se ha aumentado mediante la incorporación de nanoentidades de provenientes de la biomasa, tales como nanocristales de quitina y celulosa.

Los biopoliuretanos y bionanocomposites desarrollados en esta tesis se han caracterizado mediante diversas técnicas físico-químicas, térmicas, mecánicas, morfológicas y

superficiales, entre otras, y se ha estudiado la influencia de la naturaleza y del contenido de los reactivos y de las nanoentidades sobre las propiedades finales.

Las espumas rígidas de biopoliuretano se han sintetizado a partir de aceite de lino hidroxilado y diferentes contenidos de modificadores de la reactividad de baja masa molecular (en concentraciones comprendidas entre 0 y 20% en masa), tales como glicerol, dietilenglicol y polietilenglicol. Las propiedades finales de las espumas se han visto afectadas por los modificadores de la reactividad empleados, así como la reactividad del sistema. Las espumas con modificadores han presentado menores tiempos (crema, elevación y tacto libre) en comparación con la espuma de referencia, lo cual se atribuye a la mayor reactividad de los grupos hidroxilo de los modificadores y a la menor viscosidad inicial de los sistemas modificados.

Por otra parte, las espumas modificadas con glicerol han mostrado una mayor temperatura de transición vítrea (T_g), la cual se desplaza a mayores temperaturas a medida que aumenta el contenido de glicerol. Además, estas espumas han presentado mayor módulo de almacenamiento y propiedades a compresión superiores, debido al carácter entrecruzante del glicerol, así como a una mayor concentración de isocianato. Por lo tanto, se ha deducido que las propiedades a compresión de las espumas rígidas están altamente condicionadas por la concentración de isocianato en la formulación inicial. El análisis termogravimétrico ha revelado que el aumento de la concentración de isocianato da lugar a una mayor formación de cenizas y que las espumas con una mayor densidad de entrecruzamiento (las modificadas con glicerol) presentan mayor estabilidad térmica.

Con respecto a los poliuretanos entrecruzados, se han sintetizado dos series empleando un macrodiol derivado de aceite de ricino (CO3) y dos diisocianatos de origen renovable diferentes, LDI y DDI. En ambas series se ha utilizado trimetilolpropano (TMP) como agente de entrecruzamiento y se ha variado la concentración de diisocianato/TMP, a fin de analizar el efecto de la naturaleza del diisocianato y el contenido de diisocianato/TMP en las propiedades finales.

Los resultados obtenidos han mostrado que el empleo de diisocianatos con cadenas laterales (LDI) o con estructuras ramificadas (DDI), da lugar a biopoliuretanos con una baja T_g y que su estructura impide la cristalización del dominio rico en diisocianato. Los biopoliuretanos con LDI han mostrado una morfología con una mayor separación microfásica, dado que todos los biopoliuretanos presentan dos T_g bien definidas atribuidas a los dominios ricos en CO3 y LDI/TMP. Sin embargo, los poliuretanos con DDI presentan una única T_g que aumenta a medida que el contenido de DDI/TMP aumenta, sugiriendo una mezcla entre el DDI/TMP y

la fase amorfa del CO3. El diisocianato DDI ha mostrado una mayor tendencia a mezclarse con la parte amorfa del CO3 en comparación con el LDI. Este hecho puede ser debido a su mayor afinidad con el macrodiol. El comportamiento dinámico-mecánico de los biopoliuretanos sintetizados ha revelado que los biopoliuretanos con LDI están más entrecruzados y por lo tanto presentan una menor masa molecular promedio entre retículos. Este hecho está relacionado con el menor tamaño del LDI lo cual permite que la distancia entre los retículos sea menor y de este modo aumenta la densidad de entrecruzamiento y la temperatura de la transición α. En ambas series se ha observado que las propiedades mecánicas son dependientes de la cristalinidad del material. Además, los poliuretanos con LDI también han mostrado que la densidad de entrecruzamiento tiene un papel fundamental. Es por ello que la variación de la cristalinidad y de la densidad de entrecruzamiento permite la posibilidad de sintetizar biopoliuretanos entrecruzados con propiedades mecánicas a medida.

Los biopoliuretanos termoplásticos han sido sintetizados a partir de un macrodiol derivado de aceite de ricino (CO3) y los diisocianatos de origen renovable LDI y DDI. En los biopoliuretanos sintetizados a partir de LDI, se ha utilizado PD como extendedor de cadena, mientras que los sintetizados a partir de DDI, además de PD, también se ha utilizado DAS. Del mismo modo, se ha variado el contenido diisocianato/extendedor de cadena. Así mismo, se ha analizado tanto el efecto de la estructura de los reactivos, así como del contenido de los mismos, en las propiedades finales.

Al igual que en los biopoliuretanos entrecruzados, se ha observado que la estructura de los diisocianatos da lugar a la obtención de biopoliuretanos con baja T_g y que debido a su impedimento estérico la cristalización está más impedida. Los biopoliuretanos termoplásticos sintetizados han mostrado un comportamiento diferente en función de la naturaleza tanto del diisocianato como del extendedor de cadena. En el caso de los sintetizados a partir de PD, se han observado dos T_g diferenciadas, sugiriendo una morfología con una separación microfásica; mientras que los sintetizados con DDI han mostrado una única T_g, la cual aumenta a medida que se incrementa el contenido de DDI/extendedor de cadena, indicando una mezcla microfásica. Además, en los biopoliuretanos sintetizados a partir de DDI se ha estudiado la influencia de la estructura de los extendedores de cadena. A medida que el impedimento estérico aumenta (al emplearse DAS como extendedor de cadena) se han observado mayores T_g y una menor habilidad para la cristalización. Del mismo modo, tanto en los biopoliuretanos con LDI como los obtenidos a partir de DDI han mostrado una inversión del comportamiento de los dominios, dado que la fase cristalizable formada por el macrodiol muestra una temperatura de fusión (T_m)

mayor que la T_g de LDI/PD y DDI/PD o DDI/DAS, provocando que el macrodiol actúe como la fase rígida. Este comportamiento, difiere de los observados en la bibliografía cuando se ha empleado diisocianatos convencionales, en los cuales los segmentos formados por el diisocianato y el extendedor de cadena muestran elevadas T_g y T_m. Al igual que en los biopoliuretanos entrecruzados, las propiedades mecánicas están muy influidas por la cristalinidad total y la morfología del material. A medida que la cristalinidad aumenta se han observado mejores propiedades.

Tanto los biopoliuretanos entrecruzados como los termoplásticos han mostrado un comportamiento no tóxico y se ha observado que el DDI promueve la proliferación de las células en mayor medida. Asimismo, se ha observado que tras 7 días, las células presentan una actividad metabólica y su han observado sólo unas pocas células muertas. Es por ello, que los biopoliuretanos sintetizados muestran potencial para ser utilizados en aplicaciones biomédicas.

Además, los biopoliuretanos sintetizados a partir de LDI (tanto termoplásticos como entrecruzados) han mostrado propiedades de memoria de forma. Los poliuretanos con memoria de forma presentan la propiedad de ser capaces de recordar la forma original tras ser sometidos a una deformación y recuperarla al aplicar un estímulo externo, siendo el térmico uno de los más empleados. De este modo, al superar la temperatura de cambio (T_s) (que puede ser tanto una T_g como una T_m), la memoria del material se activa. Por ello, en este trabajo se ha analizado el efecto sobre las propiedades de memoria de forma del aumento de contenido de LDI/extendedor de cadena o agente de entrecruzamiento, así como de la variación de las condiciones del ensayo. En el caso de los termoplásticos se ha analizado la influencia de la variación del la T_s y en el de los entrecruzados la variación de la deformación límite (ε_m).

Para el análisis del efecto de la variación de la T_s en biopoliuretanos termoplásticos se han seleccionado dos temperaturas diferentes, 25 y 40 °C, las cuales se encuentran entre la T_g del domino rico en LDI/PD y la T_m del dominio rico en CO3. Los ensayos de memoria de forma a 25 °C han revelado que a medida que aumenta el contenido de LDI/PD el material muestra mayores valores de fijación, mientras que la recuperación del material aumenta a medida que aumenta el contenido de CO3. En el caso de que la T_s es 40 °C, dado que la temperatura de deformación se solapa con el principio de la entalpia de fusión, algunos cristales del dominio rico en CO3 se han fundido contribuyendo al estado caucho y con ello al aumento de la fijación. Así mismo, el aumento de la T_s acelera el proceso de recuperación.

La influencia de la deformación máxima se ha analizado sometiendo a los biopoliuretanos entrecruzados a tres deformaciones diferentes, 50, 100 y 250%. Por un lado, se ha observado que las propiedades de memoria de forma varían con la densidad de entrecruzamiento. A medida que la densidad de entrecruzamiento aumenta el material ha mostrado una menor fijación. Este hecho es debido a que el aumento de los puntos de entrecruzamiento aumenta el impedimento estérico dificultando que las cadenas puedan adoptar un estado con menor entropía. Mientras que la recuperación ha aumentado dado que los puntos de entrecruzamiento contribuyen a recordar de la forma.

De todos modos, se ha observado que la fijación de la forma para ambos sistemas está controlada por el módulo elástico en el estado vítreo. Los biopoliuretanos con un mayor módulo en el estado vítreo han mostrado mayores valores de fijación. Mientras que la fuerza impulsora para la recuperación de la forma es la tensión residual introducida en el material durante el proceso de deformación. Esta se almacena en los dominios cristalinos en los termoplásticos y en el caso de los entrecruzados también en los puntos de entrecruzamiento. Además, se ha deducido que los puntos de entrecruzamiento son más efectivos almacenando la tensión residual, dado que a pesar de la disminución de la cristalización con el aumento del contenido de LDI/TMP, se han obtenido mayores valores de recuperación.

Las propiedades de los poliuretanos pueden mejorarse adicionando diferentes nanoentidades. Por ello, en este trabajo se han preparado diversos bionanocomposites termo-sensibles por *solvent casting* incorporando nanocristales de quitina (CHNC), nanocristales de celulosa (CNC), nanopartículas de magnetita (MNP) y también una combinación de CNC y MNP a uno de los biopoliuretanos termoplásticos con memoria de forma. De esta manera se ha estudiado la influencia de la naturaleza de las nanoentidades así como de su contenido en las propiedades finales y en el comportamiento de memoria de forma.

En el caso de los bionanocomposites con CHNC, se ha observado que los CHNC interactúan con el dominio rico en LDI/PD y tienen un efecto nucleante sobre dominio rico en CO3, y por lo tanto, la cristalinidad del bionanocomposite aumenta. Además, debido a la formación de una red percolada de los CHNC y de los cristales, el módulo elástico aumenta. No obstante, los bionanocomposites con un elevado contenido de CHNC muestran una baja deformación a rotura. El análisis de las propiedades de memoria de forma ha revelado que el aumento de la cristalinidad con la adición de los CHNC permite una mayor recuperación de la forma.

En lo referente a los bionanocomposites con MNP, se ha observado que la incorporación de las nanopartículas disminuye la cristalinidad general del material obteniéndose un material más amorfo. Además, el aumento en la T_g del dominio rico en CO3 observado y la disminución de la cristalinidad relativa ha sugerido que las MNP interactúan con el dominio rico en CO3 impidiendo su cristalización. Además, se ha visto que la adición de las MNP refuerza el material dado que el modulo elástico y la tensión de rotura aumentan a medida que aumenta el contenido de las nanopartículas. Respecto a las propiedades de memoria de forma, la presencia de las MNP aumenta la fijación de la forma, debido al aumento en el módulo elástico en el estado vítreo. Así mismo, la recuperación es similar a pesar la menor cristalinidad del material, lo que ha sugerido que las MNP son capaces de absorber la energía de deformación durante el proceso de programación contribuyendo a la recuperación de la forma.

Finalmente, se han preparado bionanocomposites combinando CNC y MNP, y a modo de referencia también se ha preparado un bionanocomposite sólo con CNC. La adición de CNC ha aumentado la T_g del dominio rico en LDI/PD y no ha disminuido la habilidad del dominio rico en CO3 para cristalizar, lo que significa que los CNC interactúan, con el dominio rico en LDI/PD. Además, la adición de ambas nanoentidades ha disminuido la cristalinidad relativa, por lo que sugiere que las MNP interactúan con el dominio rico en CO3 dificultando su cristalización. Del mismo modo, en ambos bionanocomposites se ha observado que la adición de ambas nanoentidades, tanto por separado o en combinación, disminuyen la cristalización total del material. El análisis de las propiedades mecánicas ha revelado que la adición de CNC o de la combinación CNC y MNP a los bionanocomposites aumenta el módulo elástico sin comprometer en gran medida la deformación a rotura. En lo referente a las propiedades de memoria de forma, se han obtenido bionanocomposites con mayor fijación y menor recuperación debido a la menor cristalinidad del material, en comparación con sus homólogos sin CNC.

Así mismo, se ha observado que las propiedades de los bionanocomposites están influenciadas por el método de preparación de los films. Una rápida cristalización, da lugar a la obtención de materiales menos cristalinos y por lo tanto repercute en las propiedades de memoria de forma. Además, también se ha podido observar que las propiedades de memoria de forma están determinadas por el comportamiento dinámico-mecánico, así como por la naturaleza de las nanoentidades.

Por consiguiente, en este trabajo de tesis se ha conseguido aumentar el contenido de carbono renovable de biopoliuretanos porosos y sólidos, así como de los bionanocomposites, mediante la incorporación de reactivos y nanoentidades derivados de

fuentes renovables. Así mismo, se ha visto que las propiedades de los biopoliuretanos obtenidos están estrechamente relacionadas con la naturaleza y el contenido de los reactivos y nanoentidades incorporados. Por lo tanto, es posible sintetizar poliuretanos con un elevado contenido en carbono renovable con propiedades a medida controlando la naturaleza y el contenido de reactivos y nanoentidades.

The demand for the design of polyurethanes derived from renewable sources has increased in the last decades due to the depletion of the world crude oil stock and economical, environmental and social concerns. In this context, this work deals with the increase of the renewability of different porous and solid (thermoplastic and crosslinked) polyurethanes and bionanocomposites, by the incorporation of different reactants and nanoentities from renewable sources. Moreover, the influence of the nature of the reactants and nanoentities and their content on the final properties has been deeply studied.

Besides, the synthesized solid polyurethanes and bionanocomposites have shown shape-memory properties. Therefore, the effect of the programming conditions as well as reactant content and, in the case of the bionanocomposites, nanoentity nature and content on shape-memory properties has been thoroughly analyzed.